Mixing, mass transfer and energy analysis across bioreactor types in microalgal cultivation and lipid production

Sarah Melissa Jane Jones

Thesis presented for the degree of

DOCTOR OF PHILOSOPHY

Supervisors: Professor S.T.L. Harrison and Professor H. Von Blottnitz

Department of Chemical Engineering

Faculty of Engineering and the Built Environment

UNIVERSITY OF CAPE TOWN

October 2015

“You dig deeper and it gets more and more complicated, and you get confused, and it's tricky and it's hard, but... It is beautiful.”

~Brian Cox

Acknowledgments

I gratefully acknowledge the financial support of the South African Research Chairs Initiative (SARChI) of the Department of Science and Technology and the National Research Foundation (NRF) of South Africa; and I thank the University of Cape Town for the award of the JW Jagger Centenary Gift Scholarship for International Students. I also wish to extend my gratitude to the following:

Professor Sue Harrison, my supervisor, whose experience and insight guided this project and my development as a researcher. Thank you for your nurturing leadership style. Your understanding of my academic and personal growth has been pivotal in my PhD journey.

Dr Melinda Griffiths: for all your help in the laboratory, guidance during discussions and reviews, and input on this thesis. You have been a mentor to me.

Professor Harro von Blottnitz: for your knowledge and guidance on Life Cycle Analysis and environmental considerations, for broadening my understanding and motivating my interest.

Dr Tobi Louw: for your invaluable input on the power measurements in this project. It was a pleasure working with you.

Christine Richardson: for the simulated algal biodiesel production process; Murray Fraser: for circulation data in the airlift reactor; and Dr Menkin, Stellenbosch University: for calorific values.

Jo Mackie: for building, creating and advising (baffles, motors, gas units, housings); Geoff Moss: for building the oscillatory baffled reactor; Eghsaan Matthews: for helping with lights.

CeBER staff: for your assistance, care and advice in the lab (Emmanuel Ngoma, Tich Samkange, Sharon Radameyer) and with administration (Sue Jobson, Lesley Mostert, Sandra Christianson).

CeBER: whose excellent standard of science and collaborative atmosphere make me honoured to be a member; and Algae Research Group: for the inspiring discussions and useful feedback.

Dr Doug Sanyahumbi: for pointing me in the right direction, connecting me with Prof Harrison, for motivating career discussions and your advice over the years.

My family and friends: for you interest and encouragement, for listening to my excited stories about the world of algae, for sharing in my excitement and for giving soul-replenishing love, rest and fun.

Abstract

Microalgae are recognised as a source of lipids for bioenergy, nutrients and pharmaceuticals. Photobioreactors, closed vessels for microalgal cultivation, are known to have high energy consumption due to mixing and aeration. Sparging is commonly used for mixing and gas-liquid mass transfer in photobioreactors, but is energy intensive. The aim of this work was to reduce these energy requirements by optimising conventional sparging and considering surface aeration coupled with mechanical agitation as an alternative.

An airlift photobioreactor was used as a base for comparison with two novel, surface aerated reactors: oscillatory baffled and wave photobioreactors. The three bioreactors were compared in terms of power input, mixing, CO_2 mass transfer, algal growth and lipid production. Prior to comparison, each photobioreactor was optimised based on these parameters. To calculate power input, isothermal gas expansion equations were used for sparged systems and calorimetry was used for mechanically agitation systems. Mixing was investigated using a salt tracer and phenolphthalein indicator and mass transfer was measured using the gassing-in method. *Scenedesmus* sp., a high lipid-producer, was cultivated in low nitrate media across a range of mixing rates in each photobioreactor.

In the airlift photobioreactor a critical minimum CO_2 supply rate (of 2.7×10^{-5} m s^{-1}) was found, below which carbon was limiting and above which energy was spent on sparging without increased productivity (0.20 g L^{-1} d^{-1} biomass; 0.03 g L^{-1} d^{-1} lipid). In the oscillatory baffled reactor, insufficient mass transfer limited algal productivity (0.11 g L^{-1} d^{-1} biomass; 0.02 g L^{-1} d^{-1} lipid). The wave reactor had high CO_2 mass transfer coefficients (10 – 140 h^{-1}) in comparison to the airlift (2.7 – 40 h^{-1}) and oscillatory baffled reactors (6.3 – 37 h^{-1}). Sufficient biomass productivity (0.18 g L^{-1} d^{-1}) and higher lipid productivity (0.045 g L^{-1} d^{-1}) at lower power input in the wave reactor resulted in higher energy efficiency compared to the airlift reactor. Life cycle analysis of simulated algal biodiesel production showed that bioreactor energy contributed 99% of total energy consumption. Therefore, the global warming potential was reduced by 73% when the airlift reactor was operated at the critical minimum CO_2 supply (with gas compression to 2 bar) and a further 19% when the wave reactor was used.

This work offers an energy efficient alternative to sparging, through the generation of a well-mixed wave in a surface aerated bioreactor. It also offers methods for optimisation of energy usage with respect to mixing and aeration. Reducing bioreactor energy consumption is key to feasibility, and was demonstrated here to reduce energy-related environmental burdens.

Contents

List of Figures

List of Tables

Glossary

ALR	airlift reactor
A_d	cross-sectional area of downcomer (m2)
ALR High Power	airlift reactor operated at 2 L min-1 gas flowrate
ALR Optimum	airlift reactor operated at 0.5 L min-1 gas flowrate
A_r	cross-sectional area of riser (m2)
BBM	Bold's basal medium
CED	cumulative energy demand
CSR	CO2 supply rate (m s-1)
CTR	CO2 transfer rate (mol L-1 h-1)
CU_{lipid}	Carbon uptake to lipid (moles)
deg	degrees
DMSO	dimethylsulphoxide
EDTA	Ethylenediaminetetraacetic acid
F	gas flowrate (m3 s-1)
FAME	fatty acid methyl esters
g	gravitational acceleration (m s-2)
GC	gas chromatography
GHG	greenhouse gas
GWP	global warming potential
High P	High power for mixing and mass transfer
h_L	height of the liquid in the ALR (m)
IPCC	Intergovernmental Panel on Climate Change
$k_L a$	gas-liquid mass transfer coefficient (h-1)
$k_L a_{CO_2}$	CO2 mass transfer coefficient (h-1)
$k_L a_{O_2}$	O2 mass transfer coefficient (h-1)
LCA	Life Cycle Analysis
LCI	Life cycle inventory
LCIA	Life cycle impact assessment
Low P	Low power for mixing and mass transfer
n	molar gas flowrate (mol s-1)
NER	Net energy ratio
NER_{BPP}	NER for biodiesel production process

NER_{CED}	NER for cumulative energy demand
NER_{PBR}	NER for photobioreactors
OBR	oscillatory baffled reactor
OD	optical density
P/V	power input per unit volume (W m-3)
p_1	gas pressure at the top of the reactor (Pa)
p_2	gas pressure entering the reactor (Pa)
p_3	gas pressure leaving the sparger (Pa)
PBR	Photobioreactor
P_G	power for aeration (W)
PV	photovoltaic
R	ideal gas constant (8163 J K-1 kmole-1)
rpm	revolutions per minute
Sc	*Scenedesmus*
T	temperature (K)
TAG	triacylglyceride
T_m	mixing time (s)
U_G	superficial gas velocity
U_{Gr}	height averaged superficial gas velocity in riser (m s-1)
V_L	liquid volume (m3)
W	Watts
WR	wave reactor
WR Optimum	wave reactor operated at 15 rpm 4 deg
Δp	gas pressure drop across sparger (Pa)
ρ_L	liquid density (kg m-3)

Outputs arising from this work

Published journal papers

Sarah M.J. Jones and Susan T.L. Harrison (2014). Aeration energy requirements for lipid production from *Scenedesmus* sp. in airlift bioreactors. *Algal Research* 5, 249-257.

Journal papers in progress

Sarah M.J. Jones, Marc Brighton and Susan T.L. Harrison (2015). Exploring the tension between energy consumption, light provision and CO_2 mass transfer through varying gas velocity in the airlift bioreactor. *Algal Research*. Submitted to journal.

Sarah M.J. Jones and Susan T.L. Harrison (2015). An oscillatory baffled photobioreactor for cultivation and lipid production of *Scenedesmus* sp. Draft completed.

Sarah M.J. Jones, Tobias M. Louw and Susan T.L. Harrison (2015). Energy consumption due to mixing and mass transfer in a wave photobioreactor. In review.

Sarah M.J. Jones and Susan T.L. Harrison (2015). Comparison of airlift and wave photobioreactors for energy efficient microalgal cultivation. Draft in progress.

Sarah M.J. Jones and Susan T.L. Harrison (2015). Life cycle and energy analysis of algal biodiesel production using airlift and wave photobioreactors. Draft in progress.

Book chapters

Tobias M. Louw, Melinda J. Griffiths, Sarah M.J. Jones and Susan T.L. Harrison (2015). Techno-economics of algal biodiesel. In *Algal biotechnology: Products and Processes* (Editors: Faizal Bux and Yusuf Chisti).

Conference presentations

Susan T.L. Harrison, Marc Brighton and Sarah M.J. Jones (2015). Exploring the effects of aeration rate on CO_2 mass transfer and light provision for optimisation of energy efficiency in airlift bioreactors. 29th Congress of the Phycological Society of Southern Africa, St Lucia, South Africa, 22-26 June 2015 (Oral Presentation).

Susan T.L. Harrison, Marc Brighton and Sarah M.J. Jones (2015). Exploring the tension between energy consumption, light provision, and CO_2 mass transfer through varying air flowrate in the airlift bioreactor. 5th International Conference on Algal Biomass, Biofuels and Bioproducts, San Diego, USA, 7-10 June 2015 (Oral Presentation).

Sarah M.J. Jones and Susan T.L. Harrison (2014). Aeration energy requirements for lipid production by *Scenedesmus* sp. in airlift bioreactors. 28th Congress of the Phycological Society of Southern Africa, Melkbosstrand, South Africa, 13-17 January 2014 (Oral Presentation).

Sarah M.J. Jones and Susan T. L. Harrison (2013). Aeration rate and CO_2 mass transfer as key variables in airlift photobioreactors for biomass and lipid productivity, and associated energy yields, of *Scenedesmus* sp. 9th European Congress of Chemical Engineers, The Hague, The Netherlands, 21-25 April 2013.

Sarah M.J. Jones, S.T.L. Harrison, H. von Blottnitz (2012). Energy requirements and mass transfer for algal lipid production in airlift bioreactors. 8th Acia-Pacific Conference of Algal Biotechnology, Adelaide, Australia, 9 -12 July 2012. (Oral Presentation)

Sarah M.J. Jones, von Blottnitz, H. and Harrison, S.T.L (2011). Reducing energy input requirements in the bioreactor stage of algal lipid production. 17th South African Society for Microbiology Congress. Southern Sun Cape Sun Hotel, Cape Town. 6-9 November 2011.

1 Introduction and Literature Review

1.1 The role of bioprocess engineering in sustainable development

1.1.1 Advantages and limitations in bioprocesses

Technology continues to advance and expand, and with a rapidly increasing human population, is key to maintaining and improving our quality of life. Bioprocess engineering plays an important role in the global future landscape as it offers solutions to a variety of existing and imminent concerns. The use of bio-materials and biological agents for the manufacture of fine-chemical, commodity and energy products is not a new concept, but recent environmental, economic, and social pressures have sparked a new wave of interest in bio-products. Algal bioprocessing is among those receiving growing attention in research and commercialisation spaces (Anex, 2003; Demirbas, 2011; Gavrilescu and Chisti, 2005; Harun et al., 2010).

Biological systems are attractive because they have been fine-tuned by evolution to be efficient and produce biodegradable, often non-toxic products and by-products (Gavrilescu and Chisti, 2005). Industrially applied bioprocesses use mostly renewable raw materials, favourable operating conditions and highly specific and complex biologically catalysed reactions (Harding, 2008). However, it would be a misconception to assume that all industrial bioprocesses are more environmentally friendly and economically more viable than their chemical counterparts (Geigrich, 2003; Gerngross, 1999; Harding et al., 2007; Hermann and Patel, 2007). An industrial bioprocess, where a biological organism or system is harnessed to produce a product at faster than natural rates, often requires fossil fuel energy and non-renewable inputs. Appropriate resource management and innovative solutions for efficiency and adaptability are required to ensure the economic, environmental and practical feasibility of bio-based products, as well as the sought-after biological advantages (Anex, 2003). A crucial benefit is that many bioprocesses are still relatively new, allowing more scope for improvement than with more established chemical processes (Harding, 2008).

Prior to implementation, a bioprocess can be assessed for its feasibility, economics and environmental burdens using tools such as Life Cycle Analysis and energy balancing. Many of these

assessments show that energy requirements, nutrient input, productivities and yields have the largest impacts on the overall feasibility and sustainability of the investigated bioprocesses (Table 1.1). A bioprocess with high energy requirements is likely to rely on fossil-derived energy sources, have a high carbon footprint and high energy-related costs. For a bio-energy product, such as biofuel or biogas, it is essential that the energy used to create the product be lower than the energy obtained from it. For all bioproducts, it is desirable to minimise the energy footprint.

Table 1.1 Sensitivity analysis results of various Life Cycle Analyses performed on bioprocesses, showing the parameters that have the largest negative impacts on sustainability.

Bioprocess / Bioproduct	**Areas of high detrimental impact on sustainability**	**Reference**
Poly-β-hydroxybutyric acid (PHB), a bio-polymer	Energy (particularly for steam); water; toxicity (fertilizer, acids, salts)	Harding et al. (2007)
Bio-based bulk chemicals	Productivities, concentration and yields in fermentation stage	(Hermann et al., 2007)
Penicillin from *Penicillium chrysogenum*	Electricity requirements (due to large volumes caused by poor separation efficiencies; and steam requirements); agricultural inputs (for growth media)	Harding (2008)
Cellulase from microbes	Low biomass concentration = large water volumes in bioreactor = high energy requirements; lack of downstream processing = increased volumes	Harding (2008)
Lipase for biodiesel production	Low biomass concentration = large bioreactor volumes = high energy requirements	Harding (2008)
Algal biodiesel	Energy and nitrogen input in cultivation stage (bioreactor)	Lardon et al. (2009)
Bioethanol in refinery process	Large water volumes linked to energy usage (water removal by distillation, pumping and heating water)	Alvarado-Morales et al. (2009)
Algal biodiesel	Energy and nutrients in cultivation stage (bioreactor) – circulation velocity, yields, recycling, N-fertilizer, carbon dioxide input method)	Stephenson et al. (2010)
Algal biodiesel	Nitrogen and carbon dioxide inputs	Clarens et al. (2010)
Bioethanol	Biomass and ethanol yields	Singh et al. (2010)
Citric Acid from starch/molasses using *Aspergillus niger*	Electricity (for air compression and bioreactor agitation) and steam requirements	de Beer (2010)
Algal biodiesel	Reactor energy requirements; nitrogen fertilizer production	Richardson (2011)

1.1.2 Energy demand in microalgal bioprocessing

Microalgae have the potential to produce a variety of commercial bioproducts which can replace fossil fuel or chemical-based alternatives without competing with food production. This ability of microalgae to produce multiple useful compounds by harnessing energy from sunlight make them promising for sustainable development (Demirbas, 2011; Harun et al., 2010; Lehr and Posten, 2009). Key to the success of algal bioprocessing is the energy demand and cost required for generating these products. Previous reports indicate that the cultivation stage of microalgal bioprocesses significantly contributes to the overall energy consumption of the processes (Table 1.1) and thus limits their environmental and economic feasibility (Rickman et al., 2013; Slade and Bauen, 2013). Bioreactors utilised in a range of other bioprocesses also have high energy burdens (Table 1.1), indicating a need to investigate bioreactors and photobioreactors for their energy efficiency. In this work we investigated possibilities for improving the energy efficiency of algal cultivation in photobioreactors (PBRs) by optimising conventional algal cultivation methods and introducing novel PBR designs. In order for algal bioproducts to contribute to sustainable development, energy efficient cultivation is required.

1.2 Microalgal bioprocessing

1.2.1 Algal biology

Algae are a group of diverse photosynthetic aquatic organisms including eukaryotic macro- and microalgae, and prokaryotic Cyanobacteria. Cyanobacteria, also known as blue-green algae, are photosynthetic bacteria whose common ancestor was the first to evolve the capacity to use water as a source of electrons in photosynthesis more than 2450 million years ago (Knoll, 2008). The production of free oxygen by these organisms early in the Earth's history played a vital role in shaping evolution and life as it is today (Anderson, 2013). A diverse group of Cyanobacteria remained Earth's foremost autotrophic organisms until about 543 million years ago when they were joined by eukaryotic algae as major primary producers. Eukaryotic algae first evolved between about 1700 and 543 million year ago, and now include a large variety of macro- and microalgae (Knoll, 2008).

Macroalgae are plant-like multi-cellular organisms, including kelps and seaweeds. Microalgae are usually single celled microscopic organisms, sometimes occurring in colonies (Graham et al., 2009). Algae are highly diverse, spanning a variety of morphologies and ecologies, and producing a wide

array of carbohydrates, lipids and proteins (Anderson, 2013). Microalgae, used in this work, can be grouped according to morphologies and life-cycles, e.g. dinoflagellates, diatoms and haptophytes, as well as the pigments they contain, such as red, brown, gold and green algae. Green algae, *Chlorophyta*, are a large group that produce abundant quantities of chlorophylls *a* and *b*, giving them their characteristic green colour (Anderson, 2013; Graham et al., 2009).

One of the most defining features of microalgae is their ability to utilize the sun's energy for photosynthesis. Photosynthesis is a light-driven reaction in which water and carbon dioxide are converted to carbohydrates, and oxygen is released as a by-product. Photosynthetic pigments (chlorophylls, carotenoids and phycobolins) aid in light harvesting for energy provision, and transfer of excitation energy (Masojidek et al., 2013).

1.2.2 Commercial applications of microalgae

Many species of microalgae show potential as useful bioresources and a number are already used commercially in food or nutritional supplements, pharmaceuticals, animal feed, aquaculture, wastewater treatment and bioenergy (Cardozo et al., 2007; Castine et al., 2013; Christenson and Sims, 2011; Demirbas, 2010; Kuda et al., 2005). The first attempt to cultivate microalgae in a technical environment was in Germany during World War 2. In war time, microalgae presented an inexpensive protein source to replace animal proteins which were difficult to obtain. In the USA, fundamental studies on photosynthesis led to the first large-scale algal culture plant, built in 1948. In the 1950s, mass algal culture plants were established for protein production in the US and Japan but could not compete with terrestrial crop sources such as soy bean. Following this, one of the earliest commercial applications of algae was in photosynthetic wastewater treatment. Initially algal cultivation was predominantly carried out in outdoor ponds, but, in the 1960s, NASA was interested in research on closed culture systems for algal cultivation. The idea was to use these closed systems for oxygen generation during prolonged missions in outer space. In the 1970s a global oil crisis gave rise to research into algae as a biomass feedstock for methane production and a major programme on algal cultivation for biofuels (Aquatic Species Program, by the US Department of Energy) (Carvalho et al., 2006).

Today, there is continued interest in microalgae for their nutritional value, wastewater treatment and their potential role in the current energy crisis. Additionally, microalgae are used for

production of fine chemicals and high value secondary metabolites. Pigments for food colouring, cosmetics and textiles, vitamins, antioxidants, antibiotics, and high value oils (e..g omega-3 oil) are some examples of algal bioproducts (Harun et al., 2010). Algae have also been used in bioremediation and as nitrogen fixing biofertilizers, and can be used for carbon sequestration to counter the greenhouse effect (Chisti, 2007a; Harun et al., 2010). In the energy sector, many algae have high lipid content which can be extracted and used to make biodiesel. The biomass remaining after lipid extraction can then be used to make methane and bioethanol. Biohydrogen can be produced from algae by dark fermentation or pyrolysis (Harun et al., 2010; Pittman et al., 2011; Stephens et al., 2010).

The ability of algae to produce multiple commercially interesting products simultaneously, gives promise to the algal biorefinery. A biorefinery processes biomass into various co-products in order to improve the cost versus outputs of the process. Ideally, the biorefinery uses all components of the biomass to make the product range. It can also be designed as a closed system to minimise waste by recycling nutrients, water and cell-debris and integrating heat and energy released from one process to feed another (Chisti, 2007a; Demirbas and Demirbas, 2010; Singh and Gu, 2010).

1.2.3 Requirements for growth

There are several important factors for cultivating algae to desired biomass concentrations. Photosynthesis requires water, light and carbon dioxide on which algae rely to provide the raw materials necessary for growth and reproduction. In addition to photosynthetic requirements, algal growth depends on nutrients such as nitrogen, phosphorous and trace elements. Temperature, pH, salinity and removal of oxygen are also factors to consider for algal cultivation (Grobbelaar, 2000; Mata et al., 2010).

Carbon is a major constituent of algal cells (approx. 50% of algal cells by dry weight is carbon), and CO_2 is often the major or only source of carbon in algal cultivation (Chisti, 2007a). Algae typically fix 1.83 kg of CO_2 for every kg of algal biomass (Borowitzka and Moheimani, 2013; Chisti, 2007a; Pate et al., 2011). Algae utilize CO_2 from the air, but typically supplementary CO_2 in intensive cultivation systems is essential for commercially viable growth rates and productivities due to the low concentrations of atmospheric CO_2 (0.036%) (Brennan and Owende, 2010; Pate et al., 2011) and low associated mass transfer rates.

Mixing and provision of interfacial area are essential for the efficient transfer of CO_2 to the cells, and the removal of O_2. The transport of these gases in and out of solution is known as gas-liquid mass transfer, discussed in detail in Section 1.3.2 below. Mass transfer is enhanced by increasing the CO_2 content of the sparged gas (Chisti and Jauregui-Haza, 2002; Langley, 2010). The accumulation of oxygen during algal cultivation leads to decreased photosynthetic rates, thus its removal is essential to maintain growth rates. Therefore, algal cultivation relies on sufficient mass transfer (Chisti, 2007a).

Adequate mixing results in the even distribution of nutrients to all cells in the culture medium. Distribution of light and cycling of algal cells through the light and dark zones, particularly in dense cultures, also relies on sufficient mixing rates (Lehr and Posten, 2009; Pulz and Scheibenbogen, 1998). Light-dark cycling enhances photosynthetic rate; where higher frequencies of cycling induce higher growth rates (Fraser, 2011; Grobbelaar, 1991; Langley, 2010; Pulz and Scheibenbogen, 1998). At low cycling frequencies, algal growth is not inhibited as long as mixing is sufficient so that cells do not remain without light for extended periods of time. Similarly, if cells remain in constant high light conditions, photoinhibition is likely to occur, where a cell's photosynthetic machinery becomes damaged (Eilers and Peeters, 1988; Scott et al., 2010).

Algal cultivation therefore relies on a combination of inter-related factors, as illustrated in Figure 1.1. A key element in this network is the agitation (e.g. stirring, bubbling, shaking) of the algal culture. A power supply or energy input is required for agitating an algal culture; agitation is important for affecting mixing and mass transfer rates, and thus the rate of CO_2 provision as well as light and nutrient distribution, which are essential for algal growth (Figure 1.1).

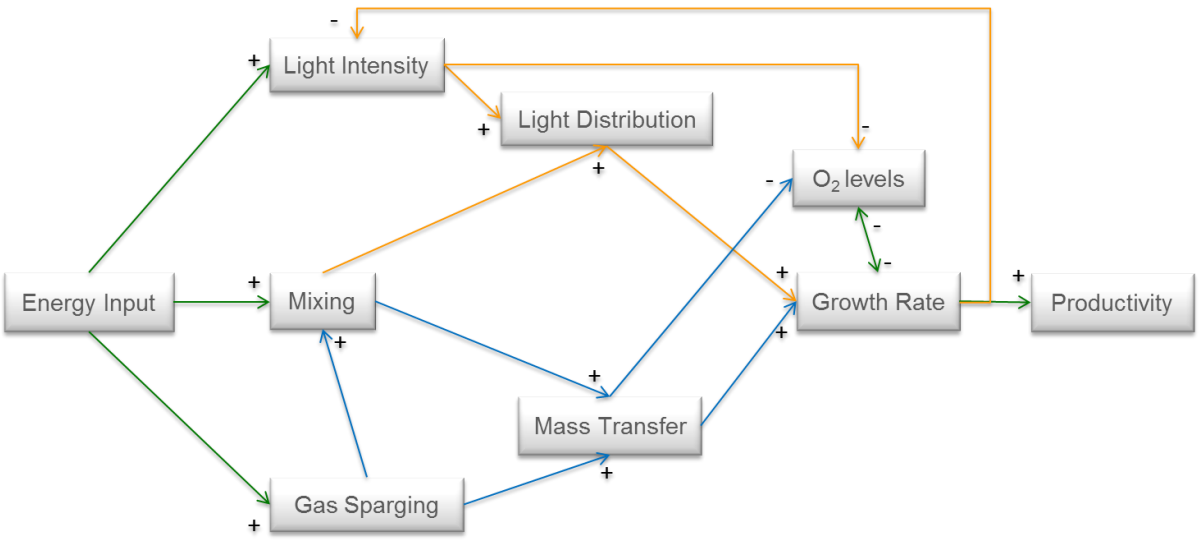

Figure 1.1 The link between energy input and parameters that are important for growth and productivities in algal PBRs. Commercial algal cultivation will be carried out under natural sunlight, and so energy for light intensity can be omitted.

1.3 Bioreactors: Mixing, mass transfer and power input

A bioreactor is a vessel used to cultivate microorganisms under conditions that enhance the production of a desired bio-product. A bioreactor requires energy for mixing, pumping, aerating, and temperature control. A variety of bioreactor configurations exist for providing the desired conditions to a biological system. Bioreactors can be divided into immobilized reactors (e.g. packed bed, membrane, biofilm) or suspended (submerged) reactors, which include stirred tank, bubble column, loop, airlift reactors and others (Moulijn et al., 2013).

1.3.1 Mixing

Mixing is a major contributor to energy consumption in bioreactor operation. Mixing is essential for the homogeneous distribution of cells, nutrients, light, gases, temperature and other factors, so that reactions can be carried out at similar rates and under similar conditions throughout a bioreactor. Limitations on transport of substrates throughout the reactor cause reductions in productivity, and so the success of a bioprocess could depend on the extent of mixing in the bioreactor (Ačai and Polakovič, 2007). Insufficient mixing results in local concentration gradients, which become more pronounced at large-scale (Ačai and Polakovič, 2007). The degree of mixing, mixing efficiencies and mixing patterns are often modelled mathematically for a better understanding of the micro-

environments and flows within a bioreactor (Ačai and Polakovič, 2007; Bouaifi and Roustan, 2001; Zahradník et al., 2001).

Hydrodynamics in a bioreactor, as well as the relationship between mixing and the transport of substances between phases (mass transfer), can be complex (Zahradník et al., 2001). Mixing time is a simple measurement for describing mixing (Regine Eibl et al., 2009; Gavrilescu and Tudose, 1997; Harvey et al., 2001; Ni et al., 2003). Mixing time is the time required to reach a specified degree of homogeneity after addition of a tracer (Hadjiev et al., 2006). Impellers, baffles, stirrers, shaking platforms, pumping and sparging (bubbling) contribute to mixing in bioreactors. It is important when studying the hydrodynamics to consider the shear stress imparted by the method of agitation, and the sensitivity of the process components (e.g. algal cells) to this stress (Pirouzi et al., 2014; Ranade et al., 1991). It is also important to consider the power input requirements. Higher power input for agitation leads to improved mixing, which in turn facilitates mass transfer in the reactor (Chisti and Jauregui-Haza, 2002; Regine Eibl et al., 2009; Harvey et al., 2001; Hewgill et al., 1993; Pirouzi et al., 2014). The energy consumed for liquid circulation and agitation is one of the major operational costs for bioreactors requiring aeration, and can be as high as 28% of the energy consumption for an algal production system (Ačai and Polakovič, 2007; Chisti, 2008a).

1.3.2 Mass transfer

Mass transfer is the net movement of a species in a mixture from one location to another, often across an interface between two phases (Henley et al., 2011). A key example of mass transfer in a bioreactor is the movement of O_2 or CO_2 from the gas phase, into solution, and from the liquid phase into microbial cells. In algal systems, adequate supply of CO_2 relies on efficient gas-liquid mass transfer. In other words, gas being supplied to the bioreactor must dissolve into solution where it is available for reaction or metabolism. Additionally, gas products, such as O_2, must be removed from reaction sites by mass transfer to prevent inhibition of the bioprocess.

Gas-liquid mass transfer can be represented adequately by the two-resistance theory where, at the interface between gas and liquid, there is a very thin gaseous layer adjacent to a very thin liquid layer (Figure 1.2). The bulk gas and liquid lie adjacent to these thin films and molecules of gas pass across the layers by diffusion into the bulk liquid. The thin films are stagnant areas where there is resistance to transfer, while the gas-liquid interface itself offers no resistance based on the

assumption that the two species at the interphase are in phase equilibrium. At steady state, the concentration gradient across the thin films is linear (Chisti, 2007b; Henley et al., 2011; Treybal, 1980; Whitman, 1962).

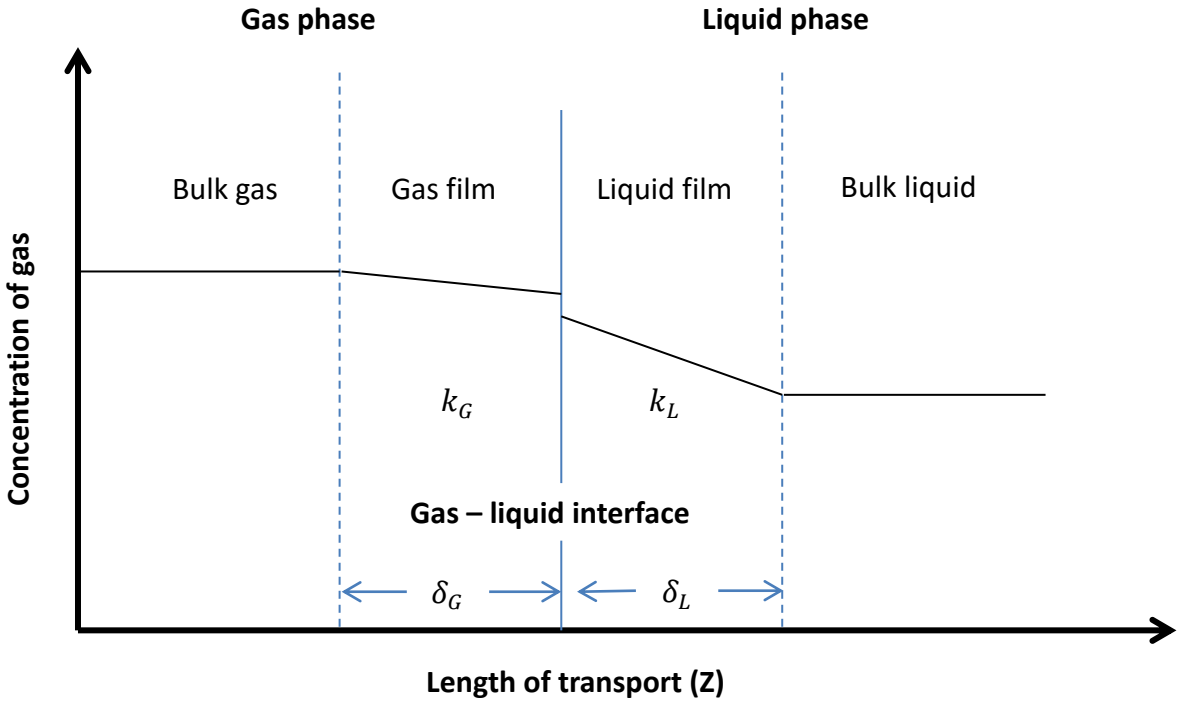

Figure 1.2 Steady-state dissolved gas concentration profile in the presence of a gas-liquid interface according to the two-resistance theory. Thin films of gas and liquid on either side of the interface have thicknesses labelled δ_G and δ_L, respectively. Gas and liquid film mass transfer coefficients are k_G and k_L, respectively, where their reciprocals represent resistance in the gas and liquid phase, respectively.

The transport of the gas into the liquid depends on the molecular diffusivity or diffusion coefficient, D, of the solute in the liquid. Gas transport into the liquid varies with temperature, liquid viscosity and the concentration of the solute (gas). The ratio of diffusivity and the film thickness, $\frac{D}{\delta}$, is known as the mass transfer coefficient, k. The transport flux or rate of transport per unit cross-sectional area (J)of a diffusing gas is dependent on the mass transfer coefficient and the concentration driving force of the gas, ΔC, according to Equation (1.1) (Bailey, 1986; Chisti, 2007b).

$$J = \frac{D}{\delta} \Delta C \tag{1.1}$$

According to the two-resistance theory, at steady-state the rate of transport of the diffusing gas is the same through the gas and liquid films as follows:

$$J = k_G(P_G - C_{Gi}) \tag{1.2}$$

$$= k_L(C_{Li} - C_L) \tag{1.3}$$

where k_G and k_L are the gas and liquid film mass transfer coefficients, respectively, P_G is the gas partial pressure in the bulk gas, C_L is the dissolved gas concentration in the bulk liquid, and i denotes the concentrations at the gas-liquid interface (Garcia-Ochoa and Gomez, 2009; Treybal, 1980).

Measurement of concentrations in the bulk phases can be determined experimentally. However, experimental detection of concentrations at the interface is impossible since these concentration differences occur over extremely small distances. Therefore, an overall effect, in terms of the bulk concentrations, can be determined by combining Equations (1.2) and (1.3). Since the interfacial concentrations (C_{L_i} and C_{G_i}) are in equilibrium because the interface offers no resistance to transfer, the overall transport rate can be written as follows:

$$J = K_L(C^* - C_L) \tag{1.4}$$

where K_L is the overall mass transfer coefficient based on the liquid film. C^* is the saturation concentration (the maximum possible value) of the diffusing gas in the bulk liquid, which for gases such as CO_2 and O_2 is related to P_G by the equilibrium relationship known as Henry's law:

$$P_G = HC^* \tag{1.5}$$

where H is Henry's constant in Pascals per molar concentration.

By substituting C^* in Equation (1.4) with P_G/H from Equation (1.5), solving Equations (1.2) and (1.3) for P_G and C_L, respectively, and subsequently substituting P_G and C_L into Equation (1.4) the mass transfer coefficients can be written as follows:

$$\frac{1}{K_L} = \frac{1}{k_L} + \frac{1}{Hk_G} \tag{1.6}$$

This shows that the overall mass transfer coefficient takes the form of addition of the liquid and gas resistances, as described in the name "two-resistance" theory. For sparingly soluble gases, such as oxygen (used for experimental determination of mass transfer in this work), H is much greater than unity. Additionally, k_G is usually larger than k_L because the gas phase diffusivities (D) are much

greater than those in liquids. Therefore, $\frac{1}{Hk_G}$ becomes negligible and Equation (1.6) can be simplified to

$$\frac{1}{K_L} \approx \frac{1}{k_L} \tag{1.7}$$

This means that the resistance to mass transfer on the gas side of the interface ($^1/_{k_G}$) is minor compared to that of the liquid film ($^1/_{k_L}$) and thus the overall mass transfer rate is said to be liquid-phase controlled.

Since the transport flux equals the rate of transport per unit gas-liquid interfacial area, Equation (1.4) can be expressed in terms of rate, as follows:

$$\frac{dC_L}{dt} = K_L a_L (C^* - C_L) \tag{1.8}$$

where C_L is the dissolved gas concentration at time t, and a_L is the gas-liquid interfacial area per unit volume of the liquid (Bailey, 1986; Chisti, 2007b, 1989; Henley et al., 2011; Treybal, 1980).

In the literature the mass transfer coefficient is often quoted to describe the mass transfer performance of a bioreactor. In light of Equation (1.7), the overall volumetric gas-liquid mass transfer coefficient, $K_L a_L$ is often expressed as $k_L a_L$ or $k_L a$ (Baird and Garstang, 1972; Chisti and Jauregui-Haza, 2002; Guo et al., 1997; Hewgill et al., 1993; Moutafchieva et al., 2013). The rate of supply of a soluble gas in a bioreactor can be determined if the $k_L a_L$ and the concentration driving force ($C^* - C_L$) are known (Bailey, 1986; Chisti, 2007b, 1989).

Sparging and agitation in bioreactors increases the gas-liquid interfacial area per unit volume and decreases the effective film thickness (δ), thus improving gas-liquid mass transfer. A review of the relationship between the mass transfer coefficient, $k_L a$ (h^{-1}) or mixing time, T_m (s), and the agitator power requirements (W m^{-3}) in a range of bioreactors reported in the literature is illustrated in Figure 1.3 (See Table A1 in Appendix A for detailed data and references). Mass transfer and mixing improve with increased power for agitation. From Figure 1.3A, it is seen that the reactors that use a combination of mechanical agitation and sparging (e.g. stirred-tank and pulsed baffled) exhibit higher $k_L a$ values, and the reactors that used sparging only (e.g. bubble columns and airlift) consumed less power.

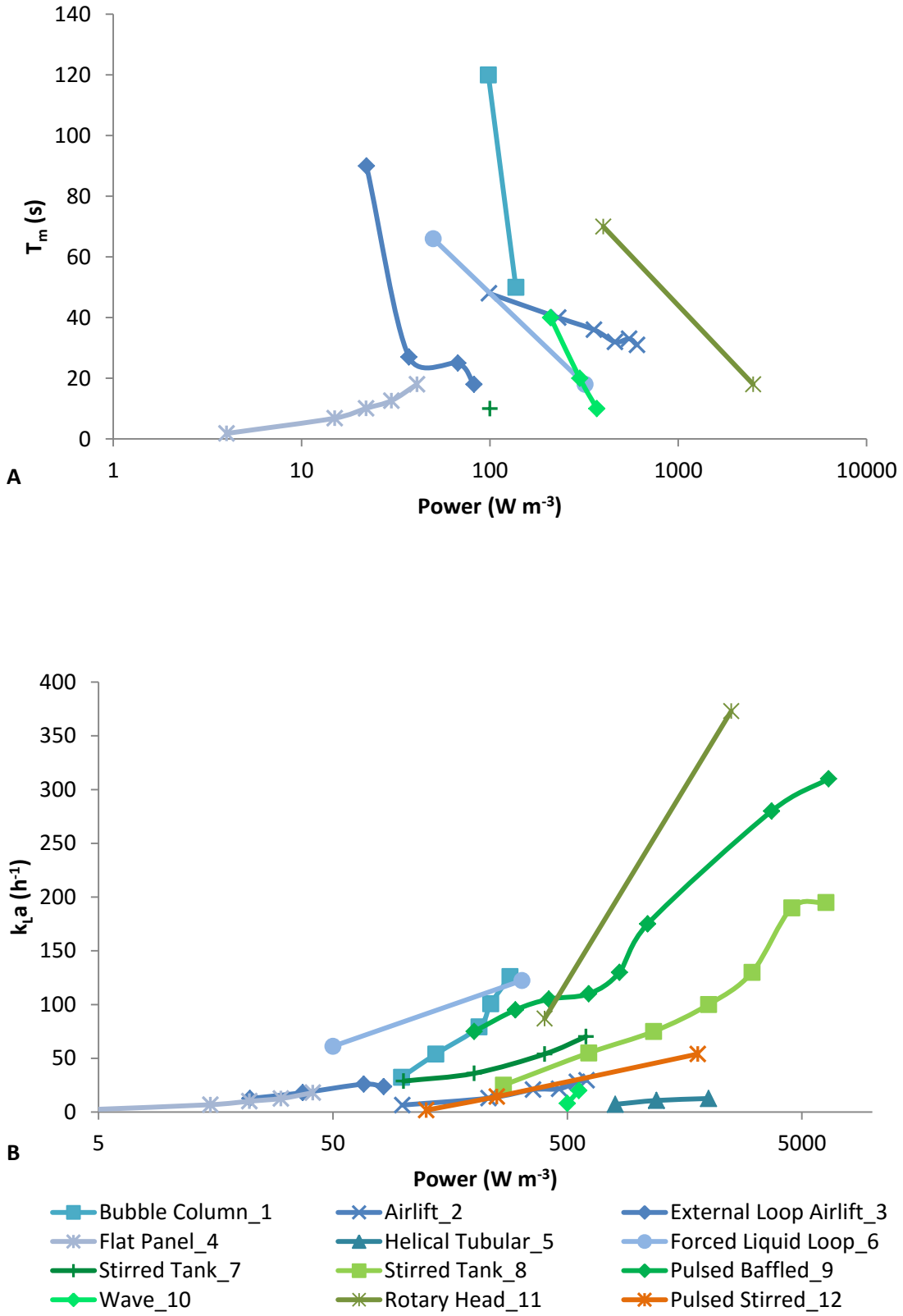

Figure 1.3 The relationship between A: mixing time (T_m, s) or B: mass transfer (k_La, h^{-1}) and power input per unit volume (W m^{-3}) for various reactor types, including sparged (blue), mechanically agitated with sparging (green), and mechanically agitated with surface aeration (orange). Numbers in series titles correspond to references according to Table A1 in Appendix A.

Figure 1.3 also includes a surface aerated reactor. Surface aeration occurs when gas moves from the headspace in a bioreactor into the liquid. The rate of surface aeration can be increased if there is sufficient renewal of the liquid surface by stirring or shaking. Surface aeration is not commonly seen in bioreactors and very rarely for algal cultivation. It may prove more energy efficient than sparging, if the correct configurations are applied (Regine Eibl et al., 2009; Eibl and Eibl, 2006; Lehmann et al., 2013).

1.4 Photobioreactors for microalgal cultivation

Currently the most prevalent large-scale algal cultivation system is the open pond or raceway. These have several drawbacks including contamination, exposure to weather, temperature fluctuations and evaporation. Closed photobioreactors (PBRs), on the other hand, provide protected environments for increased microalgal productivities, but require large amounts of energy for mixing, aeration and pumping (Chisti, 2007a; Slade and Bauen, 2013; Tredici, 2010). Other drawbacks of PBRs include high capital cost, oxygen build-up and they can be difficult to clean (Carvalho et al., 2006).

1.4.1 Open Ponds

The pioneers of mass algal cultivation in the 1950s used open pond systems which are still the most widely applied in commercial scale algal production because they are easy and cheap to construct (Carvalho et al., 2006; Pulz, 2001). Open ponds tend to have lower algal concentrations and productivities than other systems, hence the cost of harvesting large volumes of dilute biomass is high (Carvalho et al., 2006; Chisti, 2007a; Pulz, 2001). Open systems are also limited to cultivation of robust species that can withstand temperature fluctuations, exposure to weather and outcompete contaminants (Chisti, 2007a).

The most common type of open pond is the raceway, which consists of a closed loop circulation channel, typically oval, with mixing and circulation carried out by a paddlewheel. Baffles present in the flow channels are necessary for guiding the flow of liquid. Pond depths are kept low (15 to 40 cm) to allow light penetration (Hreiz, 2014).

In addition to contamination and evaporation, raceways have poor CO_2 utilization efficiency and mixing (Chisti, 2007a). In raceway ponds the paddlewheel provides pumping to develop a defined circulation through the pond. At the paddlewheel, mixing across the depth of the pond may be achieved, assisting the mass transfer of CO_2 from the surrounding air into solution. However, the mass transfer rates are low in comparison to other algal cultivation systems, and are one of the limiting factors of raceways (Brennan and Owende, 2010; Christenson and Sims, 2011; Mata et al., 2010). Mixing in raceways, particularly in areas away from the paddlewheel, is such that algae at the surface are exposed to higher light and CO_2 than the cells at the bottom of the pond (Brennan and Owende, 2010; Chisti, 2007a). Bubbling CO_2 into the ponds, via submerged aerators for example, increases this mass transfer and improves productivity (Brennan and Owende, 2010). However, with the low bubble residence time due to low liquid depth causes much of the CO_2 to be lost to the atmosphere (Christenson and Sims, 2011; Mata et al., 2010). Christenson and Sims (2011) suggest using gas-liquid contactors, similar to the rotating biological contactors used in wastewater treatment, to improve gas transfer rates.

1.4.2 Closed Photobioreactors

In light of the disadvantages of open ponds, closed PBRs have been developed. Column (airlift and bubble column), tubular (horizontal, helical and alpha-shaped) and flat-panel PBRs are the most reported designs, and various adaptions to these have been made (Carvalho et al., 2006; Lehr and Posten, 2009). Closed systems are less exposed to rain, wind and evaporation, and it is possible to provide more control over contamination compared to open ponds (Carvalho et al., 2006; Chisti, 2007a; Pulz, 2001). Mixing and gas-liquid mass transfer are superior in closed PBRs compared to open ponds, surface-area-to-volume ratios are lower, enhancing light provision, and algal productivities tend to be higher (Carvalho et al., 2006; Chisti, 2007a). However, shear stress is typically higher in these systems and the cost of construction and operation are often high (Carvalho et al., 2006; Pulz, 2001). The greater productivity in PBRs compared to open ponds has potential to reduce the cost per unit product (Chisti, 2007a). Also, PBRs are useful for cultivation of concentrated algal inoculum for large scale open ponds or in hybrid cultivation systems (Adesanya et al., 2014; Razon and Tan, 2011).

Airlift and bubble column PBRs are examples of column or vertical tubular reactors which are made from polyethylene or glass tubes to allow light to reach the algal cells. Compressed air is bubbled into the bottom of the tube, which enables simultaneous mixing of the culture and gas-liquid mass

transfer. In an airlift bioreactor there is a baffle separating the riser from the downcomer. The aerated liquid travels up the riser owing to lower average density. Following disengagement of the gas, the liquid then travels down the downcomer region (Carvalho et al., 2006; Kaewpintong et al., 2007; Lehr and Posten, 2009).

In a horizontal tubular PBR algal broth is circulated from a reservoir, or degassing column, through an array of transparent tubes, called the solar collector, where they are exposed to light before being transferred back to the reservoir. In outdoor facilities, the solar collector is orientated to optimise sunlight capture, and tubes are often placed parallel to each other, horizontal to the ground. Air is bubbled into the reservoir where an exhaust removes the accumulated oxygen (Chisti, 2007a). Tubes can also be placed in coiled, helical, or alpha-shaped arrays (Carvalho et al., 2006).

Flat-panel PBRs are of interest due to the even distribution of light as a result of the large surface-area to volume ratio (Carvalho et al., 2006; Zittelli et al., 2000). In dense algal cultures shadowing is minimised due to the short light path length. However, this may lead to heating and so temperature control is required for these PBRs (Carvalho et al., 2006; Rodolfi et al., 2009). Oxygen build up due to the high photosynthetic rates and small diameters is a disadvantage of panel PBRs (Carvalho et al., 2006). Horizontal circulation within a flat panel, and addition of alveolar plates or baffles can be used to increase turbulence and improve mixing and mass transfer (Carvalho et al., 2006; Lehr and Posten, 2009; Meiser et al., 2004; Richmond and Cheng-Wu, 2001; Zittelli et al., 2000).

Closed PBRs commonly use gas sparging to provide CO_2 (Brennan and Owende, 2010). Bubbles of gas are distributed in the liquid medium, resulting in both CO_2 mass transfer and liquid circulation (mixing). CO_2 losses from aeration are lower in closed PBRs compared to sparged open systems (Mata et al., 2010; Singh et al., 2011). However, the compression of gas for sparging is energy intensive; the feasibility of its use for large-scale algal production needs to be carefully assessed.

Improving reactor design for enhanced efficiency of mixing and gas-liquid mass transfer may reduce the energy requirement. For example, Degen et al. (2001) describe a flat-panel airlift PBR with multiple horizontal baffles which induce vortices to improve mixing and mass transfer. Iqbal et al. (1993) describe a V-shaped flat panel reactor with a very high mixing rate. Carvalho et al. (2006)

report the use of an open gas exchange unit at the bottom of a flat panel reactor for gas-liquid mass transfer. However, this increases risk of contamination. Carvalho et al. (2006) and Ferreira et al. (1998) describe membrane aeration in which CO_2 diffuses through a silicone or hollow-fibre membrane tubing. This prevents CO_2 losses that occur with bubbling, and also allows for accurate control of transfer rates and the use of pure CO_2 which would otherwise be damaging to the culture. However, large membrane surface areas are required which contribute to the cost of cultivation. High salt media, as used with marine algae, limit the diffusion across the membrane, and bacterial cells can foul the silicone membrane pores (Carvalho et al., 2006). A venturi aerator consists of a nozzle with a narrow throat. Water is circulated through the reactor via the venturi and the pressure difference in the nozzle causes air to be sucked in from the atmosphere to aerate the reactor (Jackson, 1964; Rodriguez et al., 2012). This results in good mass transfer and does not rely on delivery of compressed CO_2 from tanks. However, the venturi device has not been used for algal cultivation. Low atmospheric CO_2 concentrations and high shear rates may limit its applicability and require investigation.

To avoid the limitations of energy intensive CO_2 mass transfer, carbon can be supplied to algal cultures in the form of bicarbonate. Sea salts precipitate at high pH, so this method cannot be applied to marine algal species or species that cannot survive the highly alkaline conditions (Brennan and Owende, 2010; Chisti, 2013). Microalgae may also be grown heterotrophically, providing an organic source of carbon, such as glucose or acetate. Reports have shown very high biomass and lipid production with heterotrophic cultivation (Chisti, 2013; Rosenberg et al., 2008). However, organic carbon is costly and is derived from agricultural plants and so has implications on land and water usage. Further, the competition by heterotrophic bacteria and fungi in these systems is much greater. Agro-industrial waste could be used as a carbon source, but this is a limited resource for large-scale algal cultivation (Chisti, 2013).

1.5 Microalgal lipids and biodiesel

The looming energy crisis and global warming have sparked research into alternate sources of energy. A key candidate is energy derived from biological sources. A large portion of the research into microalgae has been focused on bio-energy. Microalgae are of particular interest as they are able to produce a range of bioenergy products, including biodiesel, algal oil, methane, hydrogen and

ethanol. Many algal species are rich in lipids (some with oil content up to 80% of their dry weight) which can be converted to biodiesel and used as a fossil-fuel replacement (Chisti, 2007a). After extraction of lipids, the algal biomass can be fermented to bioethanol, or fed into an anaerobic digester for methane production. Algae can be used to produce biohydrogen in a dark-fermentation (anaerobic) process where carbohydrates are converted to hydrogen. Algae subjected to pyrolysis and steam gasification produce a hydrogen-rich gas and bio-oil (Demirbas and Demirbas, 2010). Production of hydrogen from algae is costly and in early stages of research, and algae is one of many possible feedstocks for ethanol and methane production. The production of biodiesel from algae, however, is receiving much attention as algae are lipid-rich biological material, well suited for biodiesel production with many advantages over other sources (Demirbas and Demirbas, 2010). While biodiesel is increasingly not considered as the long term alternative for the automotive industry, it is highly advantageous as it can be implemented using the current infrastructure. In addition, it is the most promising renewable jet fuel for aviation (Louw et al., 2016).

1.5.1 Algal lipids

Lipids consist of a glycerol molecule attached via ester bonds to three fatty acids (tri-acyl glycerides, TAG's), or to two fatty acids and a phosphate (phospholipids) or carbohydrate (glycolipids). All cellular organisms produce fatty acids and lipids for their cell membranes and for signalling molecules. In some microorganisms, known as oleaginous species, the system of fatty acid and lipid biosynthesis is used for the overproduction of lipids which then serve as carbon and energy storage for the microbial cell (Griffiths and Harrison, 2009; Wynn and Ratledge, 2005). Oleaginous species accumulate lipids to more than 20% of their biomass and some species can accumulate lipids to 70% (Karatay and Dönmez, 2010; Kitcha and Cheirsilp, 2011). Among the oleaginous species are several strains of macro- and microalgae (Wynn and Ratledge, 2005). In a comparison of various marine and freshwater microalgal species, *Scenedesmus* sp. was found to have high lipid productivity (Griffiths and Harrison, 2009).

Lipid accumulation in oleaginous species is initiated by nutrient limitation or exhaustion, in the presence of excess carbon (Lin, 2011). Studies have shown that under nutrient stress, particularly under nitrogen limited conditions, microbial cells accumulate larger amounts of lipids (Bondioli et al., 2012; Griffiths et al., 2014a, 2014b; Lardon et al., 2009; Lin, 2011; Rodolfi et al., 2009). However, under these conditions algal growth rates will drop. This means that, although cells have higher lipid content, there will be fewer cells at the low growth rates thus limiting the total lipid concentration

produced by the culture (Griffiths et al., 2014a, 2014b). In order to obtain maximal lipid productivities the trade-off between cell growth and lipid content must be fully quantified. Griffiths et al. (2014a) demonstrated that there is an optimal nitrogen concentration at which biomass growth is not severely inhibited, and lipid production is high. Studies show that accumulation of lipid, as well as the fatty acid profile (and hence commercial application) are dependent on the choice of carbon source, pH and temperature (Fei *et al.*, 2011; Rupčić *et al.*, 1996).

Microalgal lipids can be used in a variety of applications, in addition to biodiesel, including biosurfactants, nutritional supplements, infant formula, aquaculture and pharmaceuticals (Harwood, 2009; Karatay and Dönmez, 2010; Kitcha and Cheirsilp, 2011; Mukherjee *et al.*, 2006). Compared to plant oils, using microalgae for oil production has several advantages in terms of cost and sustainability, including shorter production times, ease of scale-up, smaller land requirements, improved water efficiency and less dependence on season and climate (Chisti, 2007a; Griffiths and Harrison, 2009; Kitcha and Cheirsilp, 2011).

1.5.2 Algal biodiesel

Triacylglycerols (TAG) are storage lipids produced by algae in particularly high quantities during stress conditions. These are the most suitable lipids for conversion to biodiesel. Transesterification of TAG yields fatty acid methyl esters, or biodiesel. The transesterification reaction requires methanol (or an alternative alcohol) and a catalyst, producing biodiesel and glycerine. The heating value of biodiesel is 41 MJ kg^{-1}, compared to the 42.7 MJ kg^{-1} of petroleum diesel (Demirbas and Demirbas, 2010).

Algal biodiesel is considered a third generation biofuel, which has several advantages over first and second generation energy products. First generation biofuels are those produced from sugar, starch, vegetable oils and animal fats and thus rely on agricultural land and are often in direct competition with food sources. Second generation biofuels are those produced from non-food crops and agricultural waste. Their oil content is lower than in microalgae, availability of waste is limited, and crops require more land per unit of oil production compared to microalgae. Waste oil can be used to make biodiesel, but this is severely limited by available quantities (Demirbas and Demirbas, 2010).

Algae contain more lipids than crop sources, have much faster growth rates, can be cultivated on smaller areas of land, including marginal land, and do not impact food supplies or other agricultural products (Chisti, 2008a; Demirbas and Demirbas, 2010; Tredici, 2010). The areal yield of algal oil is estimated to be between 4.7 and 14 L m^{-2} $year^{-1}$ (Sheehan et al., 1998), compared to 0.54 (palm oil) (Mata et al., 2010), 0.19 (Jatropha), 0.12 (Rapeseed), 0.09 (sunflower) and 0.04 (soy) L m^{-2} $year^{-1}$ (Sazdanoff, 2006). The higher photoconversion efficiency of algae compared to plants means that algal biodiesel productivities are superior to those of terrestrial sources (Chisti, 2008b, 2007a). Algae can be grown in water that is not suitable for human consumption, and many algal species can be grown in salt water (Lehr and Posten, 2009; Mata et al., 2010; Tredici, 2010). Algae can also be used for the production of a variety of co-products which improves the economics and sustainability of an algal biodiesel process plant (Mata et al., 2010; Richardson, 2011).

Microalgal biodiesel has the potential to form part of the future energy landscape. It must first be assessed for feasibility and must be cost competitive with petroleum diesel and other biofuels. Two areas of concern for the feasibility of microalgal biodiesel are the supply of CO_2 and the process energy demand. Other major challenges include areal productivity, nutrient cost (phosphorous and nitrogen), water usage and biodiesel quality (dependent on fatty acid profile) (Louw et al., 2016).

Supplementary CO_2 for algal cultures is essential for commercial scale productivities. However, pure CO_2 can cost as much as 40 US$ per ton, contributing between 3 and 10% of overall running costs of algal production (Nagarajan et al., 2012; Richardson et al., 2014). Many studies consider industrial waste, such as flue gas, as a cheaper source of concentrated CO_2 (up to 20%) for algal cultivation (Brennan and Owende, 2010). The use of CO_2 emissions in algal culture may earn carbon credit. However, the drawbacks of using CO_2 from flue gases include location limitations, presence of potentially growth-limiting nitrogen and sulphur oxides, and limited industrial CO_2 point sources (Chisti, 2013; Pate et al., 2011). In light of these limitations, efficient mass transfer of the supplied CO_2 to the algal cells becomes vital to reduce CO_2 losses. However, even with effective mass transfer, the production of biodiesel from algae will be limited by CO_2 supply.

The availability of CO_2 from point sources seems to be a serious constraint and will limit the amount of fossil fuel replaced by algal biodiesel. As we aim to increase production of energy from renewable sources, CO_2 point sources such as coal burning power stations will decrease, further limiting CO_2

availability (Chisti, 2013). On the other hand, flue gas will become available from increasing numbers of other sources such as anaerobic digesters and bio-ethanol production plants (Takeshita, 2011). In an evaluation by Takeshita (2011), if all potential point sources of CO_2 are considered, the ratio of CO_2 required for algal biodiesel to available CO_2 emissions will be between 18.4 and 52.9 % in 2100, at biodiesel production accounting for 8 to 11 % of the global liquid fuel demand. Based on this information, algal biodiesel cannot replace all fossil based liquid fuels but can fill a niche market, such as aviation fuel, for which it is well suited. Aviation fuel consumption in the US in 2008 accounted for about 8% of the total liquid fuel consumption (Pate et al., 2011). Using conservative estimates of CO_2 availability at point sources from (Pate et al., 2011), 40 million litres of biodiesel can be produced from algae per year. This accounts for 2 – 3% of total liquid fuels but 45% of the aviation fuel demand. Algal biodiesel are superior to first generation biofuels for aviation fuel due to their high energy density and low freezing points (Brennan and Owende, 2010) .

Energy usage is another essential consideration for the feasible production of an energy product such as algal biodiesel. The energy used to cultivate algae and produce the biodiesel must be significantly lower than the energy that can be harnessed from the resulting biodiesel. If fossil fuel energy is used in the process, the environmental impacts of this must be weighed against the benefits of the resulting algal biodiesel. The cost of algal biodiesel will also be significantly affected by the energy input requirement for its production.

Following review of studies on algal biodiesel sustainability, major contributing factors to energy intensity were shown to include PBR, nutrient source, dewatering and biomass drying, and lipid extraction (Lam and Lee, 2012). Of these, the most energy intensive are the algal cultivation (for pumping, circulating and aerating) and biomass drying stages (Harun et al., 2010; Richardson, 2011; Slade and Bauen, 2013; Stephenson et al., 2010). Biomass drying can be avoided by choosing appropriate downstream processing methods (Griffiths et al., 2010; Lam and Lee, 2012), leaving energy intensity of algal cultivation as a problem yet to be solved.

Many studies have assessed the Net Energy Ratios (NERs) of algal production processes. NER is the ratio of the energy output to the energy input. Several of these studies indicate that raceway ponds have substantially lower energy requirements than tubular PBRs, the latter having a NER above 1 (more energy is being used to produce the algae than can be harvested from the biodiesel) (Lam and

Lee, 2012; Rawat et al., 2013; Slade and Bauen, 2013; Stephenson et al., 2010). Algal cultivation for energy products is not feasible unless the NER can be reduced. This may be possible by reducing the energy for mixing and CO_2 mass transfer in PBRs, while ensuring productivities that support a high NER.

1.6 Environmental impacts and Life Cycle Analysis

Development of bioprocesses has various social, economic and environmental impacts. In addition to assessing the feasibility and economics of a potential or existing process or product, there is a need to assess its environmental impacts and sustainability. Sustainable development has become a widely used term and will increasingly be considered in industrial, economic and political decisions (Gavrilescu and Chisti, 2005). It is understood that sustainable development aims to meet present needs without compromising the needs of future generations and to reconcile the economy, society and the environment (the three pillars of sustainability). One concept of sustainability states that sustainable development is only possible if the economy and society are viewed as entities within the carrying capacity of the supporting environments (Adams, 2006; Ott, 2003). If the three pillars of sustainability are considered separately then it becomes easy for economic and social sustainability to be more highly weighted than the environment, and it is important to remember that the "bottom line of sustainability is that the biosphere is limited" (Adams, 2006). Gavrilescu and Chisti (2005) explain that a challenge in the field of sustainability is to change the mind-set that prosperity is always at the cost of environmental degradation. With innovation and rigorous assessment it is possible that technological, economic and social development can continue within the bounds of our environmental constraints.

Life Cycle Analysis (LCA) is the most widely used and accepted method for assessing the environmental burdens associated with a product, process or service (Chen and Patel, 2012; Clarens et al., 2010; Harding et al., 2008; Lardon et al., 2009; Richardson, 2011; Stephenson et al., 2010). It includes a complete inventory of material and energy flows, and the environmental impact of these through impact categories. An advantage of LCA is that it includes the entire life cycle from raw materials to product, including the processing of waste and product disposal. LCA has been standardised by the International Standards Organisation (ISO) in the ISO-14040 series (International Standards Organisation, 2006). In the context of sustainability, LCA is usually associated with

assessment of environmental impacts only. For assessment of economic and social considerations Life Cycle Cost Analysis (LCCA) and Social LCA (SLCA) are used (Campbell et al., 2011; Čuček et al., 2012; Jørgensen et al., 2007; Nguyen et al., 2008). Energy balancing, including measurement of NERs, is also a commonly used method for assessing sustainability. This method can form part of an LCA, or can be used without the completion of a detailed LCA. Energy balancing is a particularly useful tool for assessing the feasibility of energy products, such as biofuels (Jorquera et al., 2010; Ruggeri et al., 2010; Stephenson et al., 2010).

Risk Assessment, Environmental Impact Assessment, Environmental Auditing, Ecological Footprint, Environmental Sustainability Index, Product Material Flow Analysis, Process Energy Analysis and Design for Environment are other methods used in sustainability assessments (Čuček et al., 2012; Finnveden, 2000; Hertwich et al., 1997; Ness et al., 2007). Čuček et al. (2012) review indices relating to environmental, social and economic footprints, including definitions and methods for measuring carbon footprint and energy footprint. In an extensive review of sustainability assessment methods Singh et al. (2009) categorises indices across a wide range applications, including product-based sustainability indices and environmental indices used in industry (often used in LCAs). Environmental assessment using LCA is recognised as the most suitable for product-based assessments, such as assessments for biofuels and bioproducts (Ness et al., 2007; Singh et al., 2009). Additionally, the methodology and indices used in LCA have been clearly defined, and there is a wide literature base of LCAs from which comparisons can be drawn (Chen and Patel, 2012; International Standards Organisation, 2006; Richardson, 2011; Ruggeri et al., 2010).

Despite the advantages of LCA and its appropriateness for assessing the environmental impacts of a bioprocess, there are a number of limitations to the method. For example, LCA does not usually include the number of products used in society, rather describes environmental impacts based on a given quantity (the functional unit) (Finnveden, 2000). Also, there is often a lack of reproducibility and disagreement between LCAs of comparative products, due to the complexity of an LCA. Differences in the choice of functional unit, scope of impacts, inventory collation, methodology and other factors affect the LCA results ad comparability (Bicalho et al., 2012; Finnveden, 2000; Reap et al., 2008). Also, LCAs are generally based on simulated models, with uncertainty when translated into real world scenarios (Finnveden, 2000; Guldbrandsson and Bergmark, 2012). However, to assess the sustainability of a product, it is usually necessary to consider its entire life-cycle, and so

LCA is an essential tool (Finnveden, 2000). Additionally, with the availability of comprehensive databases that improve regularly, LCAs provide inclusive descriptions of environmental burdens that can be globally appropriate or region-specific. Although LCAs do not always provide the type of comparable data from which decisions can be directly made, they are most useful for highlighting aspects or areas in a production process that require attention in terms of sustainability and possibilities for reduced burdens (Finnveden, 2000). Efforts continue to improve the applicability and reproducibility of LCAs by standardising methods and structuring definitions for functional units and scope (Cluzel et al., 2013; Guldbrandsson and Bergmark, 2012).

The LCAs performed on algal bioprocesses to date are predominantly for algal biodiesel. Although microalgae and algal lipids are used for a variety of commercial applications, the significance of finding a sustainable energy source drives the demand for life cycle analyses for algal biodiesel. A review of algal biodiesel LCAs is presented in Chapter 7.1.

Greenhouse gas emissions, global warming potential and abiotic (fossil-based) depletion are important and frequently documented categories in life cycle analyses on algal biodiesel (Azadi et al., 2014; Campbell et al., 2011; Sander and Murthy, 2010; Stephenson et al., 2010). They are strong indicators for the feasibility of replacing fossil derived fuel with algal fuel, and the environmental impacts of algal fuel in comparison to other biofuels. For example, the energy used for algal production will contribute to abiotic depletion and greenhouse gas emissions, depending on the source of energy. In South Africa, most electricity comes from coal-fired power stations, having considerable greenhouse gas emissions. It is important for the burdens associated with electricity consumption for algal biodiesel production to be outweighed by the reduced emissions when the biodiesel replaces liquid fossil fuel.

The nutrients required for algal cultivation, particularly nitrogen and phosphorous, also play a major role in the burdens associated with biodiesel production. In several LCAs nitrogen and phosphorous inputs have been reported to have significant effects on the global warming potential and abiotic depletion (Azadi et al., 2014; Collet et al., 2014; Lardon et al., 2009; Stephenson et al., 2010; Yang et al., 2011). This is due the large quantities of these fertilizers that must be produced and transported to the algal cultivation facility. In addition to the energy-associated burdens with these nutrients, their release affects the surrounding environment. Eutrophication and acidification potentials are

impact categories commonly discussed in LCAs of biodiesel (Clarens et al., 2010; Resurreccion et al., 2012). Eutrophication occurs when nitrogen or phosphate based fertilizers are released into the environment, changing the natural concentrations of nutrients in surrounding rivers and lakes which threatens the ecosystems. Acidification occurs when sulphur and nitrogen oxides (air pollutants) transform into their respective acids, lowering the pH of rainwater and causing damage to soil, aquatic ecosystems and to buildings.

Another major concern regarding large-scale algal cultivation is the water footprint. Large volumes of water are required to fill the PBRs and to replenish after evaporation. Fresh water has become a scarce commodity, and overuse has serious environmental and social sustainability issues. Inclusion of a water footprint analysis in biodiesel LCAs is less common than energy and nutrient-related burdens, because reports usually opt for a salt-water or wastewater usage which reduces the water requirement by as much as 90% (Clarens et al., 2010; Subhadra and Edwards, 2011; Yang et al., 2011). Also, for a bioenergy product, the LCAs usually focus on energy balances and global warming impacts to motivate for the feasibility of the bioenergy product.

1.7 Areas highlighted for further study

Review of the literature, as discussed in the sections above, revealed that although microalgae have potential as sources of bioproducts, there are key areas in algal bioprocessing where further improvement is required. The key issues highlighted for the context of this work are as follows:

1. Cultivation of microalgae accounts for a significant portion of the environmental burdens of microalgal bioprocesses.
2. Photobioreactors have significant power requirements for mixing and mass transfer which lead to high running cost and environmental burdens.
3. Sparging is a commonly used, but energy intensive method for mixing and mass transfer.
4. In algal biodiesel production the energy input for algal cultivation is currently one of the factors limiting its feasibility and reducing its NER.
5. Substantial energy consumption leads to increased fossil fuel requirement, global warming impact and cost of a bioprocess.

The issues listed above formed the basis and reasoning behind this work, from which the aims and objectives, key questions and hypotheses were formulated. In light of these areas highlighted by the literature review, it follows that further innovation for improving mixing and mass transfer efficiency in algal cultivation systems would benefit the feasibility of large-scale algal bioprocesses. In this work we propose the use of surface aeration as an alternative to sparging in PBRs with the aim of reducing the power requirements associated with compressed gas, and improving mixing and mass transfer rates. A wave bioreactor (WR) and an oscillatory baffled reactor (OBR), described in Chapter 2.3, were chosen as surface aerated reactors, novel to algal cultivation. These were compared with a conventional airlift bioreactor (ALR). We investigated these PBRs for cultivation of *Scenedesmus* sp., a high lipid producing species of freshwater microalgae. Lipids can be used for a range of products including biodiesel, as discussed in Section 1.5.1, and so lipid production was monitored in addition to algal growth. Reductions in the power requirements associated with mixing and mass transfer were incorporated into a simulated biodiesel production process as an example of improvements that can be made toward sustainable algal bioprocesses.

1.8 Aims and objectives

The following aims and objectives have been addressed through the study:

1. This work aimed to identify surface aerated PBRs that can produce mass transfer coefficients ($k_L a$) and mixing times (T_m) equivalent to sparged reactors at lower power requirements. This aim was accomplished by completing the following objectives:

    a. Investigating the relationship between power input, T_m and $k_L a$ in airlift reactors (ALR) as the base case, at different aeration rates.

    b. Comparing this to the same parameters in wave (WR) and oscillatory baffled (OBR) reactors, at varying agitation rates.

2. A second aim was to define the $k_L a$ at which algal growth and productivity becomes limited, so as not to spend excess energy on mixing and aeration. This aim was accomplished by completing the following objectives:
    a. Cultivating *Scenedesmus* sp. in each PBR (ALR, OBR and WR) at varying $k_L a$ and T_m.
    b. Comparing biomass and lipid productivities across the PBRs at given $k_L a$ and T_m.
    c. Calculating energy efficiency (biomass and lipid productivity per unit power) and Net Energy Ratios (NER) for biomass and lipid production in each PBR.

3. The third aim was to conduct a life cycle analysis of an algal biodiesel production process, substituting the airlift and wave PBRs in the cultivation stage of the process, in order to address process feasibility and key operations for improved feasibility. This aim was carried out by completing the following objectives:
    a. Incorporation of the ALR and WR in a simulated algal biodiesel flow-sheet model.
    b. Identification of areas with the highest environmental burdens, particularly with those associated with energy demand.
    c. Comparison of environmental impacts when changes to the reactor stage of the process are made.

1.9 Hypotheses

Three hypotheses are put forward to address the above aims and objectives:

1. Surface aeration in the wave and oscillatory baffled photobioreactors results in mass transfer that supports algal growth at lower energy consumption than conventional sparging (airlift photobioreactor).
2. A critical minimum power input for mixing and mass transfer exists below which algal growth and lipid productivity is significantly reduced and above which completing limitations may control productivity.
3. Reduced energy consumption for mixing and mass transfer in algal photobioreactors leads to reduced environmental burdens in an algal biodiesel production process.

1.10 Key Questions

- What are the power input, $k_L a$ and T_m ranges of a sparged bioreactor (ALR), and two surface aerated bioreactors (OBR and WR)?
- What are the lower limits of $k_L a$ and T_m for acceptable biomass and lipid productivities in each PBR (ALR, OBR and WR)?
- What mixing and aeration rates are required for comparable $k_L a$, T_m and productivities (biomass and lipid) in each PBR?
- How do the power input, $k_L a$ and T_m compare across the sparged (ALR) and surface aerated (OBR and WR) bioreactors?
- How do energy efficiency (productivity per unit power) and net energy ratios (for biomass and lipid) compare across the sparged (ALR) and surface aerated (OBR and WR) bioreactors?
- Do the novel strategies for mixing and mass transfer in algal PBRs translate to altered environmental burdens of a simulated bioprocess?

1.11 Thesis overview

In answering the key questions stated above, the materials and methods presented in Chapter 2 were used. This chapter describes methods common to all sections of this thesis. Section-specific methods are described in their corresponding chapters.

In addressing the aims and objectives of this work, the results were divided into five sections. The first results are presented in Chapters 3, 4 and 5, in which investigations of the ALR, OBR and WR, respectively, are described. The aim in these chapters was to find the mixing and mass transfer rates with the highest energy efficiency with respect to algal productivity in each biroeactor. These chapters include design and optimisation of the three PBRs for algal cultivation and lipid production.

In Chapter 6 the mixing, mass transfer, power input, biomass and lipid productivity are compared across the three PBRs operated under the most appropriate conditions determined in Chapters 3 to 5. This chapter also investigates the differences in net energy ratios across the three reactors and the implications of this for algal bioprocesses.

Chapter 7 describes a simulated algal biodiesel production process and life cycle analysis of the process. The environmental burdens for three scenarios are compared, where the bioreactor stage

of the simulated process is altered: ALR at high gas velocity at 2 bar inlet gas pressure, ALR at optimised gas velocity and 2 bar inlet pressure, and WR at optimised agitation rate.

Finally, in Chapter 8, the hypotheses of the work are examined in light of the results presented and the final conclusions and future recommendations are made.

2 Materials and Methods

2.1 Introduction

This chapter describes the microorganisms, media, culture conditions, reactor design, analytical methods and calculations used in this research. Further details on specific experiments are described in the subsequent chapters.

2.2 Microalgae cultivation and maintenance

A species of *Scenedesmus* was isolated from Upington, South Africa. Long-term stock cultures were maintained in 200 mL glass bottles, grown in 3N Bold's Basal Medium (BBM) (Bold, 1949), sparged with filtered (0.45 µm syringe filter, Membrane Solutions) air and illuminated by two cool white 18 W fluorescent bulbs (120 µmol m^{-2} s^{-1}) (Osram).

Short-term stock cultures were prepared by inoculating the long-term stock culture into 500 mL 3N BBM growth media in glass bottles to an optical density at 750 nm of 0.1 (OD 750 = 0.1). These were maintained in the same way as the long-term stock culture for a period of 7 to 10 days before inoculation into PBRs.

An adapted BBM, containing 150 mg L^{-1} NO_3 for increased lipid content, was used for cultivation in PBRs, based on results from nitrate optimisation in Chapter 3.3.1. *Scenedesmus* sp. from 500 mL stock cultures was inoculated into PBRs to an OD of 0.1 at 750 nm (approximately 0.05 g L^{-1}).

The 3N BBM medium was composed of the nutrients listed in Table 2.1.

Table 2.1 Composition of 3N BBM medium for algal cultivation, where 6 mL L^{-1} of PIV metal solution was added, which was composed of the metals in the lower section of the table.

Nutrient Component	Concentration (g L^{-1})
$NaNO_3$	0.750
$CaCl_2.3H_2O$	0.025
$MgSO_4.7H_2O$	0.075
$K_2HPO_4.3H_2O$	0.075
KH_2PO_4	0.175
NaCl	0.025
PIV metal solution:	**6 mL L^{-1}**
Na_2EDTA	0.750
$FeCl_3.6H_2O$	0.097
$MnCl_2.4H_2O$	0.041
$ZnCl_2$	0.005
$CoCl_2.6H_2O$	0.002
$Na_2MoO_4.2H_2O$	0.004

2.3 Reactor design and operation

2.3.1 Airlift photobioreactor

Airlift photobioreactors (ALR) (Figure 2.1 and Figure 2.2) consisted of a glass cylinder (600 mm height; 100 mm external diameter), with a working volume of 3.2 L, containing an inner glass column or draft tube (475 mm height; 50 mm external diameter) to separate the riser (inner tube) and downcomer regions (outer annulus) (Langley et al., 2012). Airlifts were sparged with CO_2 enriched air through a 2 µm stainless steel HPLC inlet filter at the base of the draft tube. Desired flowrates of air and CO_2 were controlled by a Brookes 5850S Thermal Mass Flow Controller and the two gas streams sent through an inline mixer and fed at a desired flowrate to the ALRs. Constant light was provided using cool white 18 W fluorescent bulbs (Osram) placed behind each airlift column (Section 2.3.4). All reactors and media were sterilized by autoclaving prior to use. Approximately 100 mL of sterile, distilled water was added daily to replace that lost by evaporation. To reduce foaming, 20 µL of antifoam (Merck) was added.

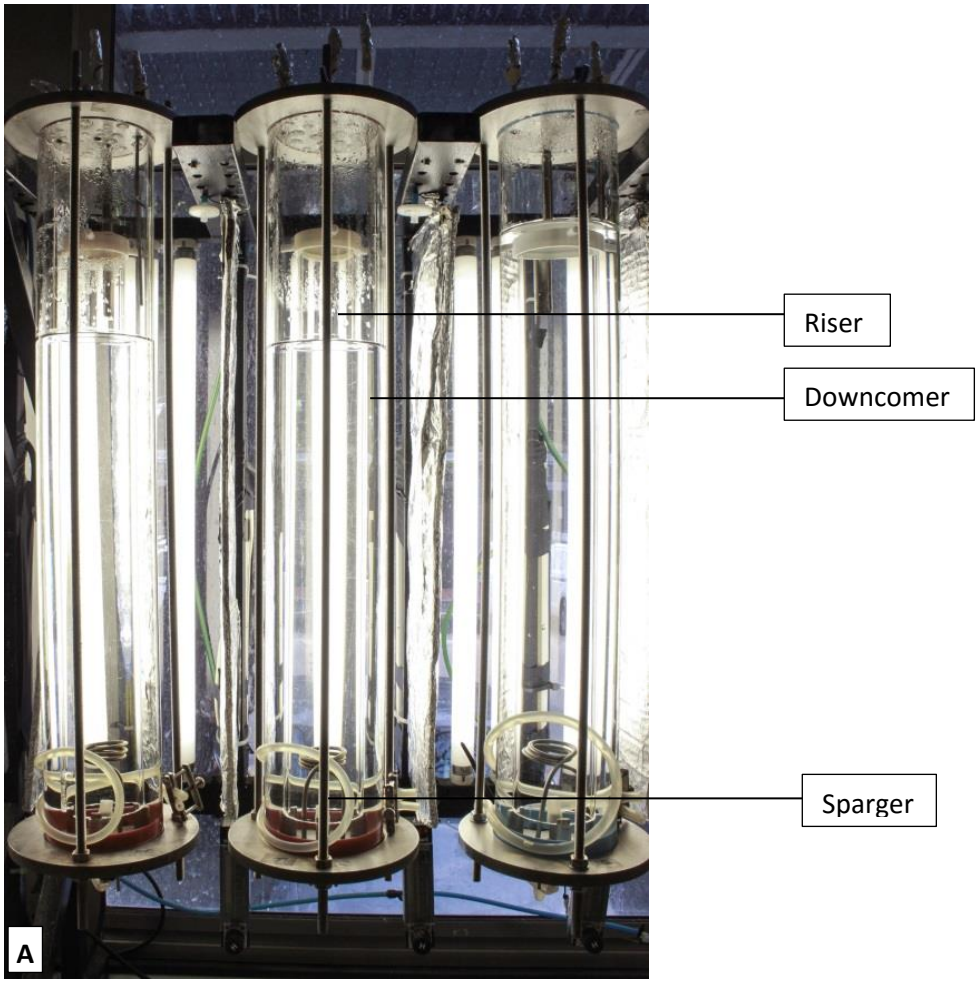

Figure 2.1 Photographs of airlift photobioreactors.

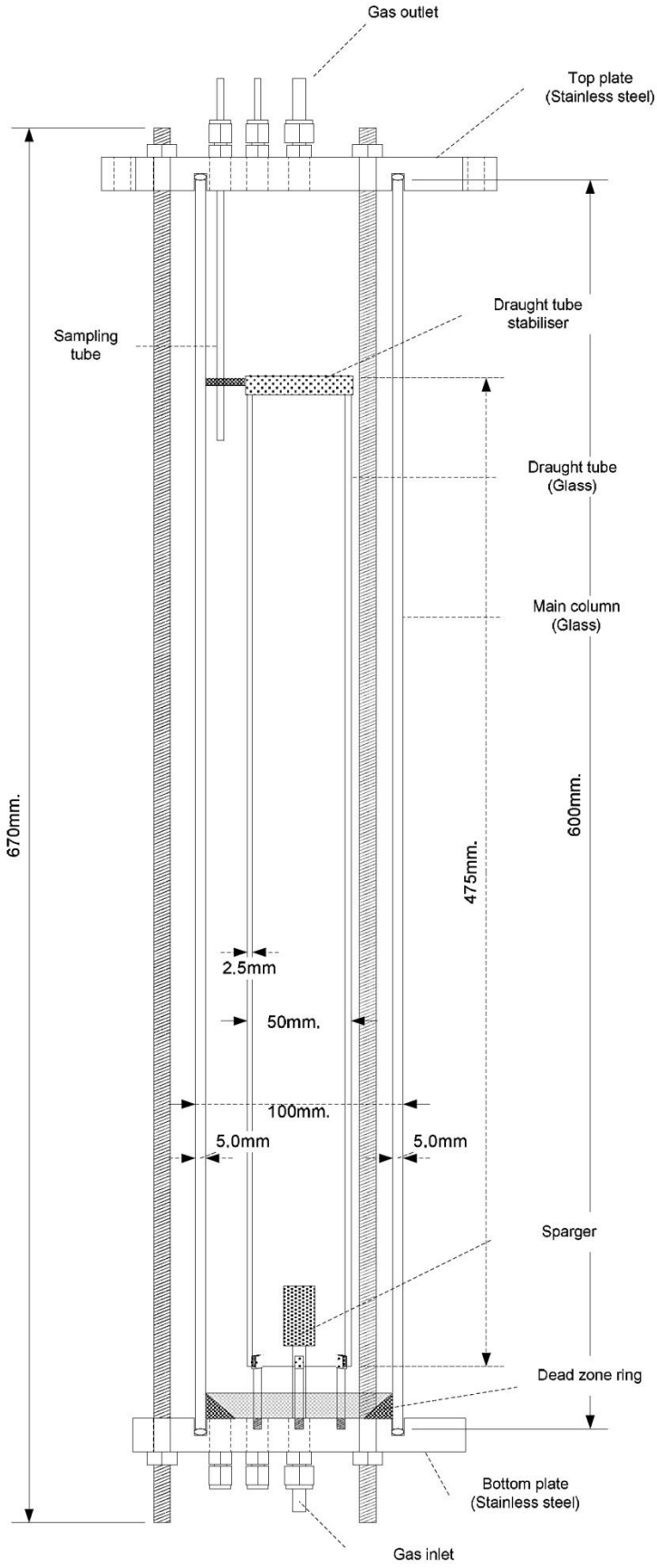

Figure 2.2 Diagram of airlift photobioreactor (Langley, 2010).

2.3.2 Oscillatory baffled photobioreactor

An oscillatory baffled PBR (OBR) was designed based on previously described oscillatory baffled and oscillatory flow columns (Ni et al., 1998; Stonestreet and Harvey, 2002), and adapted for unsparged algal cultivation. The OBR consisted of a 600 mm glass column, 100 mm in diameter and with 5 mm thick walls, supported by three steel rods and a square plate at each end of the column (Figure 2.3 and Figure 2.4). The horizontal column was attached to a 0.18 kW 380 V 4P B14 VF44A/V motor with a gear ratio of 46:1 (Bonfiglioli South Africa (Pty) Ltd). A piston connected the motor to baffles located inside the glass column. The rotation of the motor caused the piston to move the baffles back and forth inside the column. A 0.18 kW 220 V inverter (Bonfiglioli South Africa (Pty) Ltd) allowed variation in the motor speed, and thus the oscillating frequency. The working volume of the reactor was 2 L, so that the liquid height (45 mm) was just above half of the reactor diameter, leaving a headspace of gas in the upper portion of the column.

The following three baffle configurations were tested, results presented in Chapter 4:

1. Donut baffles: four donut baffles, 90 mm in diameter, with a 30 mm baffle free area, made from 3 mm thick Teflon, and spaced 140 mm apart.

2. Half-moon baffles: six half-moon baffles, 90 mm in diameter, 45 mm height, made from 7 mm thick polypropylene, and spaced 78 mm apart.

3. Perforated half-moon: six half-moon baffles as above, four of which contain 9 holes, 10 mm in diameter and spaced 10 mm apart. The two outer baffles contained no holes.

Air enriched with 1% CO_2 filled the headspace and was continuously replenished at 0.2 L min^{-1}. Flowrates of air and CO_2 were controlled by a Brookes 5850S Thermal Mass Flow Controller and the two gas streams sent through an inline mixer before reaching the gas inlet port. A gas outlet was left open to allow replacement of the gas headspace. Constant light was provided using three cool white 18 W fluorescent bulbs (Osram) placed above the column (Section 2.3.4). The reactor was sterilized prior to use by washing with 20 ppm chlorine dioxide followed by sterile, distilled water.

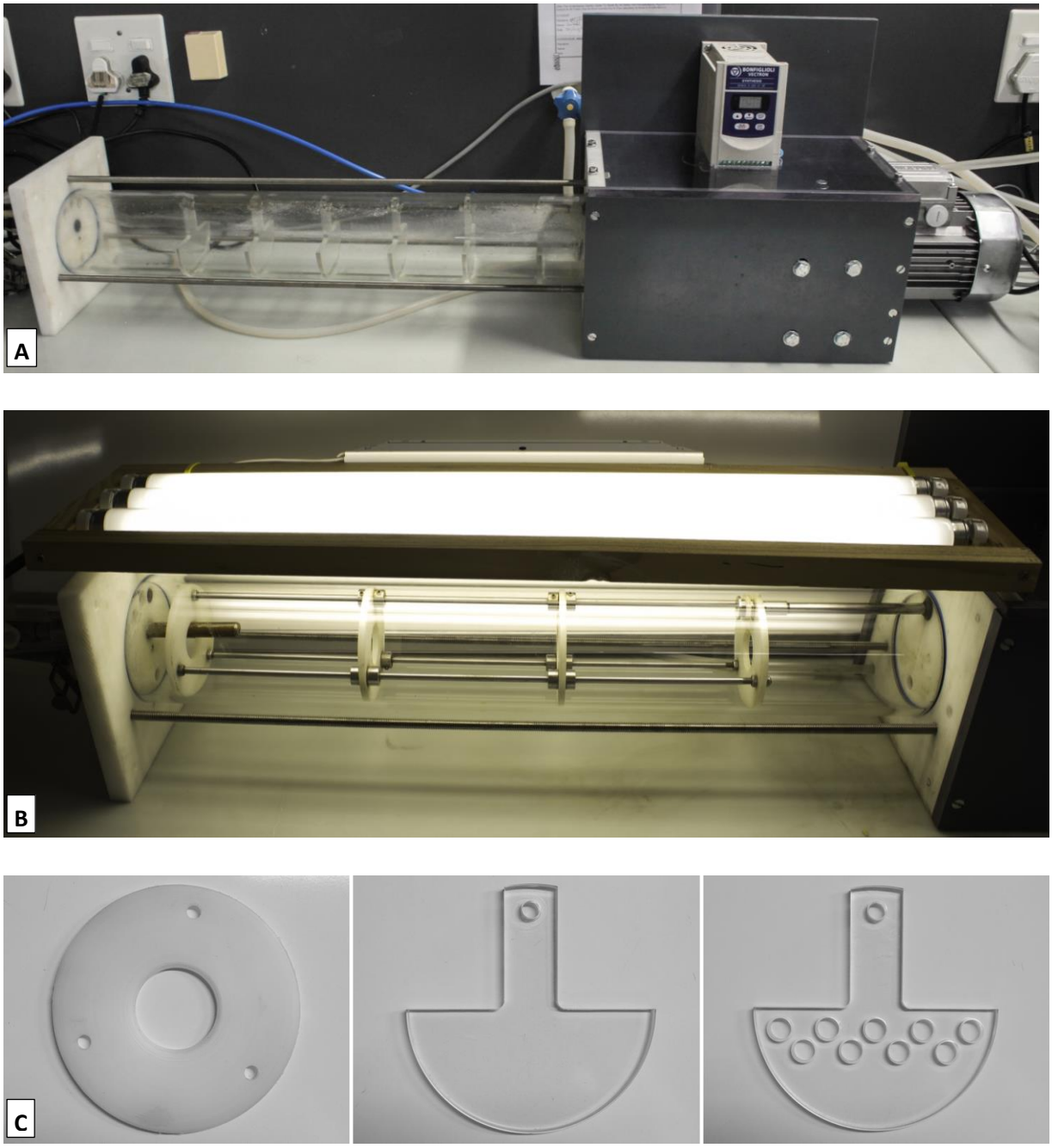

Figure 2.3 Photographs of the oscillatory baffled photobioreactor with (A) motor and inverter, (B) fluorescent lights and (C) three baffle types: donut, half-moon and perforated half-moon (from left to right, respectively).

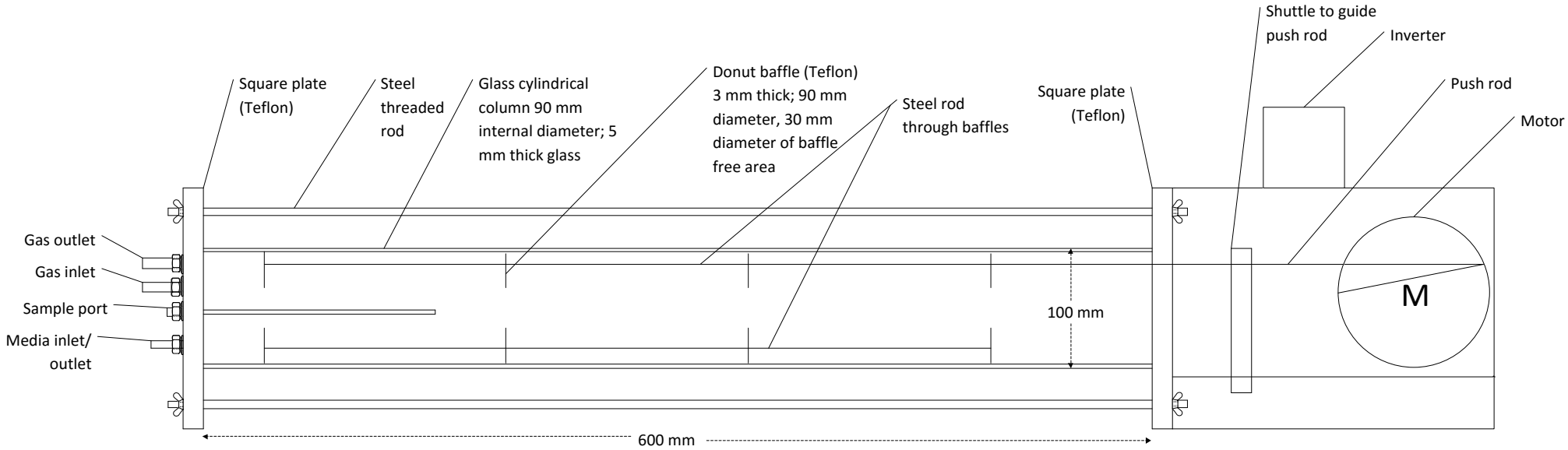

Figure 2.4 Diagram of oscillatory baffled photobioreactor.

2.3.3 Wave photobioreactor

The wave photobioreactor (WR) consisted of a WAVE Bioreactor® 20/50 (GE Healthcare) with a 10 L CellBag® (part no. CB0010L10-13). This unit consists of a rocking platform supported by a base unit (Figure 2.5 and Figure 2.6). The EVA/LDPE (ethylene-vinylacetate and low density polyethylene copolymers) cellbag, placed on top of the rocking platform, contained gas inlet and outlet, sampling, inoculation and probe ports. The cellbag (liquid working volume 2 L) was inflated with 1% CO_2 enriched air; the headspace was continuously replenished at 0.2 L min^{-1}. Flowrates of air and CO_2 were controlled by a Brookes 5850S Thermal Mass Flow Controller and the two gas streams were sent through an inline mixer before reaching the gas inlet port. A gas outlet was open to the atmosphere. The rocking speed and rocking angle were adjusted according to the experimental requirements, in the ranges 10 to 40 rpm and 2 to 10 degrees, respectively. A bank of lights was built above the wave PBR consisting of eight cool white 18 W fluorescent bulbs (Osram) to provide constant light (Section 2.3.4). The reactor was sterilized prior to use by washing with 20 ppm chlorine dioxide followed by sterile, distilled water.

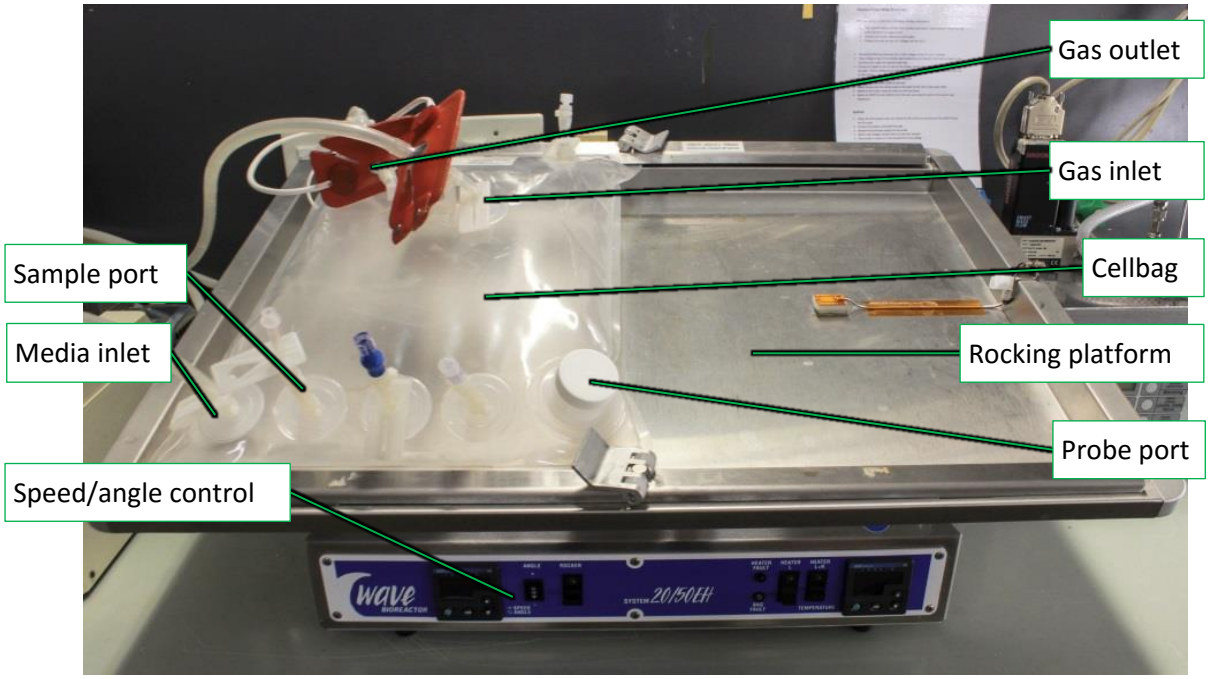

Figure 2.5 Photograph of wave photobioreactor with 10 L cellbag (2 L liquid volume).

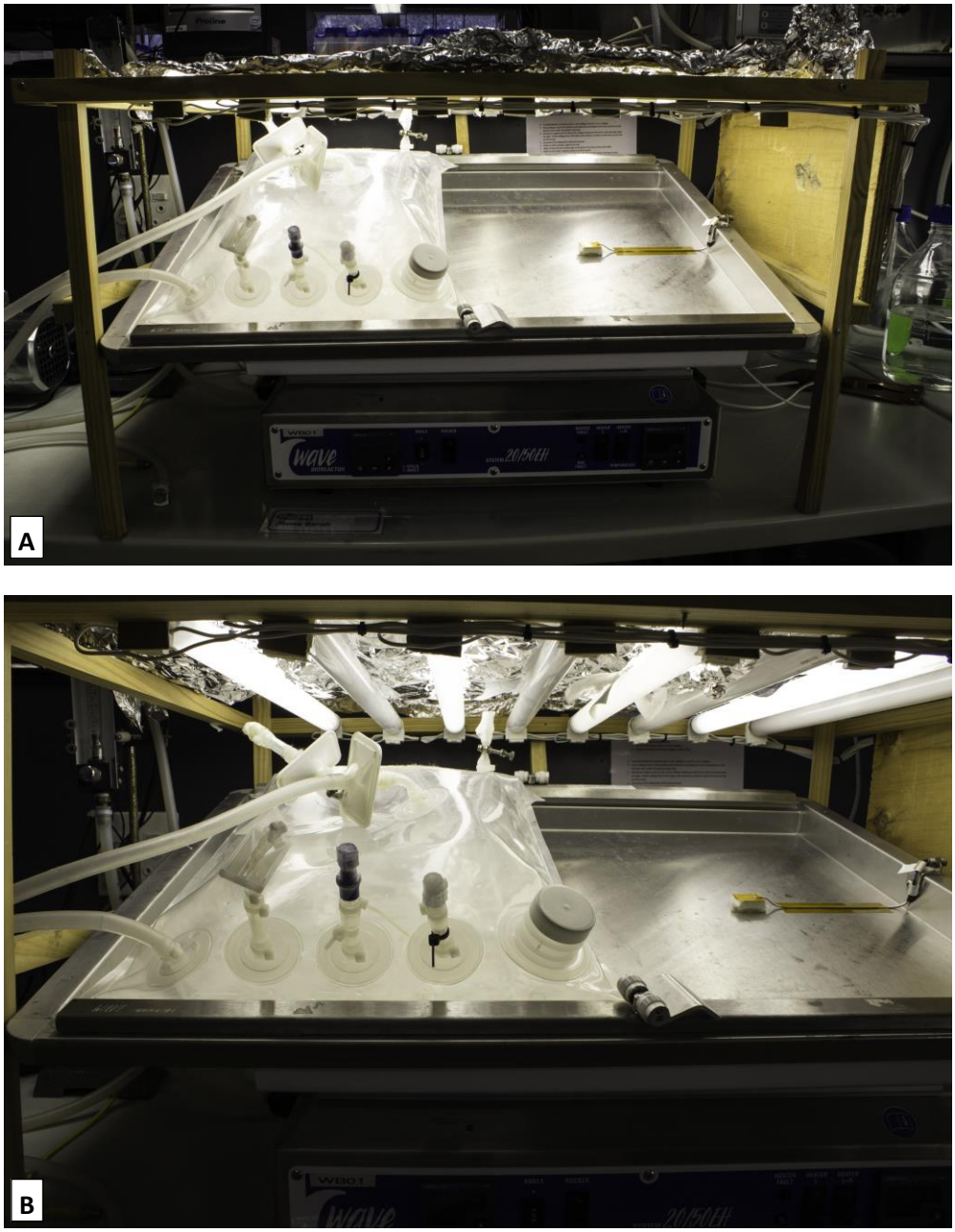

Figure 2.6 Photographs of the wave photobioreactor housed in the frame supporting the fluorescent lights.

2.3.4 Light provision

In order to compare the effects of mixing and mass transfer on algal cultivation and lipid production across the three PBRs, it was necessary to provide equivalent light to each. The light intensity to each PBR was measured at a number of points in a grid across the area of each reactor using a light meter (LI-250 photometer, Li-Cor, USA). The values at each point in the grid were averaged to give the average light intensity reaching the reactor. The readings were taken close to the light source

and at the surface of the reactor furthest from the light sources (i.e. through the airlift or oscillatory glass column, or underneath the wave cellbag).

For the ALRs, light was provided at 200 – 300 µmol m^{-2} s^{-1} at the reactor surface closest to the lights, resulting in 180 µmol m^{-2} s^{-1} measured at the central region of the reactor surface furthest from the lights (through the glass column). At the top and bottom ends of the ALRs the light intensity from the fluorescent bulbs was lower (98 - 100 µmol m^{-2} s^{-1}). This resulted in an average light intensity across the height of the ALRs of 148 µmol m^{-2} s^{-1} (Table 2.2). The averaged light intensities of the OBR and WR at the surface furthest from the light source are also shown in Table 2.2.

The total amount of light reaching each PBR was then calculated based on the surface area of the reactor exposed to light (not taking into account the light deflected due to the curve of the reactor surface). The surface area of the ALR and OBR reactors were the same, and so at equal light intensity (148 – 150 µmol m^{-2} s^{-1}), these reactors received the same amount of total light. A section of the wave cellbag was covered with tinfoil to reduce the surface area exposed to light so that the total light matched that of the ALR and OBR reactors. For the ALR and WR a second set of fluorescent bulbs were available for studies at double the light intensity.

Table 2.2 Light provision to PBR under various configurations, based on light intensity reaching the reactor contents, the surface area of the reactor exposed to light and the reactor working volume.

Reactor	Surface Area (m^2)	Sets of lights switched on	Light intensity (µmoles m^{-2} s^{-1})	Total light (µmoles s^{-1})
ALR	0.060	1	148	9
ALR	0.060	2	300	18
OBR	0.060	1	150	9
WR	0.166	1	79	13
WR	0.166	2	162	26
WR (partially covered)	0.113	1	79	9
WR (partially covered)	0.113	2	162	18

2.4 Analytical methods

2.4.1 Mixing

Mixing times in each PBR were measured using the phenolphthalein and conductivity methods for visualisation of fluid flow and accurate measurement of circulation time, respectively.

The phenolphthalein method involved adding 2 mL of Phenolphthalein Indicator Solution (Merck) to the working volume (distilled water) of each reactor, followed by 1 mL of 1 M NaOH which coloured the liquid bright pink. On the addition of 1 mL of 1M HCl, the time taken for the pink colour to disappear was measured and the mixing pattern recorded to video. This was repeated at a range of agitation rates in each reactor: 0.02 to 0.2 m s^{-1} gas velocity (ALR); 0.1 to 0.7 Hz oscillating frequency (OBR); 10 to 40 rpm rocking rate (WR).

The conductivity method involved filling each reactor to its working volume with distilled water and adding 1 mL of a 5 M NaCl tracer. A conductivity probe connected to an AZ 86555 bench-top multi-meter (AZ Instruments) was used to measure the change after addition of the tracer. Conductivity was logged to computer using data logging software (HandHeld Version 3.00). The time taken to reach 95% homogeneity was calculated as follows:

$$h = \frac{C_{t-C_\infty}}{C_\infty} \tag{2.1}$$

where h is homogeneity, C_t is the instantaneous tracer concentration and C_∞ is the final tracer concentration (Merchuk et al., 1998). The response time of the conductivity probe was measured by moving the probe from a beaker of distilled water to a beaker of 0.125 M NaCl. An average response time of 3.3 seconds was recorded.

2.4.2 Mass transfer coefficient ($k_L a_{,CO_2}$)

The gassing-in method was used to measure the O_2 mass transfer coefficient, $k_L a_{,O_2}$. Dissolved oxygen was displaced by introducing nitrogen into the reactor. The air input was then switched on. A dissolved oxygen monitor and optical oxygen measurement probe were used to measure the increase in dissolved oxygen at 5 s time intervals (ALR: M300, Mettler Toledo, response time 15 s; OBR and WR: DOOPT20, GE Healthcare, response time 3.4 ± 1 s). The gassing-in method is used to calculate $k_L a$ according to Equation (2.2):

$$\frac{dC_L}{dt} = -k_L a(C^* - C_L) \tag{2.2}$$

where C^* is the saturation concentration of dissolved oxygen and C_L is the oxygen concentration at time t (Chisti, 2007b). However, this equation does not take into the account the delay caused by the probe response time.

The response time of the oxygen probe was measured by moving the probe from oxygen saturated to oxygen deplete solutions (Mueller et al., 1967). The response time was the time taken to reach 63% of the final value, and must be less than $\frac{1}{k_L a}$ for accurate measurements. The response time was modelled as first order according to Equation (2.3):

$$\frac{dC_m}{dt} = \frac{C_L - C_m}{\tau_r} \tag{2.3}$$

where C_m is the concentration displayed on the DO meter, C_L is the actual concentration of oxygen in the liquid phase and τ_r is the response time of the probe. Solving Equation (2.3) and substituting the expression for C_L into Equation (2.2) gives Equation (2.4), which accounts for the delay in the DO probe response and gives more accurate values for $k_L a$ (Garcia-Ochoa and Gomez, 2009; Gupta and Rao, 2003).

$$C_m = C^* + \frac{C^* - C_0}{1 - \tau_r k_L a}\left[\tau_r k_L a \, exp\left(\frac{-(t - t_0)}{\tau_r}\right) - exp(-k_L a\,(t - t_0))\right] \tag{2.4}$$

The $k_L a$ measured for oxygen was converted to the $k_L a$ for carbon dioxide ($k_L a_{CO_2}$) using the relative diffusivities of these gases and Equation (2.5) (Molina Grima et al., 1999; Rubio et al., 1999; Talbot et al., 1991):

$$k_L a_{,CO_2} = k_L a_{,O_2}\left[\frac{D_{CO_2}}{D_{O_2}}\right]^{0.5} \tag{2.5}$$

where the diffusivity for oxygen (D_{O_2}) and carbon dioxide (D_{CO_2}) (Talbot et al., 1991) were taken to be 2.278 (Wilke and Chang, 1955) and 1.94 $cm^2\ s^{-1}$ (Tamimi et al., 1994), respectively, at 25°C in dilute solutions.

2.4.3 CO_2 transfer rate

The carbon dioxide transfer rate (CTR) can be described by Equation (2.6):

$$CTR = \frac{dC_{CO_2}}{dt} = k_L a_{,CO_2} * (C_{CO_2,sat} - C_{CO_2,l}) \quad (2.6)$$

where $C_{CO_2,l}$ is the residual dissolved CO_2 in the bulk liquid and $C_{CO_2,sat}$ is the saturation solubility of CO_2 at a given partial pressure, temperature and ionic strength of the growth media. $C_{CO_2,sat}$ was calculated for each CO_2 partial pressure used in these studies by thermodynamic modelling using Visual MINTEQ software version 3.0, developed by Gustafsson (2012). The CTR was then calculated using the $k_L a_{,CO_2}$ (Section 2.4.2). In this work we calculated the maximum CTR obtainable when the CO_2 is completely depleted from solution and so the $C_{CO_2,l}$ term was excluded.

2.4.4 Carbon uptake

The amount of carbon fixed into saponifiable lipid was calculated using Equation (2.7):

$$CU_{lipid} = Y * n_{lipid} \quad (2.7)$$

where CU_{lipid} is the number of moles of carbon used to produce saponifiable lipids in a given experiment, Y is the number of moles of lipid produced, and n_{lipid} is the average number of moles of carbon in a mole of lipid. Values for n_{lipid} were estimated based on the fatty acid profile of *Scenedesmus* sp. cultivated under nitrogen limitation, yielding 46.2% oleic acid (C18:1), 24.3% palmitic acid (C16:0) and 15.9% linoleic acid (C18:2) (Griffiths et al., 2012). Saponifiable lipids are those that can be hydrolysed under basic conditions and were thus detected using the method described in Section 2.4.7

2.4.5 CO_2 supply rate

The CO_2 supply rate (CSR) was calculated according to Equation (2.8):

$$CSR = U_G * C_{CO_2} \quad (2.8)$$

where CSR is the rate at which CO_2 is supplied to the reactor, given as the superficial CO_2 velocity in m s^{-1}, U_G is the superficial gas velocity of the inlet gas (calculated according to Section 3.2.2 for the ALR), and C_{CO_2} is the percentage CO_2 in the inlet gas. CSR is thus the velocity per cross-sectional area of the PBR in m^2.

2.4.6 Biomass concentration

Biomass concentration of the starter cultures was measured by optical density at 750 nm (Griffiths, 2011) using a Helios α spectrophotometer (Thermo Scientific). Samples were diluted to an OD below 0.1, to fall within the linear range of measurement.

The biomass concentration in the PBRs was quantified throughout the growth cycle by measuring the dry weight. Samples (5 – 20 mL) were filtered through pre-weighed 0.45 µm cellulose nitrate filters (Sartorius Stedim) and dried at 80°C for 48 hours before being weighed.

2.4.7 Lipid concentration

In this work the total lipid content was measured as the total fatty acid content by the direct transesterification method followed by gas chromatography (Griffiths et al., 2010). This method gives a reasonable indication of the lipid production by *Scenesdmus* sp., and is particularly relevant for biodiesel production as biodiesel is produced from fatty acids.

Throughout the growth curve, 15 mL microalgal culture samples were taken for lipid analysis. These samples were centrifuged at 1520 g for 10 minutes (U320 Centrifuge, BOECO, Germany), and the supernatant discarded. The cellular pellets were stored at -20°C until analysis. Transesterification required the addition of 500 µL of toluene to defrosted cellular pellets, followed by 0.1 mg of glyceryl triheptadecanoate internal standard (C17-TAG; Sigma), and 1 mL of 0.5 M NaOH (basic catalyst) in methanol (alkylating agent). This solution was mixed by vortexing and incubated at 80°C for 20 minutes in a shaking incubator (300 rpm). Samples were cooled for 5 minutes at room temperature before addition of 1 mL of 5% HCl (acid catalyst) in methanol and a second incubation as before. After cooling to room temperature, the transesterification reaction was stopped by adding 400 µL of water. Finally, 400 µL hexane and 0.1 mg methyl nonadecanoate internal standard (C19-ME; Fluka analytical) were added and mixed by vortexing. Tubes were centrifuged at 1520 g for 1 minute to separate the hexane-toluene layer containing the fatty acid methyl esters (FAME) which were then transferred to GC viles for analysis.

A Varian 3900 GC equipped with a flame ionisation detector and ZB-WAXplus column (30 m (length) x 0.25 mm (ID) x 0.25 µm (d_f, film thickness); Zebron, South Africa) was used to analyse the FAME

samples. Standard split/splitless injection was used with a split of 90% and an injector temperature of 270°C. The column temperature was increased from 180 to 250°C at 2°C min^{-1}. Nitrogen (25 mL min^{-1}) was used as the carrier gas and the detector temperature was 260°C. Supelco 37 Component FAME and C14:0 to C22:0 FAME standard mixtures were used to identify chromatogram peaks. The sum of the areas of chromatogram peaks was used to quantify the total fatty acid concentration.

2.5 Power input

2.5.1 Calculations for the airlift reactor

Two methods for calculating the power input to the ALRs, and other sparged reactors, are discussed in Chapter 6.3.1: the 'minimum aeration power' and 'total aeration power'. The approach to these calculations is specified here.

2.5.1.1 Minimum Aeration Power

The power input to pneumatically-agitated (sparged) reactors, like the ALR, originates from the isothermal expansion of gas as it moves up the reactor and the kinetic energy of the gas injected into the reactor. According to Chisti (1989), the kinetic energy does not contribute more than 1.5% of the total power input in airlift reactors and so can be ignored. By considering the isothermal expansion of gas, Equation 2.9 was used to calculate power in sparged reactors:

$$\frac{P_G}{V_L} = \frac{\rho_L * g * U_G}{1 + \frac{A_d}{A_r}} \tag{2.9}$$

where P_G is the power for aeration (W), V_L is the liquid volume (m^3), ρ_L is the liquid density (kg m^{-3}), g is the gravitational acceleration (m s^{-2}), U_G is the superficial gas velocity (m s^{-1}), A_d is the cross-sectional area of the downcomer (m^2), and A_r is the cross-sectional area of the riser (m^2) (Chisti, 1989).

This equation describes the power to compress gas to the pressure at which it leaves the sparger, beneath the head of liquid at the bottom of the ALR. It does not take into account the pressure of the gas entering the sparger from the pipe by which it is delivered to the ALR.

2.5.1.2 Total Aeration Power

Using isothermal expansion of gas and taking into account the inlet pressure of gas in the pipe, as it travels through the gas flow meter and into the sparger, Equation 2.10 was used:

$$\frac{P_G}{V_L} = p_2 * F * \ln(\frac{p_2}{p_1})/V_L \quad (2.10)$$

where P_G is the power for aeration (W), V_L is the liquid volume (m^3), p_1 and p_2 are gas pressures at atmospheric pressure and at the reactor inlet (Pascals), respectively, and F is the volumetric gas flowrate ($m^3\ s^{-1}$).

Equation 2.10 describes the power to compress gas to the pressure at which it enters the reactor, and thus represents the total power required to compress gas for sparging. It gives a realistic value for aeration power input. In the experiments described in this dissertation the inlet gas pressure was 2 bar, the pressure at which air is distributed in the laboratory. In Chapter 6.3.1, the effect of the compression pressure on the power requirement is also discussed and compared.

Equation (2.10) was derived using the ideal gas law. To compress 1 mole of gas, the energy (E) required can be calculated using Equation (2.11):

$$E = R * T * \ln(\frac{p_2}{p_1}) \quad (2.11)$$

where R and T are the ideal gas constant (Pa $m^3\ mol^{-1}\ K^{-1}$) and temperature (K), respectively. The power input for aeration would, therefore, be a function of the molar flowrate (n, mol s^{-1}), according to Equation (2.12):

$$P_G = n * E \quad (2.12)$$

The ideal gas law states that molar flowrate is a function of the volumetric flowrate (F, $m^3\ s^{-1}$) and the inlet gas pressure, according to Equation (2.13):

$$n = \frac{p_2 * F}{R * T} \quad (2.13)$$

Substituting n and E (Equations (2.12) and (2.13)) into Equation (2.11), gives Equation (2.10).

2.5.2 Calorimetric experiments for the oscillatory baffled and wave reactors

Power input in the OBR and WR was measured using the calorimetric method according to previous studies (Kato et al., 2004; Raval et al., 2007). Raval et al. (2007) showed that the energy consumption measured using the calorimetric method was comparable (to within 30%) of that measured by the torque method when investigating the power requirements of shaker vessels. The method is used to infer the heat generated in the reactor due to viscous dissipation of mechanical energy by measuring the heat flow out of the reactor. According to Raval et al. (2007) the heat balance for an agitated vessel with no other heat sources is given by Equation (2.14). :

$$-mC_p \frac{dT_f}{dt} = UA\left(T_f - T_o\right) - P \tag{2.14}$$

where T_f and T_o are the temperatures of the fluid inside the vessel and the surrounding air, respectively. The rate of change of the total energy of liquid in the vessel (gas-phase energy is considered negligible), is given by $mC_p \frac{dT_f}{dt}$, while $U(T_f - T_o)$ denotes the heat loss to the surroundings, and P is the heat generated by viscous dissipation.

The calorimetric method requires measurement of the temperatures T_f and T_o over time. Constant values for the total heat transfer coefficient U and the heat generation P were guessed, and the equation was solved numerically for $T_f(t)$ with experimental measurements of $T_o(t)$ used as an input. The theoretical predictions and experimental measurements of $T_f(t)$ were compared, and U and P were varied until the difference was minimized.

The validity of the calorimetric method was evaluated by measuring the energy consumption in a stirred tank reactor, and comparing the measured power to a well-established empirical correlation (Abbott et al., 2014; Holland and Chapman, 1966), given by Equation (2.15):

$$\frac{4}{\pi}\frac{N\rho d_S^5}{d_V^2 L}\omega^3 \tag{2.15}$$

where N is the power number specific to the stirrer geometry, ρ is the liquid density, d_S and d_V are the stirrer- and vessel- diameter, respectively, L is the liquid level, and ω is the rotational velocity in revolutions per second. The validation reactor consisted of a 175 cm diameter vessel with 6 cm diameter Rushton impellers (power number 5.8). The vessel was filled to a height of 20 cm and the impeller operated at a speed of 500 rpm.

To measure energy consumption in the OBR and WR, the reactors were insulated by wrapping in sheets of cotton wool wadding. This decreased the heat transfer coefficient, U, thereby ensuring the heat generation, P, was the dominant term in Equation (2.15). Temperature probes were placed inside and outside the reactor column (OBR) and cellbag (WR). A working volume of water (2 L), heated to 34°C, was added to the reactors at the start of each experiment. The temperature inside and outside each reactor was logged to a computer from the moment the rocking platform was switched on until the water temperature reached steady state. This was repeated at various mixing rates.

2.6 Net Energy Ratio

The Net Energy Ratio (NER) is the fraction of energy that can be harnessed from either the algal lipid or the whole cell, based on calorific values, divided by the energy that was consumed to agitate and aerate the PBR during the course of cultivation. The NER at each time point during the algal growth curves was calculated according to Equation (2.16) and maximum NER identified.

$$NER = \frac{E_{OUT}}{E_{IN}} \tag{2.16}$$

where E_{OUT} is the energy that could be obtained from resulting biomass or lipid (kJ), and E_{IN} is the energy required to agitate the reactors by sparging or mechanical mixing (kJ).

Values for E_{OUT} were calculated based on the calorific values of the resulting biomass (whole cell) or lipid (2.17):

$$E_{OUT} = C_X * V_r * Cal \tag{2.17}$$

where C_X is the biomass or lipid concentration (g L^{-1}), V_r is the reactor volume (L) and Cal is the calorific value of biomass or lipid (kJg^{-1}). The calorific values of high-lipid *Scenedesmus* sp. cultures grown at high (10 400 ppm) and low (3 900 ppm) CO_2 were measured using bomb calorimetry (Appendix B), and the calorific value of lipid was taken from estimates by Lardon et al. (2009).

Values for E_{IN} were calculated according to the power used for mixing and aeration (Section 2.5) and the cultivation time as follows:

$$E_{IN} = P_G * t \tag{2.18}$$

2.7 Overview of experimental approach

Chapters 3 to 5 are divided into experimental work performed on each PBR independently (ALR, OBR and WR, respectively), followed by a comparison of these reactors in Chapter 6 and finally an LCA, in Chapter 7, incorporating the best algal cultivation conditions gleaned from the experimental work.

Algal cultivation in the ALR was carried out at a range of initial nitrate concentrations in the growth media (150 – 700 mg L^{-1} nitrate), to investigate the effects on lipid production. Experiments across a range of superficial gas velocities (0.002 – 0.02 m s^{-1}) and CO_2 concentrations (400 – 10 400 ppm) were also carried out in the ALR. Mixing, mass transfer, power input, biomass and lipid concentrations were measured during algal cultivation under each set of conditions. Mixing and mass transfer were measured in the OBR using three baffle designs between 10 and 70 Hz oscillating frequency. The most promising baffle design was used for algal cultivation experiments. Mixing, mass transfer and power input were measured in the WR at a range rocking rates (10 – 40 rpm) and rocking angles (2 - 10°). *Scenedesmus* sp. was subsequently cultivated at 25 rpm 10°, 15 rpm 8° and 15 rpm 4°.

The ALR, OBR and WR were compared based on their mixing and mass transfer capabilities as well biomass and lipid productivity. The energy efficiencies, expressed as the biomass and lipid productivity per unit power, of the three reactors were also compared. Mass transfer rates in the ALR that corresponded to a standard sparging velocity and critical minimum sparging velocity were used to inform the choice of agitation rates in the OBR and WR for algal cultivation. The NERs at these 'high' and 'low' agitation rates, corresponding to 'high' and 'low' energy consumption, were compared across the reactor types.

The experimental results from the ALR and WR were used in a biodiesel production simulation to obtain data for an LCA of the theoretical process. Differences in environmental burdens were compared when using the ALR or WR in the algal cultivation stage of the process.

3 Airlift Photobioreactor: Optimisation for energy efficient *Scenedesmus* sp. cultivation and lipid production

3.1 Introduction

Mixing, gas-liquid mass transfer, nutrient supply and light distribution are all vital factors for achieving desired algal growth rates and productivities. Optimisation of algal cultivation requires consideration of all these interrelated factors, illustrated in Figure 1.1 (Chapter 1.2.3). This research project focuses on the production of lipids from microalgae that can be used in high-value industries such as cosmetics and pharmaceuticals, or for biodiesel production. As discussed in Chapter 1.5, lipid accumulation in microalgae can be increased under nitrogen limited conditions. However, there is a trade-off between biomass production and lipid accumulation, and so it is necessary to find the conditions which promote optimal overall lipid productivity as a function of cellular lipid accumulation and biomass yield. In this work, preliminary experiments were carried out in airlift PBRs (ALR) to determine which nitrate concentrations promoted the highest lipid production in *Scenedesmus* sp. This species was chosen due to its high lipid accumulation ability and its ease of use in the laboratory (Griffiths et al., 2012).

The second and major section in this chapter consists of the optimisation of mixing and gas-liquid mass transfer in ALRs for cultivation of *Scenedesmus* sp. Pneumatically agitated reactors, such as airlifts and bubble columns, are commonly used in bioprocess engineering and are popular for algal cultivation. The airlift concept comprises gas sparged from the base of the reactor, rising up in a discrete region (the riser) and down in a separate region (the downcomer) (Carvalho et al., 2006; Singh and Sharma, 2012). This concept has been used successfully for microalgal cultivation in both flat plate and tubular reactors (Chisti, 2007a; Griffiths et al., 2012; Langley et al., 2012; Sánchez Mirón et al., 2002; Sasi, 2011; Yuan et al., 2011). In reactors driven by the airlift concept, mixing and gas-liquid mass transfer both occur by sparging gas (aeration). Airlift reactors are known to have good gas-liquid mass transfer capabilities (Carvalho et al., 2006; Chisti, 2007a; Gavrilescu and Tudose, 1997). Studies have reported factors influencing improved mixing and mass transfer in airlifts to include geometric design, presence of stirrer, sparger type and bubble size (Chisti and Jauregui-Haza, 2002; Kilonzo et al., 2007; Merchuk et al., 1998; Zimmerman et al., 2011). However,

this work is the first to report optimisation of mass transfer and mixing explicitly as a function of energy input (Jones and Harrison, 2014). The results described in this chapter therefore provide useful information regarding the optimisation of energy usage in airlift PBRs.

In addition to nitrate optimisation and the optimisation of power input with regard to mixing and mass transfer, this chapter will include a brief study on the effects of increasing the light intensity provided to the ALRs. All experiments in this work were carried out under laboratory conditions, i.e. artificial lighting. This means that light played a considerable role in the rates of production in these experiments, as artificial light is varies considerably compared to sunlight. Outdoor algal cultivation is preferred at commercial scale to reduce energy inputs and light limitations. The primary focus of this research project was optimisation of mixing and mass transfer, and so light was kept constant across all experiments, except those in which the effects of light were considered (Section 3.3.3).

3.2 Materials and Methods

Scenedesmus sp. stock cultures and experimental cultures were grown according to the methods described in Chapter 2.2, with adjustments described below. All experiments were carried out in the ALRs described in Section 2.3.1. Mixing times (T_m), CO_2 mass transfer coefficient ($k_L a_{CO_2}$), CO_2 transfer rate (CTR), CO_2 uptake rate (CU) and CO_2 supply rate (CSR) were measured according to Sections 2.4.1, 2.4.2, 2.4.3and 2.4.4, respectively. The power in the ALR was measured according to the calculations for 'total aeration power' (Equation (2.9), Section 2.5.1). Algal growth experiments were analysed according to Section 2.4.6 (biomass) and 2.4.7 (lipid). Methods related to this chapter are described in detail in the following sections.

3.2.1 Nitrate optimisation for increased lipid production

Airlift PBRs were used to cultivate *Scenedesmus* sp. under various nitrate concentrations. Bold's Basal Media was adjusted to contain nitrate concentrations of 150, 300, 450 and 700 mg L^{-1}. The ALRs were operated at a gas flowrate of 2 L min^{-1} (0.02 m s^{-1} superficial gas velocity) at 1% CO_2. Constant light was provided by 18 W cool white fluorescent bulbs at 200 – 300 µmol m^{-2} s^{-1}, giving an average light intensity across the height of the ALRs, on the surface furthest from the light source, of 148 µmol m^{-2} s^{-1} (Section 2.3.4). Daily samples were analysed for biomass and lipid concentration.

The total pigment content was measured regularly during the growth curves by extraction with dimethylsulphoxide (DMSO) and spectrophotometric analysis, according to Wellburn (1994). In this method a 2 mL sample was centrifuged at 16 000 g for 3 minutes, and 2 mL DMSO (99% Saarchem) at 60°C added to the cell pellet. The cells were resuspended in DMSO by vortexing, followed by incubation at 60°C for 10 minutes, with occasional shaking. To separate the cells from the extracted pigment, the mixture was centrifuged at 16 000 g for 3 minutes. The supernatant was diluted with DMSO and optical densities at 480, 649 and 665 nm were measured on a spectrophotometer. The following calculations were used to determine the pigment content:

$$Chlorophyll\ a\ (ChlA)\ (mg\ L^{-1}) = 12.45(OD_{665}) - 3.62(OD_{649}) \quad (3.1)$$

$$Chlorophyll\ b\ (ChlB)(mg\ L^{-1}) = 25.06(OD_{649}) - 6.5(OD_{665}) \quad (3.2)$$

$$Total\ carotenoids\ (mg\ L^{-1}) = (1000(OD_{480}) - 1.29(ChlA) - 53.78(ChlB))/220 \quad (3.3)$$

$$Total\ pigments = ChlA + ChlB + Carotenoid \quad (3.4)$$

3.2.2 Height averaged superficial gas velocity

Superficial gas velocity is a function of the gas flowrate and the pressure of the gas entering the sparger. A superficial gas velocity averaged across the height of the airlift was calculated according to Chisti (1989), as follows:

$$U_{Gr} = U_G \frac{(A_r + A_d)}{A_r} \quad (3.5)$$

where U_{Gr} is the height averaged superficial gas velocity in the riser; A_r and A_d are the cross sectional areas of the riser and downcomer, respectively; and U_G, the height averaged superficial gas velocity of a reactor, can be calculated as follows:

$$U_G = \frac{n * R * T}{A * p_3} \ln(1 + \frac{p_3}{p_1}) \quad (3.6)$$

where A is the cross sectional area of the airlift, R is the gas constant (8314 J K^{-1} $kmole^{-1}$), T is the temperature in K, p_1 is the gas pressure at the top of the airlift (atmospheric pressure in Pa), $p_3$is the gas pressure leaving the sparger (given the inlet pressure and the pressure drop across the sparger (Green and Perry, 2007)) and n is the molar gas flowrate. n can be calculated as follows:

$$n = \frac{p_2 * F}{R * T} \quad (3.7)$$

where p_2 is the pressure of gas at the bottom of the ALR (inlet pressure, Pa), and F is the gas flowrate (m^3 s^{-1}). All superficial gas velocities quoted in this work are for U_{Gr}, the height averaged velocity in the riser.

3.2.3 Optimisation of gas velocity and CO_2 concentration

'Standard conditions' in the ALRs were set as a 2 L min^{-1} gas flowrate (0.02 m s^{-1} superficial gas velocity) at 1% CO_2. Following establishment of the performance of *Scendesmus* sp. under standard conditions, its performance was studied under a range of superficial gas velocities (0.0022, 0.0054, 0.011 and 0.022 m s^{-1}, equivalent to air flowrates of 0.2, 0.5, 1 and 2 L min^{-1}). At each superficial gas velocity, *Scenedesmus* sp. was cultivated at four CO_2 concentrations (400, 1 400, 5 400 and 10 400 ppm) such that the effect of CO_2 mass transfer and energy supply could be considered separately. For each set of experiments, a positive control was run under the 'standard condition' to check consistency and provide data on reproducibility. Repeats under standard conditions were used to calculate the standard deviation, where variation between these was used to represent the standard deviations across all experimental data. In addition to biomass and lipid concentration measurements, the CO_2 transfer rate, carbon uptake to lipids and CO_2 supply rate were calculated.

3.2.4 Comparison at double light intensity

Scenedesmus sp. growth curves were measured in ALRs under constant gas velocity and CO_2 concentration. Light was provided using light banks, consisting of three cool white 18 W fluorescent bulbs (Osram). One light bank was placed behind the glass column and, in the case of experiments at double light, an additional light bank was placed in front of the glass column. Each light bank provided light at 200 – 300 µmol m^{-2} s^{-1}, giving an average light intensity across the height of the ALRs, on the surface furthest from the light source, of 148 µmol m^{-2} s^{-1}. This equated to 9 µmol s^{-1} of total light, given the surface area of the airlift reactors (Section 2.3.4). With two light banks in place, the average light intensity was 300 µmol m^{-2} s^{-1}, giving 18 µmol s^{-1} of total light (double the light intensity and total light).

3.3 Results and Discussion

3.3.1 Nitrate optimisation for increased lipid production

Scenedesmus sp. was grown in four ALRs in BBM medium containing 150, 300, 450 and 700 mg L^{-1} nitrate, respectively (Figure 3.1). Light, sparging velocity, temperature and CO_2 concentrations were kept constant across the four ALRs. The maximum biomass and lipid concentrations, and correlating biomass and lipid productivities from growth curves in each ALR are shown in Figure 3.2.

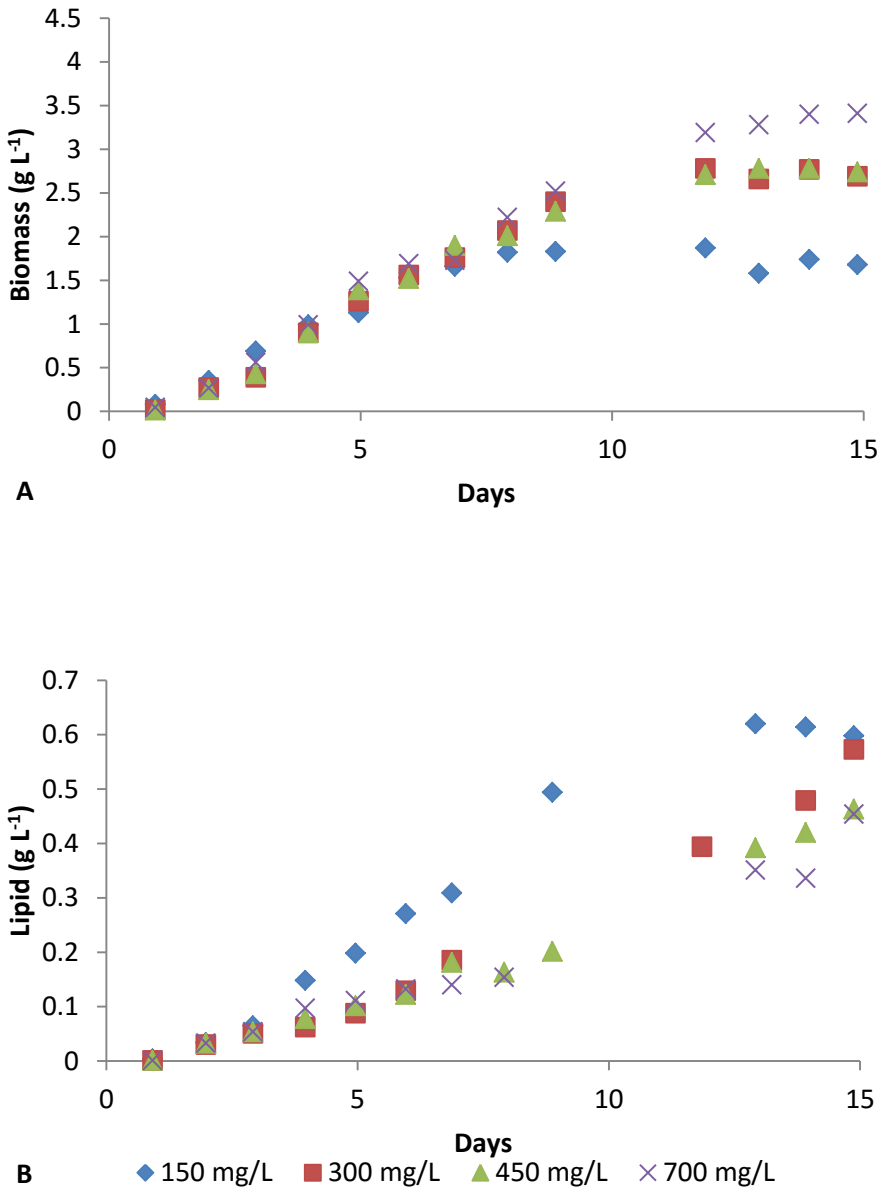

Figure 3.1 (A) Biomass and (B) Lipid concentration during *Scenedesmus* sp. growth curves in Bold's Basal Media containing 150, 300, 450 and 700 mg L^{-1} nitrate.

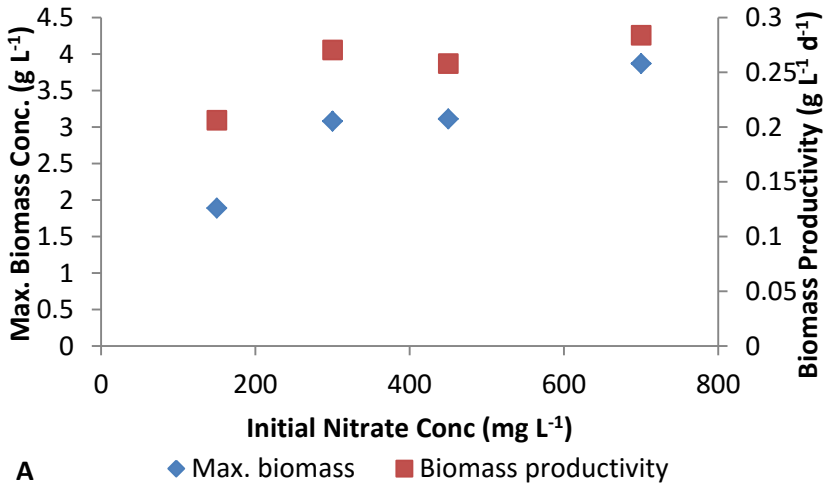

A

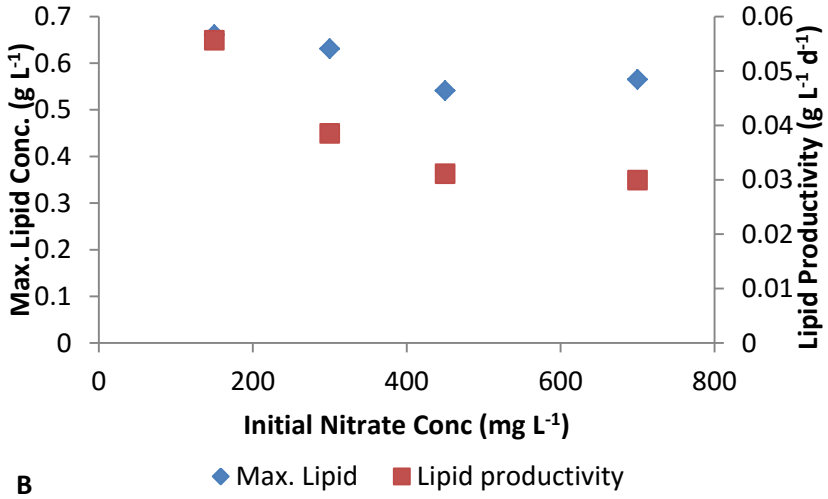

B

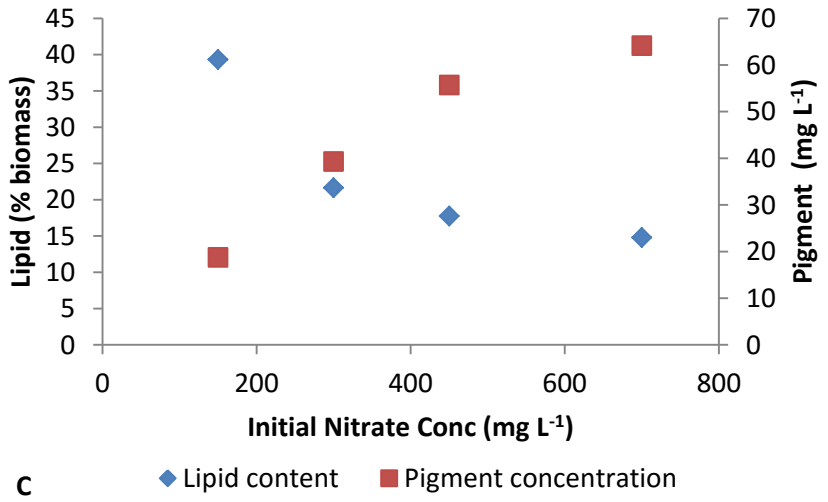

C

Figure 3.2 (A) Maximum biomass concentration and productivity; (B) maximum lipid concentration and productivity; and (C) cellular lipid content as a % of biomass concentration and total pigment concentration for *Scenedesmus* sp. grown in media containing 150, 300, 450 and 700 mg L^{-1} nitrate.

The results in Figure 3.2 indicate an increase in biomass and a decrease in lipid concentration with increasing initial nitrate concentration in the growth media. At 150 mg L^{-1} nitrate, *Scenedesmus* sp. had the highest maximum lipid concentration (0.66 g L^{-1}) and lipid productivity (0.056 g L^{-1} d^{-1}). The cellular lipid content at this nitrate concentration was sufficiently high (39% of biomass) to maintain high overall lipid production even with the lowered biomass concentration (1.89 g L^{-1}). The photosynthetic pigments in microalgae require nitrogen for their production, and so are reduced under limited nitrate conditions, in contrast to increased cellular lipid content.

These results correlate to those published previously that describe enhanced lipid production from microalgae under nitrogen stressed conditions (Griffiths et al., 2014a, 2014b; Griffiths and Harrison, 2009; Lardon et al., 2009; Lin, 2011; Rodolfi et al., 2009). Under nutrient stress, the microalgae begin to store energy in the form of lipids; the available carbon is used for these energy stores in place of cellular growth. Thus, lipid accumulation continues to increase as cellular growth moves into an early stationary phase (Figure 3.1). Reduced nitrogen for protein formation, reduction of photosynthetic pigments and favouring of energy storage over biomass production all contribute to the reduction in the maximum biomass concentration under nitrate limited growth conditions. For the purposes of this work, the best lipid concentration was obtained at 150 mg L^{-1} nitrate, despite a reduction in biomass. Therefore, in all subsequent experiments a BBM medium containing 150 mg L^{-1} nitrate was used.

3.3.2 Optimisation of gas velocity and CO_2 concentration

3.3.2.1 Mixing and mass transfer

The mixing time (T_m) and CO_2 mass transfer coefficient ($k_L a_{,CO_2}$) were measured with increasing superficial gas velocity (U_{Gr}) in an airlift reactor containing cell-free BBM media (Figure 3.3). These parameters improved (i.e. T_m decreased and $k_L a_{,CO_2}$ increased) with increasing aeration, as expected.

Similar data are found in the literature, however, $k_L a$ and mixing time vary according to the type of sparger used, the liquid viscosity and the airlift dimensions (Kilonzo et al., 2007; Luo et al., 2011; Moo-Young and Blanch, 1981). According to previous studies, mixing times in airlift reactors range from 20 to 150 s at a U_{Gr} of 0.021 m s^{-1} (Chisti and Jauregui-Haza, 2002; Merchuk et al., 1998; Molina Grima et al., 1999; Sánchez Mirón et al., 2004a). The reactor dimensions and sparger described in

this work resulted in a mixing time of 39.5 s at 0.022 m s^{-1} (Figure 3.3), i.e. at the lower (faster) end of the range found in the literature, indicating good mixing. Chisti (1989), Chisti and Jauregui-Haza (2002) and Pirouzi et al. (2014) report $k_L a$ in airlift reactors in the range 9 to 54 h^{-1}, which correlates to the range reported here (2 – 40 h^{-1}).

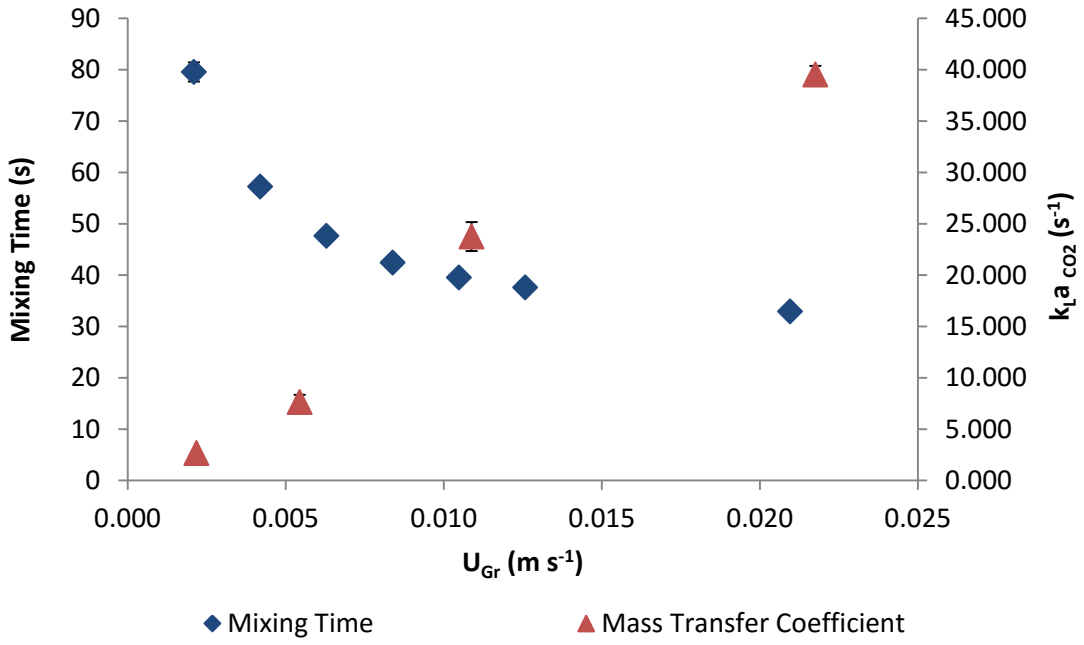

Figure 3.3 Mixing time and CO_2 mass transfer coefficient at increasing superficial gas velocity in an airlift photobioreactor. Error bars indicate the standard deviation of n = 3 replicates.

Visualisation of mixing and fluid flow in the ALR was performed using phenolphthalein indicator solution, as described in Section 2.4.1. Figure 3.4 shows the mixing patterns at a gas flowrate of 2 L min^{-1} (0.02 m s^{-1}). The HCl tracer changes the solution from pink to colourless as it circulates in a plug-flow manner from the downcomer, up the riser and down again. The conductivity raw data (Figure C.1, Appendix C) shows that the liquid circulates 5 to 6 times before the solution reaches 95% homogeneity (considered mixed). At lower gas flowrates (0.2 and 0.5 L min^{-1}) a deadzone appears at the bottom of the reactor.

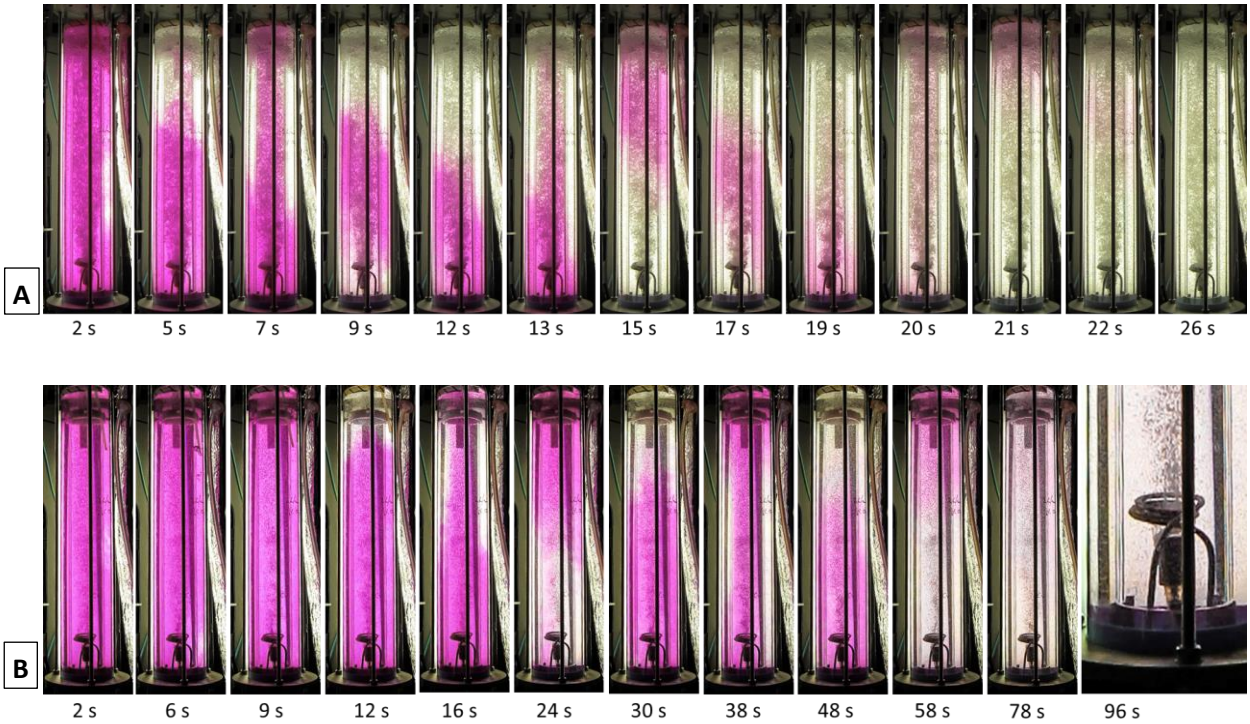

Figure 3.4 Mixing in the airlift PBR at a gas flowrate of (A) 2 L min^{-1} (0.02 m s^{-1}) and (B) 0.2 L min^{-1} (0.002 m s^{-1}) visualised using phenolphthalein indicator solution in alkali solution (pink) and a 1 M HCl tracer (colourless). After 96 s at 0.2 L min^{-1} (B) the contents were mixed except for a deadzone near the sparger.

The power input was calculated at each superficial gas velocity based on the isothermal compression of gas, according to Section 2.5.1.2. Carbon dioxide transfer rates (CTR) were calculated with respect to the saturation solubility of CO_2 at various partial pressures (400 to 10 400 ppm) and the $k_L a_{,CO_2}$ at superficial gas velocities of 0.002, 0.005, 0.01 and 0.02 m s^{-1} (Section 2.4.3). These indicated the amount of carbon available to algal cells. Figure 3.5 shows CTRs at increasing power input for aeration at the given velocities (Figure 3.4A) and at increasing CO_2 supply rates (CSR; a function of superficial gas velocity and CO_2 concentration, Figure 3.4B). This figure demonstrates the importance of high CO_2 concentrations for good CTR. The CTR increased with increased power for aeration at each CO_2 concentration, and dropped substantially with reduced CO_2 concentration. The CTR correlated well with CO_2 supply rate (superficial CO_2 velocity) across changes in both superficial gas velocity and CO_2 concentration.

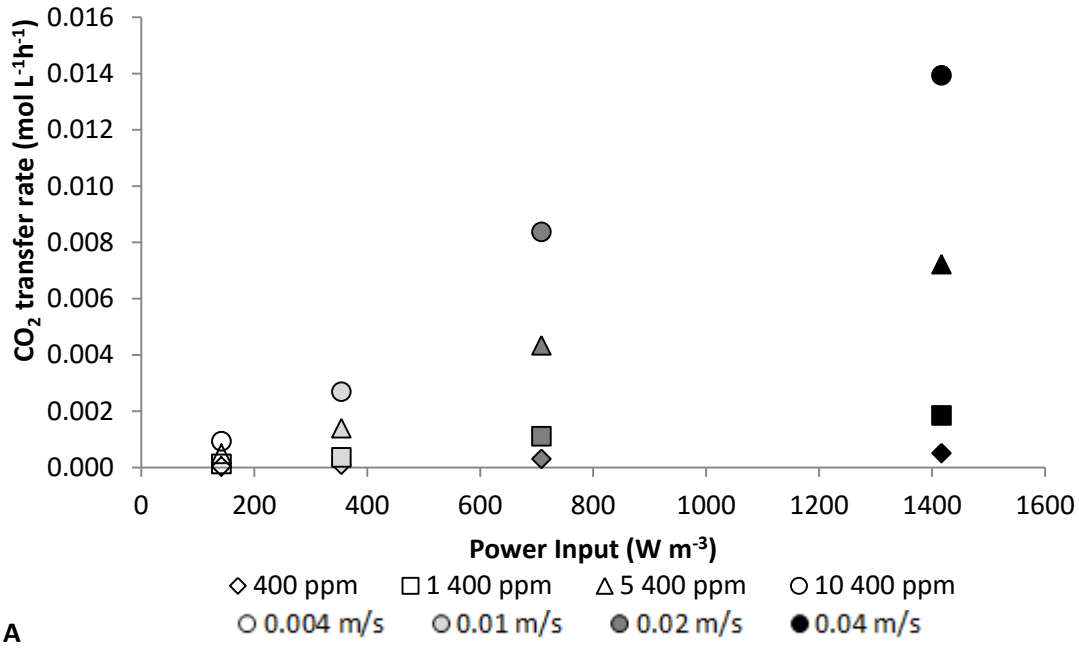

A

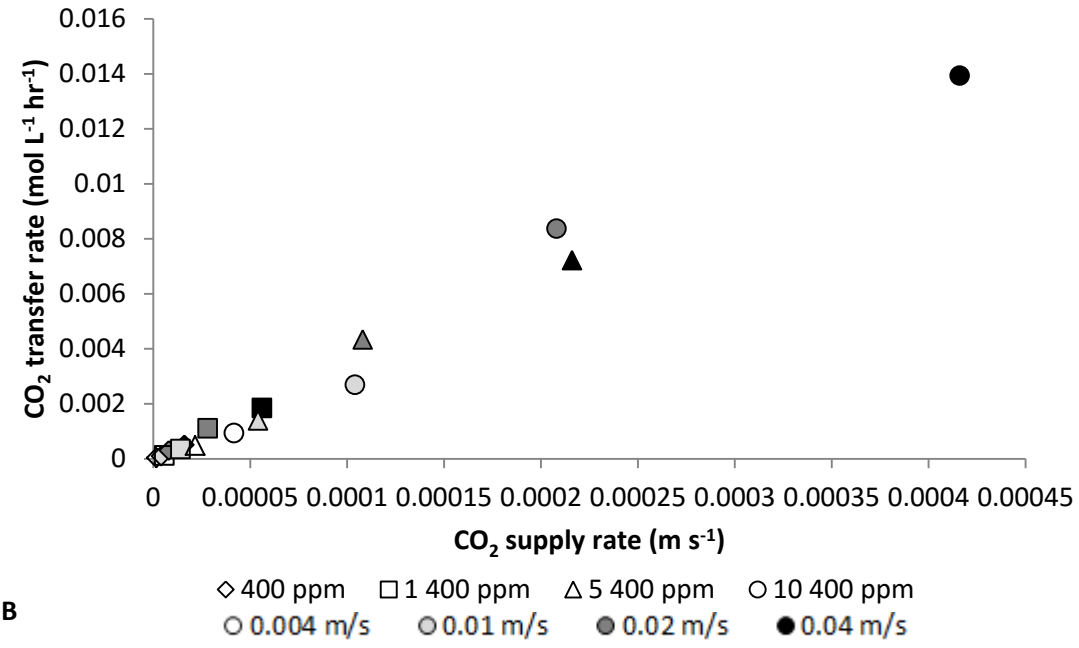

B

Figure 3.5 CO_2 transfer rates (a function of CO_2 saturation solubilities and $\boldsymbol{k_L a_{,CO_2}}$) with respect to (A) power input, and (B) CO_2 supply rate at various CO_2 partial pressures and superficial aeration velocities. Note: the deeper the shade of the point, the higher the U_{Gr}; where the black points represent data at a superficial gas velocity of 0.02 m s^{-1}.

Hall et al. (2003), Jian (2006), Linek et al. (1987), Moo-Young and Blanch (1981), Sierra et al. (2008) and others describe the increase in $k_L a$ with increased power input in different reactor types (Chapter 1.3, Figure 1.2). These are in accordance with the results in Figure 3.5 for the ALR, which highlight the dependence of carbon availability on the energy provided to the reactor for algal cultivation.

3.3.2.2 Biomass and lipid production

Figure 3.6 shows the algal growth and lipid production with respect to time under 'standard cultivation conditions' (10 400 ppm CO_2; 0.02 m s^{-1} superficial gas velocity). Maximum concentrations of 2.15 g L^{-1} biomass and 0.589 g L^{-1} lipid were measured. A maximum lipid content of 32.1% biomass, and maximum instantaneous biomass and lipid productivities of 0.306 and 0.081 g L^{-1} d^{-1}, respectively, were obtained under 'standard conditions'. Subsequent experiments assessed the effect of reduced power input for aeration on maintaining these concentrations. An ALR under 'standard conditions' was run in parallel to each set of subsequent experiments. Standard deviations were calculated based on variation across these 5 repeats at 'standard conditions' (0.144 g L^{-1} biomass; 0.029 g L^{-1} lipid).

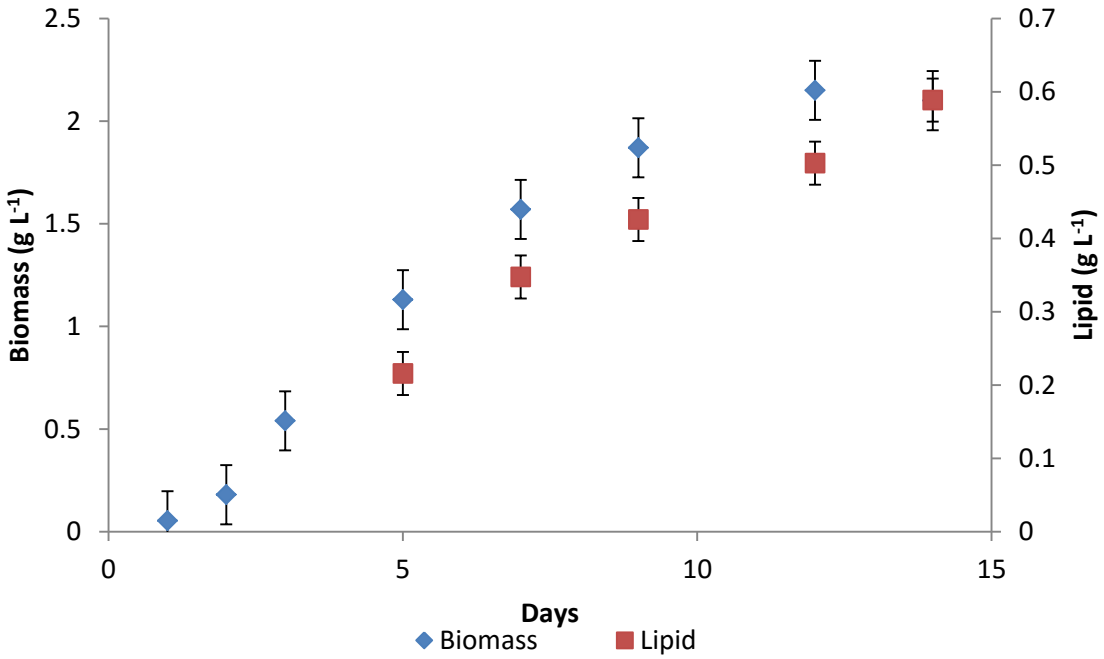

Figure 3.6 Growth curve of *Scendesmus* sp. under 'standard conditions' (10 400 ppm CO_2; U_{Gr} of 0.02 m s^{-1}) showing biomass and lipid production. Error bars show the standard deviation calculated from n = 5 repeats under 'standard conditions' (0.144 g L^{-1} biomass; 0.029 g L^{-1} lipid).

The maximum biomass and lipid concentrations in Figure 3.6 correlate with previous results from the growth of *Scenedesmus* sp. under nitrogen limited conditions (Griffiths et al., 2012). Griffiths and Harrison (2009) reviewed the maximum lipid content, biomass and lipid productivity of a wide variety of algal species. Biomass productivities were reported to range from 0.03 to 0.59 g L^{-1} d^{-1} with biomass productivity obtained in this work well within this range (0.306 g L^{-1} d^{-1}). Griffiths and Harrison (2009) reported lipid content to range from 5 to 64% biomass under nitrogen deficient conditions, and lipid productivity from 0.017 to 0.164 g L^{-1} d^{-1}. *Scenedesmus* sp. cultivated in this work reported towards the upper end of these ranges, demonstrating its potential as a lipid producer. *Scenedesmus* sp. also had higher biomass and lipid productivities under standard conditions compared to a number of freshwater algal species reviewed by Rodolfi et al. (2009) (0.17 – 0.28 g L^{-1} d^{-1} biomass and 0.03 – 0.05 g L^{-1} d^{-1} lipid).

Growth experiments at superficial gas velocity and CO_2 concentration lower than the 'standard conditions' were conducted, and biomass growth and lipid production were monitored. The superficial CO_2 velocity or CO_2 supply rate (CSR) was calculated as the product of the percentage CO_2 sparged into the reactor (400, 1 400, 5 400 and 10 400 ppm) at the four superficial gas velocities (0.002, 0.005, 0.01 and 0.02 m s^{-1}). Figure 3.7A shows the increased maximum biomass concentration with increased CSR to a maximum of 2.27 g L^{-1}. Above the critical CSR of 2.7×10^{-5} m s^{-1} (equivalent to a superficial gas velocity of 0.005 m s^{-1} and CO_2 concentration of 5 400 ppm), further increase in either CO_2 concentration or superficial gas velocity did not increase biomass production significantly. This is a significant consideration for energy input. While differences in the maximum biomass concentrations obtained may also be influenced by limitation of other nutrients, these concentrations were not altered in this study. The rate of growth during the linear phase, representing biomass productivity, is a better indication of the influence of CO_2 limitation independently of other nutrients. This productivity, given as overall and instantaneous productivity in Figure 3.7B and C respectively, follows similar trends to the maximum biomass concentration given in Figure 3.7A, where a critical CO_2 supply rate can be reached at low superficial gas velocity (0.005 m s^{-1}) and high CO_2 concentration (10 400 ppm).

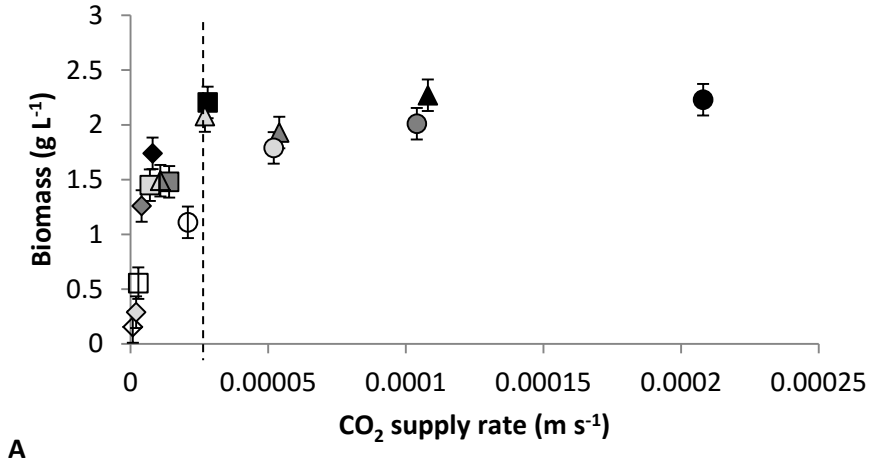

A

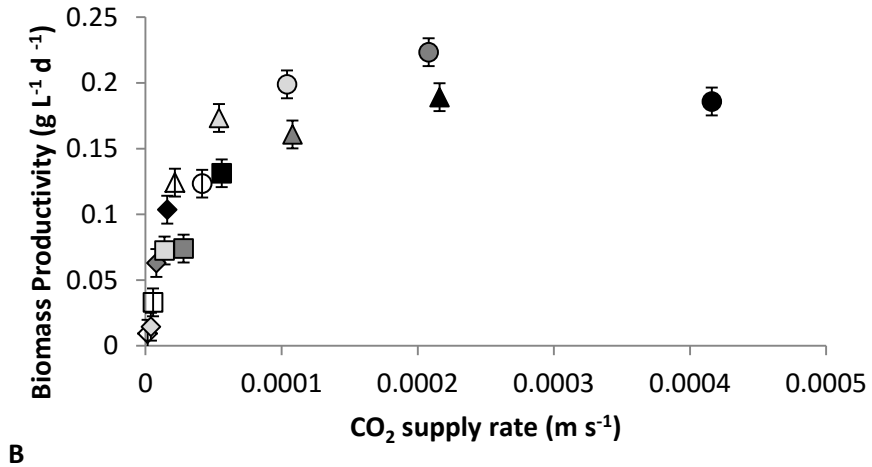

B

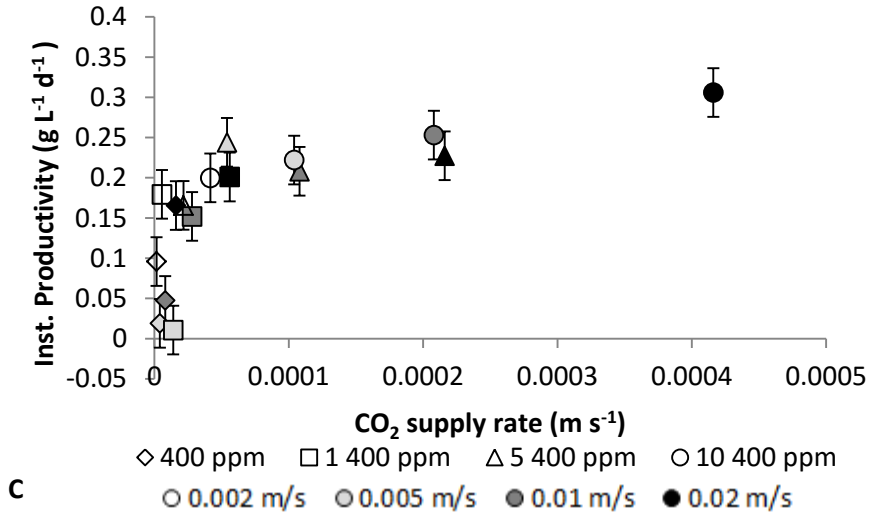

C

Figure 3.7 (A) Maximum biomass concentration, (B) overall biomass productivity (based on days to reach maximum biomass conc.) and (C) instantaneous biomass productivity in relation to the CSR. The deeper the shade of points, the higher the U_{Gr}; where black points = U_{Gr} 0.02 m s^{-1}. Dashed line indicates the critical minimum CSR. Error bars show the standard deviation calculated from n = 5 repeats under 'standard conditions' (0.144 g L^{-1} biomass; 0.011 g L^{-1} d^{-1} biomass productivity; 0.030 g L^{-1} d^{-1} instantaneous productivity).

Figure 3.8A illustrates the maximum biomass concentration attained as a function of CO_2 transfer rate (CTR). The same trend is seen as in Figure 3.7, with a critical CTR (0.00185 mol L^{-1} hr^{-1}) above which no further increase in biomass concentration is observed. Figure 3.7 and Figure 3.8 demonstrate that at 400 and 1 400 ppm CO_2, the standard superficial gas velocity of 0.02 m s^{-1}; (shown as black points on the graphs) is required to maintain maximum biomass concentrations of ≥ 2 g L^{-1}; whereas at 5 400 and 10 400 ppm CO_2, the superficial gas velocities could be reduced to 0.005 m s^{-1} without sacrificing biomass concentration or productivity. According to Figure 3.5A, this equates to a 75% reduction in the power input required for aeration.

Figure 3.8A shows that, at lower superficial gas velocities, the maximum biomass concentration is not achieved despite the critical CTR being met. This suggests that superficial gas velocity influences a second factor (in addition to carbon limitation) required for growth. This highlights the complexity of algal cultivation systems, with interdependent parameters. In an airlift reactor, gas sparging is responsible for CO_2 provision and for mixing. Mixing is important for distribution of nutrients (carbon, nitrogen, phosphorous, and other nutrients), removal of oxygen produced by the algae and access of algal cells to sufficient light for photosynthesis. Therefore, the reduction in growth at low superficial gas velocity under non-limiting CTR suggests mixing or light limitation. The latter is shown by Gani (2013). Figure 3.8B shows the decrease in biomass with decreased superficial gas velocity, which affects both CO_2 provision and mixing. The rate at which biomass increased with increased CO_2 concentration is higher at the lower gas velocities, indicating the degree of carbon limitation. Also, at higher CO_2 there is a smaller difference in biomass across superficial gas velocities.

The time taken for the algal culture to reach maximum biomass influences the energy input requirement. Productivity is therefore an important consideration. The data in Figure 3.7B is displayed in a bar graph separating the CSR into CO_2 concentration and gas velocity (Figure 3.9). Once again, at 10 400 and 5 400 ppm CO_2, the superficial gas velocity could be reduced from 0.02 to 0.005 m s^{-1} without a significant decrease in biomass productivity (Figure 3.9). This graph also clearly shows the low productivity as a result of low CO_2 concentration (400 – 1400 ppm), even at increased gas velocity.

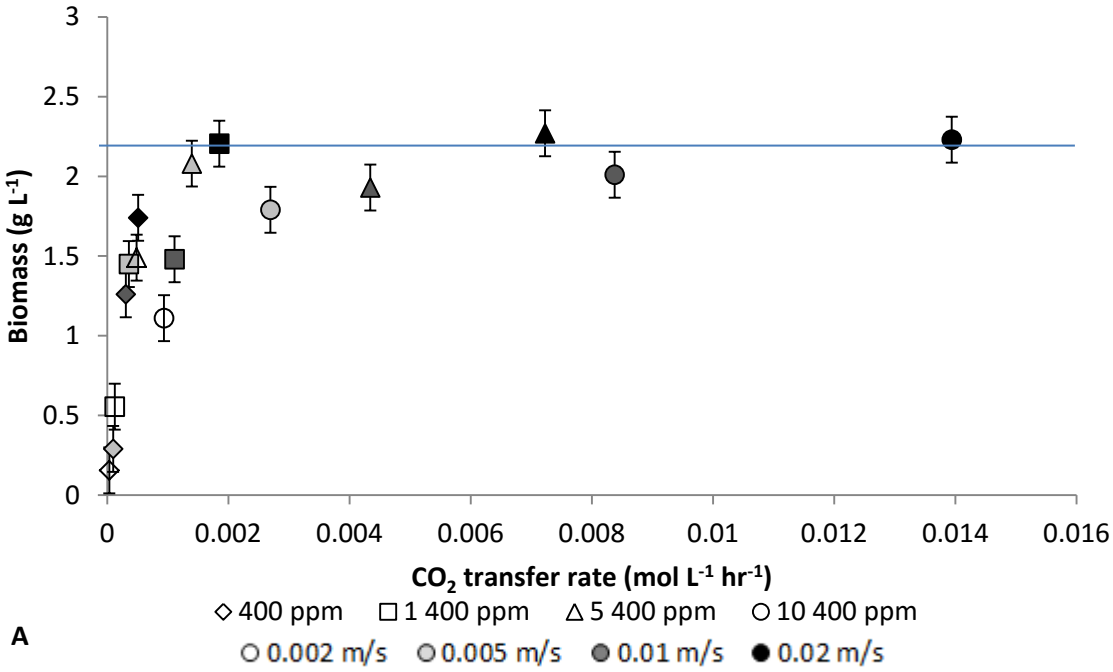

A

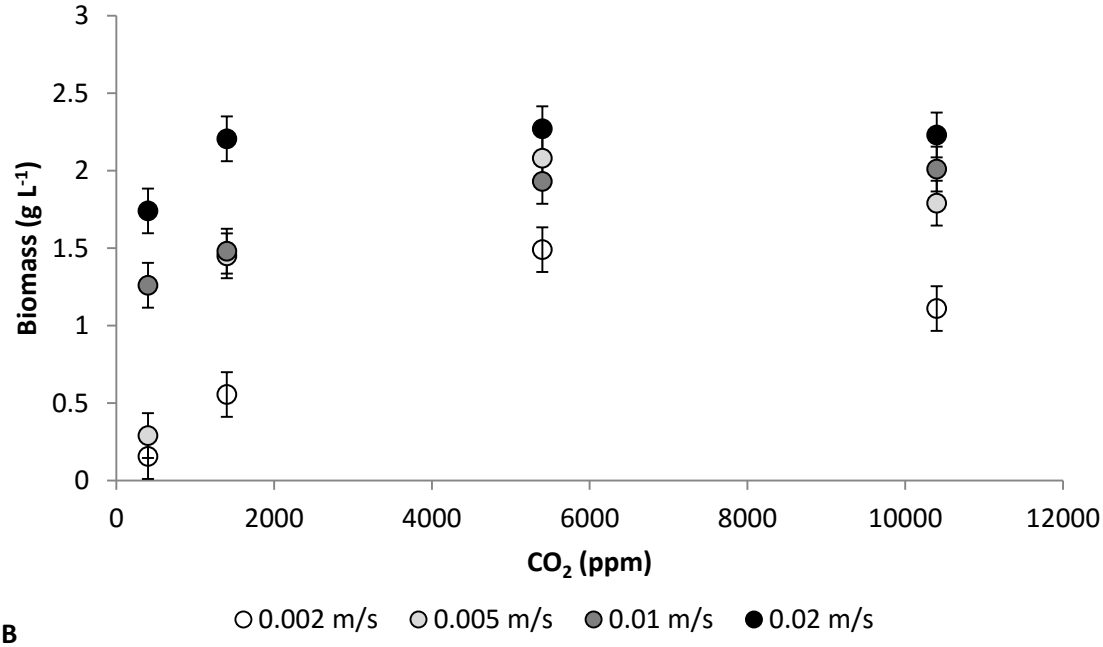

B

Figure 3.8 (A) Maximum biomass concentration with respect to CO_2 transfer rate (a function of CO_2 concentration and $k_L a_{,CO_2}$). Note: the deeper the shade of the point, the higher the U_{Gr}; the horizontal line indicates the drop from the maximum biomass, where mixing or light could be limiting. (B) Maximum biomass obtained with respect to CO_2 concentration in the sparge gas at each of the superficial gas velocities independently. Error bars show the standard deviation calculated from n = 5 repeats under 'standard conditions' (0.144 g L^{-1} biomass).

Typical CO_2 concentrations used in previous algal cultivation studies range from 10 400 to 150 400 ppm (Kaewpintong et al., 2007; Rodolfi et al., 2009; Sasi, 2011). In support of this study, results from Sasi (2011) showed that air enriched with CO_2 above 50 000 ppm does not lead to further increase in growth rate of *Chlorella vulgaris*; and similarly Langley et al. (2012) show a minimum threshold of 1 200 ppm CO_2 to maintain algal biomass productivity of *C. vulgaris*. Kaewpintong et al. (2007) investigated the effect of superficial gas velocity on the growth of *Haematococcus pluvialis* and demonstrated an increase in growth with increased velocity up to 0.04 m s^{-1}, above which no further increase occurred. These results support the claim that a critical CO_2 availability or sparging rate exists. However, the literature reports investigate either CO_2 concentration or superficial gas velocity independently, and data represented by varying only one of these factors are system-specific and of limited value to generalised application. This work is the first to report the combined effect of both CO_2 concentration and superficial gas velocity, represented as a critical CO_2 supply rate or CO_2 transfer rate.

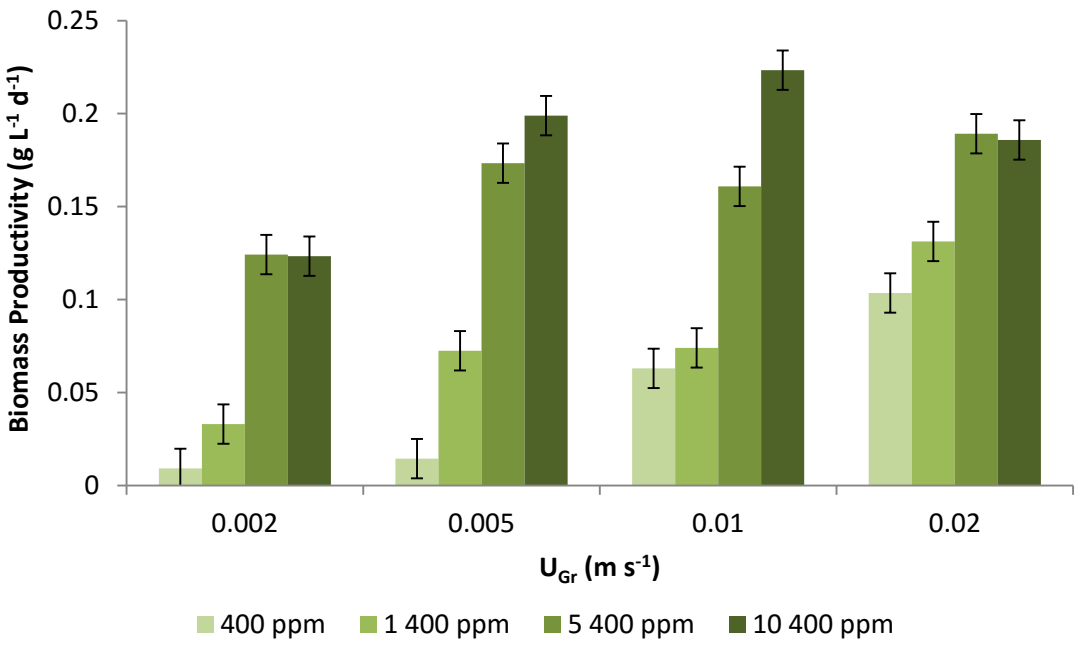

Figure 3.9 Superficial gas velocity and CO_2 concentration with respect to biomass productivity, calculated according to the number of days required to reach maximum biomass concentration. Error bars indicate standard deviation calculated from n = 5 repeats under 'standard conditions' (0.011 g L^{-1} d^{-1} biomass productivity).

Lipid production data showed a critical CSR at 1.4×10^{-5} m s^{-1} (0.02 m s^{-1} superficial gas velocity and 1 400 ppm CO_2) with lipid content as a percentage of the biomass reaching 38.3% (Figure 3.10A). Interestingly, the lipid content peaked between 1.4×10^{-5} and 2.1×10^{-5} m s^{-1} and then dropped with further increase in CSR before rising again to 36.3%. This perhaps indicates that at lower CSR (around 1.4×10^{-5} m s^{-1}) the algae favour lipid storage over cellular replication, and above this CSR the algae return to favouring cellular replication and use up the lipid stores for growth, thus leading to a reduction in the cellular lipid content. The lipid content increased again when there was excess carbon available for growth and lipid storage. A similar trend was seen in Figure 3.10B and Figure 3.10C, for volumetric lipid production (g L^{-1}) and lipid productivity (g L^{-1} d^{-1}), respectively. However, these graphs indicate that the drop in lipid production and productivity coincides with lower superficial gas velocity. This suggests a second factor, other than carbon limitation, such as mixing rates (affecting light regimes, and distribution of media components, as discussed earlier), which influences the lipid production and productivity despite the CSRs. This trend was also seen in Figure 3.11, where the moles of carbon fixed into lipid increased to a peak at a lower CSR (0.01 moles at 2.8×10^{-5} m s^{-1}), then decreased, and finally reached a maximum at high CSR (0.13 moles at 1.1×10^{-4} m s^{-1}), when superficial gas velocity is high. The graph of biomass productivity with respect to carbon transfer rate (Figure 3.8A) also pointed to limitations caused by reduced mixing. The trend was more pronounced with the lipid data, however, suggesting the sensitivity of lipid production to a factor other than CO_2 supply.

Previous studies have highlighted the link between nutrient availability and lipid production, but most of these studies have focused on nitrogen, phosphorous and silicon (Christenson and Sims, 2011; Clarens et al., 2010; Demirbas, 2010; Griffiths and Harrison, 2009). The findings in this work are important to begin understanding the relationship between carbon availability and lipid production by algae. A study by Chiu et al. (2009) reported similar results to this work, where *Nannochloropsis oculata* had biomass and lipid productivities that were poor at 400 ppm CO_2 (air), reached maximum at 20 400 ppm (0.145 g L^{-1} d^{-1} lipid), and decreased again between 50 400 to 150 400 ppm CO_2.

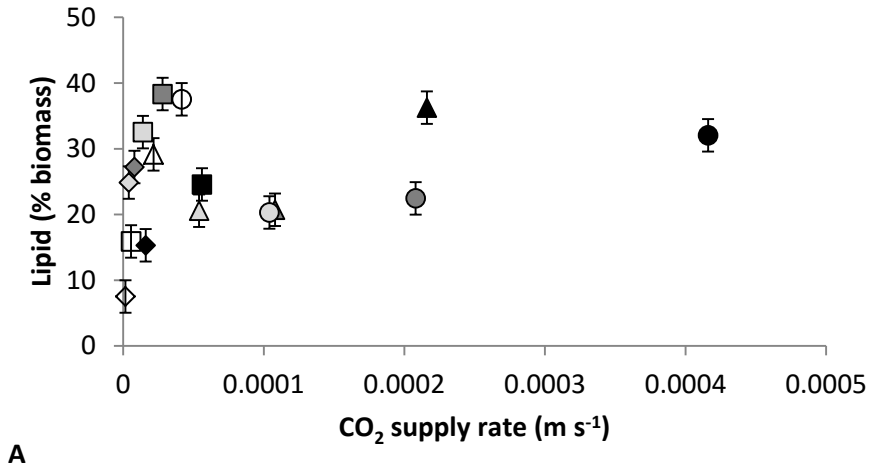

A

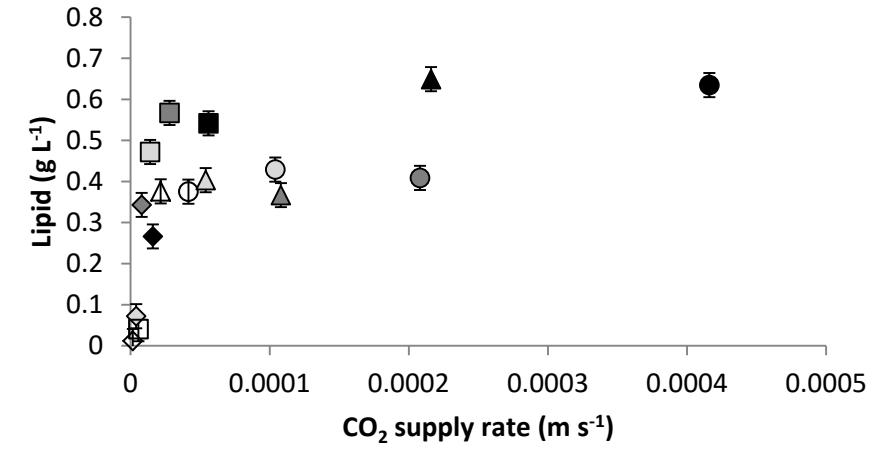

B

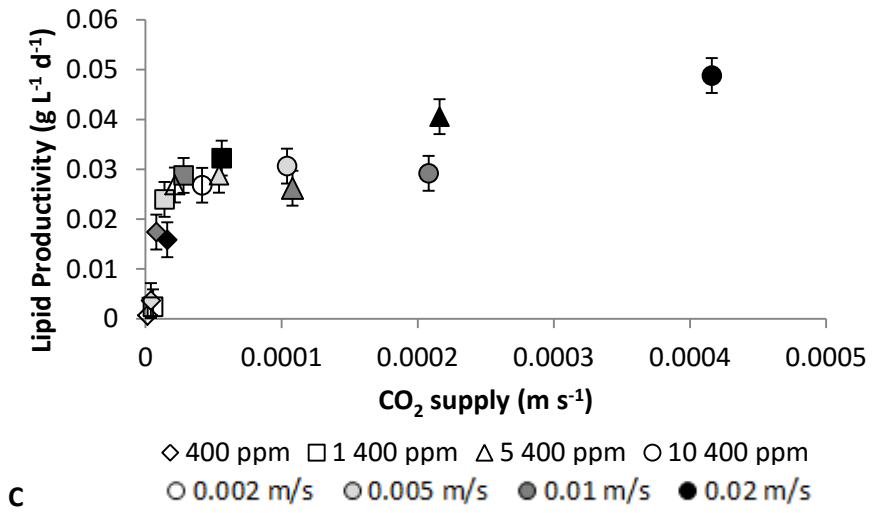

C

Figure 3.10 CO_2 supply rate in relation to (A) the maximum lipid content (as % of biomass) and (B) the maximum lipid concentration obtained during two weeks cultivation; (C) lipid productivity calculated according to the time taken to reach maximum lipid concentration. The deeper the shade of points, the higher the U_{Gr}. Error bars indicate the standard deviation calculated from n = 5 repeats under 'standard conditions' (2.47 % lipid content; 0.029 g L^{-1} lipid; 0.003 g L^{-1} d^{-1} lipid productivity).

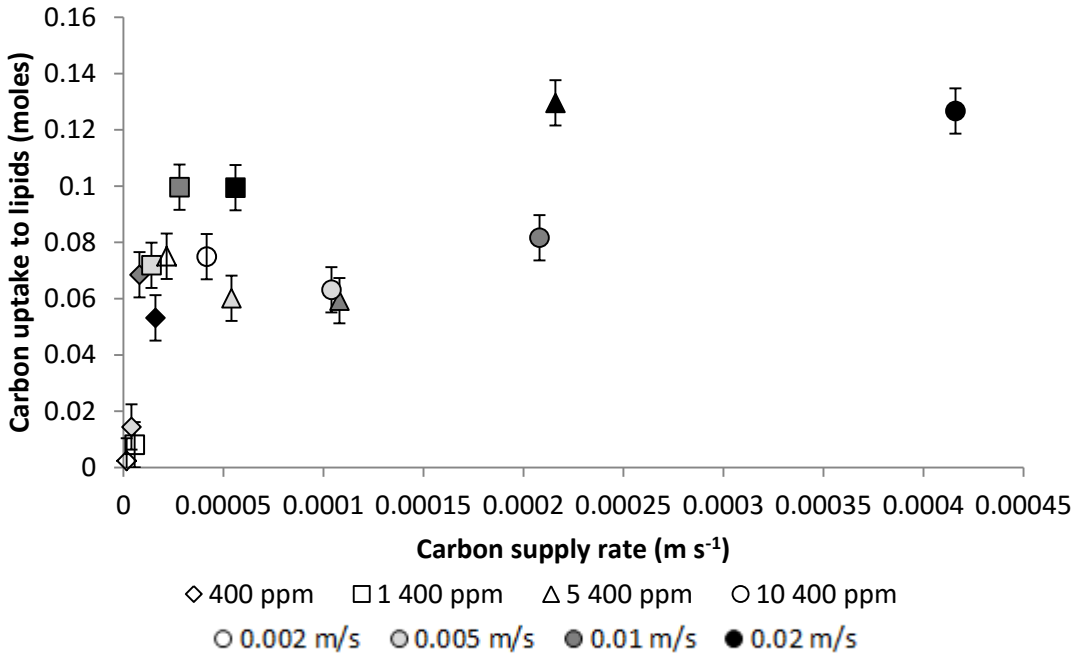

Figure 3.11 Carbon uptake, or the total number of moles of carbon fixed into lipids (calculated based on the moles of lipid produced, and the average number of moles of carbon in a mole of lipid), with respect to the CO_2 supplied to the reactor. Note: the deeper the shade of the point, the higher the $U_{Gr.}$ Error bars indicate the standard deviation calculated from n = 5 repeats under 'standard conditions' (0.008 moles).

In order to examine the energy efficiency of the ALR at the various gas velocities and CO_2 concentrations, the biomass and lipid productivity per unit power were calculated. These were based on the power input for aeration only and were calculated using 'total aeration power' equations (Section 2.5.1.2). At the 'standard' superficial gas velocity (0.02 m $s^{-1,}$) the energy required for aeration outweighed the biomass productivity and so productivity per unit power was low (Figure 3.12). For 0.002, 0.005 and 0.01 m s^{-1}, the biomass productivity per unit power was higher at 5 400 and 10 400 ppm CO_2 and dropped significantly at lower CO_2 concentrations. A maximum biomass productivity per unit power of 0.876 g W^{-1} d^{-1} was obtained at 0.002 m s^{-1} and 5 400 ppm CO_2, however, under these conditions the biomass concentration was only 1.49 g L^{-1} (compared to 2.15 g L^{-1} under 'standard conditions', Figure 3.6). A lower biomass concentration could lead to increased energy input required for harvesting and downstream processing, as well as a greater reactor volume required to yield the same amount of product. At 0.005 m s^{-1} and 5 400 ppm, on the other hand, the biomass productivity per unit power was 0.489 g W^{-1} d^{-1} and the biomass concentration was 2.08 g L^{-1}, indicating an improved power input and minor reduction in biomass compared to the 'standard conditions' (0.02 m s^{-1} and 10,400 ppm). Similar trends are seen in the

lipid productivity per unit power, but all these values were significantly lower than for biomass productivity, in the range 0.005 – 0.190 g W^{-1} d^{-1} (Figure 3.12B).

Figure 3.12 indicates that the energy efficiency of algal production can be optimised in sparged PBRs by considering the combined effects of sparging velocity and CO_2 concentration. Ketheesan and Nirmalakhandan (2012) investigated the biomass productivity of an airlift driven raceway in comparison to bubble columns, airlift and tubular PBRs reviewed from literature. Their study reports productivities in the range 0.1 to 0.7 g W^{-1} d^{-1} for these bioreactors, using power calculations that include light provision (not included in this work), and do not take into account the inlet pressure of gas in the pipe to the sparger (included in this work). Assuming an inlet gas pressure of 2 bar and disregarding energy for light provision, the productivity per unit power of the airlift driven raceway from Ketheesan and Nirmalakhandan (2012), recalculated using 'total aeration power' (Section 2.5.1.2), would be 0.8 g W^{-1} d^{-1}, comparable to the 0.876 g W^{-1} d^{-1} obtained in this work. Jorquera et al. (2010) review power (Sierra et al., 2008) and volumetric biomass productivities (Cheng-Wu et al., 2001) for a flat-panel reactor that give productivities per unit power of 0.1 – 0.5 g W^{-1} d^{-1}, assuming an inlet gas pressure of 2 bar and disregarding energy for light provision. These ranges, re-calculated from literature data, are within the range found for the ALR in this work (Figure 3.12). Due to differences in power calculations, choice of inlet gas pressure and sparger type, it is difficult to compare energy efficiencies across reported studies directly. This is will be discussed in detail in Chapter 6.3.1.

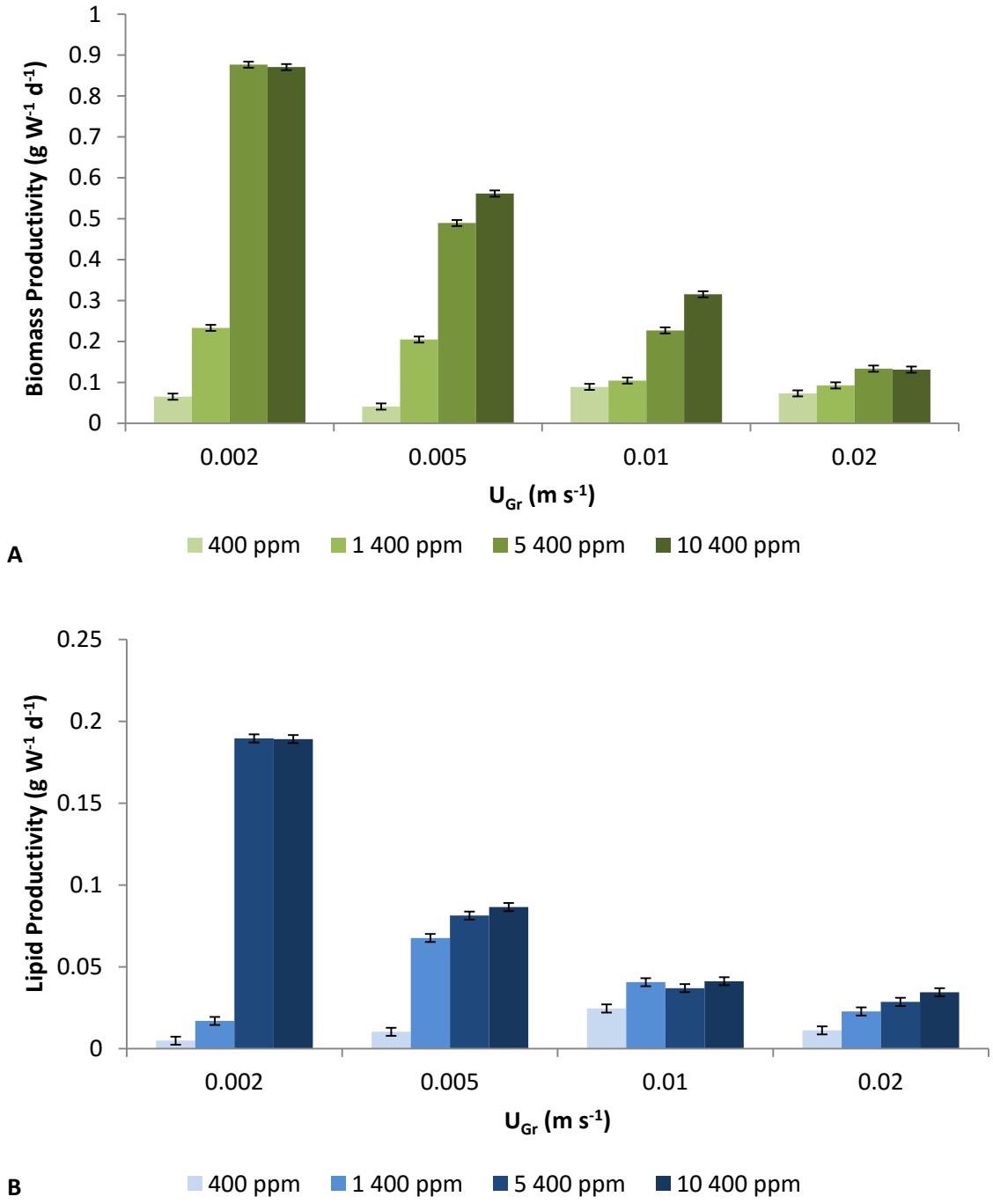

Figure 3.12 (A) Biomass and (B) lipid productivity per unit power (g W^{-1} d^{-1}) at increasing superficial gas velocity and CO_2 concentration. Error bars indicate the standard deviation calculated from n = 5 repeats under 'standard conditions' (0.07 g W^{-1} d^{-1} biomass productivity; 0.002 g W^{-1} d^{-1} lipid productivity).

3.3.3 Comparison at double light

All previous experiments in ALRs were performed at an average light intensity at the far side of the reactor of 148 µmol m^{-2} s^{-1}, totalling 9 µmol s^{-1} given the surface area of the ALRs. To investigate the effects of increased light on algal growth and lipid production, a second set of lights was added giving an average light intensity of 300 µmol m^{-2} s^{-1}, and a total light of 18 µmol s^{-1}. At double light there was an increase in the biomass productivity (Figure 3.13A). At 0.02 m s^{-1} the biomass productivity increased 1.4 times with double light. This is in accordance with studies by Bezerra et al. (2012) who report a 1.2 times increase in *Arthrospira platensis* biomass productivity at double the light intensity in a tubular PBR. These results suggest that the data shown in Section 3.3.2.2 at 0.02 m s^{-1} were light limited and further improvements to algal production efficiencies can be achieved at higher light. Commercial algal cultivation would be best outdoors under natural light, where light limitation would be considerably reduced.

Airlifts aerated at 0.005 and 0.01 m s^{-1} did not exhibit significant increases in productivity at double light (Figure 3.13). This may be due to the culture becoming carbon limited at increased light. Under increased light, growth rate increases leading to an increase in the carbon required by the culture for growth and lipid synthesis. This means that at higher light, the critical minimum CSR changes (Figure 3.14). At double light the CRS for biomass increased from 2.7×10^{-5} m s^{-1} (at 9 µmol s^{-1} light) to 1.0×10^{-4} m s^{-1} (18 µmol s^{-1}). However, at double light the maximum biomass concentration could still be reached at 0.01 m s^{-1} (half of the 'standard' gas velocity), indicating possible reductions in energy consumption with respect to carbon supply even under higher light intensities.

At 0.002 m s^{-1}, an increase in biomass productivity at double light suggests that the slow mixing at this gas velocity aggravated a light limitation, which was reduced when more light was provided. Similarly, lipid productivity increased at double light only at a sparging velocity of 0.002 m s^{-1} (Figure 3.13B). At sufficient CSR, as discussed in Section 3.3.2.2, low gas velocity resulted in a small dip in biomass and lipid concentration (Figure 3.7, Figure 3.8 and Figure 3.10), possibly caused by reduced mixing which lowers light distribution. At 0.002 m s^{-1} the doubled light intensity reduced this effect. This result is supported by a study in which *Scendesmus* sp. growth was modelled according to light path history in an ALR (Jones et al., In review).

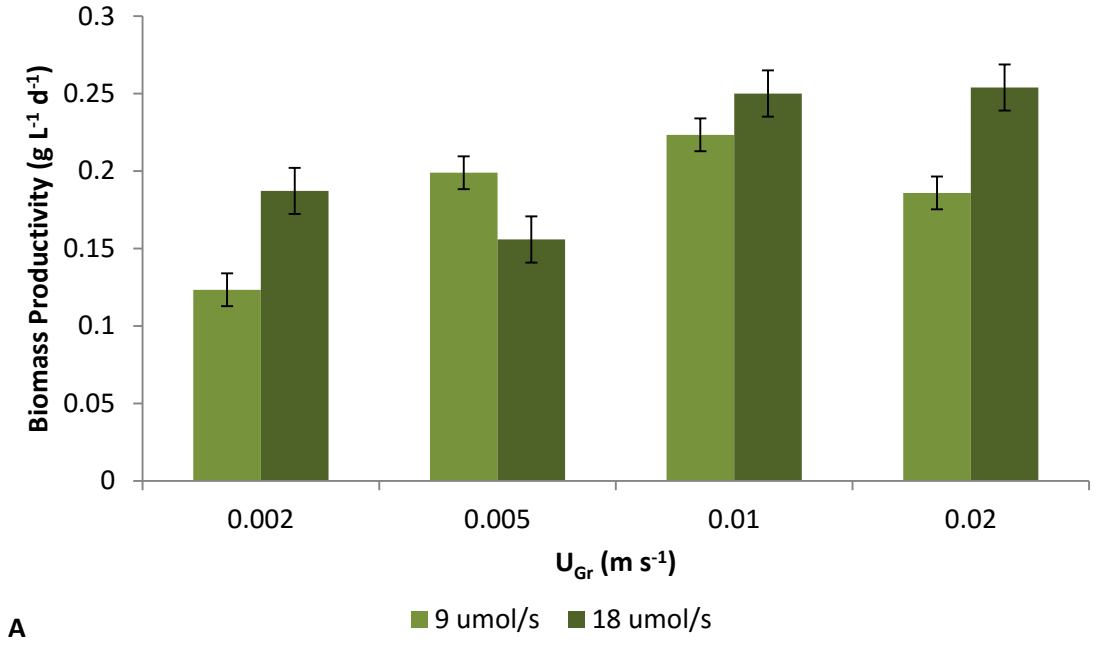

A

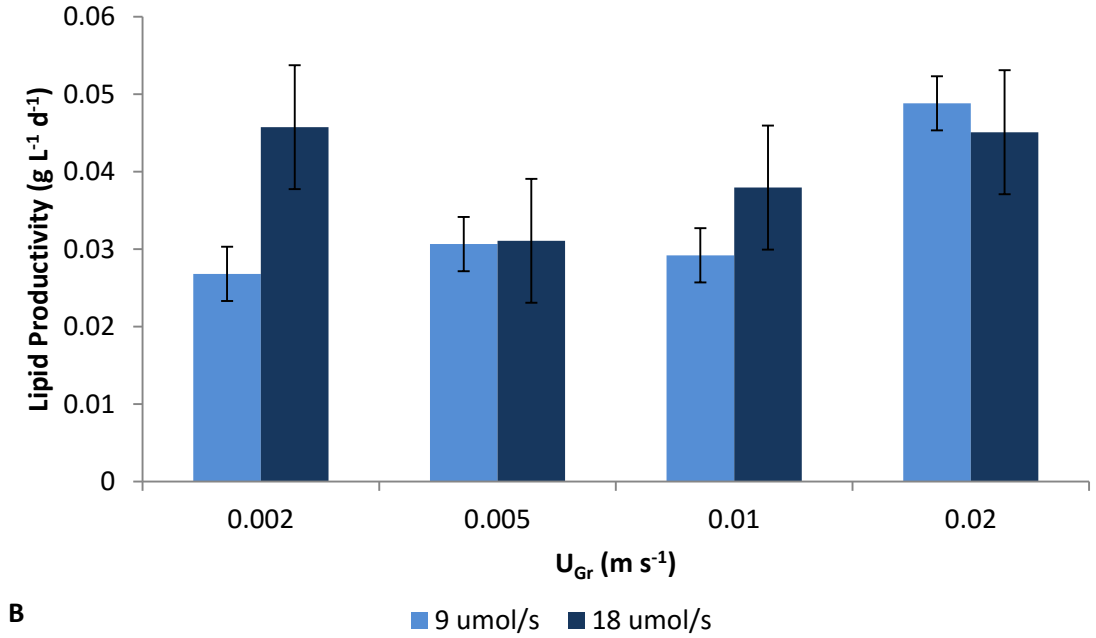

B

Figure 3.13 (A) Biomass and (B) lipid productivities of *Scendesmus* sp. grown in arlift photobioreactors at 10 400 ppm CO_2 and a total light of 9 or 18 umol s^{-1}. Error bars indicate the standard deviation calculated from n = 5 repeats under 'standard conditions' at 9 µmole s^{-1} (0.01 g L^{-1} d^{-1} biomass; 0.0035 g L^{-1} d^{-1} lipid) and n = 2 repeats at 18 µmole s^{-1} (0.015 g L^{-1} d^{-1} biomass; 0.008 g L^{-1} d^{-1} lipid).

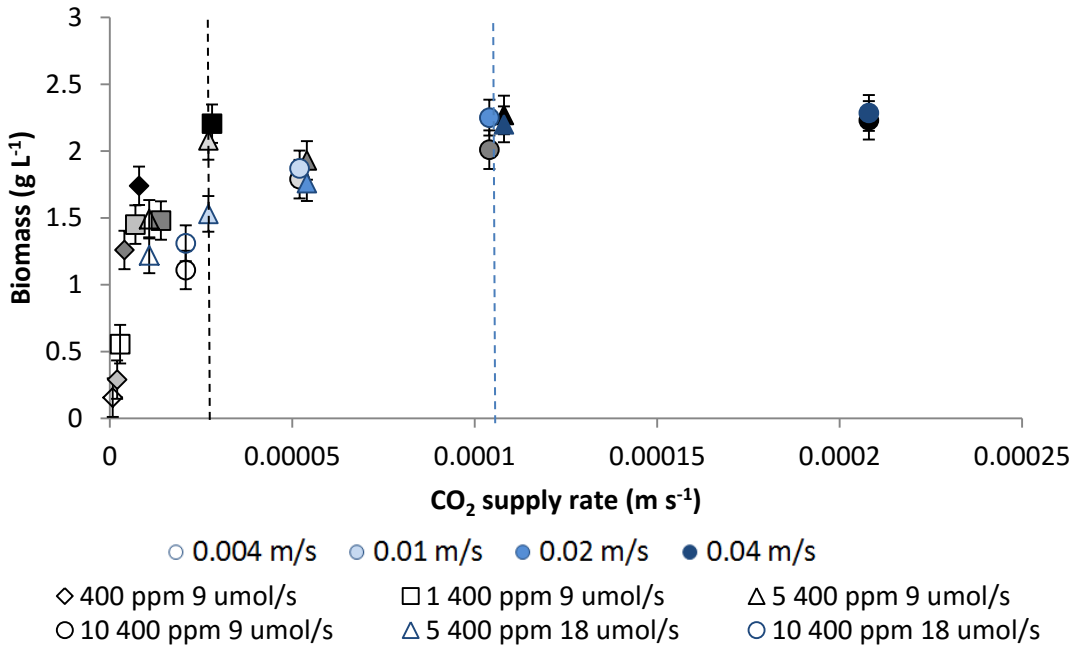

Figure 3.14 Maximum biomass concentration reached with respect to CO_2 supply rate (CSR) at increasing U_{Gr} and CO_2 concentrations in the sparged gas; a comparison at 9 and 18 umol s^{-1} total light. Dashed lines represent the critical minimum CSR at 9 (black) and 18 (blue) umol s^{-1} total light. Error bars indicate the standard deviation calculated from n = 5 repeats under 'standard conditions' at 9 µmole s^{-1} (0.144 g L^{-1}) and n = 2 repeats at 18 µmole s^{-1} (0.134 g L^{-1}).

Assuming that algal cultivation at large-scale will be outdoors and will rely on sunlight, power input was calculated according to gas velocity only. Therefore, increased productivity with increased light, led to increased productivity per unit power (Figure 3.15). Increased biomass and lipid productivity per unit power with double light was most pronounced at 0.002 m s^{-1}, where power input was lowest.

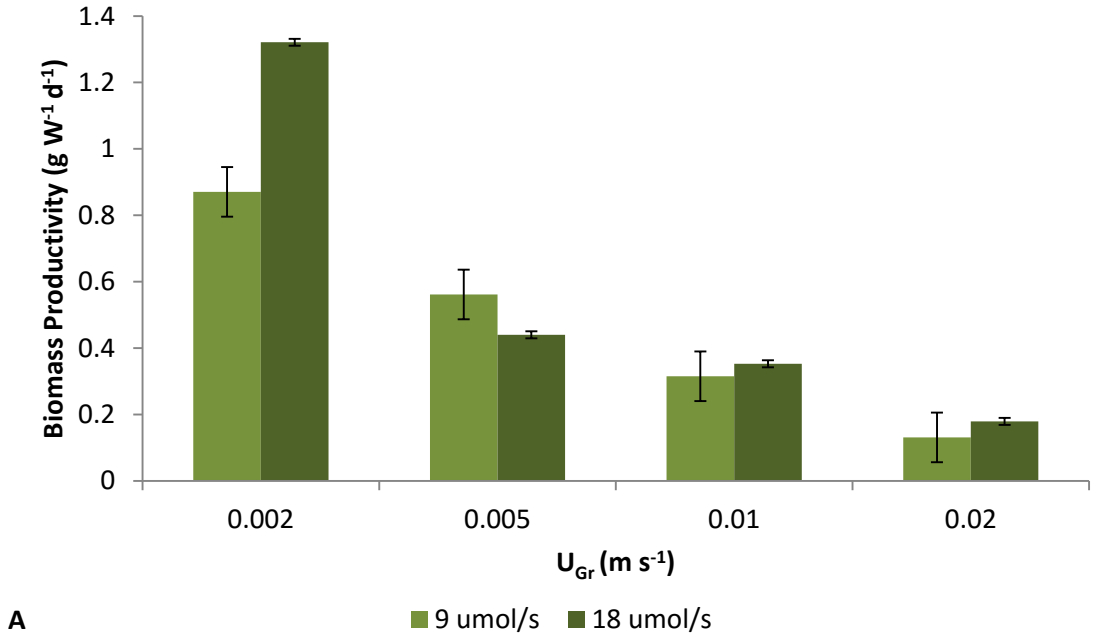

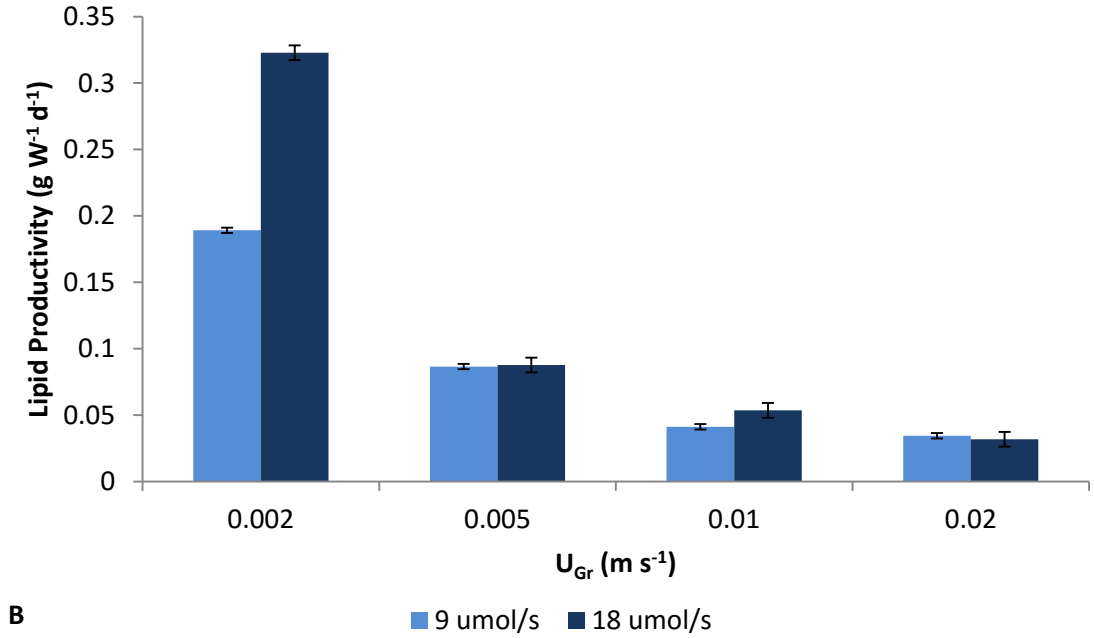

Figure 3.15 (A) Biomass and (B) lipid productivities per unit power for aeration of *Scendesmus* sp. grown in arlift photobioreactors at 10 400 ppm CO_2 and a total light of 9 or 18 umol s^{-1}. Error bars indicate the standard deviation calculated from n = 5 repeats under 'standard conditions' at 9 µmole s^{-1} (0.07 g W^{-1} d^{-1} biomass; 0.002 g W^{-1} d^{-1} lipid) and n = 2 repeats at 18 µmole s^{-1} (0.011 g W^{-1} d^{-1} biomass; 0.006 g W^{-1} d^{-1} lipid).

3.4 Conclusions

Previous studies have shown improved lipid accumulation in microalgae at reduced nitrate concentration in algal growth media. This work demonstrated that a starting nitrate concentration of 150 mg L^{-1} resulted in the highest lipid accumulation, total lipid concentration and lipid productivities by *Scenedesmus* sp., of the nitrate concentrations tested (150 – 700 mg.L^{-1}). Further reduction in nitrate concentration could result in additional cellular lipid accumulation, but at the risk of substantially lowering biomass productivities, and thus total lipid yield (Griffiths et al., 2014a). Therefore BBM containing 150 mg L^{-1} nitrate was used for all subsequent experiments, in order to promote lipid production.

Energy efficiency is an important consideration for algal bioprocesses, particularly for the effective production of algal bioenergy. This study sought to improve the energy efficiency of algal biomass and lipid production in the ALR by optimising superficial gas velocity and CO_2 concentration. At high CO_2 concentration in the gas phase (5400 – 10 400 ppm), the superficial gas velocity could be reduced fourfold (0.02 to 0.005 m s^{-1}) without substantial decrease in biomass concentration or productivity. This relates to a 75% reduction in power input, highlighting the importance of optimising aeration rate and CO_2 provision. On further reduction of superficial gas velocity (0.002 m s^{-1}) decreased biomass formation was observed. This could be attributed to compromised mixing. On sparging with gases of lower CO_2 concentration (400 – 1400 ppm), loss of productivity was observed with decreasing superficial gas velocity. This indicated CO_2 limitation, increasing in severity at lower gas velocities.

Aeration rate and CO_2 concentration were considered using the combined term, carbon supply rate (CSR, also termed CO_2 superficial velocity). A critical value for the CSR was found which, if exceeded, had no further benefit to productivity; this has not been reported previously. The power input for aeration could thus be optimised with respect to CO_2 concentration and gas velocity. By considering this approach, the biomass productivity per unit power could be increased by 1.8 times at appropriate biomass concentrations and 6.7 times at reduced biomass concentrations. The lipid productivity per unit power also increased at lower superficial gas velocity. Lipid productivity per unit power was considerably lower (in the range 0.005 – 0.19 g W^{-1} d^{-1}) than that of biomass (0.04 – 0.88 g W^{-1} d^{-1}) due to a lipid content of approximately 30% of the *Scenedesmus* sp. biomass. It

follows that it would be more energy efficient to use the whole biomass (lipid and remaining biomass) for bioenergy production, underpinning the growing interest in hydrothermal liquefaction.

When the light intensity was doubled, increases were observed in algal biomass productivity, indicating that light was a limiting factor in the initial experiments. This is an indication that under cultivation in an outdoor algal facility, where sunlight intensities far exceed those of artificial lighting under laboratory conditions, the algal biomass productivities, and thus energy efficiency with respect to sparging power may increase further. Cultivation of *Scenedesmus* sp. in ALRs outdoors would be an interesting additional study to show the magnitude of increased productivity, and the effects on the energy efficiency of the reactor.

This chapter demonstrates that airlift bioreactors can optimised according to their mixing and mass transfer rates for improved energy efficiency of algal biomass and lipid production. In Chapter 4 and 5, surface aerated PBRs are explored as potential alternatives to the ALR.

4 Oscillatory Baffled Photobioreactor: Design and optimisation for cultivation of *Scenedesmus* sp.

4.1 Introduction and Literature Review

The previous chapter (Chapter 3) describes the airlift photobioreactor, a common reactor for algal cultivation that relies on gas sparging for mixing and mass transfer. This chapter is the first of three (Chapters 4 to 6) to explore alternative approaches to providing mixing and mass transfer to an algal culture using surface aeration. This chapter focuses on the design, investigation and optimisation of an oscillatory baffled photobioreactor (OBR) for algal cultivation.

Oscillatory flow has been presented as an interesting method for enhancing mixing and mass transfer for a variety of applications in the chemical and bioprocess industries (Ghazi et al., 2008; Melendi et al., 2012; Ni et al., 2003, 2002, 1995; Stonestreet and Harvey, 2002). Oscillating reactors include tube/column reactors containing fixed baffles with liquid pulsed through the tube; or baffles connected to an oscillating piston (Ni et al., 2003, 1998). In both cases, the oscillating motion causes vortices to form between each baffle so that radial mixing is superimposed onto axial flow through the baffles, as in Figure 4.1, (Harvey et al., 2003, 2001; Ni et al., 2003).

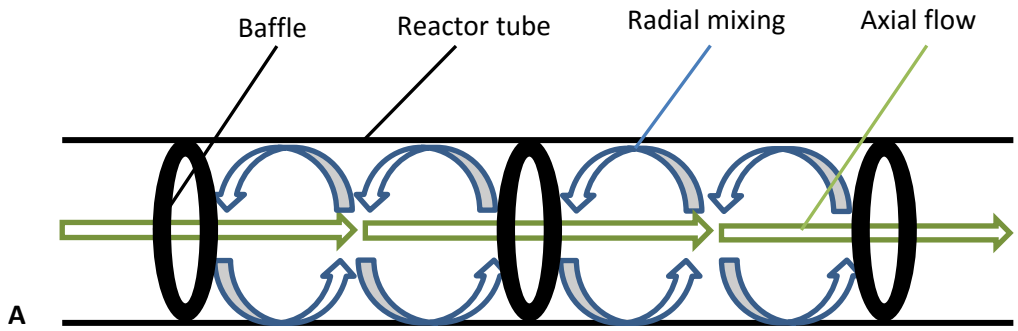

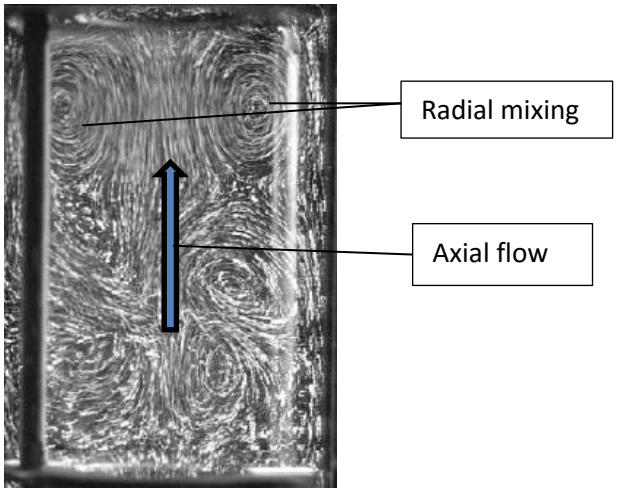

B

Figure 4.1 (A) Diagram of radial mixing (blue arrows) and axial flow (green arrows) in an oscillatory flow reactor containing donut baffles (black); (B) Photograph of flow pattern captured in an oscillatory baffled column showing axial flow (in directions of arrow) and radial mixing (spirals or eddies) (Ni et al., 2003).

4.1.1 History of oscillatory flow and oscillating reactors

The earliest reported applications of oscillatory flow were in the 1950s for enhanced solvent extraction in pulsed packed columns. The fluid was pulsed through a column, containing fixed plates or packings, either by the action of a piston or by an alternating supply and exhaust of air (Ni et al., 2003, 1998). The first reciprocating plate column was developed in the 1950s, also for enhanced solvent extraction (Karr, 1959). The plates consisted of a large number of closely spaced holes. The movement of these plates resulted in small-scale eddies to drive mixing, rather than the defined vortices produced in the more recent pulsed baffled and oscillatory baffled columns which contain annular (donut) baffles (Ni et al., 2003).

Oscillatory flow was first used for the enhancement of gas-liquid mass transfer when Baird and Garstang (1972) applied pulsation to a bubble column containing baffle plates. Bellhouse (1973) used oscillatory flow in furrowed channels for enhanced blood oxygenation. Studies on oscillatory flow for a wider variety of applications started in the 1980s (Mackley and Ni, 1991; Ni et al., 2003). Hewgill et al. (1993) reported a six-fold increase in the $k_L a$ for the mass transfer of oxygen into water in the presence of baffles and oscillations in a vertical tubular reactor. Hewgill's energy calculations suggest that the oscillatory flow column operates more efficiently than a conventional stirred tank reactor (Hewgill et al., 1993). Table 4.1 shows other applications of oscillatory flow from 1959, including current uses, improvements and scale-up of this technology.

Table 4.1 Chronological list of applications of oscillatory flow, including maximum $k_L a$ values for reactors in which this was measured (blue highlighted), and those reactors used for biological processes (green highlighted), and those in a horizontal configuration (purple highlighted) (adapted from Ni et al. (2003)).

Reactor type	Year	Application	Description	$k_L a$ (h^{-1})	Freq.; ampl.; U_G	Power	Reference
Open reciprocating-plate extraction column	1959	Solvent Extraction	Oscillating baffles				Karr (1959)
Air-pulsed water column	1967	Improved gas hold-up and power dissipation	Vertical, fixed baffle plates or rings				Baird and Garstang (1967)
Pulsed bubble column	1972	Enhanced gas-liquid mass transfer	Vertical, batch, fixed baffles, sparged	540	Freq: 1.09 – 1.35 Hz Amp: 0 – 94 mm U_G: 0.026 m s^{-1}	126 W m^{-3}	Baird and Garstang (1972)
Furrowed Channel Oxygenator	1973	Enhanced gas-liquid mass transfer	Furrowed channel				Bellhouse (1973)
Furrowed Channel	1985	Enhanced mixing (dispersion)	Furrowed channel				Sobey (1985)
Baffled U-shaped duct	1989	Enhanced mixing and observation of flow patterns	U-shaped, sharp edges and baffles				Brunold et al. (1989)
Baffled tubes	1989	Enhanced mixing and residence time distribution	Horizontal, batch, fixed triangular baffles				Dickens et al. (1989)
Pulsed baffled tube	1991	Mixing and dispersion	Fixed baffles, horizontal and vertical tubes				Mackley and Ni (1991)
Pulsatile flow bioreactor	1992	Bacterial cultivation	Vertical, fixed baffles, pulsed liquid				Harrison and Mackley (1992)
Oscillatory baffled tube	1993	Enhanced gas-liquid mass transfer	Vertical, 3 baffle types (orifice, central, helical), oscillating baffles	108	Freq: 0 – 8 Hz Amp: 0-6 mm U_G: 0.00042 – 0.0024 m s^{-1}	600 W m^{-3} (Osc and aeration)	Hewgill et al. (1993)
Baffled tube arrays	1993	Enhanced mixing	Array of vertical tubes, fixed baffles				Mackley and Ni (1993)
Pulsed baffled bioreactor	1995	Mass transfer in yeast	Vertical, batch, sparged, fixed baffles	450	Freq: 9 Hz; Amp: 10 mm; Aeration: 0.5 vvm	7700 W m^{-3} (Osc only)	Ni et al. (1995)

Reactor type	Year	Application	Description	$k_L a$ (h^{-1})	Freq.; ampl.; U_G	Power	Reference
Baffled tube	1995	Heat transfer	Horizontal heat exchanger, oscillating baffles, no aeration		Freq: 2.5 Hz Amp: 2.1mm	90 W m^{-3}	Mackley and Stonestreet (1995)
Pulsed baffled reactor	1996	Scale-up, mass transfer	Vertical, batch, sparged, fixed baffles, 50 mm diameter column vrs 100 mm	324	Freq: 3 – 8 Hz Amp: 4, 8, 12 mm U_G: 0.0021 – 0.0085 m s^{-1}	1000 W m^{-3}	Ni and Gao (1996)
Oscillatory Baffled column	1998	Enhanced mixing (wrt baffles free area, baffle thickness, baffle spacing)	Fixed baffles and oscillating baffles; vertical				Ni et al. (1998)
Baffled tube reactors	1999	Enhanced mixing and residence time distribution	Vertical, U-bend, no air, fixed baffles				Stonestreet and Van Der Veeken (1999)
Oscillatory flow parallel-plate electrochemical reactor	1999	Reduction of ferricyanide	Fixed baffles/plates				Carpenter and Roberts (1999)
Continuous oscillatory baffled reactor	2001	Droplet size for suspension polymerisation	Continuous, fixed baffles, sequence of vertical tubes				Pereira and Ni (2001)
Continuous oscillatory flow reactor	2001	Production of sterols from an ester saponification reaction	Continuous, fixed baffles, two tubes connected with U-bend				Harvey et al. (2001)
oscillatory baffled reactor	2002	Polymer product engineering	Batch, vertical, fixed baffles				Ni et al. (2002)
Oscillatory flow reactor	2002	Scale-up (polymer / sterol production)	Horizontal, not aerated, continuous				Stonestreet and Harvey (2002)
Continuous oscillatory flow reactor	2003	Biodiesel production from rapeseed oil (process intensification)	Continuous, two vertical tubes connected with U-tube				Harvey et al., (2003)
Pulsed-baffled tubular photochemical reactor	2003	Degradation of the pollutant, salicylic acid by photocatalytic oxidation	Fixed baffles				Gao et al. (2003)

Reactor type	**Year**	**Application**	**Description**	$k_L a$ **(h^{-1})**	**Freq.; ampl.; U_G**	**Power**	**Reference**
Pulsed sieve plate column	2003	Emulsion polymerisation	Continuous, fixed baffles containing many closely spaced holes				Palma and Giudici (2003)
Oscillatory baffled fermenter	2005	Biopolymer production (pullalan)	Oscillating baffles, vertical column, batch				Gaidhani et al. (2005)
Oscillatory baffled reactor	2005	Heat transfer enhancement	Helical oscillating baffles,				Solano et al. (2012)
Oscillatory flow meso reactor	2007	Biodiesel production (transesterification reaction)	Batch vs continuous, vertical, smooth periodic constriction tube (inner tube)				Zheng et al. (2007); Zheng and Mackley (2008)
Oscillating grid flotation cell	2008 2012	Flotation kinetics	Oscillating grid baffles				Changunda et al. (2008); Massey et al. (2012)
Oscillatory baffled column	2010	Cyclopentane hydrate production	Fixed orifice baffles, vertical, batch				Brown and Ni (2010)
Meso-scale Oscillatory baffles reactor	2010 2012	For laboratory use, and designed for direct scale-up	Integral, helical or axial circular baffles (fixed), sequence of vertical tubes, continuous				Phan and Harvey (2010, 2012)
Oscillatory flow reactor	2015	Algal lipid production	Horizontal tubular reactor, oscillating baffles	17	Freq: 0.7 Hz U_G: 0.01 m s^{-1}	552 W m^{-3}	THIS WORK

4.1.2 Key improvements to oscillatory flow reactors with regards to mixing and mass transfer

Many of the earlier studies on oscillatory flow, as well as some current studies, described reactors fitted with fixed baffles with oscillation or pulsation of the fluid through the baffles driven externally (Baird and Garstang, 1972; Brown and Ni, 2010; Hewgill et al., 1993; Ni et al., 2002, 1995). However, some recent designs for the oscillatory baffled rectors achieved oscillatory flow through oscillating baffles attached to a rod-shaped piston(s) (Changunda et al., 2008; Gaidhani et al., 2005; Ni et al., 1998; Solano et al., 2012).

Hewgill et al. (1993) compared the mass transfer of oxygen into water for a vertical tubular reactor containing three different baffle types: orifice (wall), central and helical (Figure 4.2). The results from this study showed that the orifice baffles gave the highest oxygen uptake rates (Hewgill et al., 1993). Mackay et al. (1991) supported this conclusion, and many subsequent studies on oscillatory flow used orifice (donut) shaped baffles (Gaidhani et al., 2005; Harvey et al., 2003; Ni et al., 1998, 1995; Ni and Gao, 1996; Stonestreet and Van Der Veeken, 1999).

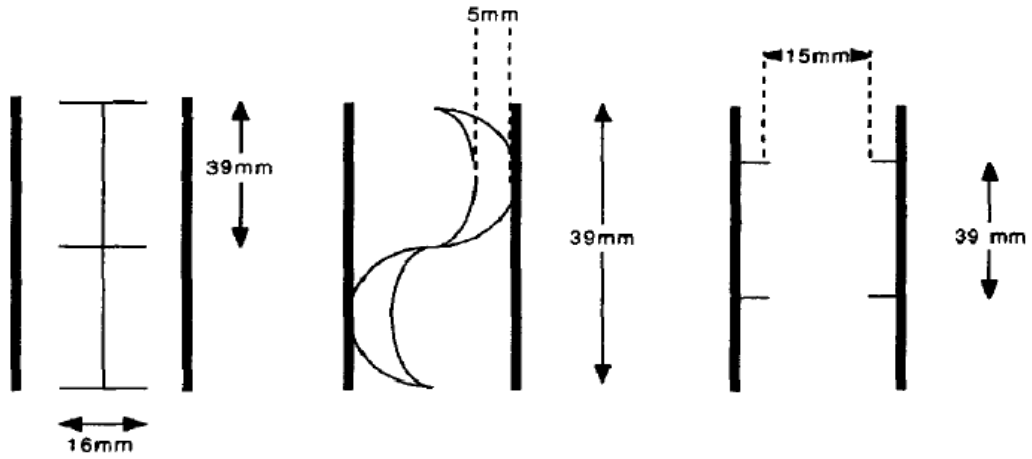

Figure 4.2 Diagrams of central, helical and orifice baffles from Hewgill et al. (1993).

Ni et al. (1998) reported a comprehensive study on the effects of baffle thickness, baffle free area and baffle spacing on the mixing time achieved in a vertical oscillatory baffled column. They concluded that a reactor containing oscillating baffles (as opposed to pulsed fluid) has optimum

mixing with a baffle thickness of 2-3 mm, a diameter of the baffle free area 20-22% of the diameter of the column, and a baffle spacing of 2 times the diameter of the column.

Ni et al. (2003) reviewed the mixing enhancements achieved though oscillatory flow for a variety of applications, and described studies that show improved heat and mass transfer, residence time distributions and shear rates using oscillatory flow compared to conventional reactors. A number of studies reported that scale-up of oscillatory flow reactors is linear and predictable (Jian and Ni, 2005; Ni et al., 2003; Ni and Gao, 1996). Ni and Gao (1996) reported improved mass transfer in large diameter reactor (100 mm) compared to a small diameter (50 mm) and that the scale-up correlation for mass transfer in pulsed baffled reactors was linear. Jian and Ni (2005) demonstrated that scale-up of the mixing properties and fluid velocities in oscillatory baffled columns can be achieved by scaling the diameter of the column.

Recently, two laboratories re-examined helical baffles (Phan and Harvey, 2010, 2012; Solano et al., 2012). It was reported that helical baffles and integral baffles, consisting of smooth periodic constrictions, (shown in Figure 4.3) were more practical at scale-up and more easily manufactured than the sharp periodic baffles of conventional oscillatory flow reactors. Reactors containing smooth baffles (helical or integral) have been developed for the production of biodiesel from oil via the transesterification reaction (Phan and Harvey, 2010; Zheng et al., 2007). Most recently, a paper describing tri-orifice baffles, and the computational modelling of the oscillatory flow when these were applied to a reactor, has been published. The report showed that tri-orifice baffles resulted in the same shear rates and mixing intensities in larger diameter tubes and so are useful for scale-up (Nogueira et al., 2013).

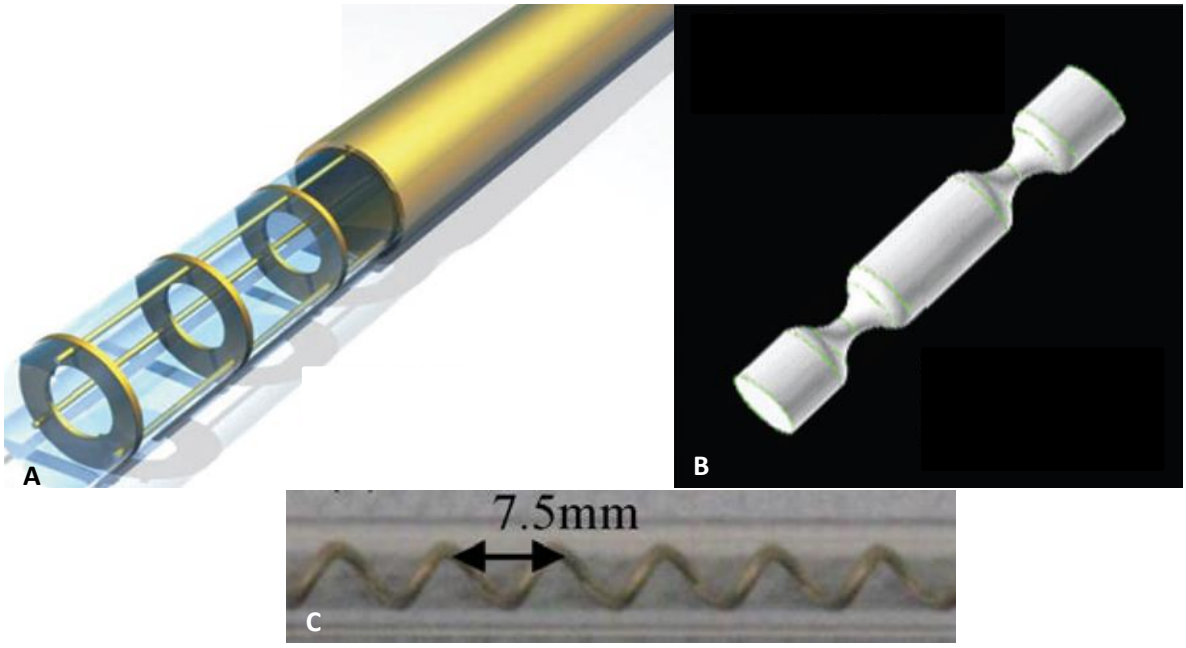

Figure 4.3 (A) Orifice baffled tube (Zheng et al., 2007); (B) integral baffles (Zheng et al., 2007); C: helical baffles (Phan and Harvey, 2010).

4.1.3 Novelty of this work

The oscillatory flow reactor described in this work is novel because it is the only oscillating-type reactor reported in the literature that is horizontal and aerated via a gas headspace (surface aeration). Oscillatory flow reactors are predominantly in the vertical orientation. All horizontal reactors in the literature are designed for chemical reactions that do not require gas, hence the tubes are completely filled with liquid (Table 4.1). The reactors in literature that are aerated, are all in the vertical orientation and aeration is via sparging (Table 4.1). This research project aimed to investigate surface aeration in comparison to sparging. The reason for choosing a horizontal configuration for the surface aerated oscillatory baffled reactor (OBR) is to increase the gas-liquid mass transfer via a headspace of gas that occupies the top third of the reactor tube. The novelty of this configuration means that although mass transfer, mixing intensities, shear rates and residence time have all been reported previously for oscillating-type reactors, none can be directly compared with the data obtained from this OBR.

Another significant feature of the literature is that, to our knowledge, there are only two reported uses of an oscillatory reactor for the growth of a microorganism: Ni et al. (1995) describe a vertical, aerated, batch column with fixed baffles and oscillating fluid for a yeast culture; and Harrison and

Mackley (1992) describe a vertical, pulsatile flow bioreactor with fixed baffles for growth of *Alcaligenes eutrophus* H16. There are no reports on the use of oscillating-type reactors for the culturing of algal species, as yet.

4.2 Materials and Methods

The OBR was designed as described in Section 2.3.2, consisting of a horizontal glass column held between two Teflon plates and containing baffles attached to an oscillating piston.

The mixing time (T_m) (Section 2.4.1), mass transfer coefficient ($k_L a_{CO_2}$) (Section 2.4.2) and power input (Section 2.5.2) were determined for a range of oscillating frequencies (0 to 0.7 Hz) at a constant centre-to-peak oscillation amplitude of 59 mm using three baffle types (donut, half-moon and perforated half-moon). This amplitude is defined as the distance moved by the baffles from their starting location to the furthest distance from the starting point.

Scenedesmus sp. were cultivated from 7 day-old stock cultures in the OBR using donut baffles at 0.2, 0.4 and 0.7 Hz. Air enriched with 1% CO_2 was continuously replenished in the headspace of the PBR at 0.2 L min^{-1}. Biomass and lipid concentrations were monitored throughout the 14 day growth cycles by measuring dry weight (Section 2.4.6) and total fatty acid content (Section 2.4.7).

4.3 Results and Discussion

4.3.1 Mixing

The mixing time (time taken to reach 95% homogeneity) in the OBR was measured by addition of a 5M NaCl tracer at various oscillation frequencies with each of the three baffle types, with subsequent determination of conductivity (AZ 86555 bench-top meter) (Figure 4.5). The conductivity probe was placed at the same end of the reactor as the tracer injection point, approximately 70 mm from the left side of the reactor (Figure 4.4). Mixing times were expected to improve (decrease) with increased agitation (oscillating frequency) (Ni et al., 1998), contrary to the

results in Figure 4.5. These results display relatively constant mixing times in the range 10 – 25 seconds for oscillation frequencies between 0.1 and 0.4 Hz for each baffle type. Half-moon and perforated half-moon baffles had higher mixing times (32 – 45 seconds) at higher frequencies (0.45 - 0.7 Hz), denoting a reduction in mixing. With donut shaped baffles the mixing time remained in the range 13 to 22 seconds at all oscillation frequencies. The best mixing time with donut baffles (13.3 seconds) was achieved at 0.3 Hz, above and below which mixing time increased slightly.

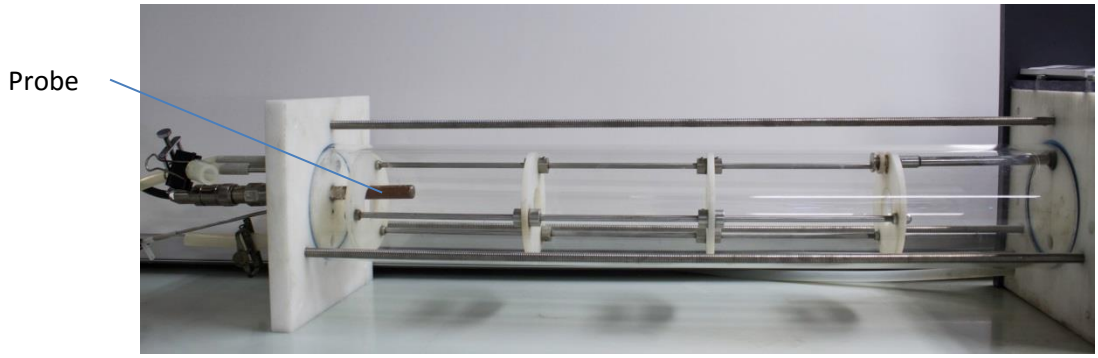

Figure 4.4 Oscillatory baffled photobioreactor containing donut baffles with probe inserted on the left side of the reactor, reaching 70 mm into the reactor.

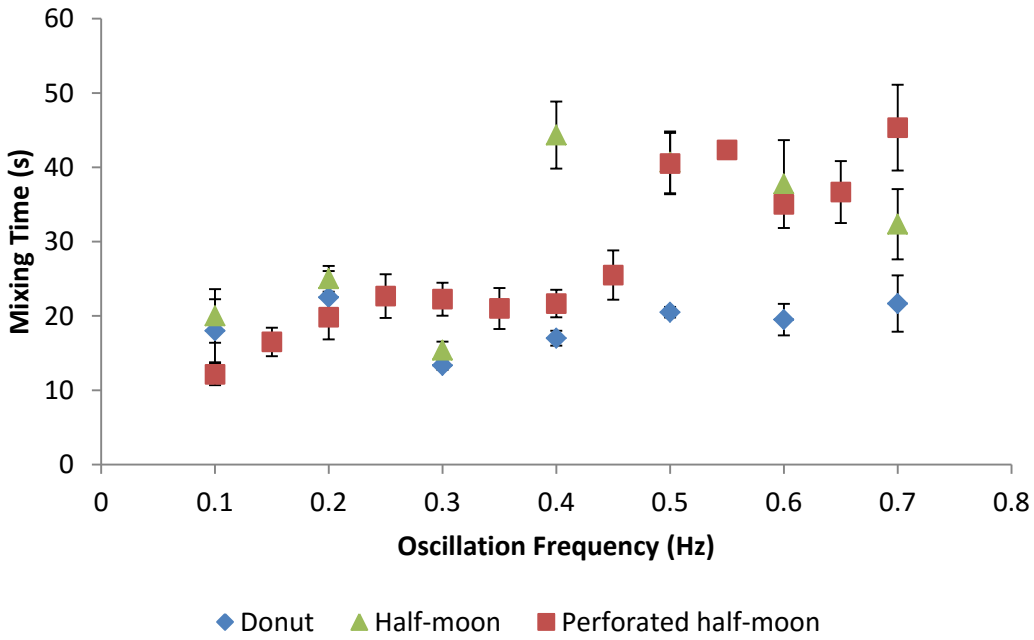

Figure 4.5 Mixing time at increasing oscillation frequency in an oscillatory baffled photobioreactor containing donut, half-moon or perforated half-moon baffles. Error bars indicate the standard deviation of n = 3 replicates.

Phenolphthalein indicator solution was used to visualise mixing patterns in the OBR. Slower mixing occurs with half-moon and perforated half-moon baffles at higher oscillation frequencies (seen in Figure 4.5) because the wave, created by baffle oscillation, collides with the returning wave. This resulted in poor transfer across the length of the reactor, affected by oscillation frequency, despite some individual inter-baffle compartments of the reactor being well mixed. Hence the tracer does not necessarily reach the section of the reactor furthest from the tracer injection point, and at high oscillation frequency the overall dispersion of the tracer in the reactor was reduced. This was demonstrated in the phenolphthalein experiments (Figure 4.6).

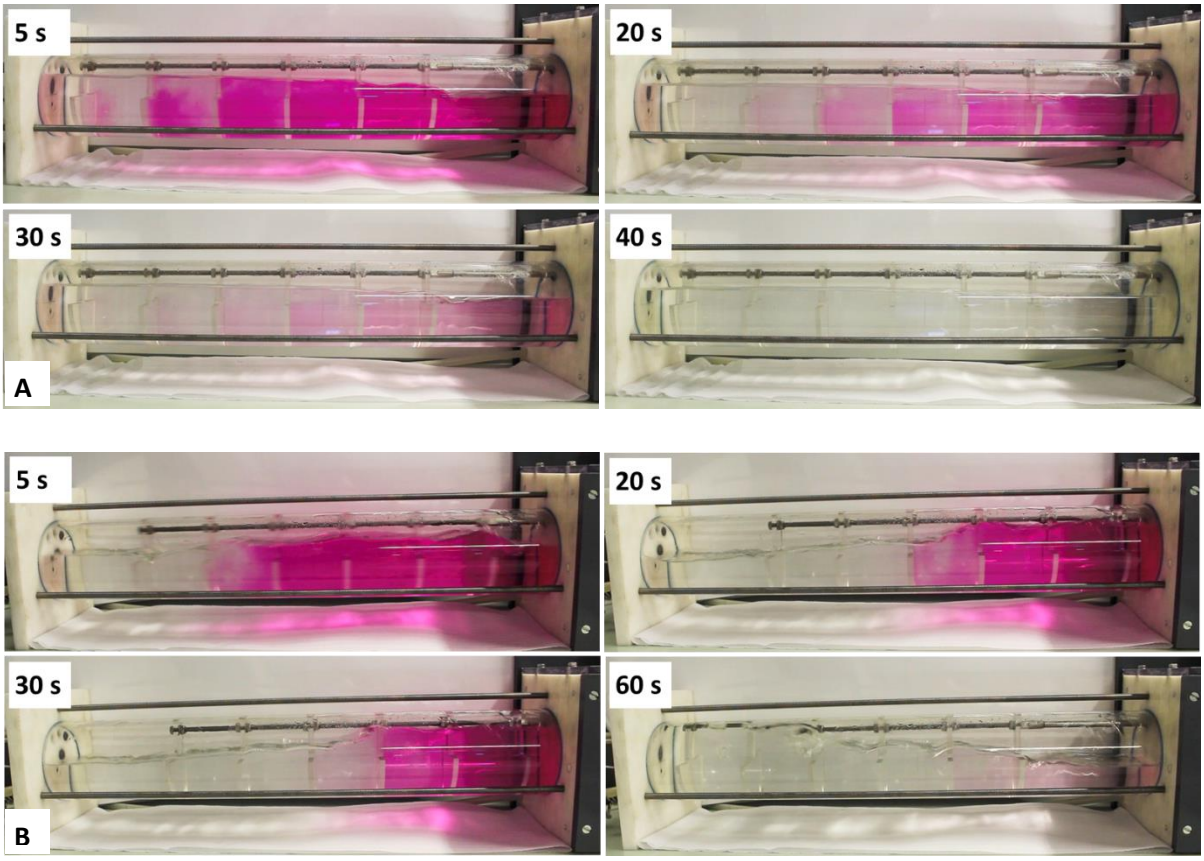

Figure 4.6 Time lapse photographs of the oscillatory baffled photobioreactor with half-moon baffles at (A) 0.2 Hz and (B) 0.7 Hz containing an alkaline solution and phenolphthalein indicator (pink) after addition of strong acid (colourless).

Figure 4.6A shows that at 0.2 Hz with half-moon baffles, complete mixing was achieved in 40 seconds, and 95% homogeneity was reached in under 30 seconds (in accordance with the conductivity tracer experiments). Figure 4.6B shows that at 0.7 Hz the alkaline solution (pink) remained in the far right of the reactor after 60 seconds, and 95% homogeneity was reached after

30 seconds (in agreement with NaCl tracer experiments). At 0.2 Hz (Figure 4.6A), and up to 0.4 Hz, the rapid tumbling of liquid over each consecutive baffle was noted, creating uniform eddies in each inter-baffle section. At these lower frequencies a wave of liquid moves back and forth in the reactor column in one direction at a time. At 0.7 Hz (Figure 4.6B), and all frequencies above 0.4 Hz, tumultuous mixing was noted, with two consecutive waves forming from each end plate of the reactor column that collide with each other, preventing transfer to the area furthest from the injection point.

Table 4.2 compares the mixing times across various reactor types, including those typically used for algal cultivation and a vertical oscillatory baffled column. The OBR described in this work has a range of mixing times lower (indicating faster mixing) than the majority of reactors in Table 4.1, comparable to the stirred tank reactor described by Camacho et al. (2011). This has significant advantages for the application of this reactor to algal cultivation and other bioprocess systems, as it results in homogenous suspensions where cells are well distributed and thus evenly exposed to nutrients and light.

Table 4.2 Comparison of mixing times across various reactor types, including photobioreactors (PBR) for algal cultivation.

Reactor type	Configuration	Mixing time	Reference
Oscillatory baffled PBR	Horizontal; 59 mm amplitude; 0.2 – 0.7 Hz frequency	12 – 45 s	This work
Oscillatory baffled column	Vertical; 0.02 m amplitude; 1 Hz frequency	50 – 100 s	Ni et al. (1998)
Stirred tank PBR		5 – 30 s	Camacho et al. (2011)
Bubble column PBR		50 – 120 s	Sánchez Mirón et al. (2004)
Airlift PBR		30 – 80 s	Jones and Harrison (2014)
Flat-panel PBR		80 – 200 s	Sierra et al. (2008)
Raceway		1.4 – 6 h	Mendoza et al. (2013)

4.3.2 Mass transfer

The mass transfer coefficient was measured in the OBR using the gassing-in method and corrected for the probe response time by using the equations described in Section 2.4.2. Increasing the oscillation frequency caused an increase in the mass transfer coefficient (Figure 4.7). Results showed that donut baffles provided superior mass transfer compared with half-moon baffles (Table 4.3 and Figure 4.7). The addition of perforations on half-moon baffles improved the mass transfer 1.5 times (5.9 to 9.5 h^{-1}), but remained 1.8 times lower than donut baffles (17.2 h^{-1}) at a frequency of 0.7 Hz (Table 4.3). Oscillating half-moon baffles caused a rippling or rolling wave over the top of the baffles that did not result in sufficient entrainment of gas (Figure 4.8A), which is necessary for gas-liquid mass transfer. Donut baffles moving through the column of liquid and gas allowed the liquid to pour through each baffle in turn (Figure 4.8B), providing more contact between gas and liquid, thus improving gas-liquid mass transfer. Likewise, Hewgill et al. (1993) and Mackay et al. (1991) found that donut baffles provided higher gas-liquid mass transfer than helical or wall baffles. Thus, the rolling wave with half-moon baffles in the OBR provided good liquid mixing but did not enhance the transfer of gas from the head space into solution.

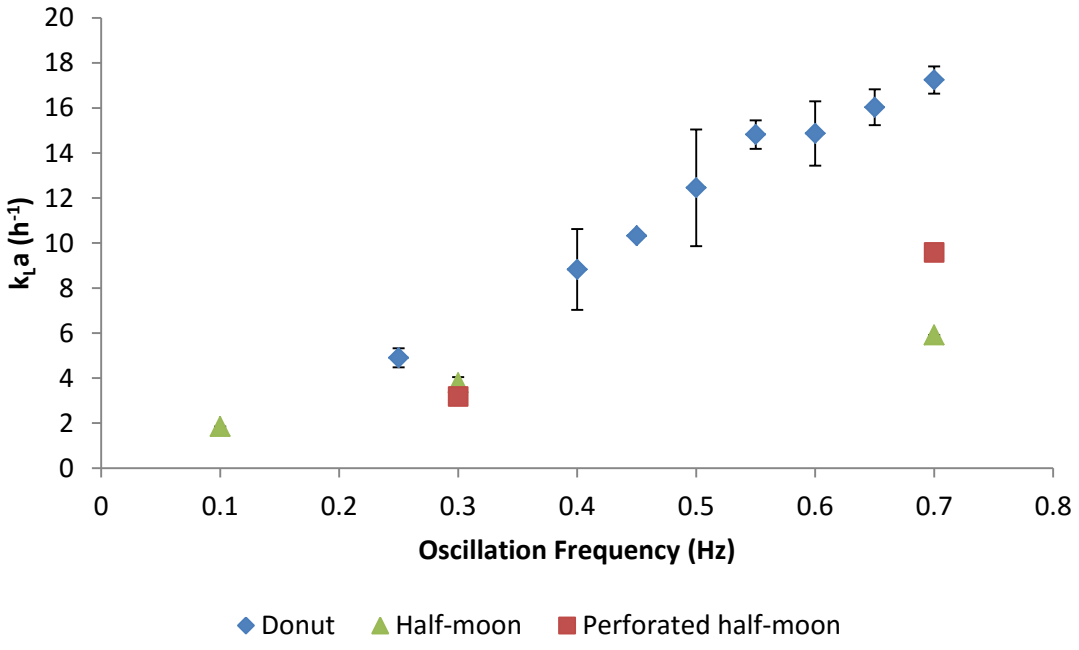

Figure 4.7 Mass transfer coefficient ($k_L a_{CO_2}$) on the oscillatory baffled photobioreactor at increasing oscillation frequency with donut, half-moon and perforated half-moon baffles. Error bars indicate the standard deviation of n = 3 replicates.

Table 4.3 The CO_2 mass transfer coefficient, $k_L a_{CO_2}$, obtained at the highest oscillation frequency (0.7 Hz) across three baffle types.

Baffle type	Maximum $k_L a_{CO_2}$ (h^{-1})	Oscillation frequency (Hz)
Donut	17.2	0.7
Half-moon	5.9	0.7
Perforated half-moon	9.5	0.7

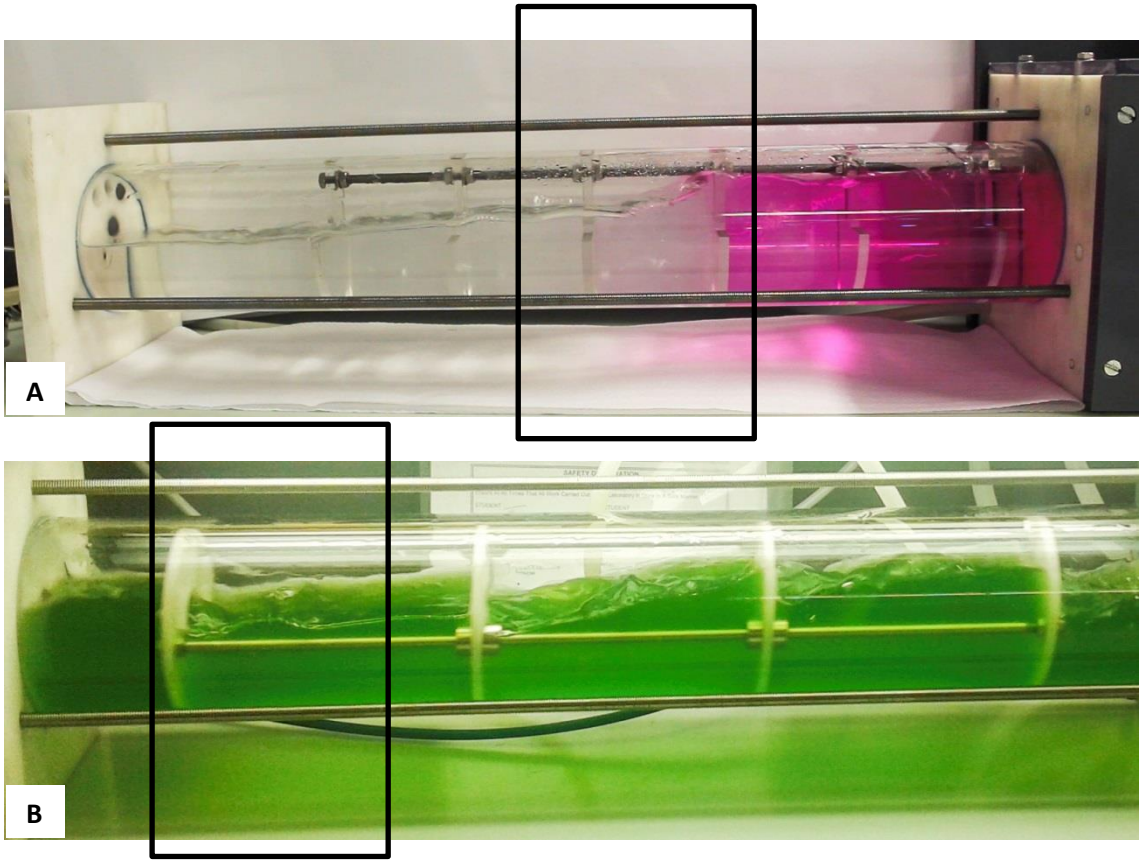

Figure 4.8 Oscillatory baffled PBR with donut baffles and half-moon baffles at 0.7 Hz. The outlined sections show the liquid rolling over the (A) half-moon baffles, or (B) pouring through the baffle free area of the donut baffles.

The power consumed by the OBR was measured using calorimetry (Section 2.5.2). Power input increased with oscillation frequency. In Figure 4.9 the increase in the mass transfer coefficient ($k_L a_{CO_2}$) with increased power input is shown, in agreement with previous studies (where power input were calculated theoretically) (Hewgill et al., 1993; Ni et al., 2003, 1995). This means that improved mass transfer comes at the price of increased energy input.

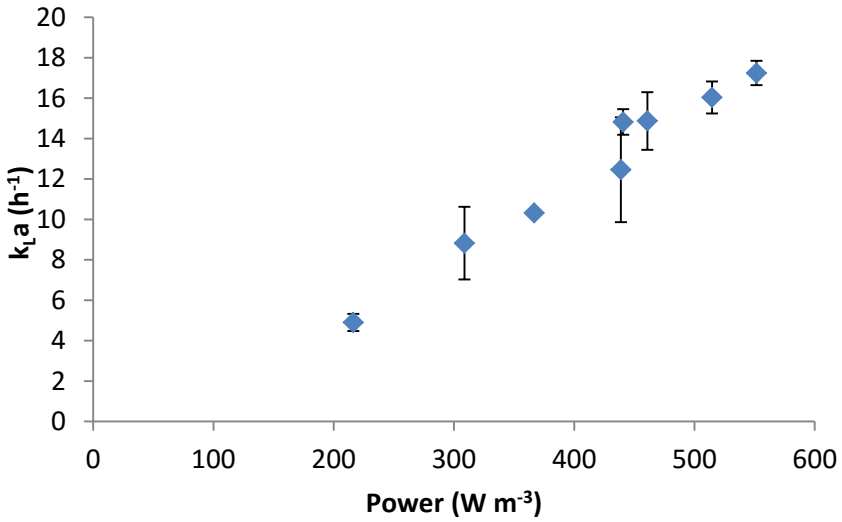

Figure 4.9 The relationship between volumetric power input and CO_2 mass transfer coefficient for the oscillatory baffled PBR with donut baffles at increasing oscillation frequency. Error bars indicate the standard deviation of n = 3 replicates.

Mass transfer coefficients reported in the literature are usually for oxygen, and so the $k_L a_{O_2}$ for the OBR was used for comparison to literature data. These values are slightly higher (4.9 – 17.2 h^{-1}) than $k_L a_{CO_2}$ (5.3 – 19.5 h^{-1}). The mass transfer in the horizontal OBR was lower than other oscillatory type reactors described in the literature (Table 4.4). Many previously reported oscillatory reactors were operated at frequencies above 1 Hz, amplitudes below 10 mm, and several include gas sparging (Hewgill et al., 1993; Ni et al., 2003, 1995; Ni and Gao, 1996). Furthermore, to date, all mass transfer studies are reported for vertical oscillatory reactors.

Increasing the oscillation frequency above 0.7 Hz and providing sparging to the OBR in this work could improve mass transfer, but at the cost of increased power input. Based on the information in Table 4.4, decreasing the oscillation amplitude at high oscillating frequency has the potential to provide higher mass transfer at comparable power input. For example, given a power input of 200 W m^{-3}, at approximately one tenth of the amplitude, and ten times the frequency used in this work, Ni et al. (1995) obtained a $k_L a$ 12-times higher (75.6 h^{-1}) than those reported here for the OBR (6.3 h^{-1}) (Table 4.4). However, the mass transfer behaviour in the vertical, sparged columns reported in literature will be considerably different to that of the horizontal, surface aerated OBR in this work. Increasing the oscillation frequency was shown to have little effect on mixing (Figure 4.5), as discussed in Section 4.3.1.

Photobioreactors with $k_L a$ as low as 1.8 to 21.6 h^{-1} have been reported to support algal cultivation (Brindley Alías et al., 2004; Sierra et al., 2008). To determine whether the OBR in this work can provide sufficient mass transfer for cultivation of *Scenendesmus* sp., this species was grown at three oscillation frequencies and the biomass and lipid concentrations recorded with time (Section 4.3.3).

Table 4.4 Reported power density and $k_L a_{O_2}$ in a variety of reactors and algal photobioreactors. Numbers in *italics* indicate the estimated $k_L a_{O_2}$ at 200 W m^{-3} extrapolated from reported graphs.

Reactor	Configuration	Power (W m^{-3})	$k_L a_{O_2}$ (h^{-1})	Reference
Oscillatory baffled PBR	Horizontal; no sparging; 59 mm amp.; 0.25 - 0.6 Hz freq.	216 – 461 *(200)*	5.3 – 17.5 *(5.3)*	This work
Pulsed baffled column	Vertical; sparged[1]; 4 – 14 mm amp.; 2 – 12 Hz freq.	200 – 6500 *(200)*	75.6 – 310 *(75.6)*	Ni et al. (1995)
Oscillatory flow reactor	Vertical; sparged; ≤ 6 mm amp.; ≤ 8 Hz freq.	100 – 500 *(200)*	64.8 – 108 *(79.2)*	Hewgill et al. (1993)
Stirred tank	Conventional; sparged	50 – 600 *(200)*	18 – 70.2 *(36)*	Hewgill et al. (1993)
Airlift	Conventional; algal cultivation	6 – 82	25.2 – 39.6	Jones and Harrison (2014)
Flat-panel PBR	Sparged; algal cultivation	5 – 55	1.8 – 21.6	Sierra et al. (2008)
Bubble column	Conventional; algal cultivation	25 – 500	14.4 – 151	Sánchez Mirón et al. (2004)

[1] Aeration power not included.

4.3.3 Biomass and lipid production

Donut baffles provided higher mass transfer rates than the half-moon and perforated half-moon baffles, and so were chosen for algal cultivation. *Scenedesmus* sp. was grown in the OBR at three oscillating frequencies (0.25 Hz, 0.4 Hz and 0.7 Hz) to investigate the relationship between power input, mass transfer and algal productivity. These oscillation frequencies correspond to $k_L a_{CO_2}$ of 4.9, 8.8 and 17.2 h^{-1}, respectively. Growth curves and lipid production under these conditions are shown in Figure 4.10 and Figure 4.11, respectively.

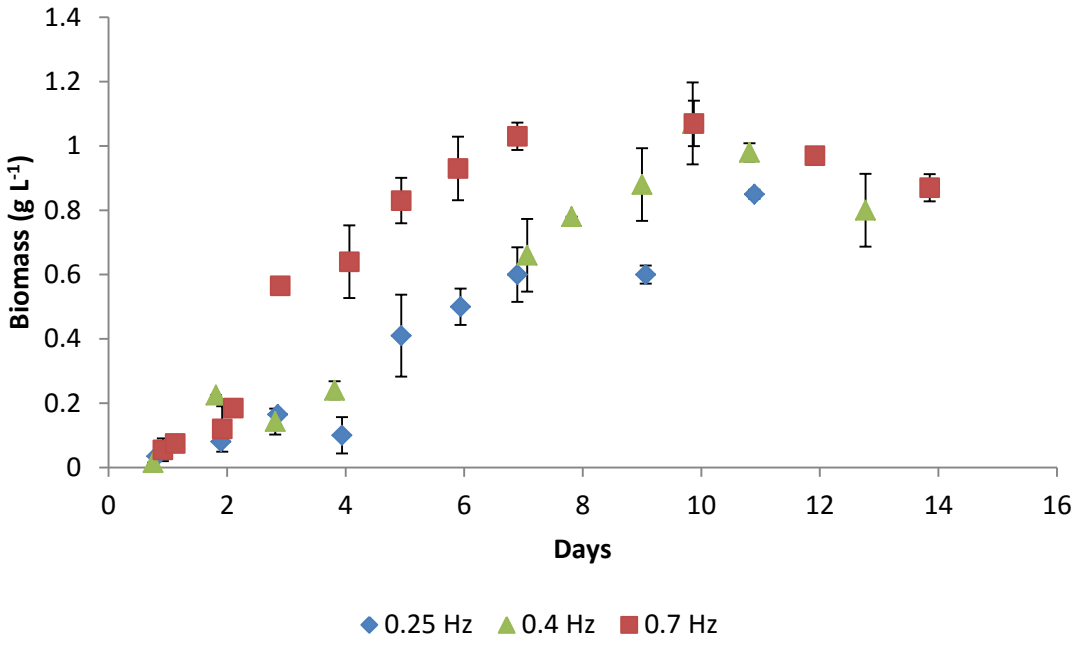

Figure 4.10 Growth curves of *Scenedesmus* sp. cultivated in the oscillatory baffled PBR with donut baffles at 0.25, 0.4 and 0.7 Hz ($k_L a_{CO_2}$ 4.9, 8.8 and 17.2 h^{-1}, respectively), 59 mm amplitude. Error bars indicate the standard deviation of n = 2 replicate dry weight samples.

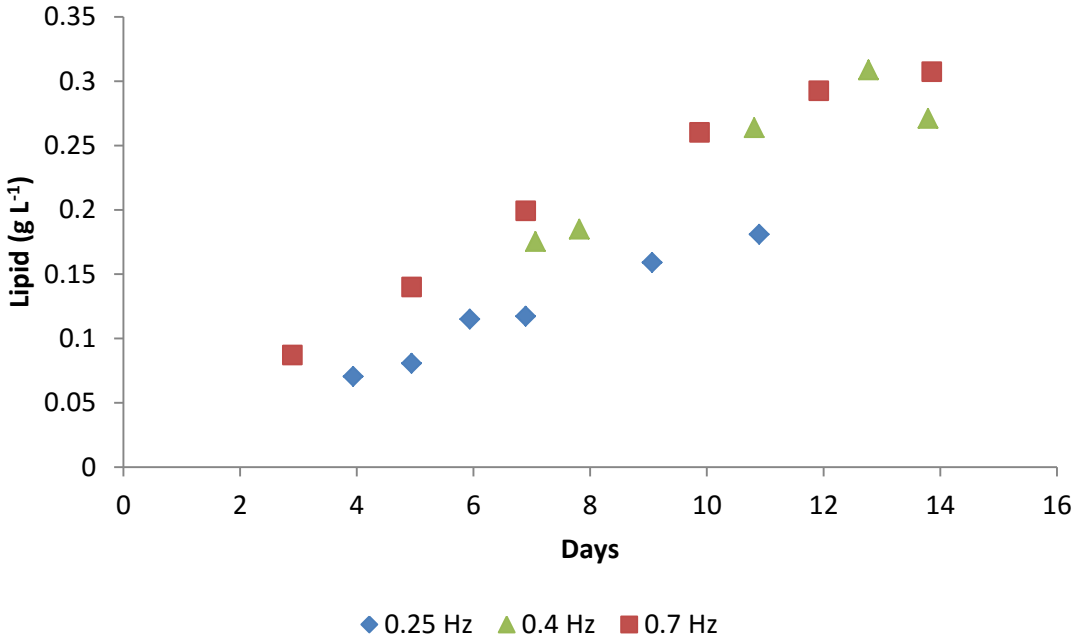

Figure 4.11 Lipid production by *Scenedesmus* sp. cultivated in the oscillatory baffled PBR at 0.25, 0.4 and 0.7 Hz ($k_L a_{CO_2}$ 4.9, 8.8 and 17.2 h^{-1}, respectively), 59 mm amplitude.

At 0.7 Hz, the culture was in exponential phase for the first three days, after which it entered linear growth until day 7 or 8 (Figure 4.10). The maximum biomass concentration reached at 0.7 Hz was 1.07 g L^{-1}, giving a biomass productivity of 0.11 g L^{-1} d^{-1}. At 0.7 Hz the lipid reaches a maximum of 0.31 g L^{-1} at 14 days, giving a lipid productivity of 21.9 mg L^{-1} d^{-1} (Figure 4.11). These values are within the range reported in an extensive review of biomass and lipid productivities for various species of *Scenedesmus* averaged across the literature (Table 4.5, Griffiths and Harrison (2009)). However, biomass and lipid productivities are lower in the OBR (0.11 and 0.02 g L^{-1} d^{-1}, respectively) than those reported in the ALR (0.17 and 0.03 g L^{-1} d^{-1}, respectively) and an airlift driven raceway pond (0.19 and 0.04 g L^{-1} d^{-1}, respectively) (Table 4.5). Although mixing times in the OBR were superior to a number of PBR configurations in the literature (Table 4.2), low mass transfer could be reducing the amount of CO_2 reaching the algal cells, and thus limiting biomass and lipid productivities. In sparged oscillatory flow reactors, radial mixing between baffles enhances gas-liquid mass transfer. However, in the surface aerated OBR, when the liquid was well mixed, there was little gas entrainment. Furthermore, the $k_L a$ values measured here represented the inter-baffle mass transfer closest to the air inlet (where the probe was placed), and may inconsistent across the length of the reactor.

The most commonly used method for increasing mass transfer in a reactor is to introduce sparged gas, which is energy intensive. Table 4.5 compares the biomass productivities per unit power in an airlift, airlift driven raceway, and the unsparged OBR. The OBR had comparable productivity per unit power (0.20 – 0.37 g W^{-1} d^{-1}) compared to the airlift (0.13 – 0.56 g W^{-1} d^{-1}) but lower than the airlift-driven raceway (0.8 g W^{-1} d^{-1}). However, the lower productivity per unit volume of the OBR compared to these reactors means that more materials, land area and capital cost would be required at large-scale. The energy efficiency of the OBR in comparison to other bioreactor types is discussed in detail in Chapter 6.

Previous reports discuss improved biomass production with increased CO_2 concentrations in the gas fed to the algal PBR, as high as 10% CO_2 (de Morais and Costa, 2007; Tang et al., 2011). Increasing the CO_2 concentration in the headspace of the OBR could be a low energy solution to improving CO_2 mass transfer without sparging. In this way the biomass and lipid production would increase with no increase in power input for sparging, resulting in further improvements to productivity per unit power.

Table 4.5 Volumetric biomass and lipid productivities, and biomass productivities per unit power, for various *Scenedesmus* species cultivated in a variety of photobioreactors. Power input for the airlift driven raceway were recalculated using 'total aeration power' (Section 2.5.1.2), for comparison with the reactors in this work.

Species	Reactor	Biomass ($g\ L^{-1}\ d^{-1}$)	Lipid ($g\ L^{-1}\ d^{-1}$)	Power ($W\ m^{-3}$)	Biomass ($g\ W^{-1}\ d^{-1}$)	Lipid ($g\ L^{-1}\ d^{-1}$)	Reference
Sc. sp.	OBR						This work
	0.7 Hz	0.11	0.022	551	0.20	0.04	
	0.4 Hz	0.09	0.024	309	0.29	0.08	
	0.25 Hz	0.08	0.017	216	0.37	0.08	
Sc. obliquus	[Averaged from literature]	0.12	0.025				Griffiths and Harrison (2009)
Sc. quadricauda		0.19	0.035				
Sc. costatum		0.08	0.013				
Sc. sp.	Airlift PBR						This work, Chapter 3
	2 L m^{-1}	0.19	0.049	1417	0.13	0.04	
	0.5 L m^{-1}	0.20	0.030	354	0.56	0.08	
Sc. sp.	Continuous airlift driven raceway	0.19	0.040	237	0.80	0.17	Ketheesan and Nirmalakhandan (2011)

4.4 Conclusions

The novel unsparged, horizontal oscillatory baffled photobioreactor (OBR) designed and tested in this work had good inter-baffle mixing in comparison to vertical oscillatory flow reactors as well as a variety of commonly used PBRs. An area of poor mixing was seen at the far end of the OBR, indicating poor transfer between baffle compartments, particularly at high oscillation frequency. Mass transfer was low in comparison to other reactors and could have been overestimated as the measurements were only taken at the end of the reactor closest to the gas inlet, and may not be consistent across the reactor. Mass transfer improved with increased frequency and thus increased power input. Comparison with previous reports on oscillatory flow reactors revealed that mass transfer could be further improved by, decreasing oscillation amplitude at high frequency, or addition of gas sparging. However, these reports describe vertical oscillatory flow reactors in contrast to the horizontal OBR. An alternative possibility for increased mass transfer in the OBR is by increasing the CO_2 concentration in the gas headspace.

Donut baffles provided higher mass transfer than half-moon and perforated half-moon baffles, due to higher contact between liquid and gas, and supported algal growth to 1.07 g L^{-1}. The algal productivity per unit power was higher at low oscillation frequency due to small differences in volumetric productivity and large differences in power input when the oscillation frequency was reduced. The algal productivity per unit power in the unsparged OBR (0.20 – 0.37 g W^{-1} d^{-1}) may be improved by increasing the CO_2 mass transfer rate, and thus CO_2 availability to the algal culture. Therefore, the OBR offers a novel approach to mixing and mass transfer that supports algal growth and lipid production to an acceptable standard. However, the design provided low CO_2 mass transfer which led to reduced algal biomass and lipid productivity compared to previously reported sparged reactor, and thus limited the energy efficiency of the OBR.

Re-design of the length to width ratio of the OBR, continuous versus batch cultivation, or recirculation of the liquid from the far end, back to the inlet might eliminate the poorly mixed area at the far end of the column and improve mass transfer. Also, increasing the surface area to volume ratio and adding a gas outlet port at the opposite end to the gas inlet may improve mass transfer, specifically. The gas outlet should be a vertical exhaust vent in the glass column to prevent loss of liquid. Testing a wider range of baffle designs could also result in further enhancements to mixing and mass transfer rates. Mixing, mass transfer and algal growth studies at approximately one tenth of the oscillation amplitude and ten times the oscillation frequency would be valuable and may result in still higher algal productivities per unit power. Furthermore, there are multiple possible configurations for surface aerated reactors. In the Chapter 5 a second surface aerated PBR, the wave bioreactor, is discussed.

5 Wave Photobioreactor: Application of surface aeration by wave motion for energy efficient cultivation of *Scenedesmus* sp.

5.1 Introduction and Literature Review

The previous chapters describe an airlift reactor (Chapter 3), widely used for algal cultivation, and a novel, surface aerated reactor, the oscillatory baffled reactor (Chapter 4). In this chapter a wave photobioreactor (WR) will be described and investigated as a second novel, surface-aerated PBR for energy efficient algal cultivation.

The Wave Bioreactor® is relatively new compared to the airlift concept and oscillatory flow-type reactors. A bioreactor using wave agitation was invented in 1996 by Vijay Singh (Singh, 2005) who first published its description, mass transfer capabilities and application to animal and plant cell culture in 1999 (Singh, 1999). The Wave Bioreactor® was then patented for animal cell culture in February 2001, extended in 2003 (Singh, 2003), and is now sold as a commercial bioreactor by GE Healthcare and previously by Wave Biotech (Singh, 2005). The invention was in response to the unsuitable existing technologies for animal cell culture which used mechanical stirring and bubbling for aeration, both of which cause shear stress to the fragile cell cultures. The technologies at the time were also arduous to sterilise, resulting in weeks of downtime before the vessels were prepared for cell culture. Stirred tank reactors adapted for animal cell culture showed promise, but were either difficult to scale-up without losses in mass transfer capability or were complex and difficult to operate. The Wave Bioreactor® offered a vessel with low shear, which was disposable, easy to operate and produced good mass transfer without bubbling (Singh, 2005, 1999). More recently, similar wave-generating bioreactors have been developed including the BioWAVE®, BIOSTAT®, AppliFlex and CELLtainer® (Eibl et al., 2009; Lehmann et al., 2013; Westbrook et al., 2014).

A Wave Bioreactor® consists of a plastic, disposable, Cellbag® sitting atop a rocking platform. The Cellbag® is inflated with gas (air) and partly filled with liquid growth medium. The rocking motion creates a wave, allowing gas transfer across the large liquid surface without the need for gas sparging. The wave also promotes bulk mixing (Eibl et al., 2009; Kadwell and Hardwicke, 2007; Singh, 1999). Singh (1999) reported mixing times as rapid as 5 to 10 seconds and $k_L a$ between 2 and 4 h^{-1} for a 10 L liquid volume in the original Wave Biroeactor® design. Wave Bioreactors® are

typically 2, 5, 10 or 20 L volumes, but have been scaled-up to a working volume of 500 L (Junne et al., 2013; Singh, 2005). The BioWAVE®, BIOSTAT®, AppliFlex and CELLtainer® bioreactors also consist of bags made from biologically inert polymers, placed on top of rocking platforms. The CELLtainer® differs from the others in that it rocks in a 2 dimensional fashion. This means in addition to rocking back and forth it moves horizontally around the axis of rotation, resulting in both horizontal and vertical displacement of the liquid wave, as in Figure 5.1 (Westbrook et al., 2014). The one dimensional wave bioreactors differ in the range of sizes, and thus possible culturing volumes, available from the manufacturers, where the AppliFlex is limited to lab-scale culturing, and the others can be up-scaled to 100 – 500 L (Eibl et al., 2009).

Since their development and commercial availability, the wave-generating bioreactors have become popular for animal, insect and plant cell cultures (Eibl and Eibl, 2006; Kadarusman et al., 2005; Kadwell and Hardwicke, 2007; Slivac et al., 2006; Tang et al., 2007; Weber et al., 2002). The Wave Bioreactor® was also the first of a number of other disposable reactor types which became widely used, particularly in the growth of microorganisms for production of biopharmaceuticals (Junne et al., 2013; Westbrook et al., 2014). Westbrook et al. (2014) cultivated *E. coli* in a rocking wave reactor for the production of recombinant proteins. The study showed $k_L a$ of 150 h^{-1} at 40 rpm, increasing to 250 h^{-1} in a CELLTainer®.

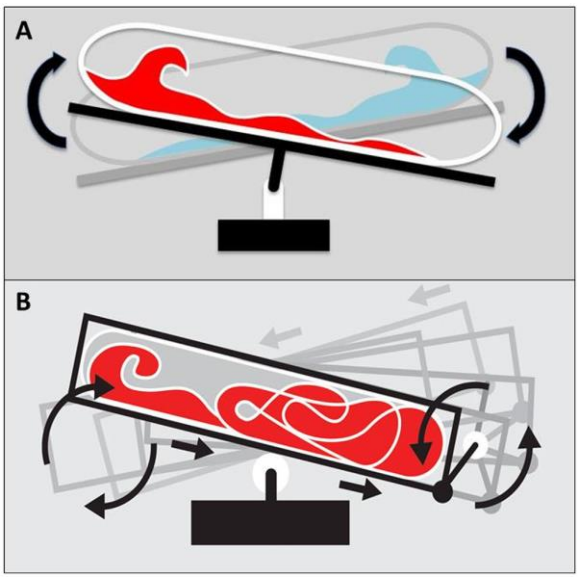

Figure 5.1 Diagram of a 1 dimensional wave bioreactor (A), and a 2 dimensional CELLTainer® (B). The 1D reactor tilts along a central pivot causing vertical displacement; the 2D reactor moves around the axis of rotation (Westbrook et al., 2014).

To our knowledge there are currently few reported applications of wave-generating bioreactors in microbial cultivation. The first of these studies was for the cultivation of aerobic yeast at high oxygen transfer rates in the Wave Bioreactor® (Mikola, 2007). In this study the $k_L a$ were between 1 and 9 h^{-1} at rocking rates up to 40 rpm for both the standard 10 L CellBag® and a novel cellbag which included an oxygen sparger. If headspace exchange is applied to the system, the $k_L a$ increases to 38 h^{-1} at 40 rpm (Mikola, 2007). The highest yeast cell dry weight obtained was 9.1 g L^{-1} in a 5 L CellBag® (0.364 g L^{-1} h^{-1}), and 6.9 g L^{-1} in a 10 L CellBag® (0.276 g L^{-1} h^{-1}). Other reports describe the successful growth of *E. coli* (0.8 – 1.1 g L^{-1} h^{-1}) and *Corynebacterium diphtheria* in wave-generating bioreactors (Glazyrina et al., 2010; Junne et al., 2013; Werner et al., 2010; Westbrook et al., 2014).

A study by Dreesen et al. (2010) is the first, to our knowledge, to describe the cultivation of algae in a Wave Bioreactor® at a rocking rate of 30 rpm, rocking angle of 6° and headspace aeration of 0.45 L min^{-1} (air, 400 ppm CO_2). They reported the successful cultivation of *Chlamydomonas reinhardtii* for the stable expression of antigens against *Staphylococcus aureus* as an oral vaccine for mice. The algal biomass reached 1.2 g L^{-1} and both biomass and antigen production yields were 20% higher than those in shake-flask cultures (Dreesen et al., 2010). Lehmann et al. (2013) compared the cultivation of the diatom *Phaeodactylum tricornutum* in an orbital shaker and two rocking wave-type reactors: a 2 L BioSTAT at 35 rpm, 10°, 0.5 vvm air at 5% CO_2; and a 10 L AppliFex at 20 rpm, 10°, 0.5 vvm air at 5% CO_2. In the wave-type reactors biomass concentrations reached 0.4 g L^{-1}. Cirés et al. (2015) cultivated a cyanobacterium, *Anabaena siamensis*, diazotrophically in a wave bioreactor. This report showed significantly increased CO_2 fixation rates, biomass productivities (0.06 g L^{-1} d^{-1}) and bioproduct productivities (phycocyanin pigment and steriodonic acid) compared to cultivation in a conventional bubbled suspension. These are currently the only publicly reported studies of algal cultivation in wave bioreactors. The current work is the first to culture *Scenedesmus* sp. in a wave bioreactor, and the first to investigate the relationships between mixing, mass transfer and algal biomass and lipid production in relation to power input in a wave bioreactor.

The aim of this chapter was to investigate the potential of using wave induced mixing and mass transfer for application in algal PBRs. Lights were placed above a Wave Bioreactor® to convert it into a photobioreactor for algal cultivation. Mixing and mass transfer rates were investigated in terms of power input for wave generation. Promising rocking rates and angles were chosen for cultivation of *Scenedesmus* sp. for lipid production.

5.2 Materials and Methods

A set of fluorescent lights in a wooden frame was used to house a Wave Bioreactor® so that the CellBag® was illuminated from above, as described in Sections 2.3.3 and 2.3.4. Dissolved oxygen and conductivity probes placed in the bottom-right port in the cellbag were used to measure the mixing time (T_m) and the CO_2 mass transfer coefficient ($k_L a_{CO_2}$), as described in Sections 2.4.1 and 2.4.2, respectively. Video footage of mixing patterns using phenolphthalein indicator solution (Section 2.4.1) was converted to photographs and used to verify conductivity results. The power input for agitation (rocking motion) in the wave photobioreactor was calculated from the temperature method, described in Section 2.5.2. Based on studies in the airlift reactor (Chapter 3), rocking rates and angles were chosen that resulted in $k_L a_{CO_2}$ supportive of algal growth at high and low energy input. Under these conditions, the biomass and lipid concentrations were measured during cultivation of *Scenedesmus* sp. in the wave photobioreactor (Sections 2.4.6 and 2.4.7, respectively).

5.3 Results and Discussion

5.3.1 Mixing

Mixing times were measured using a conductivity probe (response time 3.3 seconds), and monitored visually using phenolphthalein indicator solution. Figure 5.2 shows that after inoculation in the top right corner of the reactor, the tracer spread across the width of the cellbag as a vertical band moving back and forth along the length of the bag, aided by the rocking motion of the platform. The platform rocks up and down along the length of the reactor (Figure 5.2). The mixing times were estimated from these colour change experiments and compared to mixing times using a conductivity probe and salt tracer. There was no significant difference in the results from each method (Figure 5.3). Mixing times (from the conductivity method) decreased from 70.5 to 18.3 seconds between 10 and 40 rpm, but were not substantially affected by rocking angle at 30 and 40 rpm, e.g. ranging between 14.5 and 21.2 seconds for angles between 2 and 10° at 30 rpm (Figure 5.3).

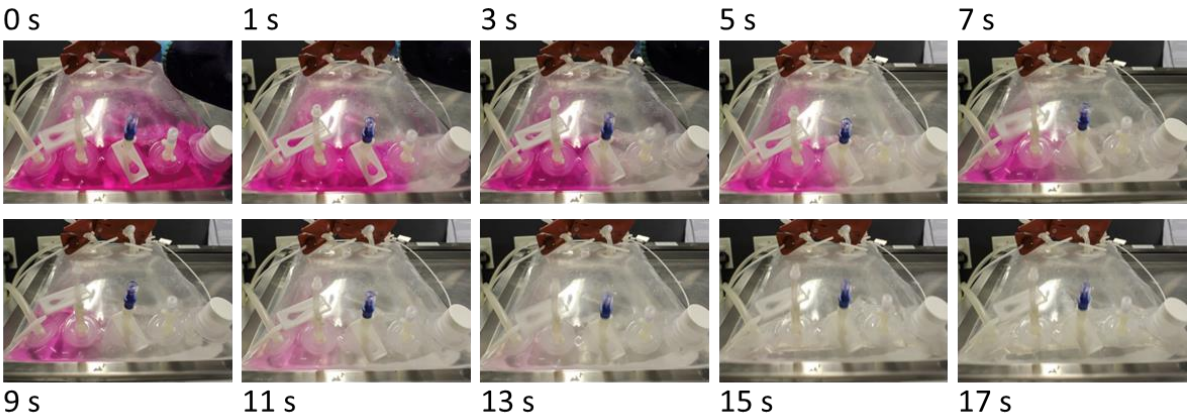

A

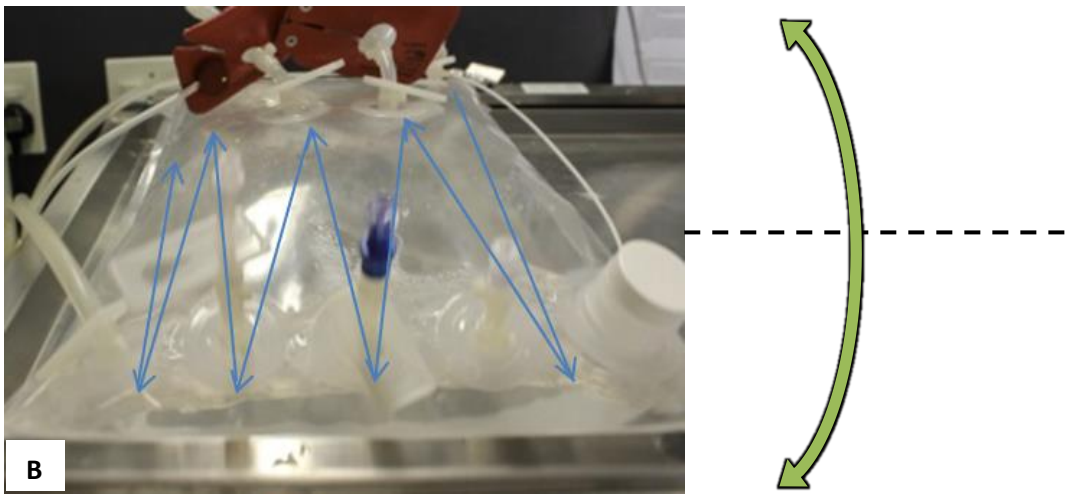

Figure 5.2 (A) Mixing pattern in the wave photobioreactor at a rocking rate of 30 rpm and rocking angle of 10° at regular time intervals shown in seconds (0 – 17 s) using phenolphthalein indicator solution in alkaline solution and a 1 M HCl tracer. (B) A simplified representation of the path travelled by the HCl tracer as the reactor rocks back and forth. The platform rocks around the horizontal axis as indicated by the green arrow.

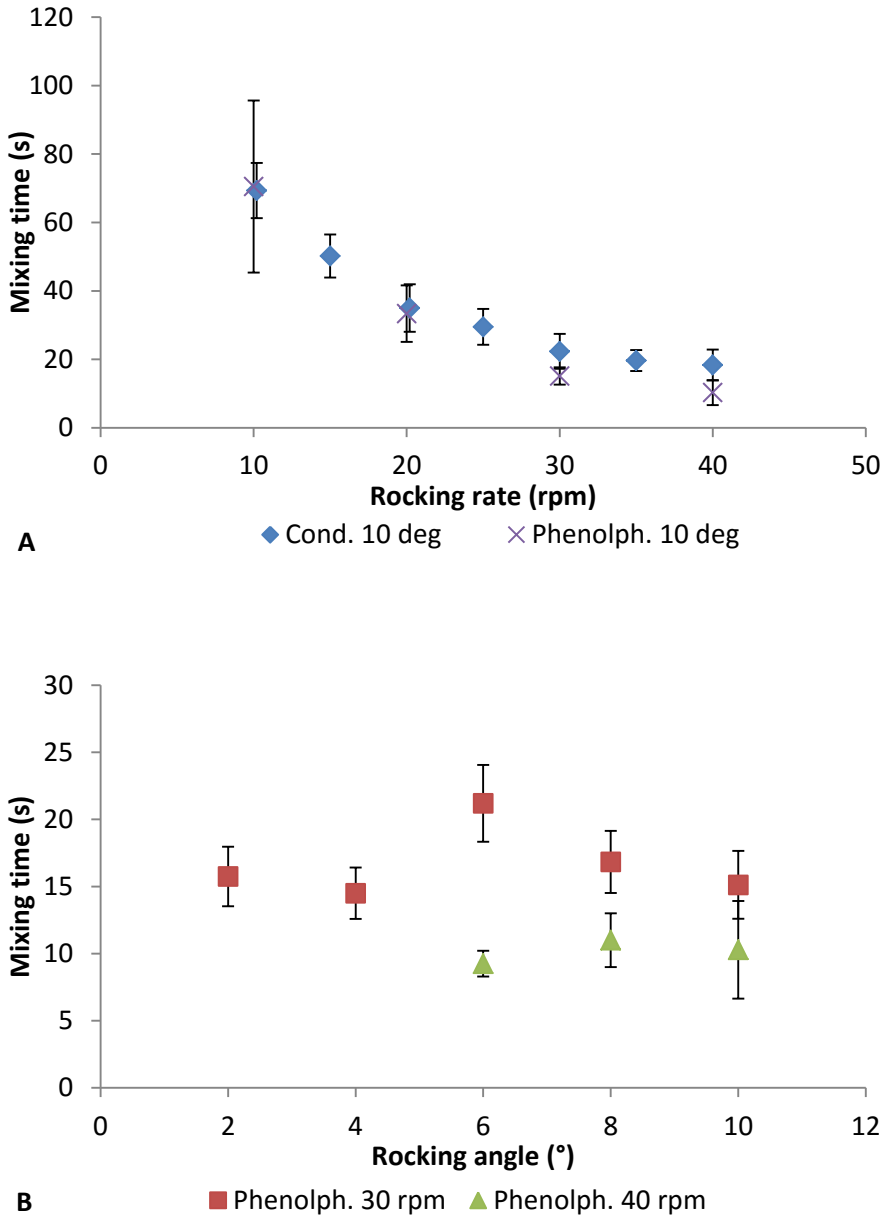

Figure 5.3 Mixing times measured using a conductivity probe and 1M NaCl tracer (Cond.), or visually using phenolphthalein indicator solution in alkaline solution and a 1 M HCl tracer (Phenolph.) at various (A) rocking rates (rpm) and (B) rocking angles (° = degrees). Error bars indicate the standard deviation of n = 3 replicates.

Typical values for mixing times found in the literature range from 16 to 5 seconds at a 10° rocking angle and rate of 30 to 40 rpm, as shown in Table 5.1 (Junne et al., 2013; Singh, 1999; Westbrook et al., 2014). The mixing times between 30 and 40 rpm in this study are slightly slower (22 – 18 seconds). The faster mixing times quoted by Junne et al. (2013) could be due to the two dimensional rocking of the CellTainer. Additionally, differences could be attributed to different cellbag geometries and working volumes, which may cause differences in wave formation and motion. Eibl

et al. (2009), Eibl and Eibl (2006) and Westbrook et al. (2014) report reduced mixing efficiency at increased working volume (as % of cellbag volume). Eibl et al. (2009) also report more efficient mixing in a smaller (2 L) cellbag compared to a 20 L cellbag. In this study a 10 L cellbag was filled to 2 L, giving a 20% working volume. The smaller cellbag used by Singh (1999) (2 L) may account for lower mixing times compared to this work. Westbrook et al. (2014) showed a mixing time of 14 seconds at 40 rpm with a working volume of 25% (20 L reactor), comparable to the 18 ± 4.5 seconds for this study. Eibl et al. (2009) report values between 100 and 20 seconds at a 10° rocking angle and 15 – 25 rpm in a 2 L cellbag (50% working volume), compared to the 50.2 and 29.5 seconds reported in Figure 5.3 for 15 and 25 rpm, respectively. The mixing times in Table 5.1 indicated that wave reactors have potential for processes requiring rapid mixing.

Table 5.1 Review of wave bioreactor investigations reporting oxygen mass transfer ($k_L a_{O_2}$), mixing time (T_m) and specific power input, where R_{vol} is reactor volume, F_{vol} is working volume, and rocking rate and rocking angle are expressed in rpm and degrees (°), respectively.

Bioreactor	Application	Rocking rate/angle	R_{vol} (L)	F_{vol} (%)	$k_L a$ (h^{-1})	T_m (s)	Power (W m^{-3})	Reference
Wave PBR	Algal culture	10 – 40 rpm 2 - 10°	10	20	9 – 152 [a] ($k_L a_{CO_2}$) 10 – 164 [a] ($k_L a_{O_2}$)	18 – 70	64 – 633	THIS WORK
Wave Bioreactor®	Cell culture	5 – 30 rpm	20	50	1.5 – 4.0 [b]	5 – 10		Singh (1999)
Sparged Wave Bioreactor®	Yeast cultivation	10 – 40 rpm 10°	20	50	2 – 9 [b] 2 – 38 [a]			Mikola (2007)
Wave and undertow reactor	Plant cell culture	15° lifting	60	33	10.0 [b]			Terrier et al. (2007)
'BioWave'	Review article	15 – 24 rpm 10°	2	50	1 – 15 [c]	20 – 100	8 – 561	Eibl et al. (2009)
CellTainer®	Bacterial culture (*E. coli*)	15 – 35 rpm	20	50	50 – 300 [a]	12 – 16		Junne et al. (2013)
1 dimensional rocking bioreactor	Bacterial cultivation	20 – 40 rpm	20	25	25 – 150 [a]	12 (40 rpm)		Westbrook et al. (2014)

[a] Headspace exchanged to remove nitrogen before initiating DO measurements for $k_L a$

[b] No headspace exchange when measuring $k_L a$

[c] Averaged from literature

5.3.2 Mass transfer

The carbon dioxide mass transfer coefficient ($k_L a_{CO_2}$) was calculated from $k_L a_{O_2}$, measured using the dynamic gassing in method and a dissolved oxygen probe (Section 2.4.2). Equation (2.4) in Section 2.4.2 was used to adjust the results to account for the probe response time. Figure 5.4 shows that at low $k_L a_{CO_2}$ there was no significant difference between values measured directly and those adjusted for the probe response time. At higher $k_L a_{CO_2}$ the values adjusted for probe response time are up to 14% higher than those measured directly. This demonstrates the importance of including the probe response time in analysis of data from the gassing-in method. All previous and subsequent $k_L a_{CO_2}$ data reported in this work were adjusted to account for the delay caused by probe response time.

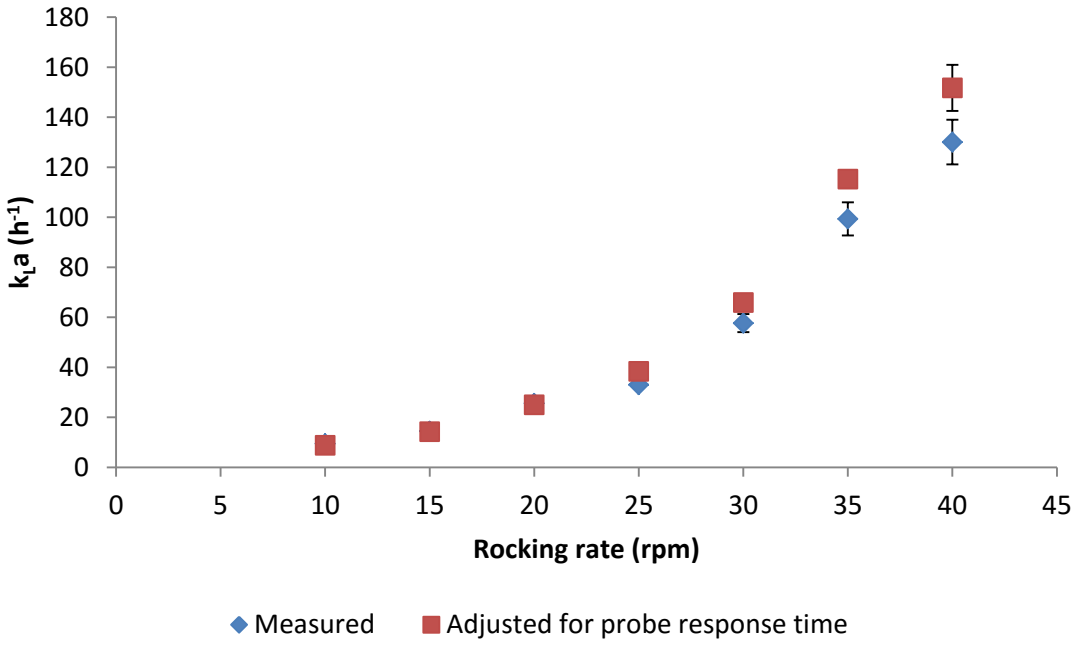

Figure 5.4 Carbon dioxide mass transfer in the wave photobioreactor at a 10° rocking angle and increasing rocking rates. Values measured directly, and adjusted for delay caused by the probe response time. Error bars indicate the standard deviation of n = 2 replicates.

The mass transfer coefficient increased exponentially with increasing rocking rate (Figure 5.4), as did the mixing efficiency (Figure 5.3A), showing the exponential relationship between mixing and mass transfer ($k_La = 4.03e^{65(1/T_m)}$). In Figure 5.5 mass transfer is plotted against rocking angle for select rocking rates. Mass transfer increased mildly with increased rocking angle at low rocking rate (15 and 25 rpm), and steeply at 30 and 35 rpm (Figure 5.5). Mixing times did not change substantially

with increased rocking angle (Figure 5.3B), implying that increased mass transfer with increased angle at 30 and 35 rpm was independent of mixing (Figure 5.5). This may be due to the splashing wave at high rocking rates and angles which increased the liquid surface area exposed to gas, and thus increased mass transfer independent of liquid mixing.

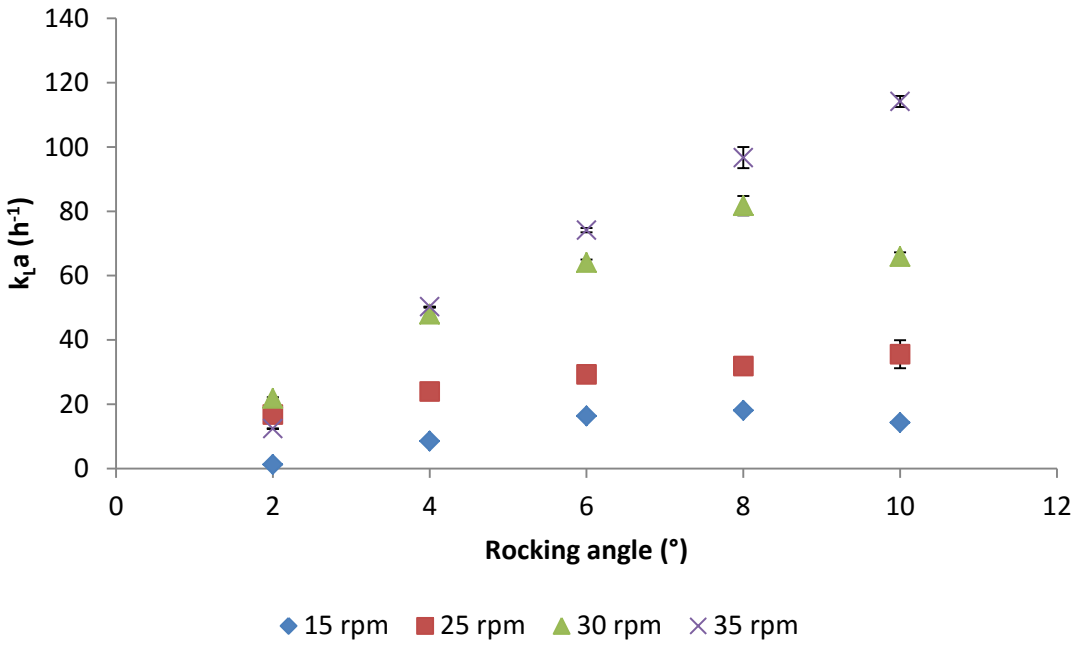

Figure 5.5 Carbon dioxide mass transfer in the wave photobioreactor at increasing rocking angle at select rocking rates. Error bars indicate the standard deviation of n = 2 replicates.

Mass transfer coefficients reported in the literature are usually for oxygen, and so the $k_La_{O_2}$ for the WR was used for comparison to literature data. The $k_La_{O_2}$ values from this study are slightly higher (9.5 – 164.4 h^{-1}) than $k_La_{CO_2}$ (8.8 – 151.7 h^{-1}), due to the higher diffusivity of O_2 in water. Literature values of $k_La_{O_2}$ for the wave reactor (Table 5.1) vary over a wide range between 1 and 300 h^{-1}. Mikola (2007) demonstrated an increase from 9 to 38 h^{-1} at 40 rpm and 10° if the nitrogen in the gas headspace was exchanged prior to the start of measurement of k_La. Therefore, the method of measurement significantly affects the comparability of literature values. Additionally, Eibl et al. (2009) and Westbrook et al. (2014) showed an increase in k_La at lower working volumes. The majority of k_La values shown in Table 5.1 were at higher working volumes (50%) than in this work (20%) and have substantially lower k_La. At a comparable 25% working volume, Westbrook et al. (2014) reported a k_La of 25 h^{-1} at 20 rpm, which matched that in this work (Figure 5.4). At 40 rpm

the $k_L a$ for the rocking bioreactor was 150 h^{-1} (Westbrook et al., 2014) which again matched the 164 h^{-1} reported for 40 rpm in this work. Lower working volumes in rocking bioreactors have the additional advantage of requiring less power to move the liquid on the platform. Mass transfer in relation to specific power input is discussed in Section 5.3.3 below.

5.3.3 Power input

Power input by the wave photobioreactor was measured using the calorimetric method as described in Section 2.5.2. This is the energy dissipated in mixing the volume of water by the wave motion caused by rocking. The mechanical energy dissipated by friction as the rocking platform is raised and lowered was not confirmed by a direct measurement in this work due to the difficulty in applying a torque meter or power meter to the complex electronic base of the wave bioreactor. Additionally, a wave motion for mixing can be generated in a variety of ways other than a rocking platform thus altering the power input requirement (discussed further in Section 5.3.4). Power input per unit volume (P/V) increased from 131 to 634 W m^{-3} with an increase in rocking rate from 10 to 40 rpm at a 10° angle, and from 50.8 to 482 W m^{-3} with an increase in rocking angle from 2 to 10° at a rocking rate of 30 rpm (Figure 5.6). Eibl et al. (2009) calculated specific power in a wave reactor using a 'static model' in which the fluid in the cellbag was assumed to display static behaviour. By determining the cellbag's point of gravity and the fluid surface area, the distribution of fluid was analysed using computer-aided design and the resulting momentums, and thus work done, was calculated. Using this method, Eibl et al. (2009) report a P/V of 210 – 560 W m^{-3} for a 2 L wave bioreactor at 50% working volume, 10° and 12 – 30 rpm. The values measured using the calorimetric method of this work were comparable to Eibl et al. (2009), with a P/V of between 480 and 503 W m^{-3} at 30 rpm and 10 ° (Figure 5.6). This is the only publically available study on power input to a wave bioreactor, to our knowledge, demonstrating the importance of this work in further investigating this reactor type in terms of energy consumption.

A plot of $k_L a$ versus P/V (Figure 5.7) shows that $k_L a$ increased exponentially with increased power input. At lower P/Vs, the wave formed inside the cellbag was a gentle rolling wave. At higher power inputs, corresponding to greater liquid motion, the wave became a more pronounced curved, crashing wave. The greater surface area of the latter type of wave, in contact with the gas headspace, may have contributed to the sharp increase in $k_L a$ after 422 W m^{-3} (Figure 5.7). At the most vigorous mixing rate, the wave splashed the roof of the cellbag creating a thin liquid film, shown in Figure 5.8, further enhancing gas-liquid mass transfer (Maier et al., 2004).

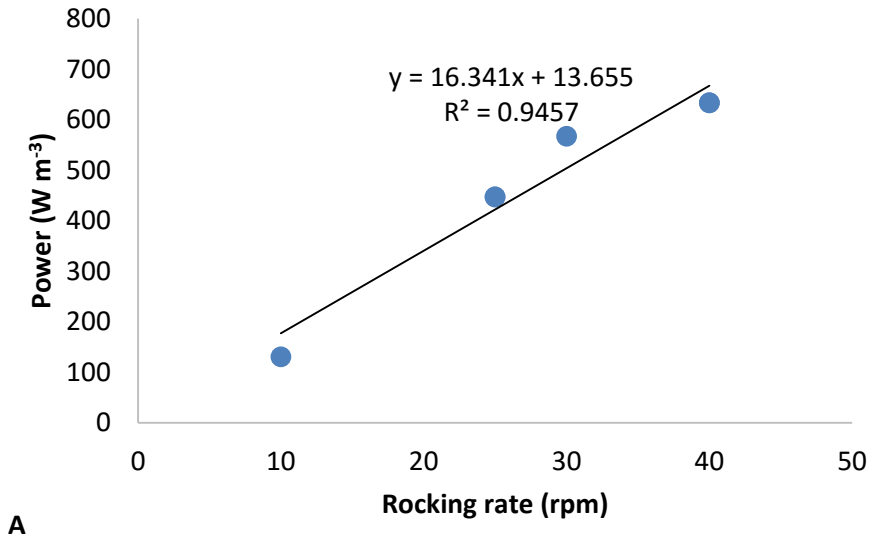

A

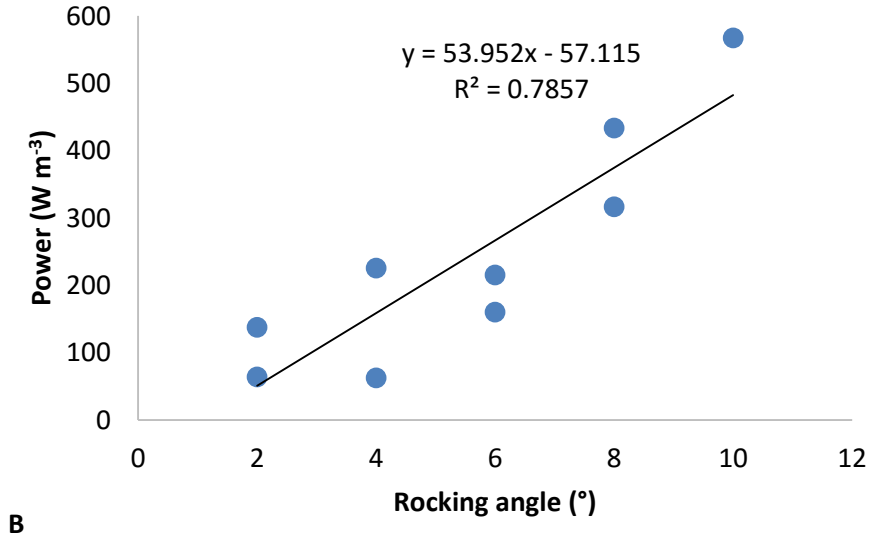

B

Figure 5.6 Power input (W m^{-3}) in the wave photobioreactor at increasing (A) rocking rate at 10° and (B) rocking angle at 30 rpm.

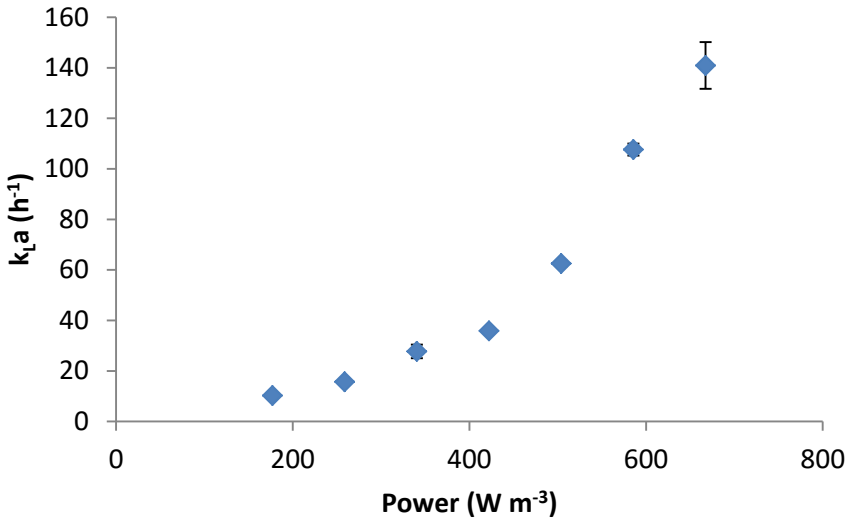

Figure 5.7 Carbon dioxide mass transfer with increasing power input in the wave photobioreactor. Error bars indicate the standard deviation of n = 2 replicates.

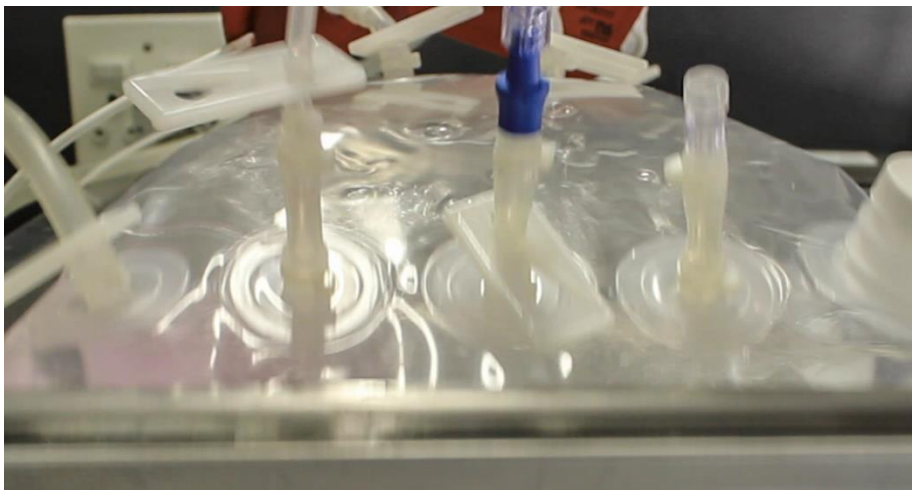

Figure 5.8 Photograph of thin liquid film on roof of wave cellbag caused by splashing wave at 40 rpm and 10°.

5.3.4 Algal biomass and lipid production

Scenedesmus sp. was grown in the wave photobioreactor using BB media and inoculum as described in Section 2.2. The OD at 750 nm was measured as an indication of the biomass concentration in two trial experiments in which a comparison was made between daily exchange of the gas headspace and constant replenishing of the headspace at 0.2 L min^{-1}. The culture grown with daily headspace exchange grew slowly to a maximum OD of 1.1 in one week at a maximum productivity of 0.35 and overall productivity of 0.22 absorbance units (750 nm) per day (Figure 5.9). With a

constant exchange of gas the culture grew to a maximum OD of 2.29 in one week at a maximum productivity of 0.70 and overall productivity of 0.48 absorbance units (750 nm) per day (Figure 5.9). This comparison revealed that, for best growth, it was necessary to use a constant flow of gas into and out of the cellbag to introduce fresh CO_2, and remove O_2 that can cause photo-inhibition at high concentrations. All subsequent experiments were performed using a 0.2 L m^{-1} gas flowrate through the headspace with the gas outlet port open.

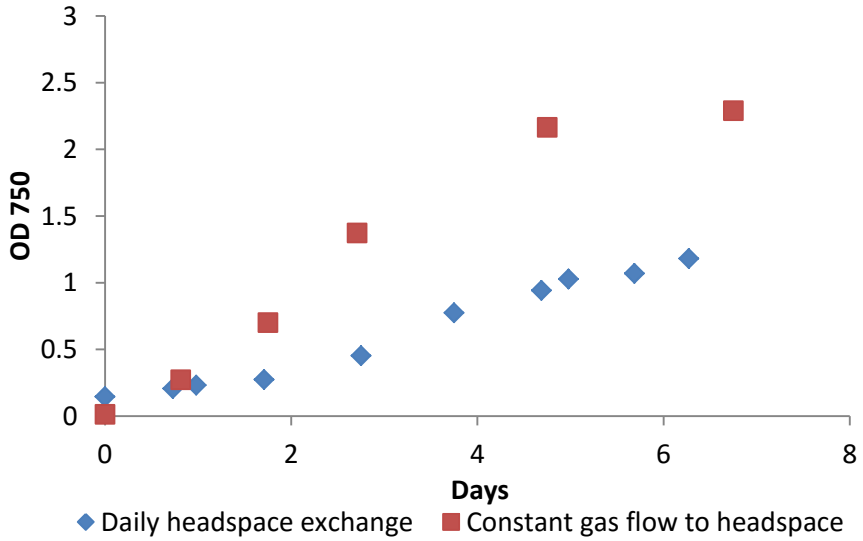

Figure 5.9 *Scenedesmus* sp. cultivation in the wave photobioreactor at 30 rpm, 10° with daily headspace exchange compared to constant gas flow in and out of the headspace.

In Table 5.2 the conditions under which *Scenedesmus* sp. was cultivated in the WR are summarised. Algal growth was monitored under three rocking conditions in the WR: 25 rpm at 10°, 15 rpm at 8° and 15 rpm at 4°. These were chosen as they provided $k_L a_{CO_2}$ comparable to the 'standard' and reduced power input conditions in the ALR (Chapter 3.3.2). The light intensity was maintained to give a total light of 9 µmol s^{-1} over the reactor area (Table 5.2), equal to the total light received by the ALR and OBR (Section 2.3.4). *Scenedesmus* sp. grew at similar rates and to similar maximum biomass concentrations under each of these conditions (Figure 5.10), despite a reduction in $k_L a_{CO_2}$ from 38 to 8.5 h^{-1}. This suggests that the rocking rate could be reduced considerably before the culture became carbon limited. However, growth was linear between days 2 and 8 in each case, showing that the culture was limited by some other factor, perhaps light. *Scenedesmus* sp. was also cultivated at 26 µmol s^{-1} light, 25 rpm and 10° (Table 5.2). Figure 5.10 shows that the culture grew more rapidly and to a higher maximum biomass concentration when the light was increased. This

indicated that the linear growth seen at 9 µmol s^{-1} was due to light limitation. A repeat of the cultivation at 26 µmol s^{-1} light was shown to demonstrate the reproducibility of these experiments. Similar results were obtained for lipid production, where lipid production was similar in all experiments at a light provision of 9 µmol s^{-1}, across the rocking rates and angles, and increased with increased light (Figure 5.10B). Power input for mass transfer can thus be reduced to 85 W m^{-3} (corresponding to a $k_L a_{CO_2}$ of 8.5 h^{-1}) without significantly affecting algal biomass and lipid production. In outdoor cultivation, where the total light exceeds 26 µmol s^{-1}, there may be further reduction in light limitation and thus the potential for further improvements to biomass and lipid production without increasing power input. However, at higher light the increased growth rates may result in increased need for carbon. Experiments at high light (26 µmol s^{-1} or outdoors) and various $k_L a_{CO_2}$ are required to investigate at what rocking rates and angles carbon limitation occurs at these higher growth rates.

Table 5.2 Conditions chosen for cultivation of *Scenedesmus* sp. in the wave photobioreactor.

Light (µmol s^{-1})	Angle (°)	Rate (rpm)	$k_L a_{CO_2}$ (h^{-1})	T_m (s)	Power (W m^{-3})
9	10	25	38.4	29.5	422
9	8	15	18.1	±19.6	201
9	4	15	8.5	±19.6	85
26	10	25	38.4	29.5	422

The overall biomass and lipid productivities were calculated from Figure 5.10 for each of the chosen cultivation conditions (based on the time taken to reach maximum biomass or lipid concentration). Figure 5.11 represents these productivities at increasing $k_L a_{CO_2}$ and CO_2 transfer rate (a function of $k_L a_{CO_2}$ and CO_2 saturation concentration at 10 400 ppm in BB media, Section 2.4.3). This shows that with increased availability of CO_2 in this range, there was slight increase in biomass productivity but no increase in lipid productivity. With increased light, the biomass productivity increased, but there was no significant increase in lipid productivity.

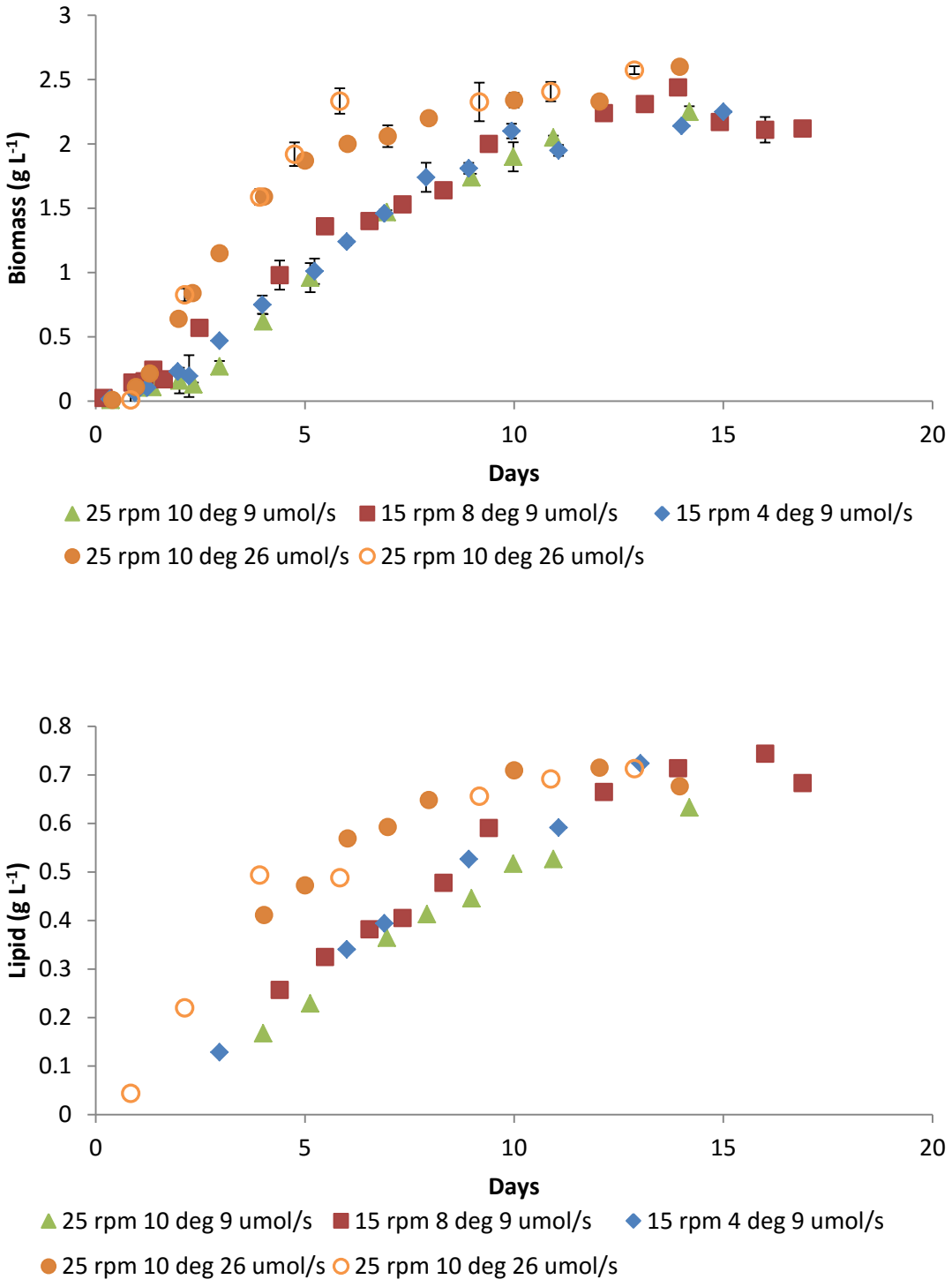

Figure 5.10 *Scenedesmus* sp. cultivation in the wave photobioreactor at various rocking rates, rocking angles and total light provision. (A) biomass growth curve (g L^{-1}), (B) lipid production (g L^{-1}). Error bars indicate the standard deviation of n = 2 replicate dry weight samples. The total light indicated is equivalent to light intensities of 79 µmol m^{-2} s^{-1} (giving 9 µmol s^{-1} at 0.13 m^{-2}) and 162 µmol m^{-2} s^{-1} (giving 18 µmol s^{-1} at 0.13 m^{-2} and 26 µmol s^{-1} at 0.17 m^{-2}).

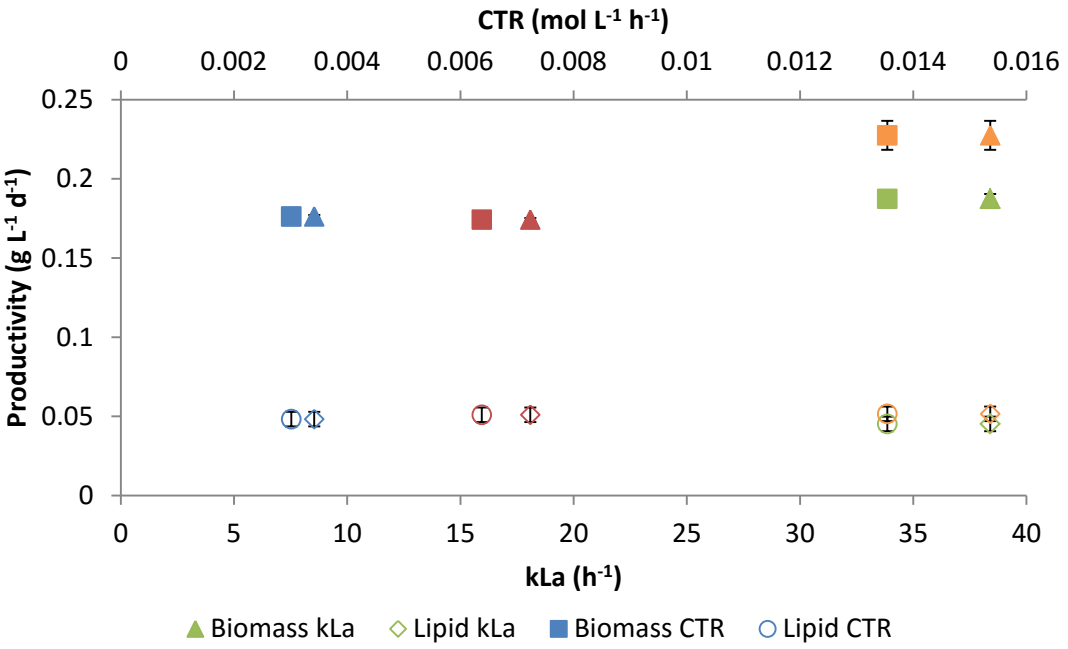

Figure 5.11 Biomass and lipid productivity (g L^{-1} d^{-1}) at increasing $k_L a_{CO_2}$ and CO_2 transfer rate (CTR) in the wave photobioreactor at 15 rpm 4° (blue), 15 rpm 8° (red), 25 rpm 10° (green) at 9 µmol s^{-1} light; and 25 rpm 10° at 26 µmol s^{-1} (orange). Error bars indicate the standard deviation from n = 2 replicate dry weight samples (biomass) and n = 2 replicates at 25 rpm 10° at 26 µmol s^{-1} (lipid).

Comparisons were made across the cultivation conditions in Table 5.2 with regards to volumetric biomass and lipid productivity. Biomass productivity decreased slightly at a $k_L a_{CO_2}$ of 8.5 h^{-1} (15 rpm and 4°) compared to 18 h^{-1} (15 rpm and 8°) and 38 h^{-1} (25 rpm and 10°) (Figure 5.12A). The increased biomass productivity at 26 µmol s^{-1} light again illustrated that when carbon was not limiting, light was the limiting factor. There was no significant difference in lipid productivity across the reactor conditions, suggesting that both carbon and light were at the minimum required for the cellular machinery to produce lipids, or another limitation (such as another nutrient) constrained lipid productivity.

Productivity on a basis of power input per unit volume was compared under each cultivation condition in the wave photobioreactor (Figure 5.12B). Since the biomass and lipid productivities did not vary greatly across the reactor conditions investigate, the biomass and lipid productivity per unit power increased substantially with lower rocking rate and rocking angle. Hence the lowest rocking rate (15 rpm, 4°) provided the most energy efficient cultivation conditions, with a maximum of 2.07 g W^{-1} d^{-1} (biomass) and 0.567 g W^{-1} d^{-1} (lipid). These productivities could be increased further in

an outdoor cultivation facility, with reduced light limitation. Comparison of these results with algal cultivation and energy efficiencies in the other PBRs is discussed in Chapter 6.

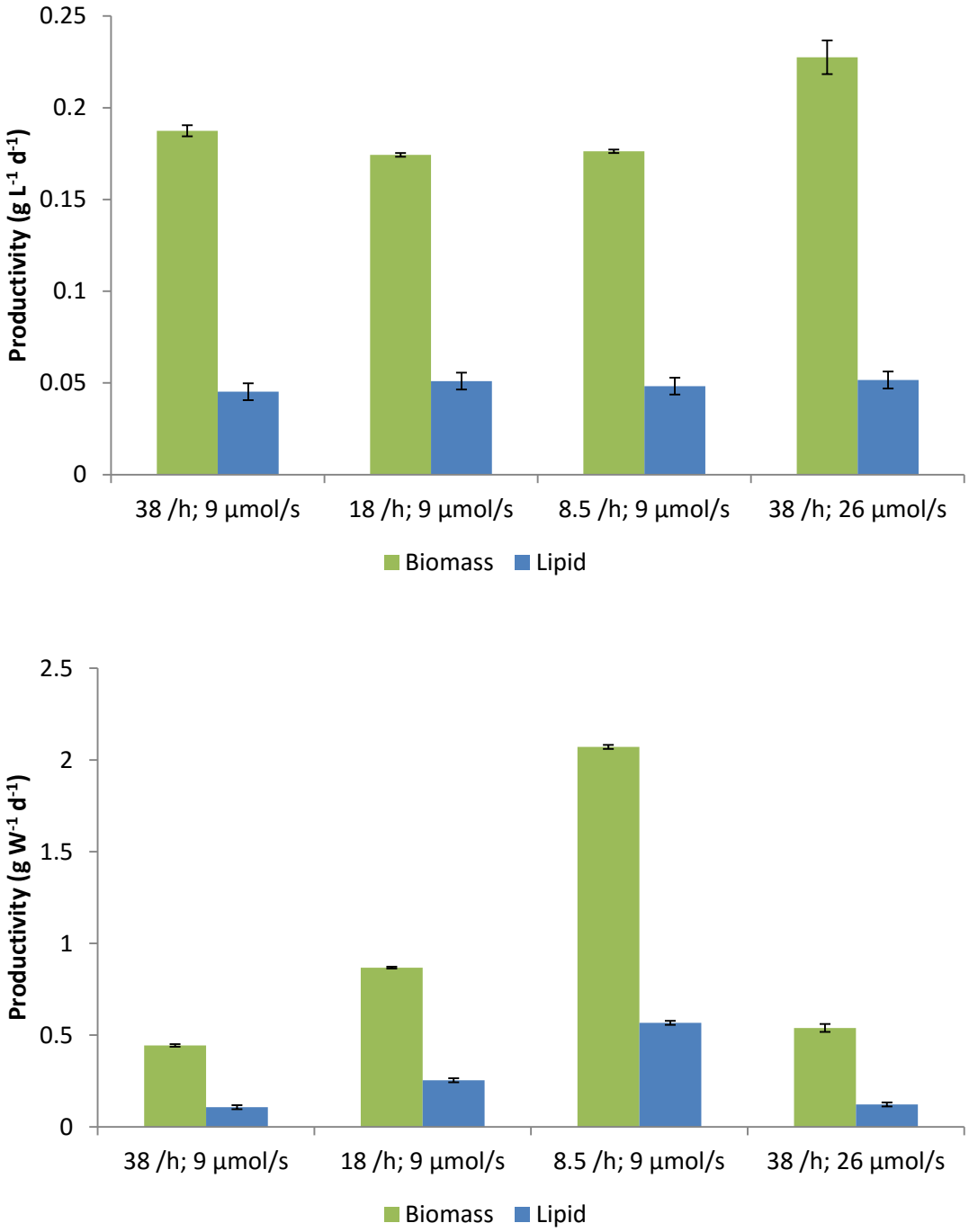

Figure 5.12 (A) Volumetric biomass and lipid productivity (g L^{-1} d^{-1}), and (B) productivity per unit power (g W^{-1} d^{-1}) under four cultivation conditions in the wave photobioreactor (25 rpm 10°; 15 rpm 8°; 15 rpm 4° and 25 rom 10° at 26 µmol s^{-1} light). X-axis is labelled with $k_L a_{CO_2}$ and total light. Error bars indicate the standard deviation from n = 2 replicate dry weight samples (biomass) and n = 2 replicates at 25 rpm 10° at 26 µmol s^{-1} (lipid).

The results presented above show that the WR has excellent potential for algal cultivation, providing sufficient mixing and mass transfer even at relatively low rocking rates. The next consideration is the scale-up of this surface aerated bioreactor. Eibl et al. (2009) calculated that the power input per unit volume relative to $k_L a$ of a rocking wave-type reactor is comparable to that of a stirred tank reactor (Chapter 1.3.2, Figure 1.2A). A significant drawback to wave reactors that sit on rocking platforms is the energy demand that will incur, particularly with scale-up, with the weight of large volumes of liquid. However, there are alternative ways to generate a wave, and still benefit from the high mixing and mass transfer seen in the Wave Bioreactor®. A unique Biowave™ reactor was developed soon after the Wave Bioreactor®, and first published in 1998 by John Hobson. Hobson (1998) used this wave-generating bioreactor to treat wastewater. The Biowave™ included a spherical wave generator, originally designed for swimming pools (WOW Technology, Belgium), placed in the middle of the treatment tank. The wave generator contained a motor attached to an oscillating weight on a vertical shaft. As the weight moves up and down the shaft, the sphere moves in and out the water, resulting in displacement, and generates a resonant wave motion that requires very little energy expenditure (Hobson, 1998). Similarly, a wave bioreactor designed by Terrier et al. (2007) consists of a cellbag on top of a horizontal platform, one or both ends of which are periodically raised to generate a wave. This results in lower energy demand in comparison to a rocking platform. Other technologies used to generate waves in aqua-parks and oceanography experiments include the use of forced air and inclined sections (Bastenhof, 1983; Idbeis, 1996). In the current study, the Wave Bioreactor® was used as a test system to investigate the conditions necessary for cultivation of *Scenedesmus* sp. using wave motion. After lab-scale assessment of this system, scale-up will be considered in an alternative wave-generating reactor more suitable for low energy wave generation in large volumes of liquid.

5.4 Conclusions

Wave bioreactors display high mixing rates with low shear forces, and provide gas-liquid mass transfer without sparging. Comparison across the literature, including the data presented in this work, showed that mixing times in wave reactors are influenced by rocking rate, rocking angle, cellbag size and working volume. Lower cellbag size and smaller working volume results in more efficient mixing (lower mixing time). Similarly, mass transfer increased with increased rocking rate and decreased working volume. To achieve the wave motion, power input per unit volume increased with increasing rocking rate and rocking angle. A rocking rate of 25 rpm and rocking angle

of 10°, required 422 Wm^{-3} to provide a $k_L a_{CO_2}$ of 38.4 h^{-1}, and a 29.5 s mixing time. *Scenedesmus* sp. reached a maximum concentration of 2.25 g L^{-1} at a biomass productivity of 0.187 g L^{-1} d^{-1} with a lipid concentration of 0.633 g L^{-1} (lipid productivity of 0.045 g L^{-1} d^{-1}) at these conditions. At one fifth of the power input for wave motion (85 W m^{-3}), the mixing time and mass transfer (19.6 s, 8.5 h^{-1}) were still sufficient to support algal biomass and lipid production at comparable productivities (0.176 and 0.056 g L^{-1} d^{-1},for biomass and lipid respectively) and maximum concentrations (2.25 and 0.724 g L^{-1}, for biomass and lipid, respectively). By reducing the rocking rate from 25 to 15 rpm, and the angle from 10 to 4°, the energy efficiency of the wave photobioreactor was 5 times higher, increasing from 0.443 to 2.07 g W^{-1} d^{-1}. Increasing the light from 9 µmol s^{-1} to 26 µmol s^{-1} revealed that growth, although not carbon limited at 9 µmol s^{-1}, was light limited. Further experiments at low rocking rates and angles and high (or unlimited) light would reveal the maximum obtainable productivities per unit power.

The results in this chapter demonstrated that *Scenedesmus* sp. can be successfully cultivated in a wave photobioreactor, and the energy efficiency of cultivation can be optimised with regard to mixing and mass transfer. This is the first study to include rigorous measurement of power input into a wave generating bioreactor. The calorimetric method used here gave power inputs that correlated well with those calculated previously (Eibl et al., 2009). The data presented here shows the excellent potential of the WR as an alternative to sparged bioreactors. The next stage is to explore scale-up strategies drawing on the work reported here. The following chapter (Chapter 6) compares the WR and the OBR with the conventional, sparged ALR.

6 Comparison of surface aerated and sparged photobioreactors

6.1 Introduction

Chapters 3, 4 and 5 show the optimisation of airlift (ALR), oscillatory baffled (OBR) and wave (WR) photobioreactors for cultivation of *Scenedesmus* sp. and lipid production at reduced power input for mixing and mass transfer. By reducing the gas velocity in the airlift reactor to a critical minimum value, a 75% reduction in power input, from 'standard conditions', was obtained without significant losses in biomass and lipid productivities. Reducing the oscillation frequency from 0.7 to 0.25 Hz in the OBR led to a 46% increase in the productivity per unit power (61% power reduction), but low total biomass and lipid concentrations were achieved. The OBR with donut baffles showed the best mass transfer and so this baffle type was used in comparison with other PBRs, presented in this chapter. The high CO_2 mass transfer rates in the WR meant that the rocking rate and rocking angle could be reduced almost to a minimum without reducing the biomass and lipid productivities, resulting in a power reduction of 80% over standard conditions. These results demonstrate the importance of optimising mixing and mass transfer to improve the energy efficiency of bioreactors, particularly for commodity products.

This chapter aims to compare the performance and energy efficiency of the three PBRs discussed in Chapters 3 to 5. The ALR is a commonly used sparged reactor type for algal cultivation. Many other PBRs (airlift, bubble column, horizontal tubular, flat panel) also use gas sparging for mixing and mass transfer. This work investigates the potential of surface aeration as an energy efficient alternative to gas sparging. Although open ponds agitated with a paddle wheel use surface aeration, these are typically gently mixed with low mass transfer. The OBR and WR were chosen as surface aerated reactors with vigorous mixing and high mass transfer rates, as reported in the literature. A comparison of the mixing and mass transfer rates as a function of power in each of the reactors is reported, and differences between sparged (ALR) and surface aerated (OBR and WR) reactors explored. The reactors are also compared for their ability to support algal cultivation and lipid production. The energy efficiencies and net energy ratios of each reactor for biomass and lipid production are discussed, with the aim of offering improvements to the high energy consumption in the bioreactor stage of algal bioprocesses that has been widely reported (Chapter 1).

6.2 Materials and Methods

The power input to each photobioreactor (ALR, OBR and WR) was calculated according to the methods described in Section 2.5. Mixing times (T_m) and CO_2 mass transfer coefficients ($k_L a_{CO_2}$) were measured in each PBR according to Sections 2.4.1 and 2.4.2, respectively. *Scenedesmus* sp. was grown under mixing rates selected to represent high power input and low power input in each PBR. Light provided to each PBR was kept constant between comparable experiments, and adjusted according to Table 2.2 in Section 2.3.4. Biomass and lipid concentrations were measured regularly with time according to Sections 2.4.6 and 2.4.7. Net energy ratios (NERs) represent the ratio of the energy obtainable from algal whole biomass or lipid to the energy consumed for mixing and aerating the PBR, calculated according to Section 2.6.

6.3 Results and Discussion

6.3.1 Power input

The electrical power required to mix the liquid contents of the ALR, OBR and WR reactors depends on the gas flowrate, oscillating frequency and rocking rate, respectively. The calorimetric method for measuring power input was used for the OBR and WR, but could not be applied to the ALR due to the majority of power being consumed for gas compression outside of the ALR column itself. This meant that the temperature change caused by energy dissipation in the ALR (as measured in the calorimetric method) would not represent the actual power consumed for sparging. A fair comparison of power input needs to be made across the three reactors, and so power calculations for the ALR are discussed below.

A commonly used method for calculating power input in airlift reactors is to calculate the energy dissipation via isothermal gas expansion equations of the gas bubbles as they rise from the sparger to the top of the reactor (Chisti, 1989). In the present work this has been described as the 'minimum aeration power' (Section 2.5.1.1) as it represents the minimum energy used for mixing the liquid in a reactor by sparging. Among pneumatic reactors, the 'minimum aeration power' is used as a common denominator (or comparable term) to represent mixing rates for comparison of other

varied factors (such as mass transfer) across various reactor geometries, configurations and sparger types and configurations.

The 'total aeration power' described in Section 2.5.1.2 is the power used to compress the gas to the pressure at which it is delivered to the airlift, entering through the sparger. Sparging would not be possible without power for gas compression, and the gas flowrate in a reactor is dependent on the inlet gas pressure of the system. Thus, the 'total aeration power' describes the total power used for aeration at the reported gas flowrates, mass transfer rates and mixing times. Table 6.1 shows the difference in power input when calculating the minimum or total aeration power.

Table 6.1 'Minimum Aeration Power' and 'Total Aeration Power' in the 3.2 L airlift photobioreactor at various sparging velocities, given as gas flowrates (L min^{-1}) and superficial gas velocities (m s^{-1}); including a comparison at a 2 bar inlet gas pressure (used in this work) and the minimum pressure required to overcome the pressure drop over the sparger at the given gas flowrates.

Gas flowrate (L min^{-1})	Superficial gas velocity (m s^{-1})	Min. Aeration Power (W m^{-3})	Total Aeration Power (W m^{-3}) at min. pressure	Total Aeration Power (W m^{-3}) at 2 bar
0.2	0.004	6	21	142
0.5	0.010	14	71	354
1.0	0.019	28	130	708
2.0	0.038	57	344	1417
3.0	0.057	85	517	2125

Figure 6.1 illustrates the difference between the two calculations ('minimum' and 'total' aeration power) and indicates the gas pressures used in each calculation. In the experimental work conducted for this dissertation, the inlet gas pressure for the ALRs (p_2) was 2 bar. Optimisation of the ALR power input could be done by reducing this gas pressure in a similar way to the optimisation of gas velocity described in Chapter 3.3.2. The gas supplied to the ALR must be at sufficient pressure to account for the frictional pressure drop across the sparger ($\Delta p = p_2 - p_3$; Figure 6.1), and the head of liquid above the sparger ($p_3 = \rho * g * h_L$; Figure 6.1). In this work a 2 µm porous stainless steel sparger was used, which will result in a frictional pressure drop between 0.05 and 0.12 bar in the range of gas velocities in this study (Green and Perry, 2007; Murhammer and Goochee, 1990; Stephenson et al., 2010). The pressure drops estimated from literature were used to calculate a minimum inlet gas pressure (p_2) to supply the ALRs. This ranged between 1.12 and 1.19 bar, dependent on gas velocity, and resulted in significantly reduced aeration energy consumption (Table

6.1). The minimum value for inlet pressure (p_2) is dependent on the sparger type used (including pore-size and material), and may increase substantially at a range of gas velocities considerably larger than those reported here (Green and Perry, 2007). Additionally, the gas pressure required to supply sparged bioreactors is also dependent on the pressure drops between the compressor and sparger, which vary according to pipe length, diameter and configuration. For this reason, the minimum inlet pressure, taken as the pressure to overcome the sparger pressure drop and head of liquid, was used in a sensitivity analysis of the results presented in this work. Data based on an inlet pressure of 2 bar was used to represent the un-optimised experimental condition. According to the ideal gas law, at reduced inlet pressure, the volumetric gas flowrates increased to maintain molar gas flowrates, and thus $k_L a$. This is accounted for in the specific power values at the minimum gas inlet (Table 6.1). The comparison of energy consumption in Table 6.1 demonstrates the importance of optimising the inlet gas pressure of a large-scale system for improved energy efficiency.

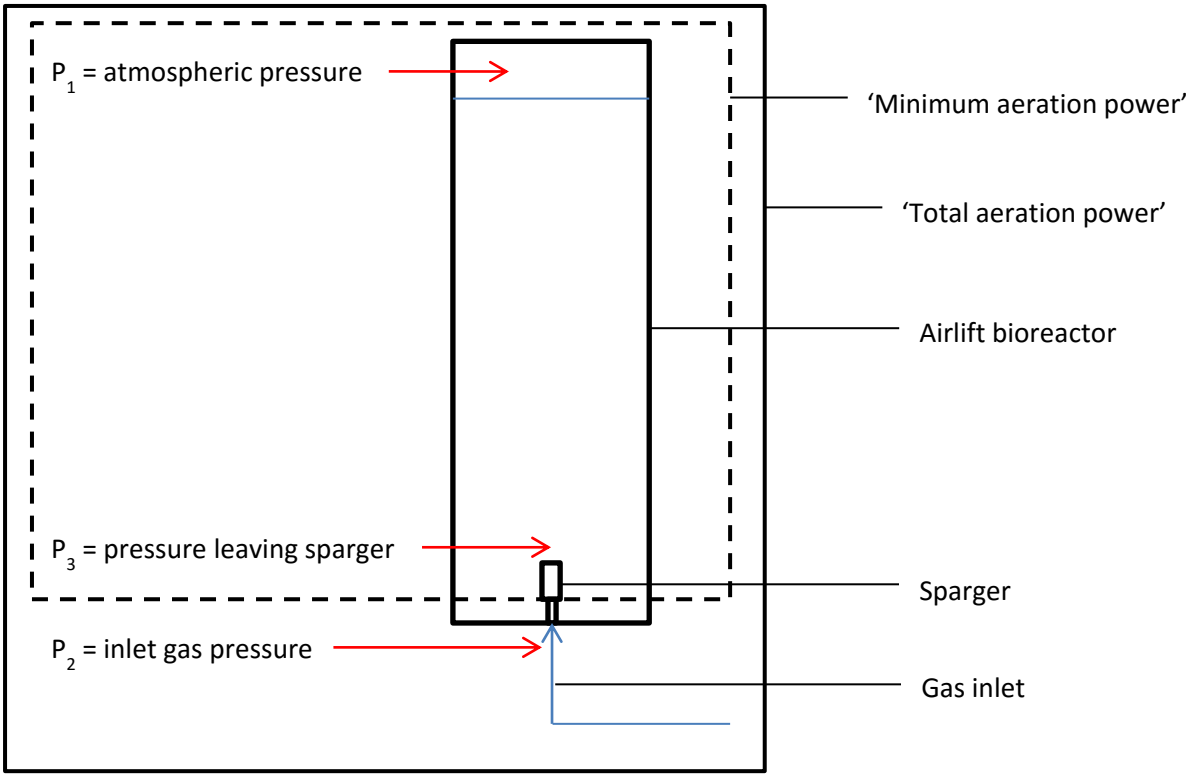

Figure 6.1 Diagram of ALR indicating gas pressures p_1, p_2 and p_3 used to calculate the power input for aeration. 'Minimum aeration power' (dashed boundary) assumes $p_3 = \rho * g * h_L$ and does not include the power requirement to compress gas to the pressure at p_2. 'Total aeration power' (solid boundary) is the power to compress gas to the pressure at p_2, the gas inlet pressure. The minimum value for p_2 is the liquid head ($p_3 = \rho * g * h_L$) plus the pressure drop across the sparger (Δp). p_2 used in this work was 2 bar.

Mixing in the OBR and WR is a result of mechanical movement. The calorimetric method measured the power input due to mechanical movement by the baffles (OBR) and rocking platform (WR), which gave rise to the mass transfer rates and mixing times reported. The calorimetric method thus gives a realistic value for the total power consumed for mixing via mechanical movement. The 'total aeration power' in the ALR better describes the actual power used to obtain the mass transfer and mixing rates recorded. For fair comparison, the 'total aeration power' for the ALR was, therefore, used in this chapter when comparing with the mechanically mixed OBR and WR reactors. Table 6.2 and Table 6.3 show the power input in OBR and WR reactors. The gentle gas flow into the headspace of these reactors did not require gas compression, making the power input for gas provision in these reactors negligible.

Table 6.2 Power input in the oscillatory baffled photobioreactor at varying oscillation frequency (Osc. Freq.) at 59 mm centre-to-peak amplitude.

Osc. Freq. (Hz)	Power (W m^{-3})
0.10	12
0.15	40
0.20	94
0.25	184
0.30	318
0.35	505
0.40	753
0.45	1072
0.50	1471
0.55	1958
0.60	2542
0.65	3231
0.70	4036

Table 6.3 Power input in the wave photobioreactor at various rocking rates and angles.

Rocking angle (°)	Rocking rate (rpm)	Power (W m^{-3})
10	10	177
10	15	259
10	20	340
10	25	422
10	30	504
10	35	586
10	40	667
2	30	51
4	30	159
6	30	267
8	30	375
10	30	482

6.3.2 Mixing and Mass Transfer

Mixing times in the ALR, OBR and WR were measured using a 5 M NaCl tracer. To compare the mixing capabilities of these reactors, the mixing times were plotted against the power consumed to generate mixing (Figure 6.2). Mixing times in the WR and OBR were superior to the ALR at a given power input, where a lower mixing time represents superior mixing. Above 753 W m^{-3} the mixing in the WR may continue to improve, possibly exceeding the OBR, where mixing in the OBR remains relatively constant at the power inputs investigated (Figure 6.2).

The CO_2 mass transfer coefficient ($k_L a_{CO_2}$) was measured in each of the three PBRs and compared based on the power input for sparging, oscillating or rocking. At the given CO_2 concentration in the inlet gas of 1%, the CO_2 transfer rates (CTR) in each PBR follow the same trend with increased power input as the $k_L a_{CO_2}$ (Figure 6.3). The WR displayed higher $k_L a_{CO_2}$ compared to the ALR and OBR at comparable power input, and increased exponentially. In the WR, the $k_L a_{CO_2}$ increased dramatically with little increase in power input above 422 W m^{-3}, at which point the wave created by the rocking motion became a curved, splashing wave, as discussed in Chapter 5.3.2. The pronounced curved wave created in the WR, resulted in the best mass transfer compared to the sparged airlift (ALR) and the rolling wave induced by oscillating baffles (OBR). This comparative result is of great significance for choice of reactor design in processes that require high mass transfer rates and energy efficient mass transfer.

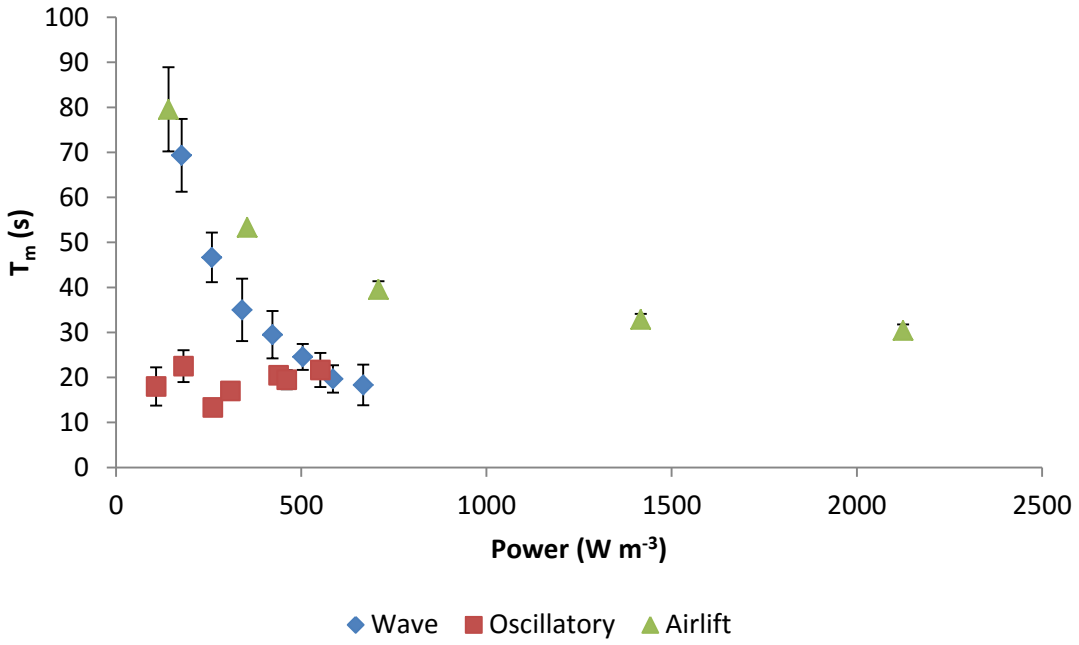

Figure 6.2 Mixing time (T_m) in seconds for each of the wave, oscillatory baffled and airlift photobioreactors at increasing power input. Error bars indicate the standard deviation of n = 3 replicates, those not visible are hidden by the data point.

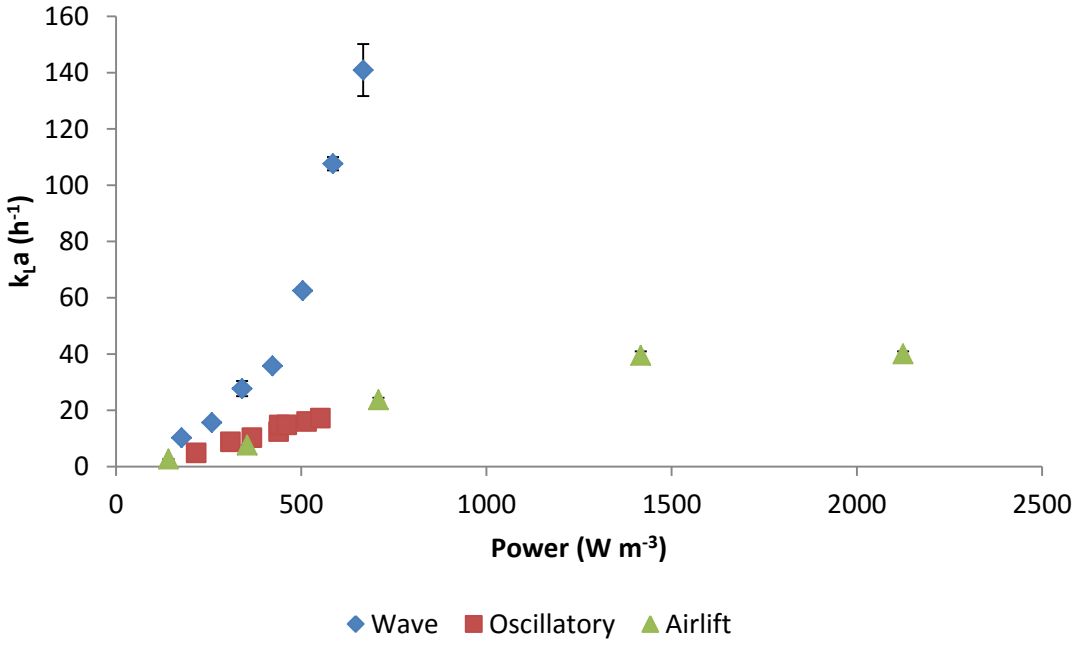

Figure 6.3 Mass transfer coefficient ($k_L a_{CO_2}$) at increasing power input in the wave, oscillatory baffled and airlift photobioreactors. Error bars indicate the standard deviation of n = 3 replicates, those not visible are hidden by the data point.

Figure 1.3 in Chapter 1.3.2 shows $k_L a$ and T_m as a function of the power input across a range of bioreactors. The graph displays the specific power as reported in the journal articles from which the information was sourced. The power input for the sparged reactors in these articles was calculated according to the 'minimum aeration power' and can thus be compared only to other sparged reactors, such as the ALR of this work (Figure 6.4). To compare with mechanically agitated reactors, in light of the discussion in Section 6.3.1, the 'total aeration power' for the ALR was used (Figure 6.5).

The mass transfer coefficient and mixing time vary across the sparged reactors (Figure 6.4), depending on sparger type, range of aeration velocity, and reactor configuration. The airlift reactor in this work (ALR) had a similar $k_L a$ to a flat panel and an external loop airlift reported in literature (Pirouzi et al., 2014; Sierra et al., 2008). The $k_L a$ of the OBR increased more steeply with power increase compared to the pulsed stirred reactor, and at higher oscillation frequencies had the potential to increase further (Figure 6.5). The $k_L a$ of the WR increased even more rapidly with increased power, and after 500 W m^{-3} had the highest rate of increase compared to all other reactor types reported in Figure 6.5. The WR of this work, had among the highest reported $k_L a$ comparable to the pulsed baffled reactor (Ni et al., 1995), the sparged stirred tank reactor (Ni, 1995) and the rotary jet head (Nordkvist, 2003). The WR and OBR of this work, the wave reactor reported by Eibl et al. (2009) and the external loop airlift (Pirouzi et al., 2014) had the fastest mixing times. Surface aeration coupled with mechanical agitation, through oscillating and wave bioreactors, thus has potential as an efficient method for providing mixing and mass transfer.

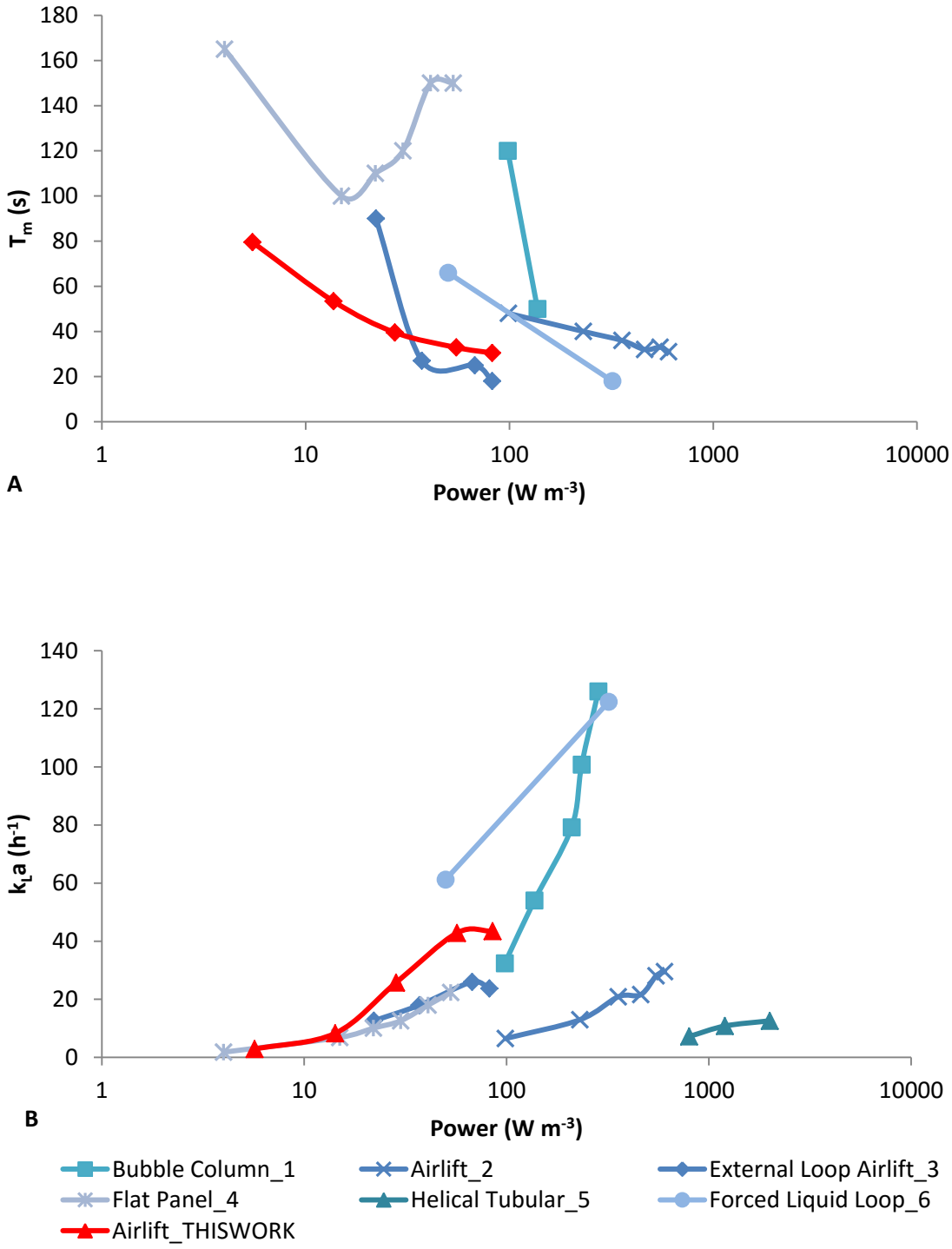

Figure 6.4 (A) Mixing time (T_m) and (B) mass transfer coefficient ($k_L a_{O_2}$) with respect to specific power input (W m^{-3}) across various sparged bioreactors, including the airlift reactor of this work. The power input in this figure represents the minimum aeration power as calculated according the expansion of gas bubbles from sparger to the top of the reactor. Numbers in series titles correspond to references: 1_Miron (1999); 2_Chisti and Jauregui-Haza (2002); 3_Pirouzi et al. (2014); 4_Sierra et al. (2008); 5_Hall et al. (2003); 6_Yazdian et al. (2010). See Table A.1 in Appendix A for detail.

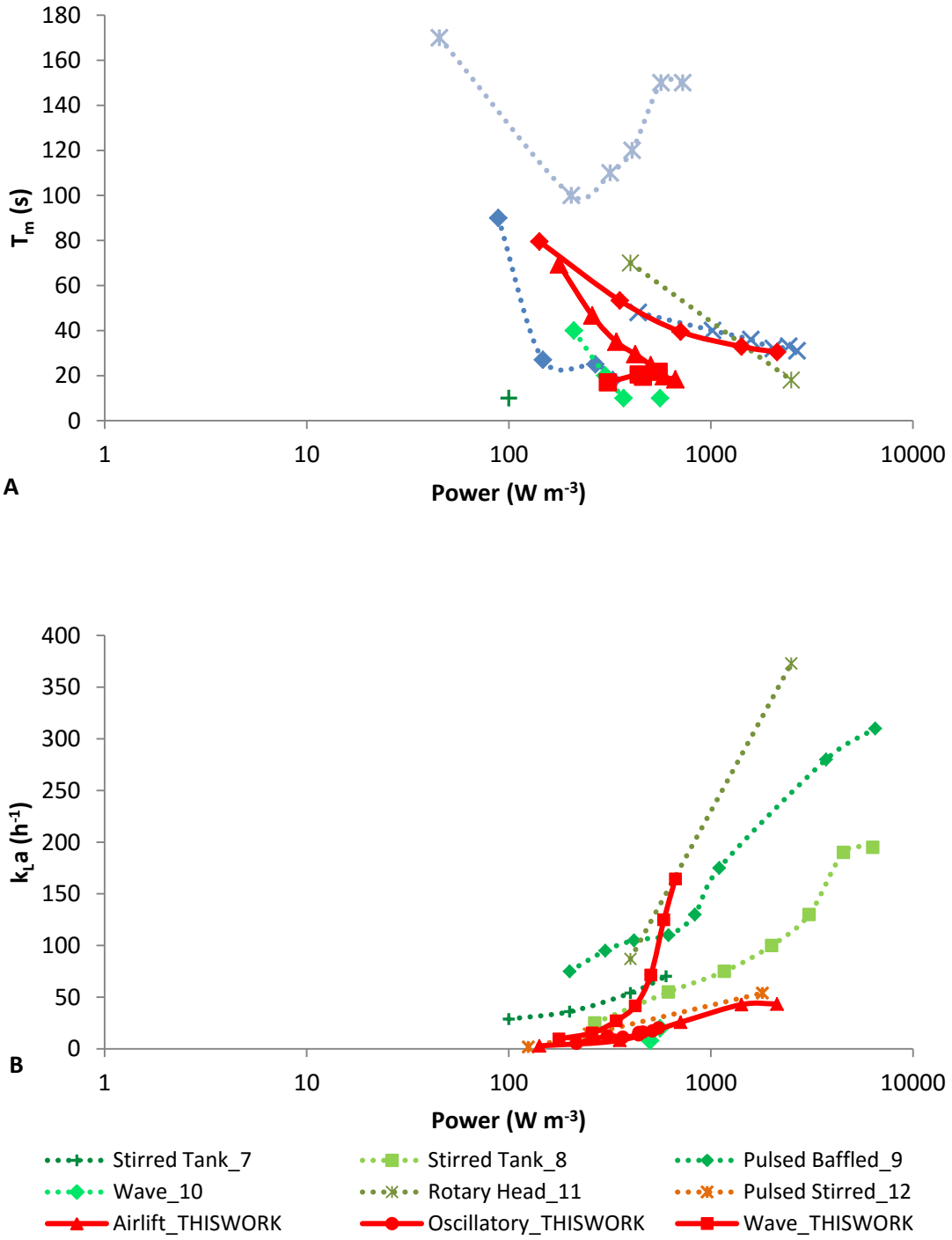

Figure 6.5 (A) Mixing time (T_m) and (B) mass transfer coefficient ($k_L a_{O_2}$) with respect to specific power input (W m^{-3}) across various sparged and mechanically mixed bioreactors, including the airlift, oscillatory baffled and wave reactors of this work. The power values in this figure represent the total power consumed for aerating or mechanically agitating the reactors. Numbers in series titles correspond to references: 7_Jian (2006); 8 and 9_Ni et al. (1995); 10_Eibl et al. (2009); 11_Nordkvist (2003); 12_Ačai and Polakovič (2007). See Table A.1 in Appendix A for detail.

The above are important findings for the improvement of mixing and mass transfer in bioreactors, where creating a wave using a rocking platform or oscillating baffles could provide a more energy efficient alternative to sparged bioreactors, comparable to bioreactors with the highest mixing and mass transfer rates reported in literature. The curved wave produced in the WR had higher $k_L a$ than the rolling wave produced by the OBR. It is important to note that, in previous chapters, a critical minimum CO_2 mass transfer rate has been demonstrated for algal cultivation, above which power was consumed at no further benefit to productivity. The high mass transfer rates obtained in the WR, and other reactors, may not be necessary for algal cultivation. This critical minimum mass transfer rate should be determined independently for different bioprocesses. To determine energy efficiency in terms of algal bioprocesses, it is thus also necessary to compare the algal growth and lipid productivity in sparged (ALR) and surface aerated (OBR and WR) photobioreactors, as done in the following sections.

6.3.3 Biomass and lipid production

Agitation rates that gave comparable $k_L a_{CO_2}$ across the ALR, OBR and WR were chosen, and the algal growth and lipid production under these conditions are presented in Figure 6.6. These results indicated that, at comparable $k_L a_{CO_2}$, *Scenedesmus* sp. had similar growth and lipid production in the ALR and WR. Further, there was no significant reduction in biomass and lipid when the $k_L a_{CO_2}$ was dropped from approximately 40 to 10 h^{-1}. This indicated that excess carbon was being supplied at these $k_L a_{CO_2}$, and only on further reduction to approximately 3 h^{-1} did carbon become a limiting factor, (as seen in the ALR data, Figure 6.6), when aerated with 1 % CO_2. Where carbon was not limiting, the growth and lipid production was limited by light. This was confirmed by an increase in biomass and lipid concentration and productivity with an increase in the light provided to the ALR and WR (Figure 6.6).

The OBR did not support growth of *Scenedesmus* sp. to the same extent as the ALR and WR even at $k_L a_{CO_2}$ of approximately 10 h^{-1} and higher (Figure 6.6). Growth in the OBR at a recorded $k_L a_{CO_2}$ of approximately 20 h^{-1} correlated to growth in the ALR at a $k_L a_{CO_2}$ of approximately 3 h^{-1}. This suggested that the $k_L a_{CO_2}$ recorded for the OBR was higher than the actual mass transfer experienced in the reactor, or that other factors were limiting, such as homogeneous mixing, light and nutrient distribution. In Chapter 4.3, a difference in mixing at either end of the OBR was

described, and additionally the $k_L a$ measurements were taken in the section closest to the gas inlet, and therefore may not represent the $k_L a$ across the length of the reactor.

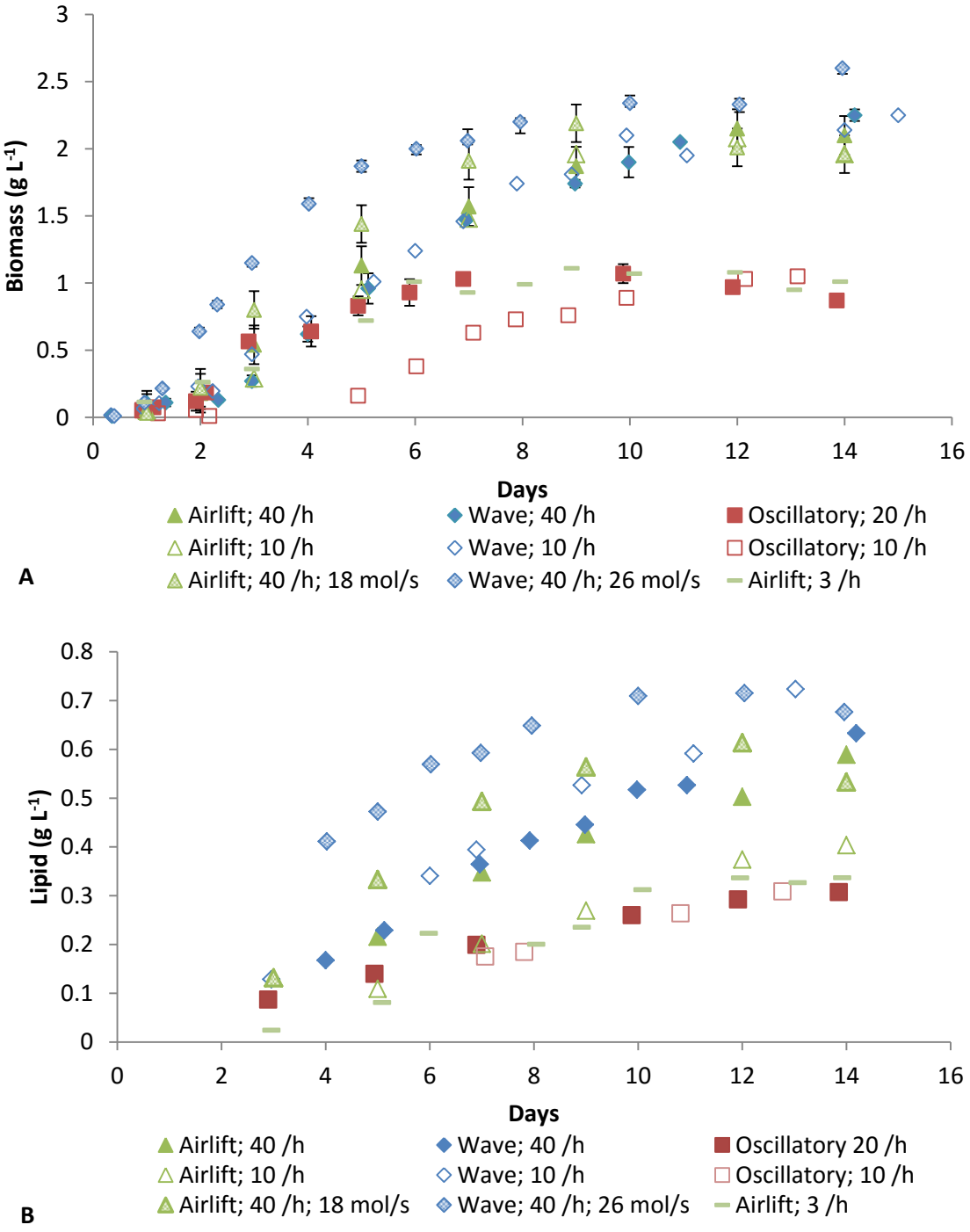

Figure 6.6 (A) Biomass and (B) lipid growth curves of *Scenedesmus* sp. in the airlift, wave and oscillatory baffled photobioreactors at given $k_L a$ (h^{-1}). 9 µmol s^{-1} total light was provided to each reactor, except in the cases indicated. Error bars indicate the standard deviation of n = 2 replicate dry weight samples.

Lipid production across the three PBRs followed similar trends to those described for algal growth, with the exception of the ALR at a $k_L a_{CO_2}$ of approximately 10 h^{-1} (Figure 6.6B). Reduced lipid production in the ALR at lower $k_L a$ could be due to a reduction in the mixing rate, leading to reduced time spent in the light, outer area of the ALR and reduced distribution of nutrients, as discussed in Section 3.3.2.2. In another study, tracer experiments were used to map the movement of an algal cell through the ALR and model the amount of light experienced in different regions of the reactor (Brighton, In review; Jones et al., In review). The results indicated that reduced gas flowrate led to a light limitation in the ALR. Light distribution in the WR was superior to the ALR at a $k_L a$ of approximately 10 h^{-1} (Figure 6.2), because the WR does not contain a distinct dark zone through which algae circulate regularly as with the draft tube of the AL. The algae in the WR are thus exposed to light more consistently, which may be the cause of higher lipid productivity at comparable mass transfer rates.

Comparisons of algal biomass and lipid productivity across the three PBRs were made at agitation rates (aeration, oscillation or rocking) that represented a high power input and a low power input (Table 6.4). The highest aeration rate investigated in the ALR (2 L min^{-1}, 0.02 m s^{-1}) was chosen for 'high power' ('High P'). A rocking rate in the WR was chosen for 'high power' that matched the $k_L a$ at 'high power' in the ALR (25 rpm 10°). The highest oscillation frequency (0.7 Hz) was chosen for the OBR 'high power'. The 'low power' ('Low P') in the ALR was chosen at the minimum aeration rate before loss of biomass and lipid productivity was seen (0.5 L min^{-1}or 0.005 m s^{-1}; Chapter 3.3.2.2). The lowest agitation required to reach similar $k_L a$ were chosen as the 'low power' in the OBR (0.25 Hz) and WR (15 rpm 4°).

Table 6.4 Mass transfer, mixing, power input, biomass and lipid productivity at a comparable high power and low power agitation rate in each of the airlift, oscillatory baffled and wave photobioreactors. All data was obtained with air enriched with 1% CO_2 and exposed to 9 µmol s^{-1} light.

	Reactor	**Agitation (1% CO_2)**	**$k_L a$ (h^{-1})**	**T_m (s)**	**Power (W m^3)**	**Biomass conc. (g L^{-1})**	**Vol. Biomass Productivity (g L^{-1} d^{-1})**	**Biomass productivity per unit power in (g W^{-1} d^{-1})**	**Lipid conc. (g L^{-1})**	**Vol. Lipid Productivity (g L^{-1} d^{-1})**	**Lipid productivity per unit power in (g W^{-1} d^{-1})**
High Power	Airlift	2 L/min airflow	39.5	33	1417	2.23	0.19	0.13	0.64	0.049	0.03
	Wave	25 rpm; 10 deg.	35.8	30	344	2.25	0.19	0.44	0.63	0.045	0.11
	Oscillatory	0.7 Hz	17.2	22	552	1.07	0.11	0.20	0.31	0.022	0.04
Low Power	Airlift	0.5 L/min airflow	7.6	53	354	1.79	0.20	0.56	0.43	0.031	0.09
	Wave	15 rpm; 4 deg.	8.5	47	71	2.25	0.176	2.07	0.72	0.056	0.65
	Oscillatory	0.25 Hz	8.8	17	216	1.05	0.08	0.37	0.31	0.024	0.11

Table 6.4 shows the mass transfer coefficients, mixing times and power input in the ALR, OBR and WR under the conditions chosen as high and low power input ('High P' and 'Low P', respectively). The OBR did not reach equivalent $k_L a_{CO_2}$, due to design constraints (Chapter 4.3.2), and so values at high power are not comparable with the ALR and WR. The ALR and WR had similar maximum biomass and lipid concentrations that did not decrease considerably between high and low power input. The OBR had lower maximum biomass and lipid concentrations than the ALR and WR, possibly due to lower actual mass transfer rates and reduced mixing experienced across the length of the reactor, as discussed above and in Chapter 4.3.

The volumetric productivity and productivity per unit of power input from Table 6.4 are also shown in Figure 6.7. As with maximum biomass and lipid concentrations, the volumetric biomass productivity were similar in the ALR and WR at both high and low power input (Figure 6.7A). This is due to similar $k_L a$ and T_m in these reactors, and an excess carbon supply at the high $k_L a$ (high power). However, at low power input, the wave had considerably higher lipid productivity (0.056 g L^{-1} d^{-1}) compared to the ALR (0.031 g L^{-1} d^{-1}). As discussed above, this may be due to slower circulation through light (downcomer) and dark (riser) zones in the ALR, causing lighted limited lipid production. The WR does not have the same light/dark zones as the ALR, and cells are exposed more consistently to light even at lower rocking rates. The lower productivity in the OBR was possibly due to lower mass transfer rates as discussed previously (Sections 6.3.2 and 4.3.3).

To compare the energy efficiency of algal cultivation and lipid production across the three PBRs, the biomass and lipid productivities were expressed as a function of the power consumed for mixing and aeration, presented in Figure 6.7B. At high power for agitation ('High P'), the productivity in g W^{-1} d^{-1} in each reactor was significantly reduced compared to 'Low P'. 'Low P' was chosen at the $k_L a$ that provided the critical minimum carbon transfer rate before loss in algal productivity. The high productivity per unit power (g W^{-1} d^{-1}) is, therefore, key in demonstrating the benefit of optimising the mixing and mass transfer rates as a function of power input in bioreactors. Furthermore, the lower power input required by the WR to produce equivalent mass transfer to the ALR meant that the biomass productivity per unit power in the WR was three times higher (1.76 g W^{-1} d^{-1}) than the ALR (0.56 g W^{-1} d^{-1}) and the lipid productivity per unit power was 7.5 times higher in the WR (0.66 g W^{-1} d^{-1}) than the ALR (0.09 g W^{-1} d^{-1}). The ALR had the highest power input (354 W m^{-3} at Low P) but the biomass productivity per unit power was greater in the ALR than the OBR (0.37 g W^{-1} d^{-1}). This

was due to the superior volumetric productivity in the ALR (0.199 g L^{-1} d^{-1}) compared to the OBR (0.08 g L^{-1} d^{-1}). Thus, a balance between high volumetric productivities and low power input resulted in superior energy efficiency. There were minimal differences in the lipid productivity in the ALR and OBR at 'Low P'.

These data demonstrated that the surface aerated WR was more energy efficient for algal cultivation and lipid production than a conventional, sparged ALR. This can be attributed to surface aeration in the WR providing ample CO_2 by mass transfer at lower energy consumption than sparging. With further improvements to oscillation amplitude and frequency (discussed in Chapter 4.3.2), the OBR may also surpass the ALR in terms of energy efficiency. Currently, most PBRs use sparging for delivery of CO_2. This work is the first to demonstrate that surface aeration offers an interesting alternative to sparging. This reactor type should be further explored for algal cultivation at large-scale and may also be applied to other bioprocesses requiring energy efficient mass transfer.

The data presented here for the ALR were calculated based on the 'total aeration power' at an inlet gas pressure of 2 bar, as used in this work. If a reduced inlet gas pressure were used (1.12 – 1.19 bar minimum, as discussed in Section 6.3.1) the productivity per unit power in the reactor would improve significantly (Figure 6.8). In this case the ALR had higher productivity per unit power than the WR for biomass. However, the lipid productivity per unit power was still superior in the WR, due to the significantly higher lipid productivity in this reactor. The significant increase in productivity per unit power in the ALR at the reduced gas inlet pressure demonstrates the importance of optimising this inlet gas pressure for reducing energy consumption and improving energy efficiency. In this work, air was supplied to the laboratory at a standard 2 bar pressure. For a large-scale algal production facility an appropriate gas inlet pressure should be chosen, taking into account the required gas flowrates through the liquid head and the pressure drops through piping (dependent on the length of piping from gas compressor to bioreactors) and across spargers (dependent on sparger type and pore size).

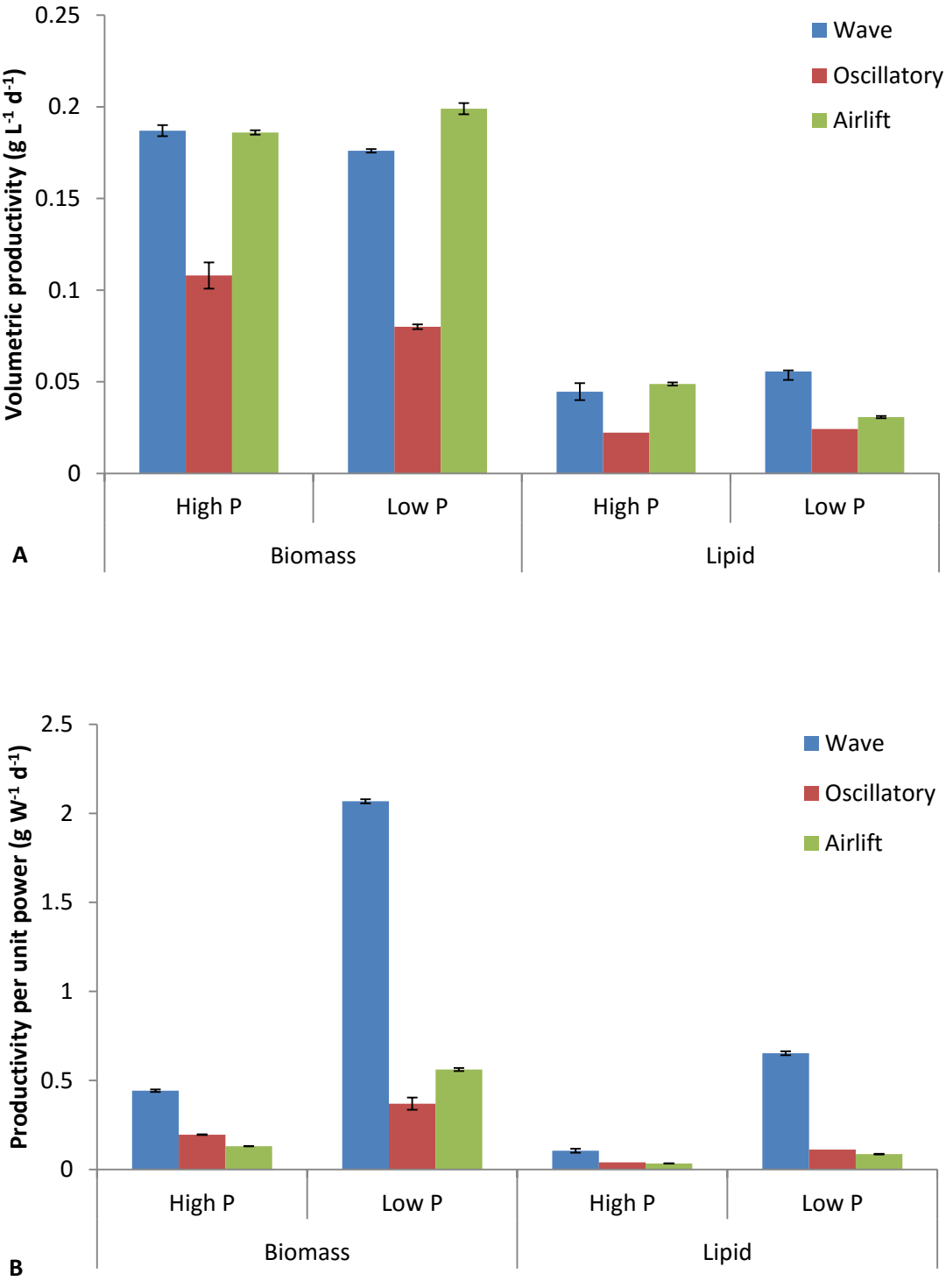

Figure 6.7 (A) Volumetric productivity and (B) productivity per unit power of *Scenedesmus* sp. in the wave, oscillatory baffled and airlift photobioreactors (at 2 bar inlet gas pressure) at high and low power (P) for agitation. See Table 6.4 for $k_L a$ and T_m under each condition. Error bars indicate the standard deviation of n = 5 replicates at 'standard conditions' in the airlift (biomass and lipid), n = 2 replicate dry weight samples in the oscillatory and wave (biomass), and n = 2 replicates of 25 rpm in the wave (lipid).

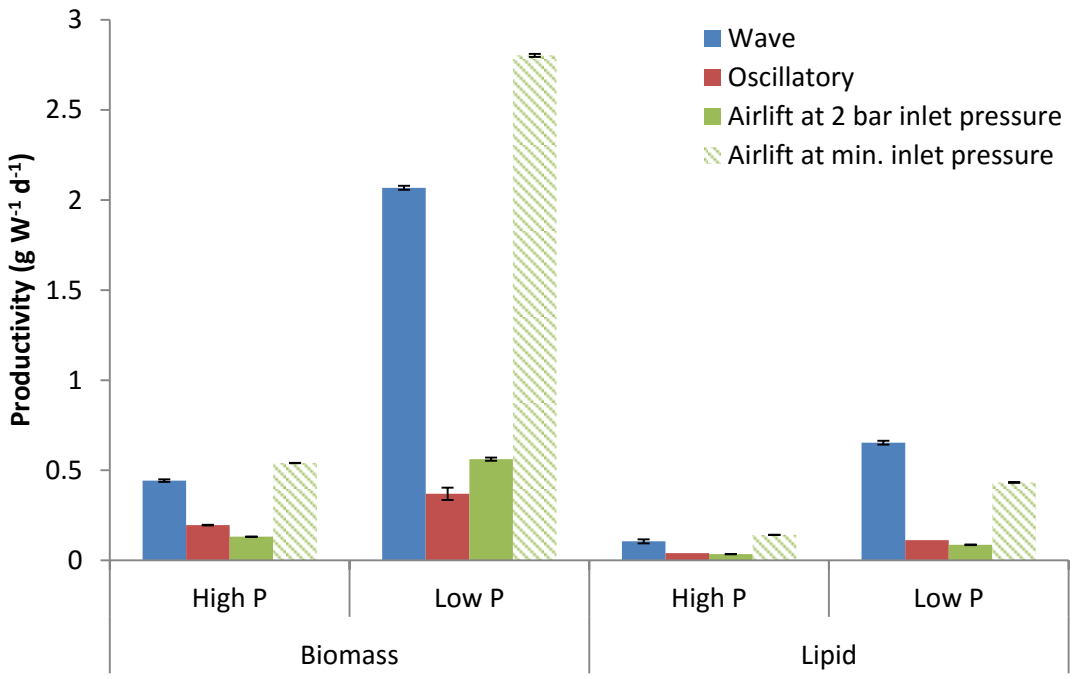

Figure 6.8 Productivity per unit power of *Scenedesmus* sp. in the wave, oscillatory baffled and airlift photobioreactors at high and low power (P) for agitation, including the airlift at a minimum gas inlet pressure (calculated in Section 6.3.1). See Table 6.4 for $k_L a$ and T_m under each condition. Error bars indicate the standard deviation of n = 5 replicates at 'standard conditions' in the airlift (biomass and lipid), n = 2 replicate dry weight samples in the oscillatory and wave (biomass), and n = 2 replicates of 25 rpm in the wave (lipid).

6.3.4 Net Energy Ratios

The net energy ratio (NER) was calculated as the energy (in Joules) that can be harvested from the algal biomass (whole cell including lipid) or lipid only, divided by the energy consumed to cultivate the algae and produce lipid (Chapter 2.6). NER is widely used for assessing the feasibility of energy products. If the NER is less than 1, it means that more energy was used in the generation of a product than can be harvested from it. A bio-energy product thus needs a NER above 1 for it to be considered feasible. In this work the NER was calculated based on the energy used for mixing and mass transfer only. It was assumed that, on scale-up, an outdoor facility utilising sunlight would be preferred to artificial lighting, and therefore the energy required for providing light was not included. The focus of this work was the comparison of PBR designs, and so the NER reported in this chapter did not include the energy for harvesting, drying, lipid extraction or other downstream processing.

If the 'minimum aeration power' for the ALR was used to calculate NER, favourable results were obtained. A NER as high as 10.5 (biomass) and 3.0 (lipid) were achieved at low superficial gas velocity and high CO_2 concentration in the sparged gas (Figure 6.9). At high gas velocity and low CO_2 concentration, the NER was below 1, indicating that more energy was used to aerate the reactor than could be gained from the resulting biomass or lipid. These results do not take into account the energy consumed to deliver the CO_2 enriched air, compressed to 2 bars, via the sparger at the given gas velocities. A more realistic NER was calculated using the 'total aeration power' and this was compared to the NERs of the WR and OB. For each reactor a high power input for mixing and mass transfer (High P), and a power input where operating conditions were optimised in terms of algal production (Low P) were chosen (Figure 6.10).

Figure 6.10A shows that the biomass and lipid NERs across ALR, OBR and WR were all below 1 at a total light of 9 μmol s^{-1}. This result was consistent with previous studies that show low NERs for sparged algal PBRs (Jorquera et al., 2010; Rodolfi et al., 2009; Stephenson et al., 2010). The NERs for the surface aerated WR were considerably higher than the ALR, but remained below unity. Utilizing the whole algal biomass for co-bioenergy-products improves feasibility (higher NERs for whole biomass, compared to lipid only NERs), as seen with methane and biodiesel production (Collet et al., 2014; Lohrey and Kochergin, 2012; Sialve et al., 2009). However, the NERs of the whole biomass in this work remained below 1.

Figure 6.10 shows that the NER of the WR reactor for whole biomass, under optimised conditions for growth and power input (Low P), was substantially higher than those of the ALR and OBR. The NERs in Figure 6.10A were calculated from biomass and lipid productivity under light limited conditions, as seen in Figure 6.6. At increased light (26 μmol s^{-1}) the NER for the WR approximately doubled at High P (Figure 6.10B). This was due to a higher productivity at higher light (Figure 6.6), meaning a shorter time was taken to reach maximum biomass concentration. Lacking experimental data, if it were assumed that at Low P the NER also doubled with increased light, then the NER for the WR becomes 1.67 (biomass) and 0.43 (lipid). At increased light (18 μmol s^{-1}) the NER of the ALR remained below 1, possibly due to the smaller increase in productivity at high light compared to the WR (Figure 6.6). In addition to the high productivity per unit power and higher mass transfer rates at comparable power input, higher NERs demonstrated the great potential of wave generating bioreactors as energy efficient alternatives to sparged bioreactors.

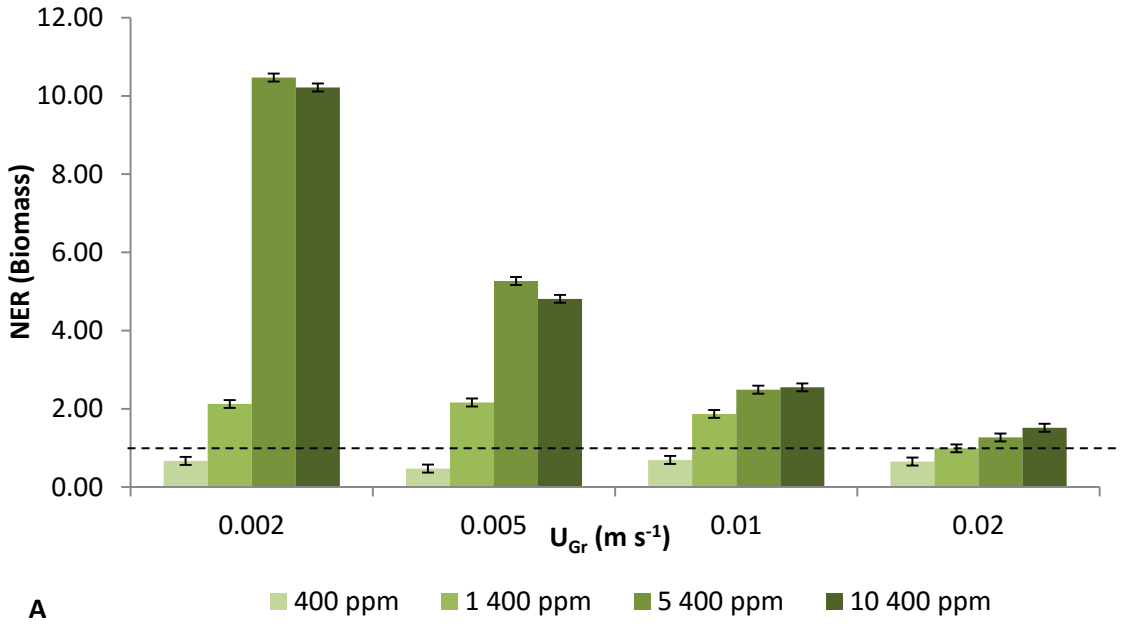

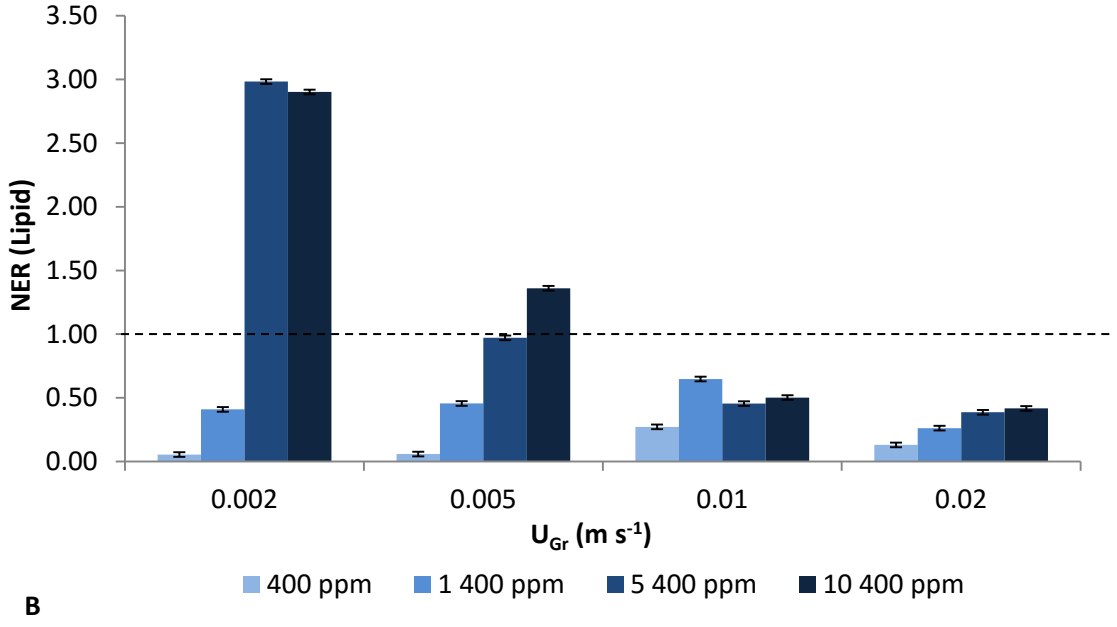

Figure 6.9 Net energy ratio for *Scenedesmus* sp. calculated using 'minimum aeration power' and based on (A) biomass (whole-cell) and (B) lipid only, at various superficial gas velocities and CO_2 concentrations in the airlift photobioreactor. Error bars show the standard deviation calculated using the propagation of variance from standard deviations in n = 5 repeats of cultivation experiments under 'standard conditions'. Dashed line indicates an NER of 1, below which more energy was consumed than can be gained from resulting biomass or lipid.

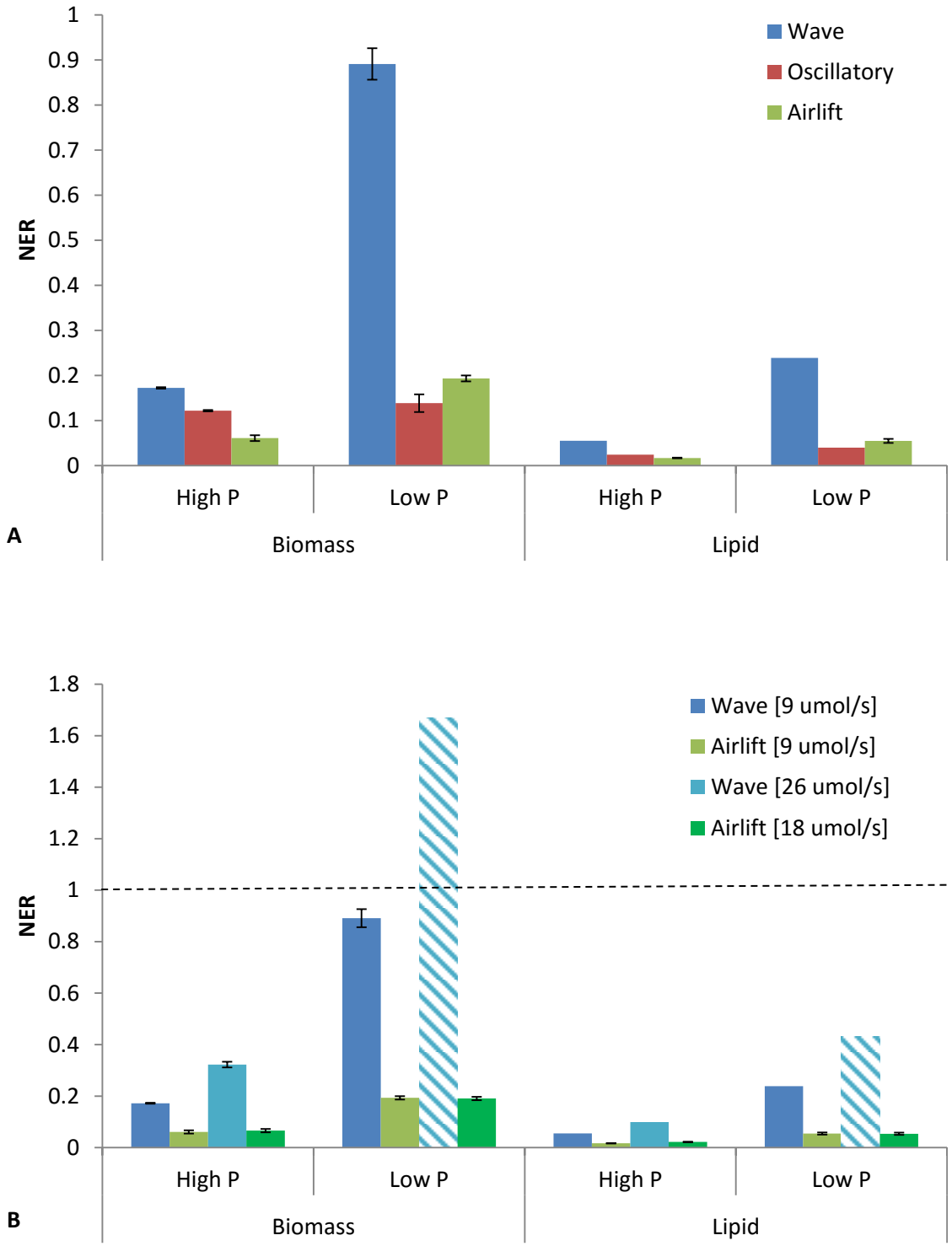

Figure 6.10 (A) Net energy ratio (NER) of *Scenedesmus* sp. for biomass (whole cells) and lipid, produced in the WR, OBR and ALR (calculated using 'total aeration power' at 2 bar inlet pressure) at 9 µmol s^{-1} total light. (B) NERs in the WR and ALR at 9 µmol s^{-1} total light and increased light (18 µmol s^{-1} in the ALR and 26 µmol s^{-1} in the WR). NERs at 26 µmol s^{-1} in the WR at Low P were estimated by extrapolation of experimental data obtained at High P (hashed symbol). High P represents operating conditions that matched the mass transfer at standard conditions in the ALR; Low P represents operating conditions optimised for energy efficiency (lower agitation rates, with productivity maintained). Error bars show the standard deviation calculated using the propagation of variance from standard deviations in biomass concentration and lipid content.

As discussed in Sections 6.3.1 and 6.3.3, if the ALR was operated at the minimum gas inlet pressure, calculated in Section 6.3.1, the power input would be significantly reduced, and thus the NERs would increase according to Figure 6.11. The NERs of the ALR at a minimum inlet gas pressure were comparable to NERs of the WR at low light (9 µmol s^{-1}). Relatively small increases in productivity in the ALR at increased light meant that the NERs at high light (18 µmol s^{-1} and 26 µmol s^{-1}) were significantly higher for the WR (extrapolated data) than the ALR. Even at the minimum gas inlet pressure, the NERs for the ALR were below unity (Figure 6.11). This is the best case scenario for the ALR in terms of optimised gas velocity and gas inlet pressure. NERs for wave generating reactors, on the other hand, may increase above unity at reduced light limitation and can be improved further by designing systems for wave generation that do not rely on rocking platforms (Chapter 5.3.4).

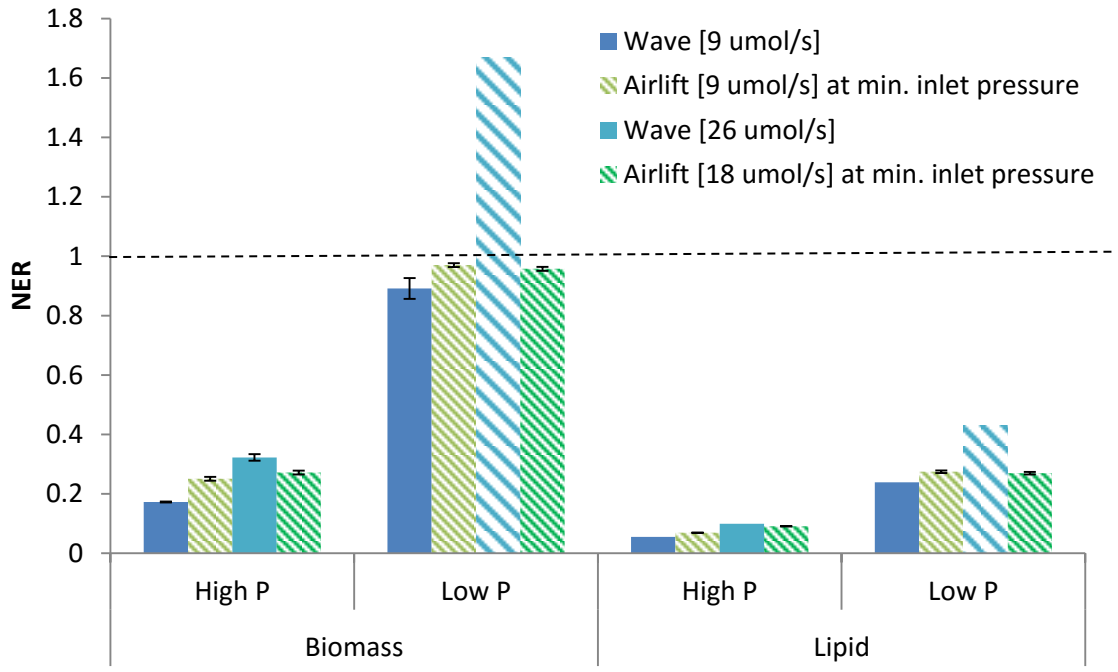

Figure 6.11 Net energy ratio (NER) of *Scenedesmus* sp. calculated using 'total aeration power' at a minimum gas inlet pressure (calculated in Section 6.3.1) for biomass / whole cells and lipid, produced in the WR and ALR at 9 µmol s^{-1} total light and increased light (18 µmol s^{-1} in the ALR and 26 µmol s^{-1} in the WR). NER at 26 µmol s^{-1} in the WR at Low P were estimated by extrapolation of experimental data obtained at High P (blue hashed symbol). Error bars show the standard deviation calculated using the propagation of variance from standard deviations in biomass concentration and lipid content.

A wide range of NERs for algal cultivation have been reported in the literature (Figure 6.12). Differences in NERs depend on the method of calculation of power input, the stages of the processes included in the power input calculation, the methods used for algal cultivation and production and

the basis for energy output (e.g. biomass, lipid, or biodiesel). In Figure 6.12 a selection of NER data from the literature have been modified for better comparability across a variety of calculations and process boundaries, using available information. All NERs in Figure 6.12 were adjusted to include only the cultivation stage of the algal process. The values in Figure 6.12 were also adjusted so that energy output was based on the whole biomass produced, eliminating differences in articles that chose biodiesel, methane, oil or biomass as the end product. After modification, variation in NERs were, therefore, due to differences in algal species, bioreactor configurations, calculations and assumptions used for energy inputs, process scale and productivity (dependent on cultivation protocol, including nutrient use and bioreactor, light availability, temperature and other factors).

The energy data for algal processes in the literature are predominantly for raceway ponds due the prevalence of the use of this cultivation system at large-scale. According to current literature, raceway ponds typically have higher NERs than closed PBRs due to the low energy inputs for mixing by paddlewheel. However, the NERs for raceways ranges from 1.05 (Clarens et al., 2010) to 17.14 (Batan et al., 2010). The wide variation in a number of factors affecting NER, make it difficult to choose correct values for comparison with PBRs.

'Minimum aeration power' was used to calculate energy input into sparged PBRs in the publications reviewed in Figure 6.12. Based on this calculation, the ALR optimised for gas velocity and CO_2 concentration ('This work (ALR)_1'), had the next highest NER (3.01) after the flat panel PBR (NER of 4.51) (Jorquera et al., 2010), in contrast to 'This work (ALR)_2' (based on 'total aeration power'). 'This work (ALR)_1' represents the NER at 5 400 ppm CO_2 and 0.005 m s^{-1} gas velocity, above the critical minimum CO_2 supply rate. In Figure 6.9 it can be seen that higher NERs are possible below critical minimum CO_2 supply rate (e.g. the NER reached 5.85 at 0.002 m s^{-1} gas velocity and 10 400 ppm CO_2), but productivity was substantially lower under these conditions.

'Total aeration power' provided fair comparison with mechanically agitated reactors, as discussed in Section 6.3.1. Based on this calculation, the wave PBR of this work at 26 µmol s^{-1} light (This work (W)_2) had the highest NER (1.67). However, this NER for the WR is based on the assumption described above and may not be the case in reality. In reality, higher algal productivity at higher light, may lead to a carbon limitation at 'Low P' in the WR. The tubular PBR in Figure 6.12 had low NER due to the high energy demand for pumping the liquid through the tubular arrays (Jorquera et

al., 2010; Stephenson et al., 2010). At 'total aeration power' the NERs of all sparged and mechanically agitated PBR were below 1, except for the wave at 26 µmol s^{-1} light, whereas even the lowest NERs for raceway ponds was above 1. In an outdoor facility, where light is not a limiting factor, the NERs of the ALR, OBR and WR could be higher than the values given here and may begin to compare with the NERs of raceway ponds, many of which are calculated based on outdoor light conditions.

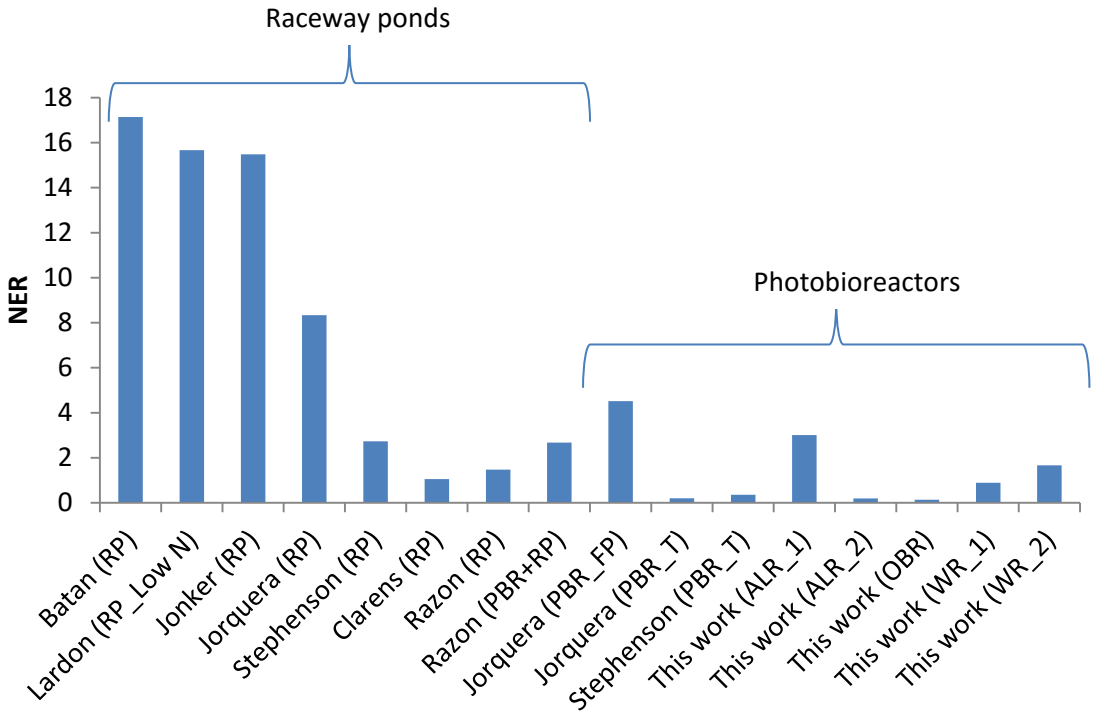

Figure 6.12 Net energy ratios (NER) from a range of studies, calculated as the energy output based on whole biomass divided by energy input for cultivation only, in raceway ponds (RP) or photobioreactors (PBR). Flat-panel (FP), tubular (T) and 'This work (ALR_1)' had energy inputs calculated based on 'minimum aeration power'. 'This work (ALR_2)' was calculated based on 'total aeration power'. 'This work (WR_1)' was at Low P, 9 µmol s^{-1} and 'This work (WR_2)' was at Low P, 26 µmol s^{-1}. Dashed line is at NER = 1. References: (Batan et al., 2010; Clarens et al., 2010; Jonker and Faaij, 2013; Jorquera et al., 2010; Lardon et al., 2009; Razon and Tan, 2011; Stephenson et al., 2010).

The energy efficiency of PBRs can be substantially improved by choice of surface aerated over sparged reactors and by optimising the agitation rate to provide the minimum critical mixing and mass transfer rates for algal production. In addition to the potential of the WR for bioenergy products, PBRs can be used for high value products, such as pigments, high value oils, pharmaceutical compounds, nutritive products, as well as wastewater treatment, carbon

sequestration and other non-energy applications. In these applications, the reductions in energy consumption demonstrated in this work will be greatly beneficial to the cost, carbon footprint and feasibility of the process.

6.4 Conclusions

The results from this work revealed that the surface aerated WR had superior mixing and mass transfer at comparable power input than a range of bioreactors reported in the literature, including sparged bioreactors. This has not been reported previously, and is important for the consideration of reactor choice in bioprocess development. Additionally, the energy efficient mixing and mass transfer provided by the WR resulted in algal productivity per unit power (2.06 g W^{-1} d^{-1}) superior to the conventional sparged ALR (0.56 g W^{-1} d^{-1}). This novel finding may be useful for reducing the energy footprint of algal photobioreactors and bioreactors across bioprocesses (Harding, 2008; Slade and Bauen, 2013).

Comparable biomass and lipid productivity in the WR at lower power input than the ALR resulted in substantially higher NERs for this surface aerated reactor. The NERs across the three PBRs were below unity, indicating the limited applicability of these reactors, under these conditions, for use in the production of bioenergy. However, it was shown that under higher light, the increased productivities led to higher NERs. An NER of 1.67 was estimated for the WR under optimised mixing and mass transfer ('lower power' conditions), and experimental data under high light or outdoor conditions are required to support this. Improvements to the NERs in the WR demonstrated its potential use in algal bioenergy production, where sparged PBRs tend to have NERs below 1.

A reduction in the gas inlet pressure of the ALR resulted in reduced power input, and higher biomass productivity per unit power (2.80 g W^{-1} d^{-1}) than the WR. This is based on the minimum gas inlet pressure required for sparging, which is system dependent and will be larger in reality due to pressure losses with gas delivery from compressor to reactor. Optimisation of the inlet gas pressure is important for improving the energy efficiency of the ALR. However, even at the minimum gas inlet, energy efficiency and NERs were limited based on lower lipid productivity in the ALR compared to the WR, and lower biomass and lipid productivity at increased light compared to the WR. This

may be due to an improvement in the relationship between mixing and light distribution in the WR compared to the ALR.

Based on algal cultivation data it was postulated that the overall mass transfer in the OBR was lower than the measured values owing to regional variation, resulting in carbon limited algal growth. This limited growth may also be due to limitation in mixing, and thus light and nutrient distribution. Improvements to the design of the OBR may increase the energy efficiency and hence potential application of this reactor.

The application of wave motion (particularly a curved wave as seen in the WR), to large-scale algal cultivation systems and other bioprocesses has interesting potential for reduced energy-related costs and environmental burdens. This research serves as the basis for increased focus on provision of mass transfer through surface aeration enhanced by wave motion. The mass transfer thus provided is applicable to both algal cultivation and other bioprocesses.

There is much variation in NERs for algal cultivation in the literature due to a range of inputs and calculations that affect NERs. From the data reviewed in Section 6.3.4, raceway ponds generally have higher NERs than PBRs. This may be biased given the light limited nature of data for the PBRs in this work and all artificially lit algal bioreactor systems. For products where energy balance is vital, such as algal biodiesel and methane, raceway ponds may still be the system of choice. For high value bio-products that require minimal contamination, and for pond inoculum development, where rapid mass transfer is important for high productivities, PBRs are preferable. Reduced energy input in these high productivity systems lowers cost, carbon footprint and overall feasibility and competiveness of the process and resulting algal bio-products.

The NERs discussed in this chapter are typically calculated as part of detailed analyses of processes for energy production. To continue the investigation, a Life Cycle Analysis was performed for algal biodiesel production by *Scenedesmus* sp. grown in the ALR and WR as described in Chapter 7.

7 Life cycle analysis of algal biodiesel using photobioreactors

7.1 Introduction and Literature Review

Previous chapters looked at PBRs in isolation and improvements that can be made with regard to mixing and mass transfer for algal cultivation. In this final chapter, the improvements to PBRs discussed in Chapters 3, 4, 5 and 6 are investigated in the context of a whole algal bioprocess using life cycle analysis. The importance of this investigation was to quantify the impact of the differences between PBRs (Chapter 6) when considered as a part of a larger bioprocess i.e. do they carry over or become diluted? For this analysis, algal biodiesel production was used as an example. Biodiesel was chosen since bioenergy products are topical, relevant in the context of reduced energy inputs and much process development work has been reported. Although low NERs discussed in Chapter 6 limit the feasibility of biodiesel production using PBRs without further improvements, changes in environmental burdens remain relevant and provide insight for other algal bioprocesses.

One of the major driving forces behind research and development of algal biodiesel is its potential as an environmentally sustainable transport fuel (Brennan and Owende, 2010; Demirbas, 2011; Lam and Lee, 2012; Slade and Bauen, 2013). As a renewable fuel source and third generation biofuel, algal biodiesel has much potential compared to fossil or crop-derived fuels. However, rigorous analysis of the production process is required to determine the environmental impacts of algal biodiesel before it can be deemed sustainable. A popular method for assessing the environmental impacts of a product or production process is Life Cycle Analysis (LCA). Many LCAs have been performed for algal biodiesel production under a variety of conditions and assumptions. These studies show that fossil energy requirement, greenhouse gas emissions (also categorised as carbon footprint or global warming potential), nutrient use, and water consumption are the major environmental concerns (Adesanya et al., 2014; Azadi et al., 2014; Campbell et al., 2011; Clarens et al., 2010; Collet et al., 2014; Kadam, 2002; Lardon et al., 2009; Sander and Murthy, 2010; Stephenson et al., 2010; Yang et al., 2011).

Table 7.1 summarises LCA results from reports on algal biodiesel, focusing on greenhouse gas emissions as well as other environmental categories such as eutrophication potential, water use and land use. There is a large amount of variation in the projected greenhouse gas emissions depending on the scope of the LCA (the process boundaries chosen for analysis) and the choice of methods for various stages of production. The choice of open raceway ponds or closed PBRs has a significant impact on the overall GHG (greenhouse gas) emissions, where Stephenson et al. (2010) show raceway ponds to result in lower emissions. CO_2 from flue gas to feed the algal cultures was commonly used in the LCA, and these studies had lower GHG emissions than those using pure CO_2, except in the case where a tubular PBR was used (Azadi et al., 2014; Stephenson et al., 2010). Harvesting and drying the biomass had substantial effects on GHG emissions (Azadi et al., 2014; Sander and Murthy, 2010). Centrifugation was commonly chosen for harvesting, but this requires a large amount of electricity, thus contributing significantly to GHG emissions from fossil-derived energy. Use of filter-press, flocculation and flotation are seen to be more environmentally sustainable alternatives (Campbell et al., 2011; Sander and Murthy, 2010; Stephenson et al., 2010). Gas-fired biomass drying releases large amounts of GHG, and is problematic for algal biodiesel sustainability. Solar drying has no GHG emissions or other environmental burdens, but is slow. Using biodiesel conversion methods that are not inhibited by wet biomass are important for improving sustainability (Azadi et al., 2014). Many of the LCAs include anaerobic digestion of the remaining biomass after lipid extraction for the production of methane, or other by-products from the process including syngas, ethanol and nutrient rich feed. Glycerol is also commonly considered a useful bioproduct from the transesterification of lipid to biodiesel. The reduction in GHG emissions and other environmental burdens associated with producing these by-products from algae as opposed to fossil sources has a significantly positive bearing on the overall LCA (Batan et al., 2010; Sander and Murthy, 2010; Stephenson et al., 2010). With these guidelines in mind, a simulated algal biodiesel production process was developed for this study.

SimaPro is widely used as an effective software package for LCA modelling with access to a selection of comprehensive databases for a variety of products and processes. The SimaPro databases contain information for country-specific production as well as global and European averaged data. Many algal bioproduct and algal biodiesel LCAs have been performed using SimaPro, and this software has been used extensively for research purposes as well as in industry (Campbell et al., 2011; Lardon et al., 2009; Razon and Tan, 2011). SimaPro was used in this current study for comparability with European LCAs and for analysis in a local, South African context, as discussed in the body of this

chapter. A number of other LCA software packages exist, some of which have been used for algal biodiesel assessments, such as OpenLCA, GaBi and GREET (Greenhouse gases, Regulated Emission and Energy in Transportation) (Adesanya et al., 2014; Batan et al., 2010; Jorquera et al., 2010; Sander and Murthy, 2010). GaBi is the least widely used with a lack of available studies with which to compare an algal biodiesel LCA. OpenLCA is the most recently developed and will undergo further developments before it is as widely used as SimaPro. GREET is specifically for energy consumption and air emissions and is often used for the assessment of algal biofuels (Miller and Theis, 2006). Additionally, GREET was developed in the USA and its databases are useful for analyses relevant to the USA (Miller and Theis, 2006). SimaPro, on the other hand, has a broader scope in terms of the impact categories, the product types for assessment and for comparability to European and global LCAs.

Table 7.1 Summary of several Life Cycle Analyses performed for algal biodiesel production with focus on global warming potential measured as CO_2 emissions, where NER is defined as the energy output (on combustion of biodiesel).divided by the energy input (for production).

Reference	Process description	LCA method	Global warming potential	Other impacts
Beal et al. (2015)	• Cultivation: Hybrid PBR and open pond system; 100 ha currently operational facility; two sepcies • Carbon from waste source • Harvest: Natural settling, settling, ring dryer • Terraced, gravity flow • Hexane extraction	• EROI(energy return on investment) for energy inputs and outputs • Economic analysis	•	• Carbon, silicon, nitrogen and phosphorous demand for ten cases • Water savings and land requirement compared over ten cases • EROI/NER = 0.6 -3
Adesanya et al. (2014)	• Cultivation: Airlift at high N, then raceway at low N • CO_2 from flue gas at 12.5% • Harvest: $Al_2(SO_4)_3$ flocculation, centrifugation • Natural-gas fired dryer • Oil extraction :Hexane in cascade of mixer-settlers • Oil refining: NaOH, H_3PO_4 • Anaerobic digestion for heat and electricity • Transesterification to biodiesel	• OpenLCA software; Ecoinvent v2.2, ELCD and NREL databases; CLM 2001 method • System boundary: algal cultivation to biodiesel production, biodiesel combustion and materials for construction of equipment. • Functional unit: 1000 kg biodiesel • Sensitivity analysis on cultivation method, TAG productivity, culture velocity in airlift / raceway, water usage, cell disruption technique, lipid recovery • Electricity: national energy network, United Kingdom	• 51.2 g CO_2/ MJ biodiesel • 21.5 g CO_2/ MJ biodiesel if mixotrophic cultivation used • 41.6 g CO_2/ MJ biodiesel if 50% lipid recovery used (instead of 99%)	• Fossil energy requirement: 31 GJ/ ton biodiesel • NER = 1.2.

Azadi et al. (2014)	• Bio-energy refinery
	• Cultivation: Raceway pond
	• Harvest: Clarification, centrifugation
	• Gas-fired/solar drying
	• Wet / dry oil extraction
	• Transesterification
	• Spent biomass used for biogas/syngas
		• System boundary: From energy, fertilizer, construction, chemicals
		• Sensitivity analyses for various strategies:
		  ○ oil extraction
		  ○ bio-energy from spent biomass
		• Electricity: average grid carbon intensities of France (i.e. 30 g e-CO2/MJe) and China (i.e. 340 g e-CO2/MJe) used as lower and upper bounds
			• Wet extraction + anaerobic digestion:
			  ○ 85 g CO_2/MJ
			• Wet extraction + hydrothermal gasification:
			  ○ 40 g CO_2/ MJ	

Reference	Process description	LCA method	Global warming potential	Other impacts
Collet et al. (2014)	• *Nannochloropsis occulata* (marine) • Cultivation: Ponds (80 Ha total) • Harvest: Flocculation (iron chloride) • Oil extraction: Hexane (from wet paste) • Alkaline transesterification	• ReCiPe midpoint method • System boundary: Production to combustion • Functional unit: 1000 MJ algal biodiesel • Electricity: European Electricity Mix	• 55.6 g CO_2 /MJ biodiesel	• Cumulative Energy Demand (CED) = 2172 MJ consumption from 2027 MJ produced • NER = 0.93
Quinn et al. (2014)	• Cultivation: down-flow open ponds • Harvest: settling, dissolved air flotation, centrifugation • Hexane extraction • Anaerobic digestion	• GREET model • System boundary: Strain to pump • Co-product allocation	• -41.7 g CO_2/MJ biodiesel	NER = 1.4
Frank et al. (2012)	• Cultivation: Open ponds • Harvest: Bio-flocculation, centrifuge • Hexane extraction • Anaerobic digestion	• GREET to compute fossil, petroleum and total energy usage • System boundary: Algal cultivation to biodiesel combustion	• 55.4 g CO_2/MJ biodiesel for baseline scenario • Compared to 101.0 g CO_2/MJ biodiesel for petroleum diesel	
Campbell et al. (2011)	• Cultivation: Raceway ponds • CO_2 from flu gas (15%) • Harvest: Flocculation, floatation and centrifugation • Transesterification • Anaerobic digestion of remaining biomass	• SimaPro 7 • System boundaries: Cradle to grave, excluding construction of production facilities • Functional unit: Combustion of enough fuel in an articulated truck to transport 1 tonne of freight 1 km. • Electricity: Energy Supply Association of Australia (mostly coal and natural gas)	• -25.86 g CO_2/MJ at production rate of 30 g/m^2/d • -11.82 g CO_2 /MJ at production rate of 15 g/m^2/d	

Reference	Process description	LCA method	Global warming potential	Other impacts
Razon and Tan (2011)	• Cultivation: Flat-panel PBR feeds into raceway pond • Harvest: Gravitational settling and microfiltration • Oil extraction: bead mill • Transesterification • Anaerobic digestion	• SimaPro 7; Cumulative Energy Demand • System boundaries: Cultivation to bioenergy production • Functional unit: 1kg algal biodiesel • Electricity: All electricity provided by a natural-gas fired combined heat and power (CHP) plant.		• NER: 0.25 – 0.54
Yang et al. (2011)	• Cultivation: Open ponds • *Chlorella vulgaris*	• Functional Unit: 1 kg biodiesel • System boundary: Cultivation to esterification		• Water footprint: 3726 kg water/kg biodiesel • Nutrient balance: 0.33 kg nitrogen; 0.71 kg phosphate

Batan et al. (2010)	• Cultivation: Sparged, polyethylene PBR bags
	• *Nanochloropsis salina*
	• CO_2 from flu gas, mixed with air at 2%
	• Harvest: Centrifugation
	• Solvent Extraction
	• Trans-esterification
	• Transport
		• GREET 1.8C analysis model
		• System boundary: "Strain-to-pump"
		• GHG emissions (CO_2, CH_4, N_2O)
		• Co-product allocation: Biomass and glycerin
		• Electricity: USA average mix; North-east mix; California mix
			• -59.49 g CO_2/MJ
			• Negative CO_2 output due to:
			  ○ algal CO_2 capture
			  ○ displacement of petroleum
			  ○ displacement of co-products
			• Lower C-footprint than conventional diesel
				•

Clarens et al. (2010)	• Cultivation: Raceway ponds • Additional CO_2 sparged in • Wastewater effluent • Harvest: Flocculation + centrifugation	• Crystal Ball modeling software • System boundary: Cradle-to-gate for dry biomass (not biodiesel) • Functional Unit: 317 GJ biomass energy	• 0.567 g CO_2/MJ	• Water use: 0.004 m3/MJ • Eutrophication potential: 1.04 g /MJ (PO_4) • Land use: 1.3 ha/MJ

Reference	Process description	LCA method	Global warming potential	Other impacts
Sander and Murthy (2010)	• Cultivation: Raceway ponds (inoculated from PBR) • Wastewater for nutrients • CO_2 from flu gas • Harvest: Chamber filter press / centrifuge • Natural gas fired dryer • Oil extraction: Hexane • Transesterification • Transport	• GREET 1.8 model (data source) • System boundary: "Strain-to-pump" • Functional Unit: 1000 MJ from algal biodiesel • Co-product allocation: Spent biomass to ethanol; distillers dry grain (DDGS)	• Growth: 0.00 g CO_2/MJ • Harvest (Filter press): 241.81 g CO_2/MJ • Separation: 6.33 g CO_2/MJ • Biodiesel conversion: 3.18 g CO_2/MJ • Co-product allocation: -273.60 • TOTAL (Filter press): -20.9 • TOTAL (Centrifuge): 135.71 g CO_2/MJ	

Stephenson et al. (2010)	• Cultivation: Raceway vs. tubular PBR
	• Flu gas (12.5% CO_2)
	• Two stage nutrient strategy: N-sufficient, N-deficient
	• Harvest: Flocculation
	• Homogenisation, solvent extraction
	• Transesterification
	• Anaerobic digestion
		• EDIP 2003 analysis method
		• System boundary: Cradle-to-gate
		• Functional Unit: 1000 kg algal biodiesel
		• Co-product allocation:
		  ○ Methane
		  ○ Glycerol
		• Electricity: Methane + National energy network (UK)
			• Tubular PBR: 315 g CO_2/MJ
			• Raceway: 18.86 g CO_2/MJ
			• Cultivation has highest CO_2 emissions.	

Jorquera et al, (2010)	• Cultivation: comparison of raceway, tubular and flatpanel PBRs • *Nanochloropsis* sp.	• GaBi software • System boundary: Cultivation only • Functional Unit: 100 tonnes biomass dry weight		• NERs: 1.58 – 7.01
Lardon et al. (2009)	• Cultivation: Raceways (100 Ha) • *Chlorella vulgaris* • Normal vs. low nitrogen • Harvest: Flocculation with lime • Oil extraction: Dry vs. wet extraction • Esterification	• CML analysis method • CED (cumulative energy demand) • System boundary: 'Cradle-to-combustion' • Functional Unit: Combustion of 1 MJ in diesel engine • Electricity: European energy mix (natural gas)		• CED = 1.66 MJ input • 2.23 MJ produced (biodiesel plus oilcake) • NER = 1.3

7.2 Life Cycle Analysis Methodology

A life cycle analysis was performed using the SimaPro 8.0.4 software package. An LCA consists of four stages including the definition of the goal and scope, the life cycle inventory or data collection, the impact assessment and the interpretation.

7.2.1 Goal and Scope

The aim of this work was to assess whether the differences in power input across sparged and surface aerated PBRs (Chapter 6) translate into significantly altered environmental burdens for an entire production process. The LCA was expected to demonstrate the importance of optimising reactor conditions and to confirm and quantify the potential of the WR for reduced environmental burdens. The LCA includes assessment of the environmental burdens for algal biodiesel production from *Scenedesmus* sp., particularly those associated with energy consumption and nutrient use, and to make comparisons across three scenarios with changes to the algal PBR stage of production. The three reactor scenarios were as follows:

1. Airlift photobioreactor at 'standard' gas velocity, 2 L min^{-1} (2 bar), denoted ALR High Power
2. Airlift photobioreactor at critical min. gas velocity, 0.5 L min^{-1} (2 bar), denoted ALR Optimum
3. Wave photobioreactor at optimum agitation rate, 15 rpm 4°, denoted WR Optimum

The functional unit of the LCA was 1000 kg of biodiesel and included all the inputs and outputs from the simulated process in Figure 7.1, including the extraction and production of raw materials. The LCA was considered a cradle-to-factory-gate analysis as the transport of the product to the regional supplier was not included. The materials and construction of the production facility were also excluded. Glycerine was included as a by-product of the process using the substitution method, meaning that the system boundaries were expanded to include impacts of this by-product. The emissions that would have occurred had this by-product been produced elsewhere were credited to the process.

7.2.2 Life Cycle Inventory (LCI)

The LCI was generated using a MATLAB process flow-sheet model, as described in Sections 7.2.3.1 to 7.2.3.7, below. Examples of the outputs from the model are given in Appendix D (Tables D1, D2 and

D3), where each stream in Figure 7.1 (1 – 27) was allocated a mass of each component (in kg). The LCA databases used were Ecoinvent 3, Agri-footprint and USLCI. The LCI included the production of all raw materials and components of the process. Where possible, data from European datasets were used (coded RER in SimaPro), for comparison with literature figures. Electricity used in the process was based on the ENTSO-E (European Network of Transmission System Operators for electricity) electricity mix (Itten et al., 2012). The LCA was repeated using datasets relevant for a South African context, including a South African electricity mix.

7.2.3 Algal biodiesel production process model

A model was developed to simulate the production of algal biodiesel at large scale. The flow-sheet of the process chosen for the model is shown in Figure 7.1. The simulated process included a cultivation stage where algae were grown in ALRs or WRs, based on experimental data collected at laboratory scale. The remainder of the process was based on data collected from various sources in the literature. The material and energy balances required for the simulation were developed in MATLAB by Richardson (2011), and updated for the current investigation. The key update was made to the reactor stage of the process, where the reactor modelled by Richardson (2011) was replaced with ALR or WR, and the inputs and outputs recalculated for these PBRs. Alterations were also made to the methods of settling and centrifugation, to make these appropriate for low energy *Scenedesmus* sp. harvesting.

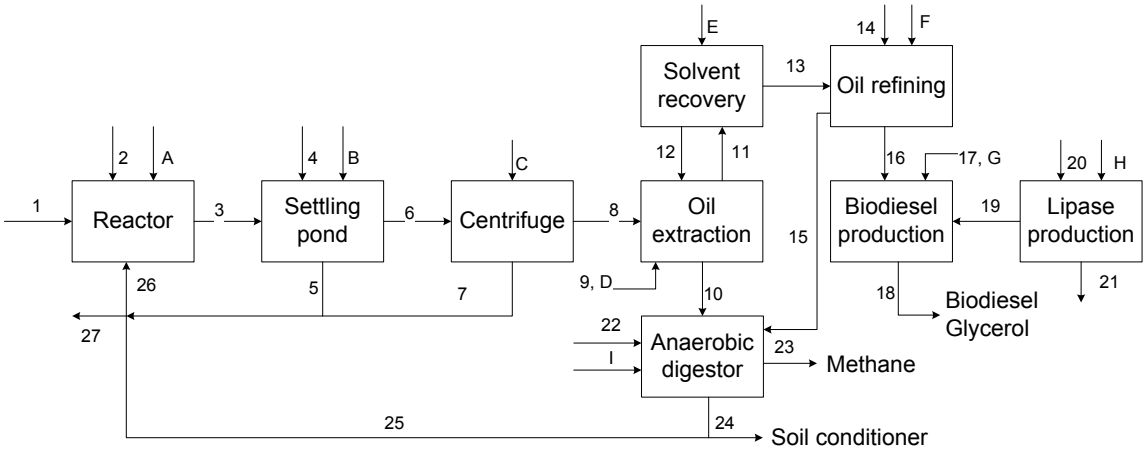

Figure 7.1 Process flow-sheet for the production of biodiesel from algae with co-production of methane from anaerobic digestion of algal residue. Annotations 1-24 refer to flow and A-I refer to energy inputs (Richardson, 2011).

7.2.3.1 Cultivation

The first stage of the process flow-sheet was cultivation of *Scenedemus* sp. in either an airlift or wave photobioreactor. Experimental data (presented in previous chapters) were used for biomass concentrations and productivities, lipid content and power input. The cultivation medium used was BBM medium, as described in Chapter 2.2, with 150 mg L^{-1} nitrate for enhanced lipid production. The scale-up of the medium was calculated in the MATLAB model according to the quantities of algae required to produce 1000 kg of biodiesel. Three cultivation scenarios were modelled:

1. ALR at 2 L min^{-1} gas flowrate, and 2 bar gas inlet pressure.
2. ALR at 0.5 L min^{-1} gas flowrate, and 2 bar gas inlet pressure.
3. WR at 15 rpm rocking rate and 4° rocking angle.

It was assumed that CO_2 was supplied at the quantity required to produce 1000 kg of biodiesel, given the growth rates and lipid productivity specified in the model.

7.2.3.2 Harvesting

Harvesting of algal cells was modelled according to Lee et al. (2010) using bioflocculation with a microbial flocculant to avoid the use of harmful chemical flocculants such as aluminium sulphate. Flocculation required mixing of the algal culture in the flocculation tanks which consumes energy at 0.0016 MJ m^{-3} (Lee et al., 2010). The settling ponds were scraped with rotating flight scrappers at 0.8 W m^{-2} of pond area to recover the biomass (Stephenson et al., 2010). A 90% recovery of biomass was assumed. To concentrate the biomass further a disc-stack centrifuge was used at an electrical efficiency of 93%. A biomass recovery of 95% was assumed at 28.8 MJ m^{-3} (Molina Grima et al., 2003). Water and nutrients were recycled to the PBR (Molina Grima et al., 2003; Richardson, 2011; Stephenson et al., 2010).

7.2.3.3 Oil extraction

Oil extraction from the algal biomass was performed using hexane in a cascade of mixer-settlers to allow sufficient contact between solvent and biomass. Hexane was supplied at half the flowrate of the biomass and a recovery of 80% lipids and chlorophyll was assumed. The power requirement for mixing was calculated as a function of the rotational speed, power number and diameter of the impeller and the two phase mixer density. A 90% motor efficiency was assumed and each mixer agitated at 5.3 Hz rotational speed and 3.4 kW m^{-3} (Adesanya et al., 2014; Richardson, 2011; Stephenson et al., 2010).

7.2.3.4 Solvent recovery

The hexane was separated from the lipid using a stripper column, resulting in recoveries of 99.5% hexane. The tops were condensed using heat exchange with the inlet stream (25 – 60°C). The heat requirement for the reboiler was 1.6 kJ kg^{-1} of lipid in hexane entering the distillation column (Adesanya et al., 2014; Stephenson et al., 2010).

7.2.3.5 Oil refining

The lipid separated from the hexane was then refined using phosphoric acid and sodium hydroxide to remove the chlorophyll (98% removed) and residual hexane (50% removed). The process required 540 kJ kg^{-1} heat, 108 kJ kg^{-1} electricity and 0.108 m^3 kg^{-1} water (Richardson, 2011; Stephenson et al., 2010).

7.2.3.6 Anaerobic digestion

The biomass remaining after oil extraction was modelled to be treated in an anaerobic digester with the addition of phosphoric acid, sodium hydroxide and urea. The anaerobic digester had a 20 day retention time and used 10 W m^{-3} of chemical oxygen demand. The methane generated would be used to run a gas-fired power station at an electrical efficiency of 60%. The energy produced from methane was assumed to be 50.1 MJ kg^{-1}. The carbon dioxide generated was recycled to the PBR (Richardson, 2011; Sialve et al., 2009; Stephenson et al., 2010).

7.2.3.7 Biodiesel production

Research by Harding et al. (2008) showed that transesterification of algal oil to biodiesel could be catalysed by the enzyme lipase in place of the conventional alkali chemical catalyst. The reaction using the enzyme catalyst is slower but is not restricted by the water content in the algae, thus eliminating the need for drying the algal biomass prior to transesterification. This considerably reduces the energy consumption of the biodiesel production. The flow-sheet simulation was generated for the production of 1000 kg of biodiesel.

7.2.4 Life Cycle Impact Assessment (LCIA) and interpretation

The LCIA involved choosing methods for analysing the inventory data under impact categories that suited the goal and scope of this LCA. CML-IA Baseline assessment method V3.02 (2013) and Cumulative Energy Demand V1.09 are reliable methods containing impact categories relevant to this work. These methods have been used in similar LCA studies in the literature (Adesanya et al., 2014; Collet et al., 2014; Harding et al., 2008; Lardon et al., 2009; Razon and Tan, 2011) and they meet all the mandatory requirements for the ISO standards. CML-IA Baseline includes impact categories widely used in LCA. The following were chosen for this study:

- Abiotic depletion (kg Sb eq.)
- Abiotic depletion, fossil fuels (MJ)
- Global warming, GWP100a (kg CO_2 eq.)
- Acidification (kg SO_2 eq.)
- Eutrophication (kg PO_4^{3-} eq.)

The abiotic depletion and global warming categories were chosen to represent the energy related impacts, through the depletion of fossil fuel reserves and emission of greenhouse gases. The abiotic depletion indicator is related to the extraction of minerals (represented by the mineral antimony, Sb) and fossil fuels (measured in MJ) due to the process inputs. Global warming is caused by increased greenhouse gases in the atmosphere. The characterisation model for this impact category was developed by the Intergovernmental Panel on Climate Change (IPCC 1996; updated in 2013). The global warming indicator is expressed as the amount of CO_2 emissions (the prominent greenhouse gas) and is expressed as the Global Warming Potential (GWP) for a time horizon of 100 years (100a).

The acidification and eutrophication categories were chosen to investigate the impacts of nutrient and chemical inputs to the process. Acidifying substances cause damage to soil, groundwater, surface water, organisms, ecosystems and buildings. The acidification impact category is expressed in kg SO_2 equivalents per kg emission. The eutrophication impact category includes all impacts due to excessive levels of macro-nutrients released into the environment. This indicator is expressed as kg PO_4 equivalents per kg emission. Details of the CML-IA method and the impact categories described above were obtained from the SimaPro Methods Manual (Pre, 2015).

Cumulative Energy Demand (CED) is a single issue LCIA method in the SimaPro 8 software package. This method investigates the energy use throughout the life cycle of a process, including the direct energy consumption and the indirect energy consumed due to use of construction materials or raw materials. The method calculates the primary energy consumption across a range of renewable and non-renewable energy sources. The method uses the upper or lower heating values of these primary energy carriers. Further details on this method are published in Frischknecht et al. (2007).

7.3 Results and Discussion

7.3.1 Life Cycle Inventory

7.3.1.1 Simulated large-scale energy consumption

The simulated biodiesel production process was modelled in MATLAB. The model calculated the amount of energy consumed at each stage of the production process. A simulation was created for each of three reactor scenarios: ALR High Power, ALR Optimum and WR Optimum. For each of these scenarios the power input for cultivation changed, and there were slight variations in the biomass and lipid concentrations obtained (based on experimental results). The model produced similar results to the lab scale results discussed in Chapter 6. The ALR at high aeration power consumed almost 4 times the energy compared to the ALR optimised to run at the critical minimum gas flowrate (0.5 L min^{-1}), which in turn consumed approximately 4 times that of the WR at optimum rocking rate and rocking angle (15 rpm, 4°) (Figure 7.2). Previous studies have shown the poor performance of PBRs in biodiesel LCA relative to open ponds, due to their higher energy demands (Jorquera et al., 2010; Lam and Lee, 2012; Stephenson et al., 2010). The findings in this work are important because they show a 93% reduction of PBR energy consumption if a wave reactor is chosen over a non-optimised sparged reactor, and mixing and mass transfer are optimised with respect to energy efficiency.

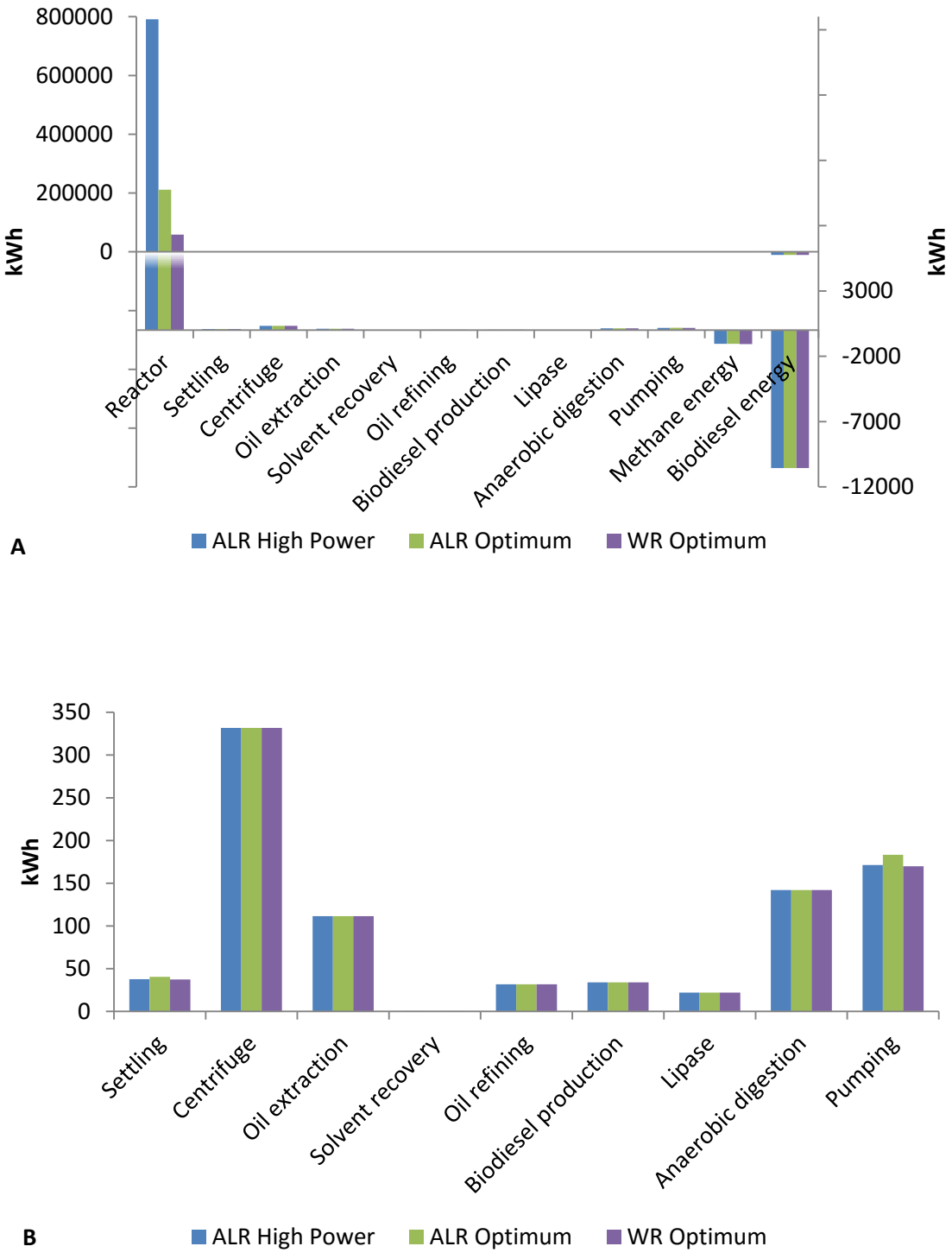

Figure 7.2 Energy consumption (kWh), per 1000 kg biodiesel, during each stage of the simulated algal biodiesel production process in Figure 7.1, where the reactor (algal cultivation stage) was an airlift run a 2 L min^{-1} gas flowrate (ALR High Power), an airlift at 0.5 L min^{-1} (ALR Optimum) or a wave reactor at 15 rpm, 4 degrees (WR Optimum). In (A) the y-axis is split to show the large values for 'Reactor' in the top half of the graph, and to magnify the remaining data in the bottom half. (B) Process stages excluding 'Reactor', on a smaller y-axis for comparison.

Literature values for the energy consumption (GJ per tonne biodiesel) of sparged PBRs were calculated based on the 'minimum aeration power' (Table 7.2). The 'minimum aeration values' from this work resulted in energy consumption values for the ALR, prior to optimisation, comparable to literature (Table 7.2). Significantly larger energy consumption for the ALR using 'total aeration power' calculations highlighted that previously reported values are not holistic representations of the energy consumed by sparged reactors, as discussed in Chapter 6.3.1. Therefore, further reductions in PBR energy consumption are necessary to be comparable to raceway ponds (Table 7.2). However, this current work demonstrates the potential for great improvements in the feasibility of PBRs in algal processes.

Table 7.2 Energy consumption in different algal culture systems. Adapted from Lam and Lee (2012).

Culture System	**Energy consumption (GJ per tonne biodiesel)**	**Reference**
Raceway	4 – 11	Lardon et al. (2009)
Raceway	13 – 15	Jorquera et al. (2010)
Raceway	22 - 30	Stephenson et al. (2010)
Raceway	55 – 158	Campbell et al. (2011)
Airlift tubular	195 – 231[a]	Stephenson et al. (2010)
Airlift tubular	537[a]	Jorquera et al. (2010)
Airlift (2 L min^{-1})	2848[b] (201[a])	This work; Jones and Harrison (2014)
Airlift (0.5 L min^{-1})	761[b] (54[a])	This work; Jones and Harrison (2014)
Wave (15 rpm, 4°)	211	This work

[a] Energy consumption (GJ per tonne biodiesel) based on 'minimum aeration power' for sparged reactors.

[b] Energy consumption (GJ per tonne biodiesel) based on 'total aeration power' for sparged reactors.

The energy consumed by the reactor (Figure 7.2) was higher than all the other stages of the simulated process (98.5% of total energy demand for WR Optimum, and higher for the ALR), followed by harvesting (0.62%), pumping (0.28%), anaerobic digestion (0.24%) and oil extraction (0.18%). The methane produced by anaerobic digestion was used for the generation of a small amount of electricity (1061 kWh; 1.8% of the total energy consumed) that was re-used in the biodiesel production process. If the electricity from methane is deducted from the energy demand, the cultivation energy rises to 100% of the total. This means the electricity from methane was sufficient to run all the process stages after cultivation. A number of previous studies agree that algal biodiesel production is limited by its large energy requirements, mainly due to the cultivation stage (Harun et al., 2010; Slade and Bauen, 2013; Stephenson et al., 2010). According to a review of

studies on algal biodiesel sustainability, major contributing factors to energy intensity include PBR design, nutrient source, dewatering and biomass drying, and lipid extraction (Lam and Lee, 2012). Recycling of nutrients (as done in this simulation) can reduce the energy consumption of cultivation (Razon and Tan, 2011), but the high power requirements of mixing and providing CO_2 remain (Louw et al., 2016).

Harvesting of algal biomass has also been described to have significant energy consumption (Harun et al., 2010; Lam and Lee, 2012; Slade and Bauen, 2013). Centrifugation is commonly used because it is a quick and easy method of harvesting biomass. However, it is highly energy intensive and not recommended for algal biodiesel production (Lam and Lee, 2012; Louw et al., 2016; Sander and Murthy, 2010). Filtration is also energy intensive, but other methods of harvesting, including gravity sedimentation, flocculation and flotation, have minor energy requirements, usually for pumping the culture to the harvest area (Brennan and Owende, 2010; Rawat et al., 2013). In the simulation modelled here, the primary method of harvesting was bioflocculation, followed by a low through-put centrifugation step. This method required substantially less energy than if centrifugation was used as the primary harvesting method (Sander and Murthy, 2010). According to calculations by Sander and Murthy (2010), if centrifugation were used as the primary harvesting method the energy consumption for harvesting would be 66 473 kWh (53% of the total energy consumption). The mixers and scrapers used in the settling ponds contributed significantly to the energy demand of harvesting, but remained small in comparison to reactor energy.

The difference in energy consumption for pumping and settling between the three reactor scenarios is due to the difference in algal biomass concentration, where the ALR Optimum produced the lowest biomass concentration and the WR Optimum the highest. In other words, the WR Optimum produced the lowest volume of algal culture per 1000 kg of biodiesel. This is an example of the importance of high biomass productivity to avoid dilute algal suspensions (large volumes) that require more energy to process. This is in agreement with previous LCA findings (Harding et al., 2008; Richardson, 2011; Stephenson et al., 2010). However, in the overall process, the magnitude of this effect is relatively minor (Figure 7.2).

Biomass drying can contribute significantly to the energy demand of algal biodiesel production, as much as 69% of total consumption has been reported (Adesanya et al., 2014; Brennan and Owende, 2010; Sander and Murthy, 2010). In the simulation discussed in this work, biomass drying was avoided by using a direct transesterification for lipid extraction that did not require dry biomass (Lam and Lee, 2012; Stephenson et al., 2010). In agreement with previous studies, the lipid extraction accounted for a relatively small portion of the total energy consumption (Sander and Murthy, 2010; Stephenson et al., 2010).

The total energy consumption of each scenario was as follows:

- ALR High Power: 792 131 kWh
- ALR Optimum: 212 281 kWh
- WR Optimum: 59 499 kWh

These values were entered into the LCA software as the total amount of electricity, minus 1048 (ALR) or 1061 kWh (WR) for electricity production from methane.

7.3.1.2 Material flows

In addition to energy, the material inputs and outputs of the algal biodiesel flow-sheet (Figure 7.1) were generated by the MATLAB model. Tables D1, D2 and D3 in Appendix D show the mass in kg of each component in each of the numbered streams in Figure 7.1. From these, the total input and output of each component was calculated and tabulated (Table 7.3,Table 7.4 and Table 7.5). Together with total energy consumption, the data in these tables was entered into the LCA software for the production of 1000 kg of biodiesel.

Table 7.3 Inputs and outputs of the simulated biodiesel production process in Figure 7.1 using an airlift at 2 L min^{-1} (ALR High Power).

kg	Input	Output
Water	410038	409953
Cells	0	1958
$NaNO_3$ (growth media)	771	0
KH_2PO_4 (growth media)	124	0
Hexane (oil extraction)	42	0
Phosphoric acid (oil refining)	9	0
NaOH (oil refining)	59	0
Methanol (biodiesel production)	111	2
Biodiesel	**0**	**1000**
Glycerol (bi-product of biodiesel)	0	106
Cooling water	120	120
Glucose (lipase production)	6	0
Yeast (lipase production)	4	0
Precipitating chemical (lipase production)	2	2
CO_2	7627	8
O_2	0	5547
Phosphates (lipase production)	0	1
Urea (anaerobic digestion)	3	0
Methane (anaerobic digestion)	0	126
TOTAL	418916	418824

Table 7.4 Inputs and outputs of the simulated biodiesel production process in Figure 7.1 using an airlift at 0.5 L min^{-1} (ALR Optimum).

kg	Input	Output
Water	438071	437954
Cells	0	1958
$NaNO_3$ (growth media)	771	0
KH_2PO_4 (growth media)	124	0
Hexane (oil extraction)	42	0
Phosphoric acid (oil refining)	9	0
NaOH (oil refining)	59	0
Methanol (biodiesel production)	111	2
Biodiesel	**0**	**1000**
Glycerol (bi-product of biodiesel)	0	106
Cooling water	120	120
Glucose (lipase production)	6	0
Yeast (lipase production)	4	0
Precipitating chemical (lipase production)	2	2
CO_2	7627	8
O_2		5547
Phosphates (lipase production)	0	1
Urea (anaerobic digestion)	3	0
Methane (anaerobic digestion)	0	126
TOTAL	446949	446825

Table 7.5 Inputs and outputs of the simulated biodiesel production process in Figure 7.1 using a wave reactor at 15 rpm, 4° (WR Optimum).

kg	Input	Output
Water	406562	406502
Cells	0	1958
$NaNO_3$ (growth media)	771	0
KH_2PO_4 (growth media)	124	0
Hexane (oil extraction)	42	0
Phosphoric acid (oil refining)	9	0
NaOH (oil refining)	59	0
Methanol (biodiesel production)	111	2
Biodiesel	**0**	**1000**
Glycerol (bi-product of biodiesel)	0	106
Cooling water	120	120
Glucose (lipase production)	6	0
Yeast (lipase production)	4	0
Precipitating chemical (lipase production)	2	2
CO_2	7640	8
O_2	0	5556
Phosphates (lipase production)	0	1
Urea (anaerobic digestion)	3	0
Methane (anaerobic digestion)	0	127
TOTAL	415453	415383

7.3.2 Life Cycle Impact Assessment

Data from the LCI (Section 7.3.1) was input into the LCA software (SimPro 8.0) for assessment of environmental burdens of the algal biodiesel production process. Analysis was performed under impact categories chosen from the CML-IA 2 Baseline assessment method V3.02, and comparisons made across the three process scenarios (Figure 7.3). The normalised data from the LCA of the three process scenarios decreased significantly with reduced gas flowrate in the ALR, and when the ALR is replaced with the WR (Figure 7.3). With the exception of Abiotic Depletion, the environmental burdens shown in Figure 7.3 dropped by 73% between ALR High Power (2 L min^{-1}) and ALR Optimum (0.5 L min^{-1}), and dropped a further 19% between ALR Optimum and WR Optimum. The consistency of these differences across the impact categories indicates that a single factor affected each impact category to a far greater degree than any other factor in the biodiesel production process. Abiotic depletion (kg Sb eq) decreased by 56% with reduced air flow-rate, and a further 16% when the ALR is replaced with the WR (Figure 7.3). Improvements to the PBR, as discussed in previous chapters, therefore translate to improved environmental burdens of the whole biodiesel production process.

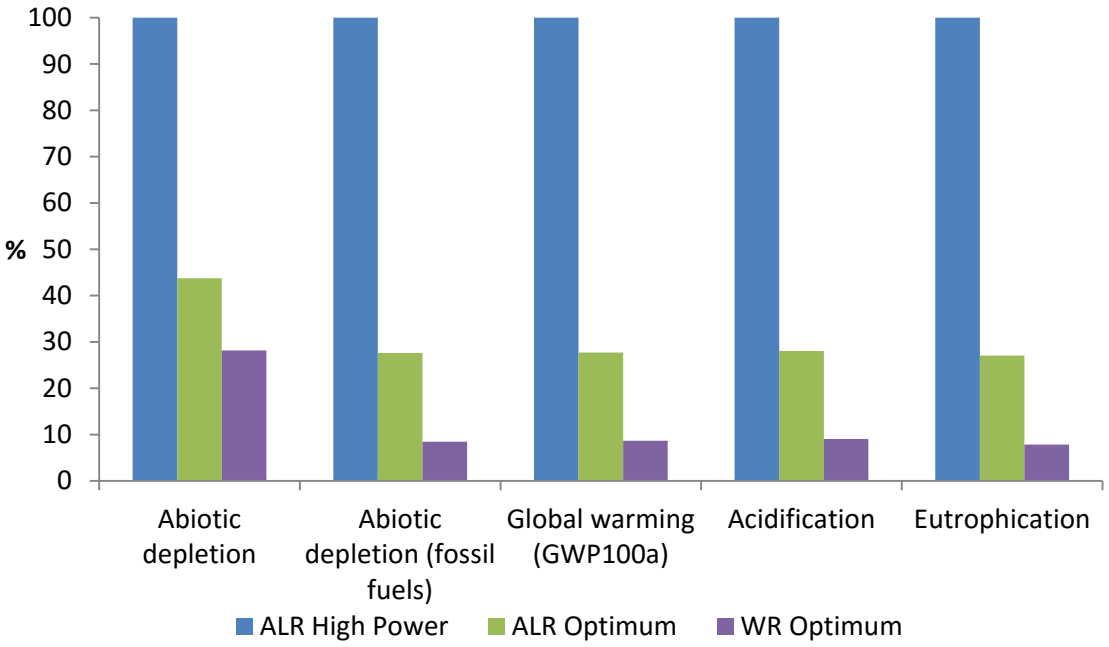

Figure 7.3 Normalised data from life cycle analysis of the simulated algal biodiesel production process in Figure 7.1, where the reactor (algal cultivation stage) was an airlift run at 2 L min^{-1} gas flowrate (ALR High Power), an airlift at 0.5 L min^{-1} (ALR Optimum) or a wave reactor at 15 rpm, 4 degrees (WR Optimum). Impact categories included abiotic depletion (kg Sb eq), abiotic depletion (fossil fuels, MJ), global warming potential (kg CO_2), acidification (kg SO_2 eq) and eutrophication (kg PO_4 eq).

In order to consider the effects of each factor of the biodiesel production process, the four impact categories were explored in more detail without normalisation. The factors that had the most prominent effects in each impact category are shown in Figure 7.4. The electricity input for the process had by far the greatest effect in each impact category compared to all other factors. Figure 7.2 shows that the majority of the energy consumption (i.e. electricity) was required for mixing and aerating the reactor. Reducing the electricity demand of the reactor stage of the biodiesel production process is the only way to ensure significant improvements in the impact categories discussed here. The lower electricity usage of the WR to produce roughly the same biomass and lipid concentrations led to the large reduction in environmental burdens. A trade-off with this reactor, however, is the larger land area required for a wave reactor compared to an airlift. The ALR is a vertical reactor, whereas the WR lies horizontally and thus would occupy substantially more land. At large scale a wave PBR could be arranged as an array of channels stacked vertically to reduce land use.

Previous LCAs have also reported that electricity requirements have the largest burdens in algal biodiesel production (Adesanya et al., 2014; Azadi et al., 2014; Collet et al., 2014; Lardon et al., 2009; Richardson, 2011; Stephenson et al., 2010). As expected, this is particularly the case for fossil fuel depletion and global warming potential. Reports have also shown that algal cultivation has the highest burdens compared to other stages of production (Adesanya et al., 2014; Collet et al., 2014; Richardson, 2011; Stephenson et al., 2010). However, there are considerable variations in the values obtained across LCA studies (Table 7.1). This is due to LCA results being dependent on a number of factors that vary widely based on the researcher's choice of assumptions. For example, the design of the flow-sheet and the choices made for each unit process have large effects on LCA outcomes, particularly with respect to bioreactor, harvesting and drying methods (Jorquera et al., 2010; Sander and Murthy, 2010). Algal productivities also play a role in variation across biodiesel LCA as shown by sensitivity analyses (Adesanya et al., 2014; Richardson, 2011; Stephenson et al., 2010). Assumptions made on equipment and technique efficiencies and outputs also affect LCA results. Adesanya et al. (2014) demonstrated that varying lipid recoveries from 99% to 50% vastly changed the global warming potential. The report also stated that the functional unit chosen for the LCA (where many studies use either 1 MJ or 1 tonne of biodiesel) affects the end results (Adesanya et al., 2014). The most prominent difference between the LCA presented here and others (Table 7.1) is the basis for calculating the energy requirement for the airlift photobiroeactor. Here, the 'total aeration power' based on a 2 bar inlet pressure was used, whereas many LCAs report energy requirements for sparged reactors based on the 'minimum aeration power', as discussed in Chapter 6. The 'total aeration power' gives a more realistic value, particularly for cross reactor comparison and determination of overall impact.

Nitrate and phosphate required for the algal cultivation media also had considerable environmental burdens (Figure 7.4). This was consistent with previous studies (Azadi et al., 2014; Collet et al., 2014; Lardon et al., 2009; Stephenson et al., 2010). This is mostly due to the energy demand for producing these fertilizers (Lardon et al., 2009; Stephenson et al., 2010).

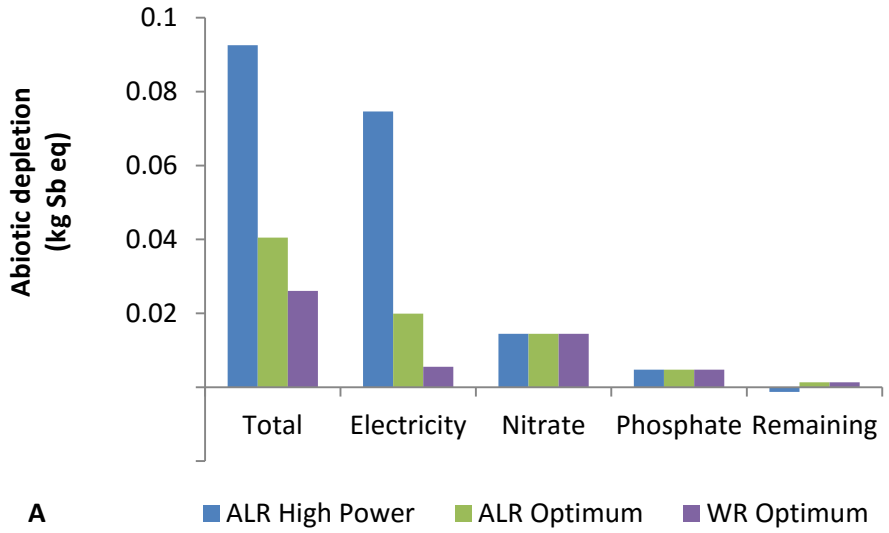
Abiotic depletion (kg Sb eq)
0.1
0.08
0.06
0.04
0.02
Total
Electricity
Nitrate
Phosphate
Remaining
ALR High Power
ALR Optimum
WR Optimum

A

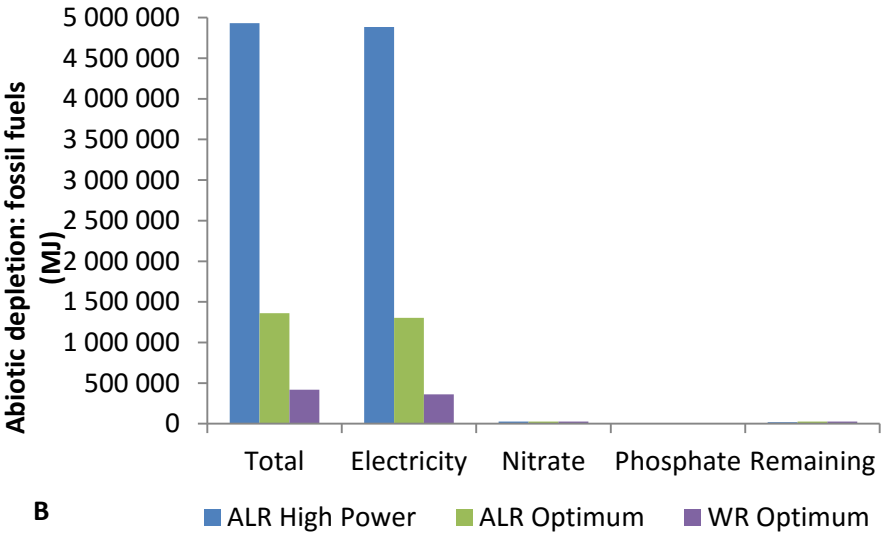
Abiotic depletion: fossil fuels (MJ)
5 000 000
4 500 000
4 000 000
3 500 000
3 000 000
2 500 000
2 000 000
1 500 000
1 000 000
500 000
0
Total
Electricity
Nitrate
Phosphate
Remaining
ALR High Power
ALR Optimum
WR Optimum

B

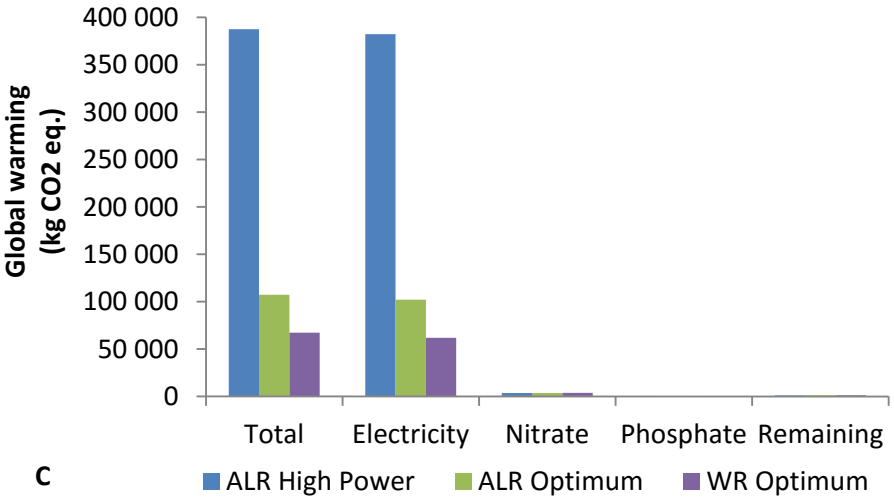
Global warming (kg CO2 eq.)
400 000
350 000
300 000
250 000
200 000
150 000
100 000
50 000
0
Total
Electricity
Nitrate
Phosphate
Remaining
ALR High Power
ALR Optimum
WR Optimum

C

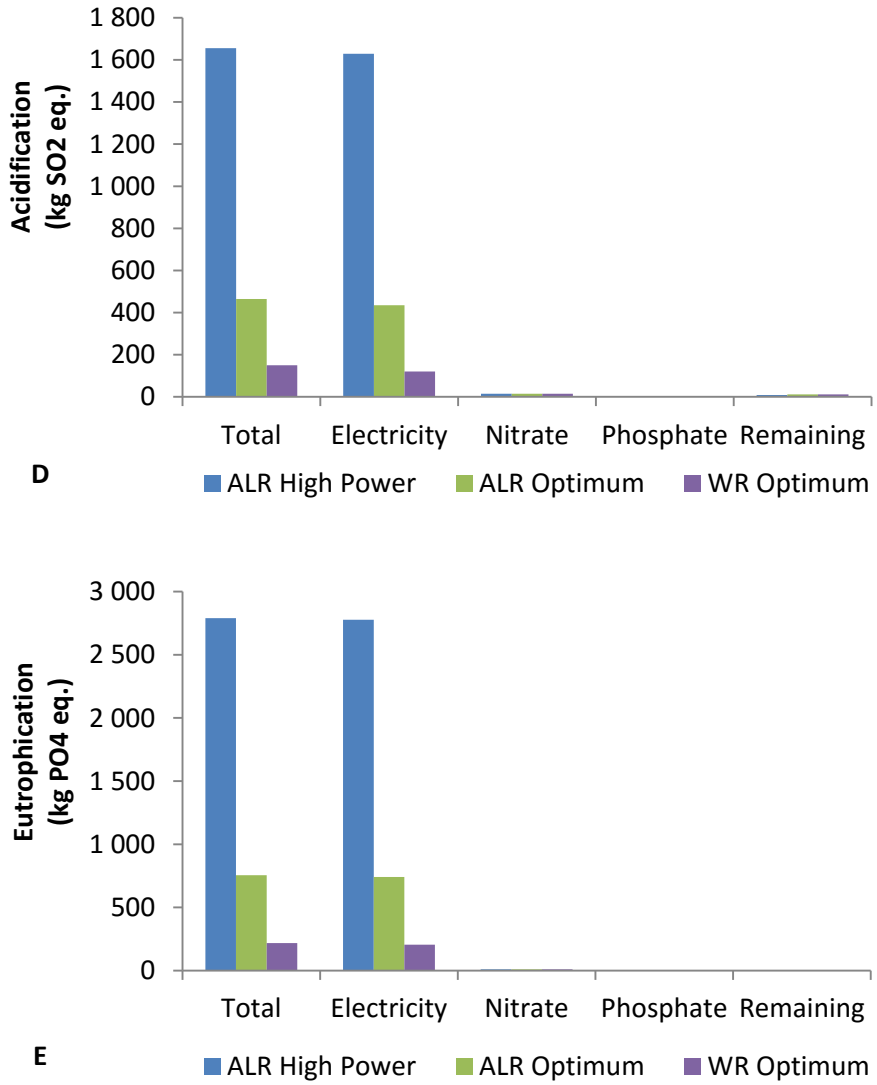

Figure 7.4 Process inputs that contribute most significantly to the impact categories: (A) abiotic depletion, (B) abiotic depletion specific to fossil fuels, (C) global warming, (D) acidification and (E) eutrophication.

The LCA described above was repeated using datasets appropriate for a South African context, particularly a South Africa electricity mix. This resulted in significantly higher impacts on depletion of fossil fuels, global warming potential and acidification (Figure 7.5). These differences were mainly due to the different sources of electricity used in South Africa. As discussed in Section 7.3.3 below, South African electricity is largely coal generated, and the European electricity mix has higher contributions from nuclear and renewable sources.

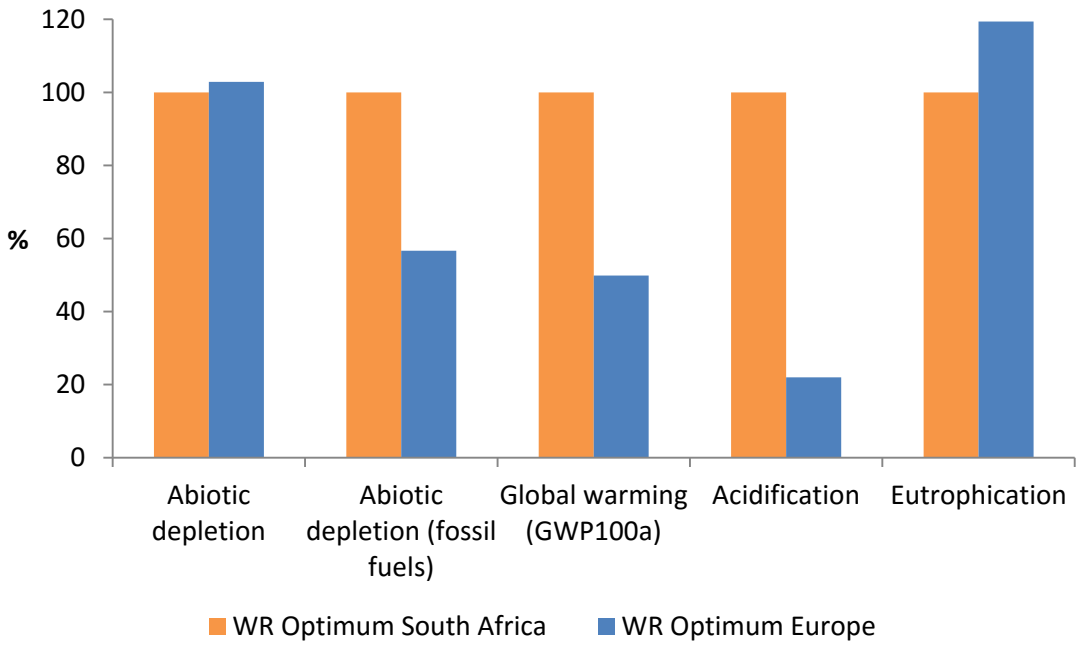

Figure 7.5 Normalised data from life cycle analysis of the simulated algal biodiesel production process in Figure 7.1, where LCA datasets for a South African context are compared to a European context. Impact categories included abiotic depletion (kg Sb eq), abiotic depletion (fossil fuels, MJ), global warming potential (kg CO_2), acidification (kg SO_2 eq) and eutrophication (kg PO_4 eq).

7.3.3 Cumulative Energy Demand and Net Energy Ratios

Results presented in the previous sections demonstrated that electricity inputs to the algal biodiesel production process caused the highest impacts on abiotic depletion, global warming, acidification and eutrophication (Section 7.3.2); and at least 98% of this electricity was used in the PBRs for mixing and aeration (Section 7.3.1). Cumulative Energy Demand (CED) was used to calculate the energy consumption of the algal biodiesel life cycle from its primary energy sources. The electricity used in the LCA was the ENTSO-E, an average European electricity mix, consisting of large portions of fossil and nuclear generated electricity, and small amounts of hydroelectric, renewable biomass and wind/solar/geothermal (Figure 7.6A). A South African Electricity mix was used for a local algal biodiesel LCA scenario. In South Africa electricity is mostly coal-generated (non-renewable fossil fuel) with small contributions from hydroelectric, nuclear, wind/solar/geothermal and renewable biomass (Figure 7.6B).

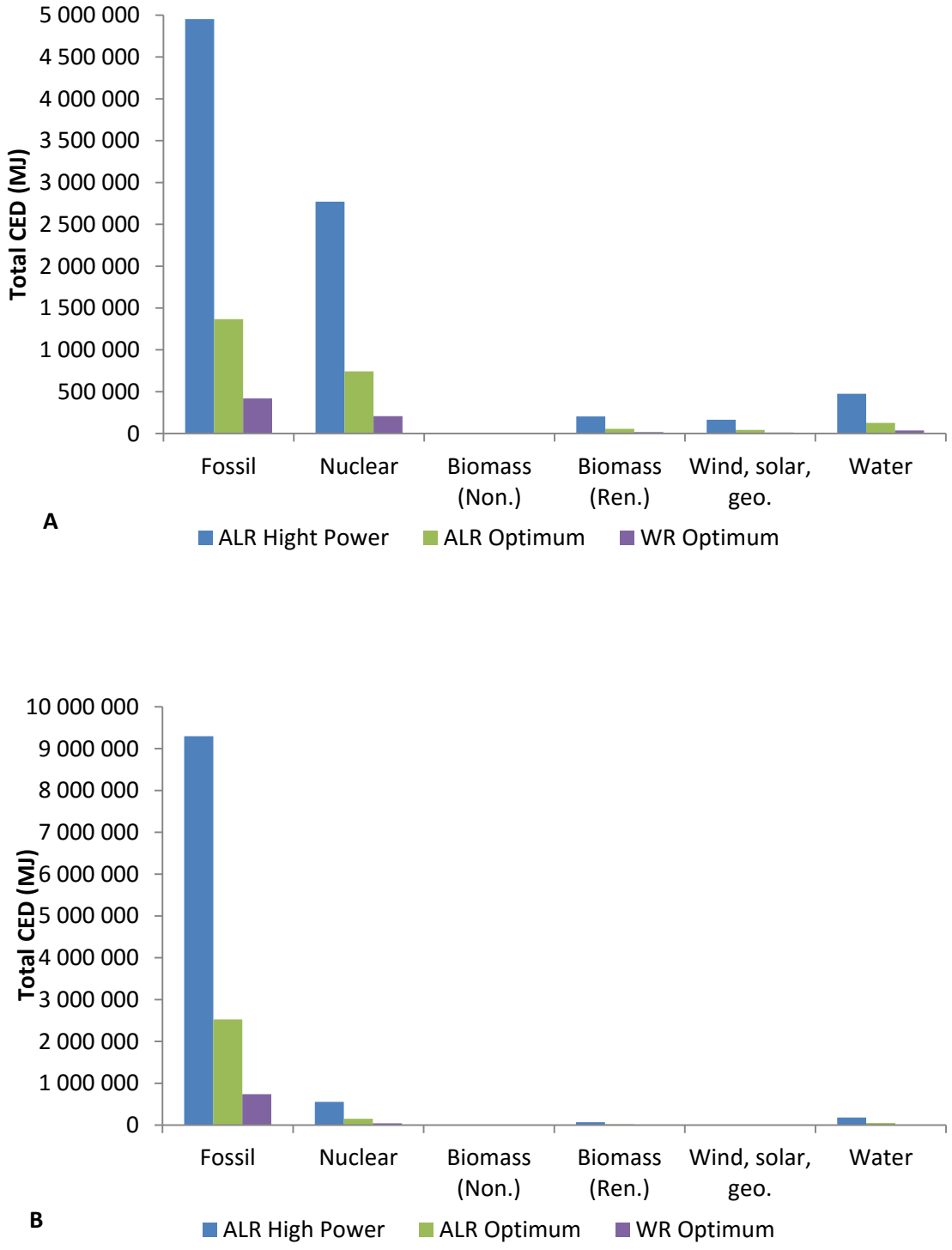

Figure 7.6 Cumulative Energy Demand for the production of 1000 kg of algal biodiesel according to the flow-sheet in Figure 7.1, where ALR High Power used airlift reactors at 2 L min^{-1}, ALR Optimum used airlifts at 0.5 L $mins^{-1}$, and WR Optimum used wave reactors at 15 rpm, 4°. (A) European electricity mix (ENTSO-E), (B) South African electricity mix. Non-renewable energy sources include fossil, nuclear and non-renewable biomass (non.), and renewable sources include biomass (ren.), wind/solar/geothermal and water.

Net energy ratios (NERs) were calculated using the total energy output from 1000 kg algal biodiesel divided by the total CED for the process (the energy input). Energy output was calculated based on the calorific value of algal biodiesel (37 MJ kg^{-1}) (Demirbas, 2007; Nautiyal et al., 2014; Razon and Tan, 2011) and energy from methane was deducted from the energy input of the process. In Chapter 6, the NERs for the PBRs were discussed. In Table 7.6, these are compared with the NERs for the whole biodiesel production process. The NERs for the PBRs (based on lipid production) are similar to the NERs based on the total electricity usage for 1000 kg biodiesel (Section 7.3.1). This is because at least 98% of the total electricity was used in the reactors. The NERs based on the CED are between 4 and 5 times lower because, in addition to the direct electricity usage, the CED includes the primary energy sources and the energy consumption for producing the electricity used in the process. In all cases the NERs are below 1, meaning that more energy is used to produce the biodiesel than the biodiesel provides. This suggests that although large improvements were seen using the more energy efficient WR (NER increased by 70 – 80%), the production of algal biodiesel was still unfeasible. It is important to note that the cultivation data was obtained under light limited conditions, and the NER would improve significantly if outdoor growth data was used

Table 7.6 NERs (defined as the energy produced / energy consumed) for ALR and WR photobioreactors (NER_{PBR}) measured according to the lipid concentration produced and its calorific value, compared with the NERs for the algal biodiesel production process (NER_{BPP}) measured using the total electricity used for 1000 kg biodiesel, and the NERs for 1000 kg biodiesel based on the Cumulative Energy Demand of the process (NER_{CED}). The per-cent increase between the ALR Optimum and the WR Optimum (AL:W % Increase) was calculated for each NER. These data are based on the LCA performed using European datasets.

Scenario	**NER_{PBR}**	**NER_{BPP}**	**NER_{CED}**
ALR High Power	0.017	0.013	0.004
ALR Optimum	0.055	0.048	0.016
WR Optimum	0.239	0.172	0.054
ALR:WR % Increase	77%	72%	70%

7.3.4 Photovoltaic solar electricity to reduce environmental burdens

The best location for an algal cultivation facility is one that receives large amounts of sunlight. This location would also be suitable for harvesting energy through solar panels. If a portion of the algal production facility were dedicated to photovoltaic (PV) solar energy capture, the reliance on coal-produced electricity could be reduced. An LCA scenario was designed to incorporate 10 acres of open ground multi-silicon PV cell solar panels into the algal biodiesel production process described

in Figure 7.1. The wave reactor at optimum agitation efficiency was used in this scenario to illustrate further possible improvements to the best case scenario highlighted by this research. The LCA was performed using datasets appropriate to a South African context to show possible improvements to a local algal biodiesel production scenario.

South Africa receives an annual average solar radiation of 4.5 kWh (along the eastern coast) to 6.0 kWh (in the north west of the country) (Munzhedzi and Sebitosi, 2009). The efficiency of current photovoltaic technology ranges between 12 and 38% (Green et al., 2015), with the current average for mainstream multi-silicon PV cells at approximately 15% (EnergyTrend PV, 2014). A PV solar panel at 15 % efficiency exposed to 5 kWh of solar energy, is expected to give 0.75 kWh m^{-2}. For 10 acres (40468.6 m^2) of open ground multi-silicon PV solar panels, this results in 30 351 kWh of electricity. This is roughly half of the total energy demand of the biodiesel process using the WR Optimum (58 438 kWh). The CED for this scenario shows a 43% reduction in fossil energy usage for the process (Figure 7.7A). This resulted in reductions in abiotic depletion of fossil fuels, global warming, acidification and eutrophication (Figure 7.7B). Abiotic depletion of minerals (kg Sb equivalent) increased 4 times due to minerals required for construction of the solar panels. The total CED across the types of energy sources in Figure 7.7A also decreased, leading to an increased NER of 0.064, compared to 0.054 when solar panels were not included.

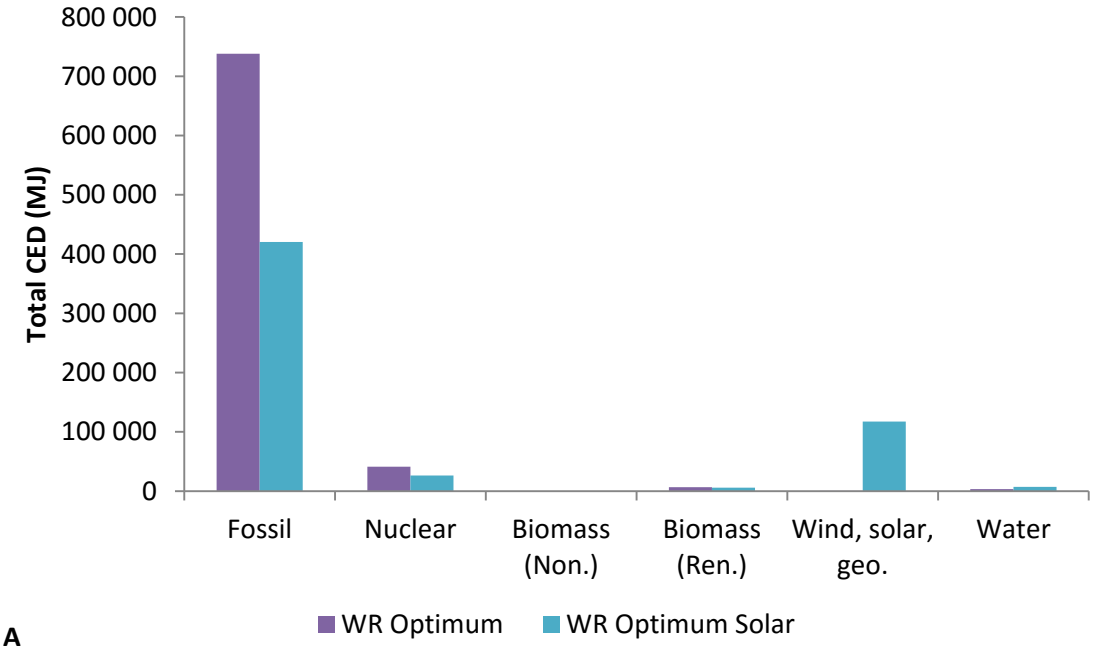

A

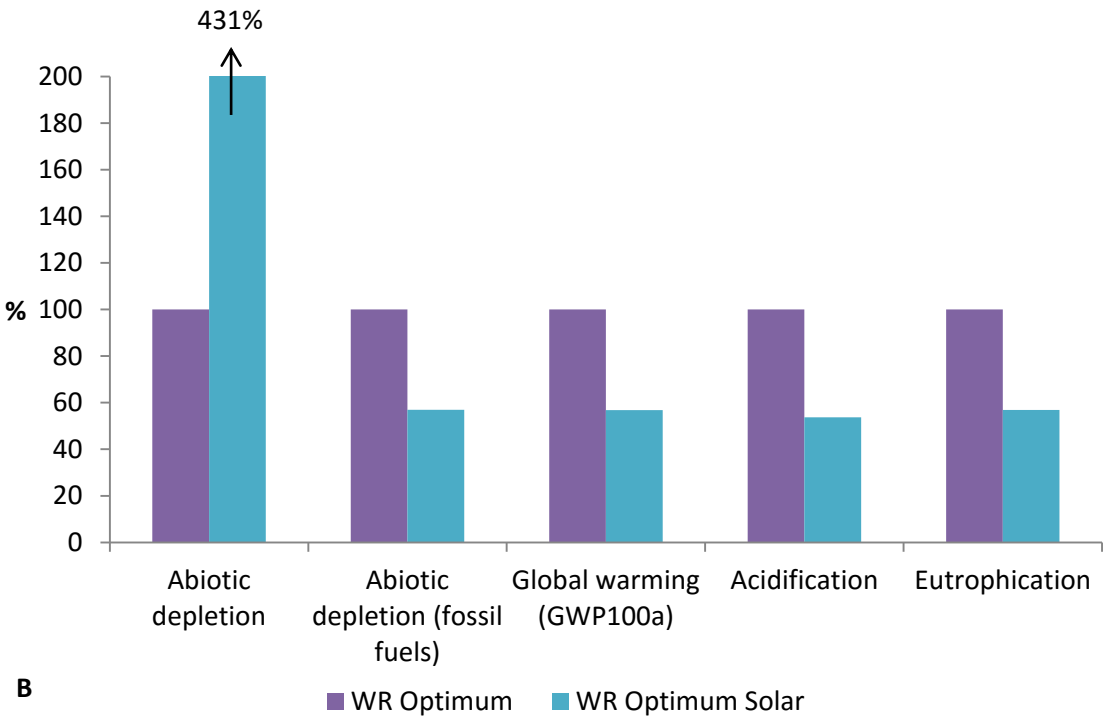

Figure 7.7 (A) Cumulative Energy Demand and (B) normalised data using CML-IA LCA methodology for 1000 kg of algal biodiesel using a wave bioreactor at optimum agitation efficiency (WR Optimum) for cultivation, with the addition of 10 acres of open ground multi-silicon PV solar panels to contribute to the electricity requirement (WR Optimum Solar). Impact categories included abiotic depletion (kg Sb eq), abiotic depletion (fossil fuels, MJ), global warming potential (kg CO_2), acidification (kg SO_2 eq) and eutrophication (kg PO_4 eq). These data are based on the LCA performed using South African datasets.

7.4 Conclusions and recommendations

The aim of this chapter was to consider the work done on PBRs (detailed in previous chapters) in the context of a whole bioprocess, in this case algal biodiesel production. The electricity consumption for the reactor stage of the process consisted of 98% of the total. This means that the differences in energy consumption seen in Chapter 6 across the three PBRs were carried over in the LCA. The NER of the whole biodiesel production process were slightly lower than those calculated for the PBRs only, and significantly lower for the life-cycle based cumulative energy demand (CED) indicator (Table 7.6). Improvements in NER with optimisation of energy efficiency, and use of the surface aerated WR instead of the sparged ALR were also carried over in the LCA, with a 77% improvement of NER_{PBR} and a 72% improvement of NER_{BPP}. Therefore, the PBR energy consumption was a major concern and key area for improvement in the context of the bioprocess.

In the LCA, the high energy demand in the reactor stage caused high impacts in depletion of fossil fuels (MJ), global warming, acidification and eutrophication. These impacts were reduced by 73% when the ALR was run at optimum (energy efficient) gas velocity, and a further 19% when the ALR was replaced with the WR. However, abiotic depletion (kgSb eq.) was not reduced to the same extent as the other impact categories. This was due to the impacts to this category caused by nitrate and phosphate inputs, which were consistent across the three PBR scenarios (Figure 7.4A).

In Europe and South Africa electricity is predominantly sourced from non-renewable fossil fuels, which meant that the Cumulative Energy Demand (CED) for the algal biodiesel production process was highest for fossil derived energy. This was reduced by 44% by allocating 10 hectares of the algal facility to PV solar panels, thus reducing the environmental burdens with respect to fossil fuel depletion, global warming, acidification and eutrophication.

The NER for the process was below 1 for all scenarios, meaning that more energy was used to produce the algal biodiesel that can be harnessed from it. It would be interesting to perform the LCA using data from outdoor algal cultivation to reduce the effects of light limitation. It would also be useful to obtain data for a pilot-scale wave reactor to inform the LCA of algal concentrations and power input on scale-up. It would be interesting to compare this LCA (using a pilot scale wave reactor) to that using a pilot scale raceway pond. Differences in NERs between these systems would inform the future applicability of PBRs for the production of bioenergy products. A scenario where a PBR is used as a primary cultivation step before inoculation of a pond would also be informative.

The LCA described in this chapter focussed on impacts related to energy usage, to stay within the scope of the thesis. A more comprehensive LCA including water footprint and land use would be an interesting addition to this work. It would be valuable to use LCA methods to perform an economic analysis of algal biodiesel using a wave reactor, and to compare this to the cost of second generation biofuels and fossil derived diesel. Additionally, although the results in this chapter indicate limitation to use of PBRs for biodiesel production, the study will inform bioreactor selection and optimisation for the range of products and processes to which microalgae can be applied.

8 Conclusions

8.1 Significant findings

Previous publications have reported that bioreactors have substantial power requirements and much of this is due to the energy used for mixing and aeration (Harding et al., 2008; Louw et al., 2016; Slade and Bauen, 2013; Stephenson et al., 2010). In algal bioprocesses, this energy demand limits the feasibility of bioproducts, particularly energy products, by increasing cost, fossil fuel reliance and environmental burdens. Previous work on bioreactors for algal cultivation has resulted in a number of improvements to reactor design (Carvalho et al., 2006; Lehr and Posten, 2009). However, PBRs are still predominantly aerated by sparging. In this work, the impact of optimising sparging rates was considered. Further, the use of surface aeration as an alternative was proposed, with the aim of reducing power requirements for algal cultivation.

The airlift concept is a popular method of sparging algal PBRs. This was used as the base case in this study to compare with novel surface aerated reactors. First, an airlift PBR (ALR) was investigated, with the aim of studying the effects of decreasing the power input for sparging on algal productivity and to elucidate the lower limits of mixing and mass transfer required for alga cultivation, as set out in the research questions. To date, there has been some research on altering the CO_2 concentration or sparging rates, independently, in sparged algal PBRs (Kaewpintong et al., 2007; Sasi, 2011). The current study is the first to investigate the combined effects of these parameters with respect to power input. The current investigation revealed a critical minimum CO_2 supply rate (CSR, a function of CO_2 concentration and sparging rate), above which energy would be spent on aeration with no further increase in algal productivity (0.2 g L^{-1} d^{-1} biomass and 0.03 g L^{-1} d^{-1} lipid) . This means that if the CO_2 concentration was sufficiently high (5 400 – 10 400 ppm), the superficial gas velocity could be reduced fourfold (0.02 to 0.005 m s^{-1}), resulting in a 75% reduction in the aeration power input (1417 to 354 WR m^{-1}). Optimisation of aeration in this way had considerable effects on the energy efficiency of the ALR, where biomass productivity per unit power increased from 0.13 to 0.56 g W^{-1} d^{-1}. The critical minimum CSR for algal biomass production in this work was 2.7×10^{-5} m s^{-1}. This value is specific to energy efficient cultivation of *Scenedesmus* sp. and will change with algal species (according to carbon uptake rate) and altered growth conditions, such as light intensity and nitrate concentration. This work demonstrated the value of implementing an optimisation step to

determine the system specific critical CO_2 supply rate in sparged bioreactors to increase energy efficiency.

Reductions in biomass and lipid concentration were seen at lower gas velocities despite the critical CSR being met. This may be caused by reduced mixing, which affected the distribution of nutrients and light in the culture. An increase in light intensity (150 to 300 µmol m^{-2} s^{-1}) resulted in increased biomass and lipid productivity at the lowest gas velocity (0.002 m s^{-1}). This suggested a reduction in the light limitation caused by slow circulation between light (downcomer) and dark (riser) areas of the ALR. This demonstrated the importance of considering mixing and light provision in addition to the CO_2 supply rate. These factors are strongly interrelated. At 0.01 and 0.005 m s^{-1}, increased light led to an increase in carbon required by the algal culture (an increase in the critical minimum CO_2 supply rate). This caused algal productivity to remain constant with increased light intensity at these gas velocities. At gas velocities of 0.02 m s^{-1} (higher CO_2) or higher, productivity increased again.

Two surface aerated PBRs were investigated in this work with focus on power input, mixing and mass transfer rates and algal productivity in order to answer the research questions presented in Section 1.10. The first surface aerated PBR investigated was the oscillatory baffled reactor (OBR), which was designed during this research project. It is the first publically available report on the use of an oscillatory flow or oscillatory baffled reactor for algal cultivation, and the first currently known reactor of this kind to use surface aeration. Oscillatory motion, which causes inter-baffle eddies, has been reported to result in high mixing and mass transfer rates, and to provide more energy efficient mass transfer than stirred tank reactors (Ni et al., 2003). For this reason, oscillatory motion in a surface aerated reactor was chosen for this research. Several parameters, such as baffle type, distance between baffles, baffle free area, oscillation frequency and oscillation amplitude, effect the mixing and mass transfer in oscillatory flow reactors (Ni et al., 1998). A comparison of baffle design in the OBR of this work revealed that donut baffles were superior to half-moon and perforated half-moon baffles with respect to mass transfer, and so were chosen for subsequent studies.

The mixing times in the OBR (12 – 45 s) were superior to a range of bioreactors reported in the literature, but the mass transfer was lower (4.9 – 17.2 h^{-1}). However, an area of poor mixing was present in the reactor column at high oscillating frequencies. Also, limited mass transfer resulted in lower algal biomass and lipid productivity than expected (0.1 g L^{-1} d^{-1} biomass and 0.02 g L^{-1} d^{-1} lipid).

Re-designing the OBR to eliminate the dead-zone and improve mass transfer is key to improving its energy efficiency. This could be done by increasing the length to width ratio, operating the OBR as a continuous reactor, or recirculating the liquid from the far end of the column, back to the inlet. Improvements specific to mass transfer enhancement include increasing the surface area to volume ratio and improving the flow of gas through the headspace, across the length of the reactor, by inclusion of an appropriately designed and positioned gas outlet vent. Increasing the CO_2 concentration in the headspace, increasing oscillation frequency and reducing oscillation amplitude could also increase the mass transfer in the OBR. This work demonstrated the ability of the OBR to support algal cultivation, and after the suggested improvements to design, the OBR may offer solutions to energy efficiency in bioprocesses.

The second surface aerated bioreactor investigated in this work was the wave PBR (WR). Wave bioreactors are relatively new, the first reported in 1999, and have thus far been used predominantly for plant and animal cell culture (Singh, 1999). A small number of recent studies have shown their applicability to microbial cultivation, and two known studies reported their use for algal or diatom cultivation (Dreesen et al., 2010; Lehmann et al., 2013). The current work is the first to use a wave bioreactor for cultivation of *Scenedesmus* sp. and production of algal lipids. This is also the first work to carry out a detailed investigation of mixing and mass transfer with respect to power input and optimisation for energy efficient algal productivity.

The WR used in this work consisted of a 10 L cellbag filled to 2 L with liquid medium (20% working volume), with the remaining volume filled with CO_2 enriched air. A comparison between the WR and wave reactors from previous studies showed that mixing and mass transfer are affected by the total volume of the cellbag and the working volume. Reports that used similar cellbag volumes or similar working volumes to the WR used in this work had comparable mixing times and mass transfer coefficients. Reports demonstrated that smaller working volume resulted in higher mass transfer (Eibl et al., 2009; Westbrook et al., 2014), which had the added benefit of reduced energy for supporting a smaller volume of water on the rocking platform. There is only one publically available study that reports the power input of a wave bioreactor, to our knowledge. The power input obtained from the calorimetric method in this work was comparable to the previous study (Eibl et al., 2009), giving power in the range 64 – 633 W m^{-3}. It was observed that from 422 W m^{-3} (25 rpm, 10°), vigorous rocking caused the liquid wave to splash the roof of the cellbag, creating a thin film of

liquid. This film provided a large surface area for mass transfer, and resulted in a sharp increase in CO_2 mass transfer. An important feature for wave bioreactors is, therefore, a crashing wave rather than a rolling wave (or gentle swells), for increased mass transfer.

In order to answer the research question presented in Section 1.10 - "What are the lower limits of mixing and mass transfer for biomass and lipid productivity?" – algal cultivation experiments were carried out in the WR. Preliminary cultivation experiments in the WR showed that *Scenedesmus* sp. required a slow but continuous inlet of CO_2 enriched air. With exchange of the gas headspace only once daily, the limited CO_2 provision and O_2 build-up caused the culture to be severely inhibited, and so further experiments were conducted with continuous gas flow. At rocking conditions that gave $k_L a_{CO_2}$ in the range 8.5 to 38 h^{-1}, there were only small differences in algal biomass and lipid productivity (0.15 – 0.17 g L^{-1} d^{-1} biomass and 0.045 – 0.050 g L^{-1} d^{-1} lipid). This means that rocking could be lowered to 15 rpm at 4° ($k_L a_{CO_2}$ 8.5 h^{-1}) while maintaining sufficient CO_2 supply that supports *Scenedesmus* sp. growth and lipid production at the given light conditions and nutrient concentrations. This equates to an 80% reduction in power input compared to rocking at 25 rpm, 10° (422 WR m^{-3} reduced to 85 WR m^{-3}). This in turn led to substantial increases in energy efficiency of the WR (0.4 to 1.8 g W^{-1} d^1 biomass and 0.1 to 0.6 g W^{-1} d^1 lipid). Optimisation of rocking rate and angle are, therefore, essential for optimising the energy efficiency of wave bioreactors. The minimum mass transfer rate sufficient for the cultivation and production will depend on of the species under investigation, and the growth conditions (e.g. nutrients and light).

Linear growth in the WR under conditions that were not limited by CO_2 mas transfer was thought to be caused by a light limitation. Experiments at double the light intensity demonstrated an increase in biomass productivity. As with the ALR experiments, it was concluded that 9 µmol s^{-1} of total light was insufficient. Under outdoor conditions, with plenty of sunlight, the algal productivity and energy efficiency of the WR is expected to improve, provided photoinhibition is avoided.

The research questions presented in Section 1.10 set out to analyse the power input to the three bioreactor types investigated, and also compare the power input, energy efficiency and NERs across the sparged and surface aerated PBRs with respect to mixing, mass transfer and algal productivity. Power input in sparged reactors is usually calculated as the 'minimum aeration power', which is

based on the expansion of gas from the sparger to the top of the reactor. This power value is useful as a common term across sparged reactors, which can then be compared based on mixing rate, expressed as specific power. However, the 'minimum aeration power' does not include the power used to compress the gas to the pressure at which it is delivered to the reactor. Changes to this inlet pressure alter the gas flowrates and hence the mixing and mass transfer rates. The aim of this work was to compare the energy efficiencies across sparged and surface aerated reactors. The 'total aeration power', which takes into account the inlet gas pressure, provides a more realistic value for energy usage in sparged reactors, for better comparison with mechanically agitated reactors. The 'total aeration power' was considerably higher than the 'minimum aeration power', and thus the NERs of the ALR were much lower when using the 'total aeration power'. Many previously reported NERs use 'minimum aeration power' calculations for theoretical algal processes. Here, the NERs were a realistic representation of the burden of gas compression. The NERs based on 'total aeration power' were also more appropriate for comparison to the NERs of the OBR and WR. Significant improvements to the 'total aeration power' can be made by reducing the inlet gas pressure, which considerably improves the productivity per unit power and NERs of sparged reactors. This was demonstrated by calculating minimum gas inlet pressures for the ALR at the given gas velocities. The minimum gas inlet pressure required for a sparged reactor is system specific, as it varies with liquid height, sparger type and gas piping configurations. It should be incorporated as part of the optimisation of operating conditions for sparged reactors.

Comparison across the ALR, OBR and WR reactors showed that the WR had far higher mass transfer capability than the ALR and OBR. Comparing these to various reactors reported previously, the WR had among the highest mass transfer capability, with $k_L a$ increasing with power input more rapidly than any other reactor above 500 W m^{-3}. The WR and OBR had among the fastest mixing times across the range of reactors reviewed in this study. There is, therefore, much potential for surface aerated reactors, with the WR demonstrating higher energy efficiency with respect to mixing and mass transfer compared to the ALR and other sparged reactors. This is an important finding with useful implications for improving the energy consumption related to the bioreactor stage of a bioprocess.

The research question – "What mixing and aeration rates are required for comparable $k_L a$, T_m and algal productivity across the three PBRs?" – was addressed by replicating favourable cultivation

conditions demonstrated for the ALR in the OBR and WR, with respect to mixing and mass transfer. In the ALR the $k_L a_{CO_2}$ at 'standard conditions' was 39.5 h^{-1}, and a $k_L a_{CO_2}$ of 7.6 h^{-1} was sufficient for algal cultivation at the critical minimum CSR ('optimised conditions': 0.005 m s^{-1}, 10 400 ppm CO_2). To replicate these conditions, algae was cultivated in the WR at 25 rpm, 10°, giving a $k_L a_{CO_2}$ of 38.4 h^{-1} (similar to the ALR 'standard'), and 15 rpm, 4°, giving a $k_L a_{CO_2}$ of 8.5 $h^{-1.}$ (close to the ALR optimised). Similarly, conditions were chosen in the OBR to replicate the mass transfer in the ALR and WR as well as possible. The $k_L a_{CO_2}$ values were rounded off to the nearest 10 to make a simpler comparison. At comparable $k_L a_{CO_2}$, biomass and lipid growth curves and productivity were alike in the ALR and WR, and were not significantly different at $k_L a_{CO_2}$ of approximately 40 h^{-1} and 10 h^{-1}. At $k_L a_{CO_2}$ 3 h^{-1} algae growth became severely limited by the reduced availability of carbon. These results demonstrated the sensitivity of algal production to CO_2 mass transfer. They showed that carbon availability was key to maintaining growth rates across varied BPR designs. When designing the cultivation stage of a bioprocess, first the critical minimum mass transfer rate must be ascertained, and then a reactor choice can be made based on the lowest energy consumption to achieve that mass transfer rate, while meeting the necessary mixing and light delivery requirements.

A comparison between the three PBRs showed that the WR could achieve comparable $k_L a_{CO_2}$, and T_m at lower power input. The WR was, therefore, more energy efficient, as shown by the algal productivity per unit power (0.37 g W^{-1} d^{-1} for the OBR; 0.56 g W^{-1} d^{-1} for the ALR; 2.07 g W^{-1} d^{-1} for the WR). Sparging in the ALR required a large power input, so that even though the algae grew at comparable rates in the ALR and WR, when carbon was not limiting, the energy efficiency of the ALR was lower. The WR matched the rates of growth and lipid production of the ALR at lower power input. The OBR had poor algal growth compared to the ALR and WR, likely due to the low mass transfer in the reactor. Algal growth experiments in the OBR revealed that even at a reported $k_L a_{CO_2}$ of 10 h^{-1} (sufficient for growth in the ALR and WR), algal growth was limited. Mass transfer was measured in only one section of the reactor, and it is suggested that the $k_L a_{CO_2}$ was not consistent across the length of the reactor, resulting in parts of the reactor experiencing $k_L a_{CO_2}$ below 10 h^{-1}. Therefore, the data reported here for all experiments in the OBR could represent carbon limited algal growth, and so was not an equal comparison to the ALR and WR data.

Optimisation of the gas inlet pressure to the ALR was shown to result in significant improvements in the energy efficiency of this reactor by a sensitivity analysis using calculations for theoretical

minimum gas inlet pressure. At this reduced gas inlet pressure, the biomass productivity per unit power of the ALR improved beyond that of the WR, reaching 2.80 g W^{-1} d^{-1}. However, the volumetric lipid productivity in the WR was superior to the ALR, such that even at the minimum gas inlet pressure the lipid productivity per unit power in the ALR (0.45 g W^{-1} d^{-1}) was lower than that in the WR (0.65 g W^{-1} d^{-1}). Furthermore, at increased light, the NER for the ALR at the minimum gas inlet pressure was 0.96, compared to the 1.67 estimated for the WR. These differences may be due to the improved relationship between mixing and light distribution in the WR compared to the ALR. Additionally, the values calculated for the ALR were the best case scenario with likely increases in inlet gas pressure. Conversely the WR energy efficiency could be improved further, as discussed below.

The WR created a curved, splashing wave in the liquid media with a large surface area of the liquid in contact with the gas in the headspace of the reactor. The wave created in a raceway pond, and also seen in the OBR, is a rolling wave, or gentle swell, that does not extend far above the surface of the liquid. Surface aeration in a gently agitated system is likely to have lower mass transfer rates, as seen in raceway ponds and the current OBR design. Conversely, surface aeration in the dynamically agitated WR resulted in more efficient mass transfer than sparging, with a power requirement of 85 W m^{-3} to reach a $k_L a_{CO_2}$ of 8.5 h^{-1}, compared to 354 W m^{-3} required by the ALR to reach a $k_L a_{CO_2}$ of 7.6 h^{-1}. However, the NER of the WR, under the conditions described in this work, was below 1. This means that even with more energy efficient mixing and mass transfer through surface aeration, PBRs are still energy intensive to operate. It is important to note, however, that there were a number of conditions in this work that reduced the NER of the WR, leaving room for increases on further optimisation.

Algal cultivation in the ALR and WR under sufficient CO_2 mass transfer was limited by light. The NER at higher light increased significantly, and may further improve in an outdoor facility. Also, the lowest $k_L a_{CO_2}$ investigated in the WR was 8.5 h^{-1}, whereas in the ALR the critical minimum CSR was obtained at a $k_L a_{CO_2}$ of 7.6 h^{-1} and at 3 h^{-1} growth was clearly limited. It is, therefore possible that in the WR, the rocking rate and angle could be reduced further before significant reductions in productivity are seen. Experiments at lower rocking rate and higher light could thus result in higher NER, although optimisation of these interrelated factors is required. Ultimately, scale-up of the WR would require designing a system that recreates the liquid motion without using a rocking platform.

By using technologies developed for recreational wave pools, for example, the energy consumption of a wave bioreactor could be further reduced, again improving the NER.

A review of NERs, including previous publications and the current study, indicated that open raceway ponds have higher NERs than PBRs. After optimisation of energy efficiency using the critical minimum CO_2 supply rate, and when using surface aeration instead of sparging, this remains the case. This suggests that PBRs may be better suited to high-value products, requiring low contamination and high productivity. Bioenergy products require cultivation systems with high NER. If the NER of the WR could be substantially improved, using methods suggested above, it may become comparable to the NERs for raceways (which were calculated based on outdoor sunlight) and thus become competitive for energy products.

An LCA of a simulated algal biodiesel production process was performed using the ALR and WR in the cultivation stage of the process. This was performed in order to answer the research question stated in Section 1.10 – "Do the novel strategies for mixing and mass transfer in algal PBRs translate to altered environmental burdens of a simulated bioprocess?" The electricity demand generated by the flow-sheet model for algal biodiesel production showed that the PBR had far higher electricity usage than the rest of the process, including harvesting and pumping (at least 98% of the total). This large electricity input led to heavy environmental burdens in the LCA impact categories analysed (abiotic and fossil fuel depletion, global warming potential, acidification and eutrophication). The area of highest environmental impact in algal biodiesel production was, therefore, the PBR, whose power requirement for mixing and mass transfer were the primary cause of this burden. This highlights the importance of improvements to mixing and mass transfer in the PBR and confirms the purpose of this research. Furthermore, the improvements to PBRs made in this work led to substantial reductions in environmental burdens in the context of the whole biodiesel production process:- 73% reductions with an optimised ALR, and a further 18% when the surface aerated WR was used instead of the sparged reactor. Reductions in environmental burdens of this magnitude are a major advantage for a bioprocess. A push to more sustainable systems, driven by global environmental degradation, will lead to support for bioprocesses which offer lowered environmental impacts. Additionally, the large reductions in electricity input of a bioprocess, as shown in this work, would lead to considerable improvements in the cost of the bio-product. This has positive

implications for bioproducts when considering their cost competitiveness with non-renewable alternatives.

8.2 Final conclusions

In this research it was hypothesised that surface aeration would provide sufficient mass transfer for algal cultivation at lower energy consumption than conventional sparging. To investigate this, we compared the mass transfer and algal cultivation in airlift (ALR), oscillatory baffled (OBR) and wave (WR) PBRs across a range of power inputs. The research described in this dissertation supported the hypothesis in the case of the WR compared to the ALR, but not in the case of the OBR. Improvements to the OBR design could lead to improved mass transfer, and further investigation is recommended in future work. The superior energy efficiency of the WR compared to ALR has significant impacts on future bioreactor choice by researchers and process engineers. It might also stimulate further investigation into the use of surface aeration.

The second hypothesis of this research stated that a critical minimum power input for mixing and mass transfer exists before algal growth and lipid productivity is significantly reduced. This was demonstrated in the ALR and WR, where there was a critical mass transfer rate above which there were no significant changes in algal biomass and lipid productivity. Agitation rates (sparging and rocking, respectively) could thus be reduced accordingly. In the ALR the objective was to find the critical minimum CO_2 supply rate, based on aeration and CO_2 concentration. Applying a critical minimum power for mixing and mass transfer in this way caused substantial improvements to the energy efficiencies of the reactors. It is suggested that the critical minimum power input be ascertained by the methods shown in this work, for the energy efficient operation of any PBR in future applications.

In the final section of this research, it was hypothesised that reductions in energy consumption for mixing and mass transfer, demonstrated in previous sections, would lead to reduced environmental burdens in an algal biodiesel production process. An LCA of a simulated biodiesel production process was used to investigate this hypothesis, using the data from the ALR and WR obtained from previous sections. The LCA showed that the energy consumption by the bioreactors was key to

reducing the impacts of the process. Therefore, the reductions in energy consumption achieved by PBR optimisation, and using a wave reactor in place of a sparged reactor, led to substantial reductions in the environmental burdens of the whole bioprocess.

8.3 Future recommendations

Cultivation of *Scenedesmus* sp. under conditions that are not light limiting would be of considerable benefit. Outdoor cultivation, under sunlight, would provide data closer to that obtained at a large-scale facility (which are predominantly outdoors). Investigations of varied reactor dimensions with respect to light penetration and mass transfer would be necessary. Shallower volumes would promote light distribution, but this would lead to larger land requirements at large-scale.

Construction of a pilot-scale wave-generating PBR that simulates the wave motion of the WR in this work would also be beneficial. Possible differences in energy consumption across different wave generating technologies would be a useful comparison for future design choices.

Improvements on design also need to be made to the OBR, with a focus on the eddy formation reported by previous studies to increase mass transfer. Waves and oscillations can be achieved in a variety of ways, leaving much scope for design of novel surface aerated reactors. Other reactors, such as orbital shakers, also provide surface aeration. A comparison across a range of surface aerated reactors would provide more insight into the benefits of this method of aeration. These need to be weighed against the low energy raceway ponds.

Although the WR was more energy efficient than the ALR, the land use might be larger. A more detailed LCA including land use would reveal such trade-offs. Water footprint is also an important aspect of algal cultivation which can be studied in an LCA. The low NERs of PBRs suggests that they have limited application for bioenergy products. The use of PBRs for inoculum into large-scale ponds should be explored further, including an LCA on such a scenario. A comparison between this hybrid (PBR-pond) system and a system that uses PBRs only or ponds only, would be useful for process

design choices. An LCA of a non-energy, high value algal product, in comparison to its chemical counterpart, would also be useful for understanding the niche for PBRs.

An economic assessment would be an informative addition to the energy balance and environmental assessment of algal biodiesel reported in this work, or other algal products from PBRs. The economic benefits of reduced reactor energy inputs would be significant, and would improve the feasibility of algal biodiesel compared to other biofuels and fossil diesel, and increase competiveness of other algal bioproducts.

References

Abbott, M.S.R., Valente Perez, G., Harvey, A.P., Theodorou, M.K., 2014. Reduced power consumption compared to a traditional stirred tank reactor (STR) for enzymatic saccharification of alpha-cellulose using oscillatory baffled reactor (OBR) technology. Chemical Engineering Research and Design, Green Processes and Eco-technologies 92, 1969–1975.

Ačai, P., Polakovič, M., 2007. Design of a large-scale surface-aerated bioreactor for biomass production using a VOC substrate. Journal of Biotechnology 132, 149–155.

Adams, W.M., 2006. The Future of Sustainability: Re-thinking environment and development in the twenty-first century (Report of the IUCN Renowned Thinkers Meeting).

Adesanya, V.O., Cadena, E., Scott, S.A., Smith, A.G., 2014. Life cycle assessment on microalgal biodiesel production using a hybrid cultivation system. Bioresource Technology 163, 343–355.

Anderson, R., 2013. The Microalgal Cell, in: Handbook of Microalgal Culture: Applied Phycology and Biotechnology. Wiley, pp. 3–20.

Anex, R., 2003. Something New under the Sun? The Industrial Ecology of Biobased Products. Journal of Industrial Ecology 7, 1–4.

Azadi, P., Brownbridge, G., Mosbach, S., Smallbone, A., Bhave, A., Inderwildi, O., Kraft, M., 2014. The carbon footprint and non-renewable energy demand of algae-derived biodiesel. Applied Energy 113, 1632–1644.

Bailey, J.E., 1986. Biochemical Engineering Fundamentals. McGraw-Hill, New York.

Baird, M.H.I., Garstang, J.H., 1972. Gas absorption in a pulsed bubble column. Chemical Engineering Science 27, 823–833.

Baird, M.H.I., Garstang, J.H., 1967. Power consumption and gas hold-up in a pulsed column. Chemical Engineering Science 22, 1663–1673.

Bastenhof, D., 1983. Surf wave generator. US Patent 4522535 A.

Batan, L., Quinn, J., Willson, B., Bradley, T., 2010. Net Energy and Greenhouse Gas Emission Evaluation of Biodiesel Derived from Microalgae. Environmental Science & Technology 44, 7975–7980.

Beal, C.M., Gerber, L.N., Sills, D.L., Huntley, M.E., Machesky, S.C., Walsh, M.J., Tester, J.W., Archibald, I., Granados, J., Greene, C.H., 2015. Algal biofuel production for fuels and feed in a 100-ha facility: A comprehensive techno-economic analysis and life cycle assessment. Algal Research 10, 266–279.

Bellhouse, B.J., 1973. A high efficiency membrane oxygenator and pulsatile pumping system, and its application to animal trials. ASAIO Journal: A peer-reviewed journal of the American Society for Artifical Internal Organs 19, 72.

Bezerra, R.P., Matsudo, M.C., Sato, S., Perego, P., Converti, A., Carvalho, J.C.M. de, 2012. Effects of photobioreactor configuration, nitrogen source and light intensity on the fed-batch cultivation of Arthrospira (Spirulina) platensis. Bioenergetic aspects. Biomass and Bioenergy 37, 309–317.

Bicalho, T., Richard, J., Bessou, C., 2012. Limitations of LCA in environmental accounting for biofuels under RED. Sustainability 3, 218–234.

Bold, H.C., 1949. The Morphology of Chlamydomonas chlamydogama, Sp. Nov. Bulletin of the Torrey Botanical Club 76, 101–108.

Bondioli, P., Della Bella, L., Rivolta, G., Chini Zittelli, G., Bassi, N., Rodolfi, L., Casini, D., Prussi, M., Chiaramonti, D., Tredici, M.R., 2012. Oil production by the marine microalgae Nannochloropsis sp. F&M-M24 and Tetraselmis suecica F&M-M33. Bioresource Technology 114, 567–572.

Borowitzka, M.A., Moheimani, N.R., 2013. Sustainable biofuels from algae 13–25.

Bouaifi, M., Roustan, M., 2001. Power consumption, mixing time and homogenisation energy in dual-impeller agitated gas–liquid reactors. Chemical Engineering and Processing: Process Intensification 40, 87–95.

Brennan, L., Owende, P., 2010. Biofuels from microalgae—A review of technologies for production, processing, and extractions of biofuels and co-products. Renewable and Sustainable Energy Reviews 14, 557–577.

Brighton, M., In review. Tracing Particle Movement for Simulation of Light History and Algal Growth in Airlift Photobioreactors using Positron Emission Particle Tracking (PEPT). University of Cape Town.

Brindley Alías, C., García-Malea López, M. C., Acién Fernández, F. G., Fernández Sevilla, J. M., García Sánchez, J. l., Molina Grima, E., 2004. Influence of power supply in the feasibility of Phaeodactylum tricornutum cultures. Biotechnology and Bioengineering 87, 723–733.

Brown, C.J., Ni, X., 2010. Evaluation of rate of cyclopentane hydrate formation in an oscillatory baffled column using laser induced fluorescence and energy balance. Chemical Engineering Journal 157, 131–139.

Brunold, C.R., Hunns, J.C.B., Mackley, M.R., Thompson, J.W., 1989. Experimental observations on flow patterns and energy losses for oscillatory flow in ducts containing sharp edges. Chemical Engineering Science 44, 1227–1244.

Camacho, F.G., Rodríguez, J.J.G., Mirón, A.S., Belarbi, E.H., Chisti, Y., Grima, E.M., 2011. Photobioreactor scale-up for a shear-sensitive dinoflagellate microalga. Process Biochemistry 46, 936–944.

Campbell, P.K., Beer, T., Batten, D., 2011. Life cycle assessment of biodiesel production from microalgae in ponds. Bioresource Technology 102, 50–56.

Cardozo, K.H.M., Guaratini, T., Barros, M.P., Falcão, V.R., Tonon, A.P., Lopes, N.P., Campos, S., Torres, M.A., Souza, A.O., Colepicolo, P., Pinto, E., 2007. Metabolites from algae with economical impact. Comparative Biochemistry and Physiology 146, 60–78.

Carpenter, N.G., Roberts, E.P.L., 1999. Mass Transport and Residence Time Characteristics of an Oscillatory Flow Electrochemical Reactor. Chemical Engineering Research and Design 77, 212–217.

Carvalho, A., Meireles, L.A., Malcata, F.X., 2006. Microalgal reactors: A review of enclosed system designs and performances. Biotechnology Progress 22, 1490.

Castine, S.A., Paul, N.A., Magnusson, M., Bird, M.I., de Nys, R., 2013. Algal bioproducts derived from suspended solids in intensive land-based aquaculture. Bioresource Technology 131, 113–120.

Changunda, K., Harris, M., Deglon, D.A., 2008. Investigating the effect of energy input on flotation kinetics in an oscillating grid flotation cell. Minerals Engineering 21, 924–929.

Chen, G.-Q., Patel, M.K., 2012. Plastics derived from biological sources: present and future: a technical and environmental review. Chemical Reviews 112, 2082–2099.

Cheng-Wu, Z., Zmora, O., Kopel, R., Richmond, A., 2001. An industrial-size flat plate glass reactor for mass production of Nannochloropsis sp. (Eustigmatophyceae). Aquaculture 195, 35–49.

Chisti, Y., 2013. Constraints to commercialization of algal fuels. Journal of Biotechnology 167, 201–214.

Chisti, Y., 2008a. Response to Reijnders: do biofuels from microalgae beat biofuels from terrestrial plants? Trends in Biotechnology 26, 351.

Chisti, Y., 2008b. Biodiesel from microalgae beats bioethanol. Trends in Biotechnology 26, 126–131.

Chisti, Y., 2007a. Biodiesel from microalgae. Biotechnol.Adv. 25, 294–306.

Chisti, Y., 2007a. Mass Transfer, in: Kirk-Othmer Encyclopedia of Chemical Technology. John Wiley & Sons, Inc.

Chisti, Y., 1989. Airlift Bioreactors. Elsevier Science Publishers Ltd, England.

Chisti, Y., Jauregui-Haza, U.J., 2002. Oxygen transfer and mixing in mechanically agitated airlift bioreactors. Biochemical Engineering Journal 10, 143–153.

Chiu, S.-Y., Kao, C.-Y., Tsai, M.-T., Ong, S.-C., Chen, C.-H., Lin, C.-S., 2009. Lipid accumulation and CO2 utilization of Nannochloropsis oculata in response to CO2 aeration. Bioresource Technology 100, 833–838.

Christenson, L., Sims, R., 2011. Production and harvesting of microalgae for wastewater treatment, biofuels, and bioproducts. Biotechnology Advances In Press, Corrected Proof.

Cirés, S., Alvarez-Roa, C., Heimann, K., 2015. First use of the WAVE™ disposable rocking bioreactor for enhanced bioproduct synthesis by N2-fixing cyanobacteria. Biotechnology and Bioengineering 112, 621–626.

Clarens, A.F., Resurreccion, E.P., White, M.A., Colosi, L.M., 2010. Environmental life cycle comparison of algae to other bioenergy feedstocks. Environmental Science and Technology 44, 1813–1819.

Cluzel, F., Leroy, Y., Yannou, B., 2013. Toward a structured functional unit definition framework to limit LCA results variability, in: 6th International Conference on Life Cycle Management - LCM 2013. Gothenburg, Sweden, p. Paper no. 484.

Collet, P., Lardon, L., Hélias, A., Bricout, S., Lombaert-Valot, I., Perrier, B., Lépine, O., Steyer, J.-P., Bernard, O., 2014. Biodiesel from microalgae – Life cycle assessment and recommendations for potential improvements. Renewable Energy 71, 525–533.

Čuček, L., Klemeš, J.J., Kravanja, Z., 2012. A Review of Footprint analysis tools for monitoring impacts on sustainability. Journal of Cleaner Production, Recent Cleaner Production Advances in Process Monitoring and Optimisation 34, 9–20.

Degen, J., Uebele, A., Retze, A., Schmid-Staiger, U., Trösch, W., 2001. A novel airlift photobioreactor with baffles for improved light utilization through the flashing light effect. Journal of Biotechnology, Biochemical Engineering: Trends and Potentials 92, 89–94.

Demirbas, A., 2010. Use of algae as biofuel sources. Energy Conversion and Management 51, 2738–2749.

Demirbas, A., 2007. Importance of biodiesel as transportation fuel. Energy Policy 35, 4661–4670.

Demirbas, A., Demirbas, M.F., 2010. Algae Energy: Algae as a New Source of Biodiesel. Springer Science & Business Media.

Demirbas, M.F., 2011. Biofuels from algae for sustainable development. Applied Energy 88, 3473–3480.

de Morais, M.G., Costa, J.A.V., 2007. Biofixation of carbon dioxide by Spirulina sp. and Scenedesmus obliquus cultivated in a three-stage serial tubular photobioreactor. Journal of Biotechnology 129, 439–445.

Dickens, A.W., Mackley, M.R., Williams, H.R., 1989. Experimental residence time distribution measurements for unsteady flow in baffled tubes. Chemical Engineering Science 44, 1471–1479.

Dreesen, I.A.J., Hamri, G.C.-E., Fussenegger, M., 2010. Heat-stable oral alga-based vaccine protects mice from Staphylococcus aureus infection. Journal of Biotechnology 145, 273–280.

Eibl, R., Eibl, D., 2006. Design and use of the wave bioreactor for plant cell culture, in: Gupta, S.D., Ibaraki, Y. (Eds.), Plan Tissue Culture Engineering, Focus on Biotechnology. Springer Netherlands, pp. 203–227.

Eibl, R., Werner, S., Eibl, D., 2009. Bag Bioreactor Based on Wave-Induced Motion: Characteristics and Applications. Advances in Biochemical Engineering / Biotechnology Disposable bioreactors, 55–87.

Eilers, P.H.C., Peeters, J.C.H., 1988. A model for the relationship between light intensity and the rate of photosynthesis in phytoplankton. Ecological Modelling 42, 199–215.

EnergyTrend PV, 2014. Advances in PV Technology – 2014 Review 2/4. TrendForce Corp.

Ferreira, B.S., Fernandes, H.L., Reis, A., Mateus, M., 1998. Microporous hollow fibres for carbon dioxide absorption: Mass transfer model fitting and the supplying of carbon dioxide to microalgal cultures. Journal of Chemical Technology & Biotechnology 71, 61–70.

Finnveden, G., 2000. On the limitations of life cycle assessment and environmental systems analysis tools in general. The International Journal of Life Cycle Assessment 5, 229–238.

Frank, E.D., Han, J., Palou-Rivera, I., Elgowainy, A., Wang, M.Q., 2012. Methane and nitrous oxide emissions affect the life-cycle analysis of algal biofuels. Environ. Res. Lett. 7, 014030.

Fraser, M., 2011. Modelling airlift photobioreactors for algal bioenergy, using Scenedesmus sp. as the model species (MSc Dissertation). University of Cape Town, South Africa.

Frischknecht, R., Jungbluth, N., Althaus, H.J., Doka, G., Dones, R., Hischier, R., Hellweg, S., Humbert, S., Margni, M., Nemecek, T., Spielmann, M., 2007. Implementation of Life Cycle Impact Assessment Methods: Data v2.0. ecoinvent report No. 3.

Gaidhani, H.K., McNeil, B., Ni, X., 2005. Fermentation of Pullulan Using an Oscillatory Baffled Fermenter. Chemical Engineering Research and Design 83, 640–645.

Gani, A., 2013. Effect of light supply in photobioreactors on the biomass productivity and energy efficiency of Scenedesmus sp. (MSc Dissertation) University of Cape Town, Cape Town.

Gao, P., Han Ching, W., Herrmann, M., Kwong Chan, C., Yue, P.L., 2003. Photooxidation of a model pollutant in an oscillatory flow reactor with baffles. Chemical Engineering Science 58, 1013–1020.

Garcia-Ochoa, F., Gomez, E., 2009. Bioreactor scale-up and oxygen transfer rate in microbial processes: An overview. Biotechnology Advances 27, 153–176.

Gavrilescu, M., Chisti, Y., 2005. Biotechnology—a sustainable alternative for chemical industry. Biotechnology Advances 23, 471–499.

Gavrilescu, M., Tudose, R.Z., 1997. Mixing studies in external-loop airlift reactors. Chemical Engineering Journal 66, 97–104.

Geigrich, J., 2003. Modern Times and Imperfect Cycles: Managing the Waste from Biobased Products. Journal of Industrial Ecology 7, 10–12.

Gerngross, T.U., 1999. Can biotechnology move us toward a sustainable society? Nature Biotechnology 17, 541.

Ghazi, A.T.I.M., Resul, M.F.M.G., Yunus, R., Yaw, T.C.S., 2008. Preliminary design of oscillatory flow biodiesel reactor for continuous biodiesel production from jatropha triglycerides. Journal of Engineering Science and Technology 3, 138.

Glazyrina, J., Materne, E.-M., Dreher, T., Storm, D., Junne, S., Adams, T., Greller, G., Neubauer, P., 2010. High cell density cultivation and recombinant protein production with Escherichia coli in a rocking-motion-type bioreactor. Microbial Cell Factories 9 – 42.

Graham, L.E., Graham, J.M., Wilcox, L.W., 2009. Algae, 2nd ed. Benjamin Cummings, San Francisco.

Green, D., Perry, R., 2007. Perry's Chemical Engineers' Handbook, Eighth Edition, 8 edition. ed. McGraw-Hill Professional.

Green, M.A., Emery, K., Hishikawa, Y., Warta, W., Dunlop, E.D., 2015. Solar cell efficiency tables (Version 45). Progress in Photovoltaics: Research and Applications 23, 1–9.

Griffiths, M.J., 2011. Optimising microalgal lipid productivity for biodesel production (PhD Dissertation). University of Cape Town, South Africa.

Griffiths, M.J., Harrison, S.T.L., 2009. Lipid productivity as a key characteristic for choosing algal species for biodiesel production. Journal of Applied Phycology 21, 493.

Griffiths, M.J., Hille, R.P. van, Harrison, S.T.L., 2014a. The effect of nitrogen limitation on lipid productivity and cell composition in Chlorella vulgaris. Applied Microbiology and Biotechnology 98, 2345–2356.

Griffiths, M.J., Hille, R.P. van, Harrison, S.T.L., 2014b. The effect of degree and timing of nitrogen limitation on lipid productivity in Chlorella vulgaris. Applied Microbiology and Biotechnology 98, 6147–6159.

Griffiths, M.J., van Hille, R.P., Harrison, S.T.L., 2012. Lipid productivity, settling potential and fatty acid profile of 11 microalgal species grown under nitrogen replete and limited conditions. - Journal of Applied Phycology 24, 989–1001.

Griffiths, M.J., van Hille, R.P., Harrison, S.T.L., 2010. Selection of direct transesterification as the preferred method for assay of fatty acid vontent of microalgae. - Lipids 45, 1053–1060.

Grobbelaar, J.U., 2000. Physiological and technological considerations for optimising mass algal cultures. Journal of Applied Phycology 12, 201–206.

Guldbrandsson, F., Bergmark, P., 2012. Opportunities and limitations of using life cycle assessment methodology in the ICT sector, in: Electronics Goes Green 2012+ (EGG), 2012. Presented at the Electronics Goes Green 2012+ (EGG), 2012, pp. 1–6.

Guo, Y.X., Rathor, M.N., Ti, H.C., 1997. Hydrodynamics and mass transfer studies in a novel external-loop airlift reactor. Chemical Engineering Journal 67, 205–214.

Gupta, A., Rao, G., 2003. A study of oxygen transfer in shake flasks using a non-invasive oxygen sensor. Biotechnology and Bioengineering 84, 351–358.

Gustafsson, J.P., 2012. Visual MINTEQ.

Hall, D.O., Acién Fernández, F.G., Guerrero, E.C., Rao, K.K., Grima, E.M., 2003. Outdoor helical tubular photobioreactors for microalgal production: Modeling of fluid-dynamics and mass transfer and assessment of biomass productivity. Biotechnology and Bioengineering 82, 62–73.

Harding, K.G., 2008. A generic approach to environmental assessment of microbial bioprocesses through Life Cycle Assessment (LCA) (PhD Dissertation). University of Cape Town.

Harding, K.G., Dennis, J.S., von Blottnitz, H., Harrison, S.T.L., 2008. A life-cycle comparison between inorganic and biological catalysis for the production of biodiesel. Journal of Cleaner Production 16, 1368–1378.

Harding, K.G., Dennis, J.S., von Blottnitz, H., Harrison, S.T.L., 2007. Environmental analysis of plastic production processes: Comparing petroleum-based polypropylene and polyethylene with biologically-based poly-β-hydroxybutyric acid using life cycle analysis. Journal of Biotechnology 130, 57–66.

Harrison, S.T.L., Mackley, M.R., 1992. A pulsatile flow bioreactor. Chemical Engineering Science 47, 490–493.

Harun, R., Singh, M., Forde, G.M., Danquah, M.K., 2010. Bioprocess engineering of microalgae to produce a variety of consumer products. Renewable and Sustainable Energy Reviews 14, 1037–1047.

Harvey, A.P., Mackley, M.R., Seliger, T., 2003. Process intensification of biodiesel production using a continuous oscillatory flow reactor. Journal of Chemical Technology & Biotechnology 78, 338–341.

Harvey, A.P., Mackley, M.R., Stonestreet, P., 2001. Operation and Optimization of an Oscillatory Flow Continuous Reactor. Industrial & Engineering Chemistry Research 40, 5371–5377.

Henley, E.J., Seader, J.D., Roper, D.K., 2011. Separation Process Principles. Wiley.

Hermann, B.G., Blok, K., Patel, M.K., 2007. Producing bio-based bulk chemicals using industrial biotechnology saves energy and combats climate change. Environmental science & technology 41, 7915–7921.

Hermann, B.G., Patel, M., 2007. Today's and tomorrow's bio-based bulk chemicals from white biotechnology: a techno-economic analysis. Applied Biochemistry and Biotechnology 136, 361–388.

Hertwich, E.G., Pease, W.S., Koshland, C.P., 1997. Evaluating the environmental impact of products and production processes: a comparison of six methods. Science of The Total Environment 196, 13–29.

Hewgill, M.R., Mackley, M.R., Pandit, A.B., Pannu, S.S., 1993. Enhancement of gas-liquid mass transfer using oscillatory flow in a baffled tube. Chemical Engineering Science 48, 799–809.

Hobson, J., 1998. BiowaveTM: A novel reactor for the treatment of wastewater. Water Research 32, 2556–2561.

Holland, F.A., Chapman, F.S., 1966. Liquid mixing and processing in stirred tanks. Reinhold Publishing Corporation.

Hreiz, R., 2014. Experimental and numerical investigation of hydrodynamics in raceway reactors used for algaculture. Chemical Engineering Journal 250, 230.
Idbeis, B., 1996. Aquarium sea current generator. US Patent 5535702 A.
International Standards Organisation, 2006. Environmental Management—Life Cycle Assessment—Principles and Framework; ISO report 14040:2006(E).
Iqbal, M., Grey, D., Stepan-Sarkissian, F., Fowler, M.W., 1993. A flat-sided photobioreactor for culturing microalgae. Aquacultural Engineering 12, 183–190.
Itten, R., Frischknecht, R., Stucki, M., 2012. Life cycle inventories of electricity mixes and grid. (Technical Report). Paul Scherrer Institute, Switzerland.
Jackson, M.L., 1964. Aeration in Bernoulli Types of Devices.
Jian, H., Ni, X., 2005. A Numerical Study on the Scale-Up Behaviour in Oscillatory Baffled Columns. Chemical Engineering Research and Design 83, 1163–1170.
Jian, M.I.N., 2006. Large eddy simulations of mixing time in a stirred tank. Chinese Journal of Chemical Engineering 14, 1.
Jones, S.M.J., Brighton, M., Harrison, S.T.L., In review. Exploring the tension between energy consumption, light provision and CO2 mass transfer through varying gas velocity in the airlift bioreactor. Algal Research.
Jones, S.M.J., Harrison, S.T.L., 2014. Aeration energy requirements for lipid production by Scenedesmus sp. in airlift bioreactors. Algal Research 5, 249–257.
Jonker, J.G.G., Faaij, A.P.C., 2013. Techno-economic assessment of micro-algae as feedstock for renewable bio-energy production. Applied Energy 102, 461–475.
Jørgensen, A., Bocq, A.L., Nazarkina, L., Hauschild, M., 2007. Methodologies for social life cycle assessment. The International Journal of Life Cycle Assessment 13, 96–103.
Jorquera, O., Kiperstok, A., Sales, E.A., Embiruçu, M., Ghirardi, M.L., 2010. Comparative energy life-cycle analyses of microalgal biomass production in open ponds and photobioreactors. Bioresource Technology 101, 1406–1413.
Junne, S., Solymosi, T., Oosterhuis, N., Neubauer, P., 2013. Cultivation of Cells and Microorganisms in Wave-Mixed Disposable Bag Bioreactors at Different Scales. Chemie Ingenieur Technik 85, 57–66.
Kadam, K.L., 2002. Environmental implications of power generation via coal-microalgae cofiring. Energy 27, 905–922.
Kadarusman, J., Bhatia, R., McLaughlin, J., Lin, W.R., 2005. Growing Cholesterol-Dependent NS0 Myeloma Cell Line in the Wave Bioreactor System: Overcoming Cholesterol-Polymer Interaction by Using Pretreated Polymer or Inert Fluorinated Ethylene Propylene. Biotechnol Progress 21, 1341–1346.
Kadwell, S., Hardwicke, P., 2007. Production of baculovirus-expressed recombinant proteins in wave bioreactors. Methods in Molecular Biology 388, 247.
Kaewpintong, K., Shotipruk, A., Powtongsook, S., Pavasant, P., 2007. Photoautotrophic high-density cultivation of vegetative cells of Haematococcus pluvialis in airlift bioreactor. Bioresource Technology 98, 288–295.
Karr, A.E., 1959. Performance of a reciprocating-plate extraction column. AIChE Journal 5, 446–452.
Kato, Y., Peter, C.P., Akgün, A., Büchs, J., 2004. Power consumption and heat transfer resistance in large rotary shaking vessels. Biochemical Engineering Journal 21, 83–91.
Ketheesan, B., Nirmalakhandan, N., 2012. Feasibility of microalgal cultivation in a pilot-scale airlift-driven raceway reactor. Bioresource Technology 108, 196–202.
Ketheesan, B., Nirmalakhandan, N., 2011. Development of a new airlift-driven raceway reactor for algal cultivation. Applied Energy 88, 3370–3376.
Kilonzo, P.M., Margaritis, A., Bergougnou, M.A., Yu, J., Ye, Q., 2007. Effects of geometrical design on hydrodynamic and mass transfer characteristics of a rectangular-column airlift bioreactor. Biochemical Engineering Journal 34, 279–288.

Kitcha, S., Cheirsilp, B., 2011. Screening of Oleaginous Yeasts and Optimization for Lipid Production Using Crude Glycerol as a Carbon Source. 9th Eco-Energy and Materials Science and Engineering Symposium 9, 274–282.

Knoll, A.H., 2008. Cyanobacteria and Earth History, in: The Cyanobacteria: Molecular Biology, Genomics, and Evolution. Horizon Scientific Press, pp. 1–20.

Kuda, T., Tsunekawa, M., Goto, H., Araki, Y., 2005. Antioxidant properties of four edible algae harvested in the Noto Peninsula, Japan. Journal of Food Composition and Analysis 18, 625–633.

Lam, M.K., Lee, K.T., 2012. Microalgae biofuels: A critical review of issues, problems and the way forward. Biotechnology Advances 30, 673–690.

Langley, N., 2010. Strategies for carbon delivery to microalgal cultures and their potential for the reduction of emissions (MSc Dissertation). University of Cape Town.

Langley, N.M., Harrison, S.T.L., van Hille, R.P., 2012. A critical evaluation of CO2 supplementation to algal systems by direct injection. Biochemical Engineering Journal 68, 70–75.

Lardon, L., Helias, A., Sialve, B., Steyer, J.-P., Bernard, O., 2009. Life-cycle assessment of biodiesel production from microalgae. Environmental Science & Technology 43, 6475–6481.

Lee, A.K., Lewis, D.M., Ashman, P.J., 2010. Energy requirements and economic analysis of a full-scale microbial flocculation system for microalgal harvesting. Chemical Engineering Research and Design 88, 988–996.

Lehmann, N., Rischer, H., Eibl, D., Eibl, R., 2013. Wave-Mixed and Orbitally Shaken Single-Use Photobioreactors for Diatom Algae Propagation. Chemie Ingenieur Technik 85, 197–201.

Lehr, F., Posten, C., 2009. Closed photo-bioreactors as tools for biofuel production. Current Opinion in Biotechnology 20, 280–285.

Linek, V., Vacek, V., Beneš, P., 1987. A critical review and experimental verification of the correct use of the dynamic method for the determination of oxygen transfer in aerated agitated vessels to water, electrolyte solutions and viscous liquids. The Chemical Engineering Journal, An International Journal of Research and Development 34, 11–34.

Lin, J., 2011. Lipid production by Lipomyces starkeyi cells in glucose solution without auxiliary nutrients. Journal of Biotechnology 152, 184–188.

Lohrey, C., Kochergin, V., 2012. Biodiesel production from microalgae: Co-location with sugar mills. Bioresource Technology 108, 76–82.

Louw, T.M., Griffiths, M.J., Jones, S.M.J., Harrison, S.T.L., 2016. Techno-economics of algal biodiesel, in: Algae Biotechnology - Products and Processes | Springer, Green Energy and Technology.

Luo, L., Liu, F., Xu, Y., Yuan, J., 2011. Hydrodynamics and mass transfer characteristics in an internal loop airlift reactor with different spargers. Chemical Engineering Journal 175, 494–504.

Mackay, M.E., Mackley, M.R., Wang, Y., 1991a. Oscillations flow within tubes containing wall or central baffles. Chemical engineering research & design 69, 506–513.

Mackay, M.E., Mackley, M.R., Wang, Y., 1991. Oscillations flow within tubes containing wall or central baffles. Chemical Engineering Research and Design 69, 506–513.

Mackley, M.R., Ni, X., 1993. Experimental fluid dispersion measurements in periodic baffled tube arrays. Chemical Engineering Science 48, 3293–3305.

Mackley, M.R., Ni, X., 1991. Mixing and dispersion in a baffled tube for steady laminar and pulsatile flow. Chemical Engineering Science 46, 3139–3151.

Mackley, M.R., Stonestreet, P., 1995. Heat transfer and associated energy dissipation for oscillatory flow in baffled tubes. Chemical Engineering Science 50, 2211–2224.

Maier, U., Losen, M., Büchs, J., 2004. Advances in understanding and modeling the gas–liquid mass transfer in shake flasks. Biochemical Engineering Journal, Applied Shaking Technology 17, 155–167.

Masojidek, J., Torzillo, G., Koblizek, M., 2013. Photosynthesis of Microalgae, in: Handbook of Microalgal Culture: Applied Phycology and Biotechnology. Wiley, pp. 21–36.

Massey, W.T., Harris, M.C., Deglon, D.A., 2012. The effect of energy input on the flotation of quartz in an oscillating grid flotation cell. Minerals Engineering 36–38, 145–151.
Mata, T.M., Martins, A.A., Caetano, N.S., 2010. Microalgae for biodiesel production and other applications: A review. Renewable and Sustainable Energy Reviews 14, 217–232.
Meiser, A., Schmid-Staiger, U., Trösch, W., 2004. Optimization of eicosapentaenoic acid production byPhaeodactylum tricornutumin the flat panel airlift (FPA) reactor. Journal of Applied Phycology 16, 215–225.
Melendi, S., Bonyadi, S., Castell, P., Martinez, M.T., Mackley, M.R., 2012. The functionalization of carbon nanotubes using a batch oscillatory flow reactor. Chemical Engineering Science 84, 544–551.
Mendoza, J.L., Granados, M.R., de Godos, I., Acién, F.G., Molina, E., Banks, C., Heaven, S., 2013. Fluid-dynamic characterization of real-scale raceway reactors for microalgae production. Biomass and Bioenergy 54, 267–275.
Merchuk, J.C., Contreras, A., García, F., Molina, E., 1998. Studies of mixing in a concentric tube airlift bioreactor with different spargers. Chemical Engineering Science 53, 709–719.
Mikola, M., 2007. Evaluation of a novel Wave Bioreactor® cellbag for aerobic yeast cultivation. Bioprocess and Biosystems Engineering 30, 231.
Miller, S.A., Theis, T.L., 2006. Comparison of Life-Cycle Inventory Databases: A Case Study Using Soybean Production. Journal of Industrial Ecology 10, 133–147.
Mirón, A.S., 2004. Mixing in bubble column and airlift reactors. Chemical Engineering Research and Design 82, 1367.
Miron, A.S., 1999. Comparative evaluation of compact photobioreactors for large-scale monoculture of microalgae. Journal of Biotechnology 70, 249.
Molina Grima, E., Belarbi, E.-H., Acién Fernández, F.., Robles Medina, A., Chisti, Y., 2003. Recovery of microalgal biomass and metabolites: process options and economics. Biotechnology Advances 20, 491–515.
Molina Grima, E., Fernández, F.G.A., García Camacho, F., Chisti, Y., 1999. Photobioreactors: light regime, mass transfer, and scaleup. Journal of Biotechnology 70, 231–247.
Moo-Young, M., Blanch, H.W., 1981. Design of biochemical reactors: Mass transfer criteria for simple and complex systems. Advances in Biochemical Engineering 19, 1–69.
Moulijn, J.A., Makkee, M., Diepen, A.E. van, 2013. Chemical Process Technology. John Wiley & Sons, Inc., USA.
Moutafchieva, D., Popova, D., Dimitrova, M., Tchaoushev, S., 2013. Experimental determination of the volumetric mass transfer coefficient. Journal of Chemical Technology and Metallurgy 48, 351–356.
Mueller, J.A., Boyle, W.C., Lightfoot, E.N., 1967. Effect of the response time of a dissolved oxygen probe on the oxygen uptake rate. Applied Microbiology 15, 674.
Munzhedzi, R., Sebitosi, A.B., 2009. Redrawing the solar map of South Africa for photovoltaic applications. Renewable Energy 34, 165–169.
Murhammer, D.W., Goochee, C.F., 1990. Sparged animal cell bioreactors: mechanism of cell damage and pluronic F-68 protection. Biotechnol. Prog. 6, 391–397.
Nagarajan, S., Chou, S.K., Cao, S., Wu, C., Zhou, Z., 2012. An updated comprehensive techno-economic analysis of algae biodiesel. Bioresource Technology.
Nautiyal, P., Subramanian, K.A., Dastidar, M.G., 2014. Kinetic and thermodynamic studies on biodiesel production from Spirulina platensis algae biomass using single stage extraction–transesterification process. Fuel 135, 228–234.
Ness, B., Urbel-Piirsalu, E., Anderberg, S., Olsson, L., 2007. Categorising tools for sustainability assessment. Ecological Economics 60, 498–508.
Nguyen, T.L.T., Gheewala, S.H., Bonnet, S., 2008. Life cycle cost analysis of fuel ethanol produced from cassava in Thailand. The International Journal of Life Cycle Assessment 13, 564–573.

Ni, X., 1995. A study of mass transfer in yeast in a pulsed baffled bioreactor. Biotechnology and Bioengineering 45, 165.

Ni, X., Brogan, G., Struthers, A., Bennett, D.C., Wilson, S.F., 1998. A Systematic Study of the Effect of Geometrical Parameters on Mixing Time in Oscillatory Baffled Columns. Chemical Engineering Research and Design 76, 635–642.

Ni, X., Gao, S., 1996. Scale-up correlation for mass transfer coefficients in pulsed baffled reactors. The Chemical Engineering Journal and the Biochemical Engineering Journal 63, 157–166.

Ni, X., Gao, S., Cumming, R.H., Pritchard, D.W., 1995. A comparative study of mass transfer in yeast for a batch pulsed baffled bioreactor and a stirred tank fermenter. Chemical Engineering Science 50, 2127–2136.

Ni, X., Mackley, M.R., Harvey, A.P., Stonestreet, P., Baird, M.H.I., Rama Rao, N.V., 2003. Mixing through oscillations and pulsations—a guide to achieving process enhancements in the chemical and process industries. Chemical Engineering Research and Design 81, 373–383.

Ni, X., Murray, K.R., Zhang, Y., Bennett, D., Howes, T., 2002. Polymer product engineering utilising oscillatory baffled reactors. Powder Technology 124, 281–286.

Nogueira, X., Taylor, B.J., Gomez, H., Colominas, I., Mackley, M.R., 2013. Experimental and computational modeling of oscillatory flow within a baffled tube containing periodic-tri-orifice baffle geometries. Computers & Chemical Engineering 49, 1–17.

Nordkvist, M., 2003. Applying rotary jet heads for mixing and mass transfer in a forced recirculation tank reactor system. Chemical Engineering Science 58, 3877.

Ott, K., 2003. The case for strong sustainability, in: Ott, K., Thapa, P. (Eds.), Greifswald's Environmental Ethics. Steinbecker, Greifswald, pp. 59–64.

Palma, M., Giudici, R., 2003. Analysis of axial dispersion in an oscillatory-flow continuous reactor. Chemical Engineering Journal 94, 189–198.

Pate, R., Klise, G., Wu, B., 2011. Resource demand implications for US algae biofuels production scale-up. Applied Energy 88, 3377–3388.

Pereira, N.E., Ni, X., 2001. Droplet size distribution in a continuous oscillatory baffled reactor. 16th International Conference on Chemical Reactor Engineering 56, 735–739.

Phan, A.N., Harvey, A., 2010. Development and evaluation of novel designs of continuous mesoscale oscillatory baffled reactors. Chemical Engineering Journal 159, 212–219.

Phan, A.N., Harvey, A.P., 2012. Characterisation of mesoscale oscillatory helical baffled reactor—Experimental approach. Chemical Engineering Journal 180, 229–236.

Pirouzi, A., Nosrati, M., Shojaosadati, S.A., Shakhesi, S., 2014. Improvement of mixing time, mass transfer, and power consumption in an external loop airlift photobioreactor for microalgae cultures. Biochemical Engineering Journal 87, 25–32.

Pittman, J.K., Dean, A.P., Osundeko, O., 2011. The potential of sustainable algal biofuel production using wastewater resources. Bioresource Technology 102, 17–25.

Pre, 2015. SimaPro Database Manual, Methods Library, Report 2.8.

Pulz, O., 2001. Photobioreactors: production systems for phototrophic microorganisms. Applied Microbiology and Biotechnology 57, 287–293.

Quinn, J.C., Smith, T.G., Downes, C.M., Quinn, C., 2014. Microalgae to biofuels lifecycle assessment — Multiple pathway evaluation. Algal Research, Progress and Perspectives on Microalgal Mass Culture 4, 116–122.

Ranade, V.V., Bourne, J.R., Joshi, J.B., 1991. Fluid mechanics and blending in agitated tanks. Chemical Engineering Science 46, 1883–1893.

Raval, K., Kato, Y., Büchs, J., 2007. Comparison of torque method and temperature method for determination of power consumption in disposable shaken bioreactors. Biochemical Engineering Journal 34, 224–227.

Rawat, I., Ranjith Kumar, R., Mutanda, T., Bux, F., 2013. Biodiesel from microalgae: A critical evaluation from laboratory to large scale production. Applied Energy 103, 444–467.

Razon, L.F., Tan, R.R., 2011. Net energy analysis of the production of biodiesel and biogas from the microalgae: Haematococcus pluvialis and Nannochloropsis. Applied Energy, Special Issue of Energy from algae: Current status and future trends 88, 3507–3514.

Reap, J., Roman, F., Duncan, S., Bras, B., 2008. A survey of unresolved problems in life cycle assessment. The International Journal of Life Cycle Assessment 13, 374–388.

Resurreccion, E.P., Colosi, L.M., White, M.A., Clarens, A.F., 2012. Comparison of algae cultivation methods for bioenergy production using a combined life cycle assessment and life cycle costing approach. Bioresource Technology 126, 298–306.

Richardson, C., 2011. Investigating the role of reactor design to maximise the environmental benefit of algal oil for biodiesel (MSc Dissertation). University of Cape Town.

Richardson, J.W., Johnson, M.D., Zhang, X., Zemke, P., Chen, W., Hu, Q., 2014. A financial assessment of two alternative cultivation systems and their contributions to algae biofuel economic viability. Algal Research, Progress and Perspectives on Microalgal Mass Culture 4, 96–104.

Richmond, A., Cheng-Wu, Z., 2001. Optimization of a flat plate glass reactor for mass production of Nannochloropsis sp. outdoors. Journal of Biotechnology 85, 259–269.

Rickman, M., Pellegrino, J., Hock, J., Shaw, S., Freeman, B., 2013. Life-cycle and techno-economic analysis of utility-connected algae systems. Algal Research 2, 59–65.

Rodolfi, L., Zittelli, G.C., Bassi, N., Padovani, G., Biondo, N., Bonini, G., Tredici, M.R., 2009. Microalgae for oil: Strain selection, induction of lipid synthesis and outdoor mass cultivation in a low-cost photobioreactor. Biotechnology and Bioengineering 102, 100.

Rodriguez, G., Dorado, D., Bonsfills, A., Sanahuja, R., Gamisans, X., 2012. Optimization of oxygen transfer through venturi-based systems applied to the biological sweetening of biogas 854–860.

Rosenberg, J.N., Oyler, G. a., Wilkinson, L., Betenbaugh, M.J., 2008. A green light for engineered algae: redirecting metabolism to fuel a biotechnology revolution. Current Opinion in Biotechnology 19, 430–436.

Rubio, F.C., Fernández, F.G.A., Pérez, J.A.S., Camacho, F.G., Grima, E.M., 1999. Prediction of dissolved oxygen and carbon dioxide concentration profiles in tubular photobioreactors for microalgal culture. Biotechnology and Bioengineering 62, 71–86.

Ruggeri, B., Tommasi, T., Sassi, G., 2010. Energy balance of dark anaerobic fermentation as a tool for sustainability analysis. International Journal of Hydrogen Energy 35, 10202–10211.

Sánchez Mirón, A., Cerón García, M.-C., García Camacho, F., Molina Grima, E., Chisti, Y., 2004a. Mixing in bubble column and airlift reactors. Chem.Eng.Res.Design 82, 1367–1374.

Sánchez Mirón, A., Cerón García, M.-C., García Camacho, F., Molina Grima, E., Chisti, Y., 2004. Mixing in Bubble Column and Airlift Reactors. Chemical Engineering Research and Design 82, 1367–1374.

Sánchez Mirón, A., Cerón García, M.-C., García Camacho, F., Molina Grima, E., Chisti, Y., 2002. Growth and biochemical characterization of microalgal biomass produced in bubble column and airlift photobioreactors: studies in fed-batch culture. Enzyme and Microbial Technology 31, 1015–1023.

Sánchez Mirón, A., Contreras Gómez, A., García Camacho, F., Molina Grima, E., Chisti, Y., 1999. Comparative evaluation of compact photobioreactors for large-scale monoculture of microalgae. Journal of Biotechnology, Biotechnological Aspects of Marine Sponges 70, 249–270.

Sander, K., Murthy, G.S., 2010. Life cycle analysis of algae biodiesel. The International Journal of Life Cycle Assessment 15, 704–714.

Sasi, D., 2011. Growth kinetics and lipid production using Chlorella vulgaris in a circulating loop photobioreactor. Journal of Chemical Technology and Biotechnology 86, 875–880.

Sazdanoff, N., 2006. Modeling and Simulation of the Algae to Biodiesel Fuel Cycle (Dissertation). The Ohio State University.

Scott, S.A., Davey, M.P., Dennis, J.S., Horst, I., Howe, C.J., Lea-Smith, D.J., Smith, A.G., 2010. Biodiesel from algae: challenges and prospects. Current Opinion in Biotechnology, Energy biotechnology – Environmental biotechnology 21, 277–286.

Sheehan, J., Dunahay, T., Benemann, J., Roessler, P., 1998. Look Back at the U.s. Department of Energy's Aquatic Species Program: Biodiesel from Algae; Close-Out Report (No. NREL/TP-580-24190). National Renewable Energy Lab., Golden, CO. (US).

Sialve, B., Bernet, N., Bernard, O., 2009. Anaerobic digestion of microalgae as a necessary step to make microalgal biodiesel sustainable. Biotechnology Advances 27, 409–416.

Sierra, E., Acién, F.G., Fernández, J.M., García, J.L., González, C., Molina, E., 2008. Characterization of a flat plate photobioreactor for the production of microalgae. Chemical Engineering Journal 138, 136–147.

Singh, A., Nigam, P.S., Murphy, J.D., 2011. Mechanism and challenges in commercialisation of algal biofuels. Bioresource Technology, Special Issue: Biofuels - II: Algal Biofuels and Microbial Fuel Cells 102, 26–34.

Singh, J., Gu, S., 2010. Commercialization potential of microalgae for biofuels production. Renewable and Sustainable Energy Reviews 14, 2596–2610.

Singh, R.K., Murty, H.R., Gupta, S.K., Dikshit, A.K., 2009. An overview of sustainability assessment methodologies. Ecological Indicators 9, 189–212.

Singh, R.N., Sharma, S., 2012. Development of suitable photobioreactor for algae production – A review. Renewable and Sustainable Energy Reviews 16, 2347–2353.

Singh, V., 2005. The Wave Bioreactor Story.

Singh, V., 2003. Disposable perfusion bioreactor for cell culture. US Patent 6544788 B2.

Singh, V., 1999. Disposable bioreactor for cell culture using wave-induced agitation. Cytotechnology 30, 149.

Slade, R., Bauen, A., 2013. Micro-algae cultivation for biofuels: Cost, energy balance, environmental impacts and future prospects. Biomass Bioenergy.

Slivac, I., Srček, V.G., RadoŠević, K., Kmetič, I., Kniewald, Z., 2006. Aujeszky's disease virus production in disposable bioreactor. Journal of Biosciences 31, 363–368.

Sobey, I.J., 1985. Dispersion caused by separation during oscillatory flow through a furrowed channel. Chemical Engineering Science 40, 2129–2134.

Solano, J.P., Herrero, R., Espín, S., Phan, A.N., Harvey, A.P., 2012. Numerical study of the flow pattern and heat transfer enhancement in oscillatory baffled reactors with helical coil inserts. Chemical Engineering Research and Design 90, 732–742.

Stephens, E., Ross, I.L., Mussgnug, J.H., Wagner, L.D., Borowitzka, M.A., Posten, C., Kruse, O., Hankamer, B., 2010. Future prospects of microalgal biofuel production systems. Trends in Plant Science 15, 554–564.

Stephenson, A.L., Kazamia, E., Dennis, J.S., Howe, C.J., Scott, S.A., Smith, A.G., 2010. Life-Cycle Assessment of Potential Algal Biodiesel Production in the United Kingdom: A Comparison of Raceways and Air-Lift Tubular Bioreactors. Energy Fuels 24, 4062–4077.

Stonestreet, P., Harvey, A.P., 2002. A Mixing-Based Design Methodology for Continuous Oscillatory Flow Reactors. Chemical Engineering Research and Design 80, 31–44.

Stonestreet, P., Van Der Veeken, P.M.J., 1999. The Effects of Oscillatory Flow and Bulk Flow Components on Residence Time Distribution in Baffled Tube Reactors. Chemical Engineering Research and Design 77, 671–684.

Subhadra, B.G., Edwards, M., 2011. Coproduct market analysis and water footprint of simulated commercial algal biorefineries. Applied Energy, Special Issue of Energy from algae: Current status and future trends 88, 3515–3523.

Takeshita, T., 2011. Competitiveness, role, and impact of microalgal biodiesel in the global energy future. Applied Energy 88, 3481–3491.

Talbot, P., Gortares, M.P., Lencki, R.W., de la Noüe, J., 1991. Absorption of CO2 in algal mass culture systems: A different characterization approach. Biotechnology and Bioengineering 37, 834–842.

Tamimi, A., Rinker, E.B., Sandall, O.C., 1994. Diffusion Coefficients for Hydrogen Sulfide, Carbon Dioxide, and Nitrous Oxide in Water over the Temperature Range 293-368 K. Journal of Chemical & Engineering Data 39, 330–332.

Tang, D., Han, W., Li, P., Miao, X., Zhong, J., 2011. CO2 biofixation and fatty acid composition of Scenedesmus obliquus and Chlorella pyrenoidosa in response to different CO2 levels. Bioresource Technology 102, 3071–3076.

Tang, Y.-J., Ohashi, R., Hamel, J.-F.P., 2007. Perfusion Culture of Hybridoma Cells for Hyperproduction of IgG2a Monoclonal Antibody in a Wave Bioreactor-Perfusion Culture System. Biotechnology Progress 23, 255–264.

Terrier, B., Courtois, D., Hénault, N., Cuvier, A., Bastin, M., Aknin, A., Dubreuil, J., Pétiard, V., 2007. Two new disposable bioreactors for plant cell culture: The wave and undertow bioreactor and the slug bubble bioreactor. Biotechnology and Bioengineering 96, 914–923.

Tredici, M.R., 2010. Photobiology of microalgae mass cultures: understanding the tools for the next green revolution. Biofuels 1, 143–162.

Treybal, R.E., 1980. Mass-transfer Operations. McGraw-Hill.

Weber, W., Weber, E., Geisse, S., Memmert, K., 2002. Optimisation of protein expression and establishment of the Wave Bioreactor for Baculovirus/insect cell culture. Cytotechnology 38, 77–85.

Wellburn, A.R., 1994. The Spectral Determination of Chlorophylls a and b, as well as Total Carotenoids, Using Various Solvents with Spectrophotometers of Different Resolution. Journal of Plant Physiology 144, 307–313.

Werner, S., Eibl, R., Lettenbauer, C., Röll, M., Eibl, D., De Jesus, M., Zhang, X., Stettler, M., Tissot, S., Bürkie, C., Broccard, G., Kühner, M., Tanner, R., Baldi, L., Hacker, D., Wurm, F.M., 2010. Innovative, Non-stirred Bioreactors in Scales from Milliliters up to 1000 Liters for Suspension Cultures of Cells using Disposable Bags and Containers – A Swiss Contribution. CHIMIA International Journal for Chemistry 64, 819–823.

Westbrook, A., Scharer, J., Moo-Young, M., Oosterhuis, N., Perry Chou, C., 2014. Application of a two-dimensional disposable rocking bioreactor to bacterial cultivation for recombinant protein production. Biochemical Engineering Journal 88, 154–161.

Whitman, W.G., 1962. The two film theory of gas absorption. International Journal of Heat and Mass Transfer 5, 429–433.

Yang, J., Xu, M., Zhang, X., Hu, Q., Sommerfeld, M., Chen, Y., 2011. Life-cycle analysis on biodiesel production from microalgae: Water footprint and nutrients balance. Bioresource Technology 102, 159–165.

Yazdian, F., Hajiabbas, M.P., Shojaosadati, S.A., Nosrati, M., Vasheghani-Farahani, E., Mehrnia, M.R., 2010. Study of hydrodynamics, mass transfer, energy consumption, and biomass production from natural gas in a forced-liquid vertical tubular loop bioreactor. Biochemical Engineering Journal 49, 192–200.

Yuan, X., Kumar, A., Sahu, A.K., Ergas, S.J., 2011. Impact of ammonia concentration on Spirulina platensis growth in an airlift photobioreactor. Bioresource Technology 102, 3234–3239.

Zahradník, J., Mann, R., Fialová, M., Vlaev, D., Vlaev, S.D., Lossev, V., Seichter, P., 2001. A networks-of-zones analysis of mixing and mass transfer in three industrial bioreactors. Chemical Engineering Science, 16th International Conference on Chemical Reactor Engineering 56, 485–492.

Zheng, M., Mackley, M., 2008. The axial dispersion performance of an oscillatory flow meso-reactor with relevance to continuous flow operation. Chemical Engineering Science 63, 1788–1799. doi:10.1016/j.ces.2007.12.020

Zheng, M., Skelton, R.L., Mackley, M.R., 2007. Biodiesel Reaction Screening Using Oscillatory Flow Meso Reactors. Process Safety and Environmental Protection 85, 365–371.

Zimmerman, W.B., Zandi, M., Hemaka Bandulasena, H.C., Tesař, V., James Gilmour, D., Ying, K., 2011. Design of an airlift loop bioreactor and pilot scales studies with fluidic oscillator induced microbubbles for growth of a microalgae Dunaliella salina. Applied Energy 88, 3357–3369.

Zittelli, G.C., Pastorelli, R., Tredici, M.R., 2000. A Modular Flat Panel Photobioreactor (MFPP) for indoor mass cultivation of Nannochloropsis sp. under artificial illumination. Journal of Applied Phycology 12, 521–526.

Appendix A

A. Detail for graphs comparing kLa and T_m across a variety of bioreactors

In Chapters 1 and 6, mixing and mass transfer are discussed as a function of power input across a wide variety of bioreactors. Figures 1.2, 6.3 and 6.4 report the mixing time (Tm, seconds) and mass transfer coefficient (k_La, h^{-1}) of bioreactors from literature studies to compare with the AL, OB and W photobioreactors of this study. The references for the data sourced from the literature, as well as some details of the bioreactor and bioprocess studied, are listed in Table A.1. The reference numbers in Table A.1 correspond to the labels in Figures 1.2, 6.3 and 6.4. Table A.1 is divided into sparged biroeactors, bioreactors that are mechanically agitated and sparged, and those that are mechanically agitated without sparging.

Table A.1 Mixing, mass transfer and power input across various bioreactor types. V, T_m and k_La denote reactor volume, mixing time and mass transfer coefficient, respectively. P_1 represents the power, as reported in the corresponding journal article, and P_2 represents the power recalculated according to the total aeration power described in Chapter 2.5.1.2 of this thesis.

SPARGED BIOREACTORS:								
Ref. number on graph	**Bioreactor**	**Bioproduct / process**	**V (L)**	**T_M (s)**	**k_La (h^{-1})**	**P_1 (W m^{-3})**	**P_2 (W m^{-3})**	**Reference**
1	Bubble column	Algal production		50 – 120 [a]	32.4 54.0 79.2 100.8 126.0	98.1 137.3 209.9 235.4 284.5	680.0 952.0 1455.2 1632.0. 1972.0	Mirón (2004); Sánchez Mirón et al. (1999)
2	Airlift bioreactor	Reactor design	1100	48 40 36 32 33 31	6.5 13.0 21.0 21.6 28.1 29.5	98.8 230.6 356.8 461.1 549.0 603.9	98.8 30.6 356.8 461.1 549.0 603.9	Chisti (1989); Chisti and Jauregui-Haza (2002)
3	External loop airlift bioreactor	Microalgae culture	63	90 27 25 18	12.62 18 26 23.72	22.1 37.2 67.6 82.3	88.6 147.4 268.2 326.9	Pirouzi et al. (2014)
4	Flat-panel photobioreactor	Microalgae production	250	170 100 110 120 150 150	3.6 7.2 9 13.68 18 22.32	4 15 22 30 41 53	45.3 204.0 317.3 408.0 566.7 725.3	Sierra et al. (2008)
5	Helical tubular photobioreactor	Microalgal cultivation	75	-	7.2 10.8 12.6	800 [b] 1200 2000	-	Hall et al. (2003)
6	Forced liquid vertical tubular loop bioreactor	Biomass (bacteria for feed/fodder)	-	66 18	61.2 122.4	50 320	-	Yazdian et al. (2010)

MECHNICALLY AGITATED WITH SPARGING:								
Ref. number on graph	**Bioreactor**	**Bioproduct / process**	**V (L)**	**T_M (s)**	**$k_L a$ (h^{-1})**	**P_1 (W m^{-3})**	**P_2 (W m^{-3})**	**Reference**
7	Stirred tank, sparged	Mathematical correlation for determining mass transfer	-	10	28.8 36 54 70.2	100 200 400 600	-	Jian, 2006; Linek et al. (1987)
8	Stirred tank, sparged	Yeast fermentation	2	-	25.2 54 75.6 97.2	267 617 1667 2000	-	Ni et al. (1995)
9	Pulsed baffled column, vertical, sparged[c]	Yeast fermentation	1	-	75.6 93.6 111.6 130.0 280.0	200 300 417 833 3717	-	Ni et al. (1995)
10	Wave bioreactor, sparged, gas head-space exchanged[a]	Yeast cultivation / cell culture	5	40 20 10 10	 8 20 40	210 300 370 420 500 560	-	Eibl et al. (2009); Mikola (2007); Singh (1999)
11	Forced recirculation tank reactor with rotary jet heads	Improving mixing and mass transfer for scale-up		18 – 70	87 – 373	400 - 2500	-	Nordkvist (2003)

MECHANICALLY AGITATED BIOREACTORS:								
Ref. number on graph	**Bioreactor**	**Bioproduct / process**	**V (L)**	**T_M (s)**	**$k_L a$ (h^{-1})**	**P_1 (W m^{-3})**	**P_2 (W m^{-3})**	**Reference**
12	Pulsed-batch stirred, surface aerated, large-scale	Bacterial biodegradation of volatile organic compounds	10 000		0.0005 0.004 0.015	125 250 1800	-	Ačai and Polakovič (2007)
13	Raceway (Sparged) Raceway (Unsparged)	Microalgae cultivation	20 000 5600	7200 6480 2000 500		1.5 4 17 39	-	Mendoza et al. (2013) Hreiz (2014)

[a] Rough approximations from studies of varying volumes and agitation conditions

[b] Power calculations included power for circulation (pumping) through helical section of reactor

[c] Power calculations did not include power input as a result of sparging

Appendix B

B. Calorific values of Scenedesmus sp.

The calorific values of high-lipid *Scenedesmus* cultures grown at high (10 400 ppm) and low (3 900 ppm) CO_2 were measured using bomb calorimetry (Department of Forest and Wood Science, University of Stellenbosch, South Africa), and used for calculations of energy output and NER, according to Section 2.6

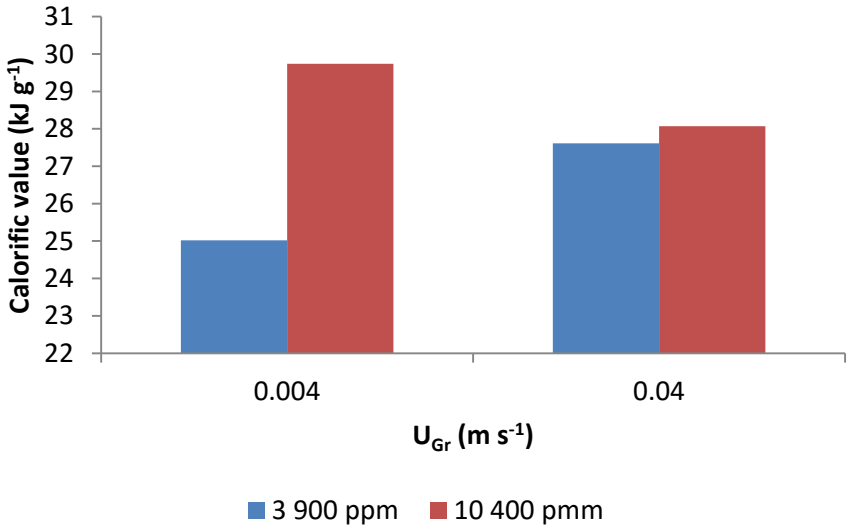

Figure B.1 Calorific values of *Scendesmus* sp. whole cells harvested in stationary phase after cultivation at the given CO_2 concentrations (ppm) and superficial gas velocities (U_{Gr}, m s^{-1}).

Appendix C

C. Raw data for conductivity experiments used for measurement of Tm

Figure C.1 is an example of the raw data obtained for the measurement of mixing time using the conductivity method in the airlift reactor. The tracer in the liquid makes a number of circulations through the riser and downcomer before the solution becomes mixed. Similar raw data was recorded at a range of gas flowrates (0.1 – 2 L min^{-1}).

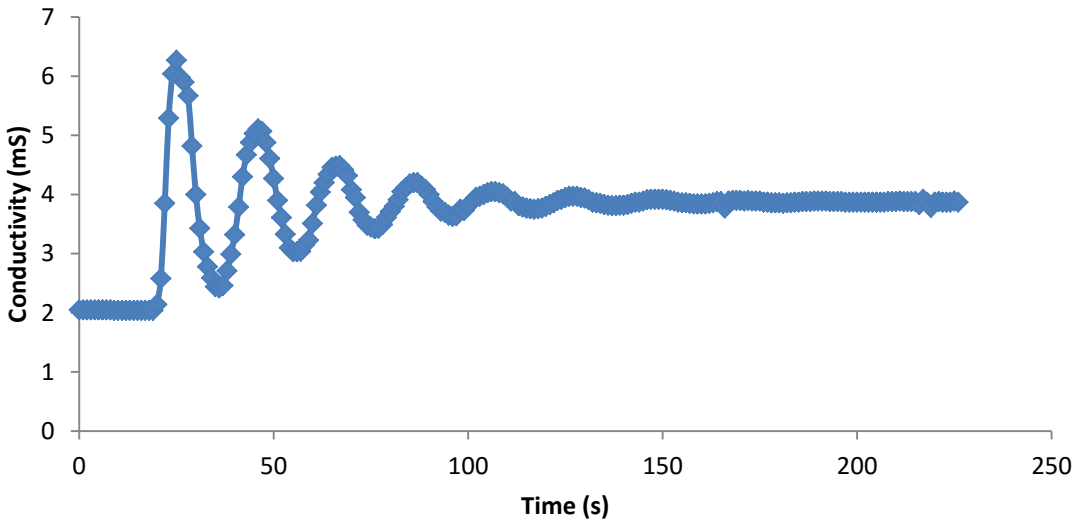

Figure C.1 Raw data from measurement with conductivity probe in airlift photobioreactor at 0.1 L min^{-1} gas flowrate. Peaks indicate circulation time as the tracer passes the probe. The time take for peaks to subside is the mixing time (T_m). This data was courtesy of Fraser (2011).

Figure C.2 is an example of the raw data obtained for the measurement of mixing time using the conductivity method in the wave photobioreactor. On the addition of NaCl tracer, the conductivity measurement spikes. Over time the rocking motion of the wave reactor causes the NaCl tracer to become mixed into the liquid contents of the reactor and the peak dissipates, and the conductivity graph plateaus. Similar raw data was obtained for a range of oscillating frequencies (10 – rpm) and angles (2 - 10°). Similar raw data was also obtained for the oscillatory baffled photobioreactor for a range of oscillating frequencies (10 – 70 Hz) (Figure C.3).

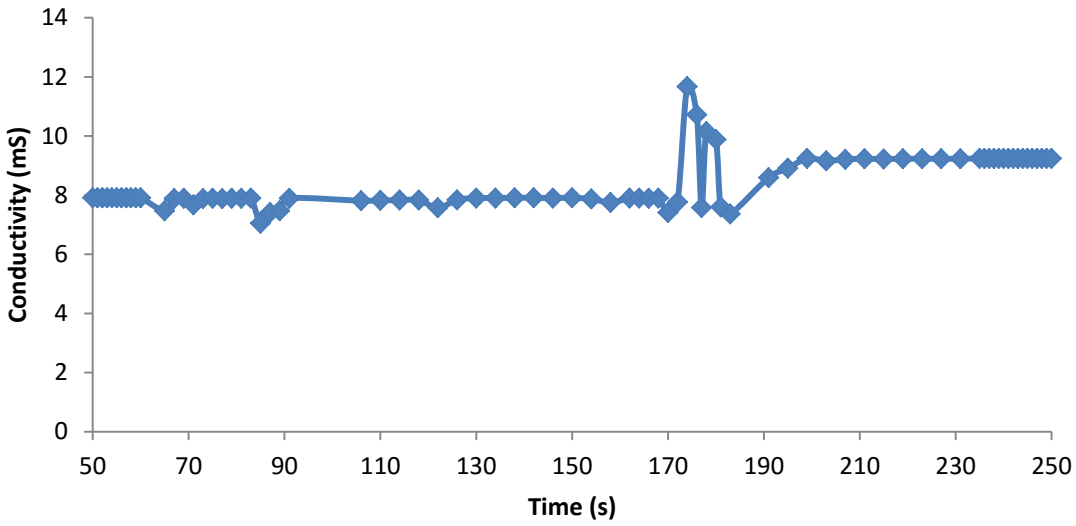

Figure C.2 Raw data from measurement with conductivity probe in wave photobioreactor at 30 rpm, 10°. The peak indicates the NaCl tracer and the time taken from the point of injection to levelling out of the graph is the mixing time (T_m).

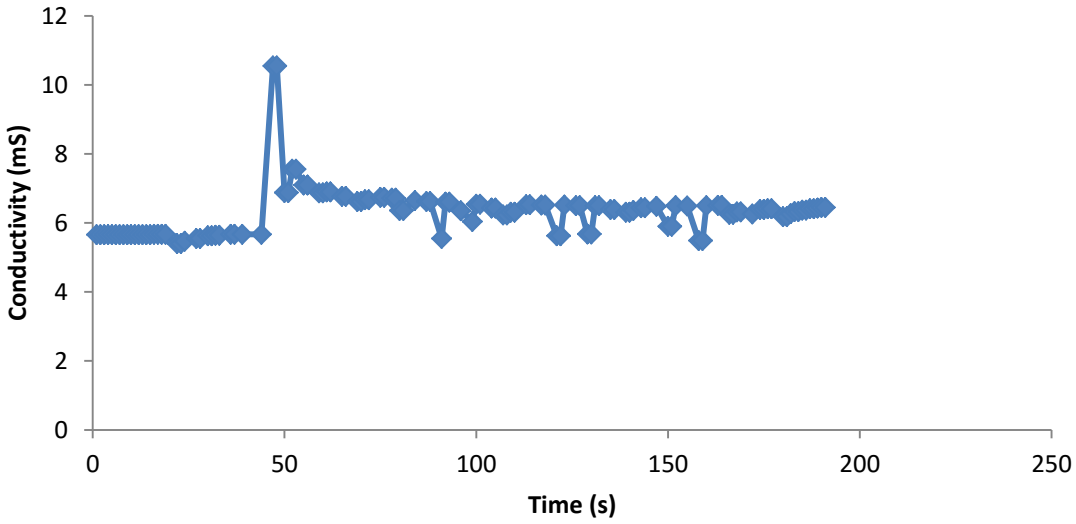

Figure C.3 Raw data from measurement with conductivity probe in oscillatory baffled photobioreactor at 40 Hz. The peak indicates the NaCl tracer and the time taken from the point of injection to levelling out of the graph is the mixing time (T_m).

Appendix D

D. Input and outputs used in Life Cycle Analysis of algal biodiesel production

A model was developed to simulate the production of algal biodiesel at large scale according to the process flow-sheet in Figure D.1. This model was developed by Richardson (2011) and refined for this work. The model was used to inform a life cycle analysis comparing the use of the airlift and wave photobioreactors in the reactor stage of the process. The model calculated all the relevant inputs and outputs for the streams labelled in Figure D.1, and exported the data to Tables D.1, D.2 and D.3.

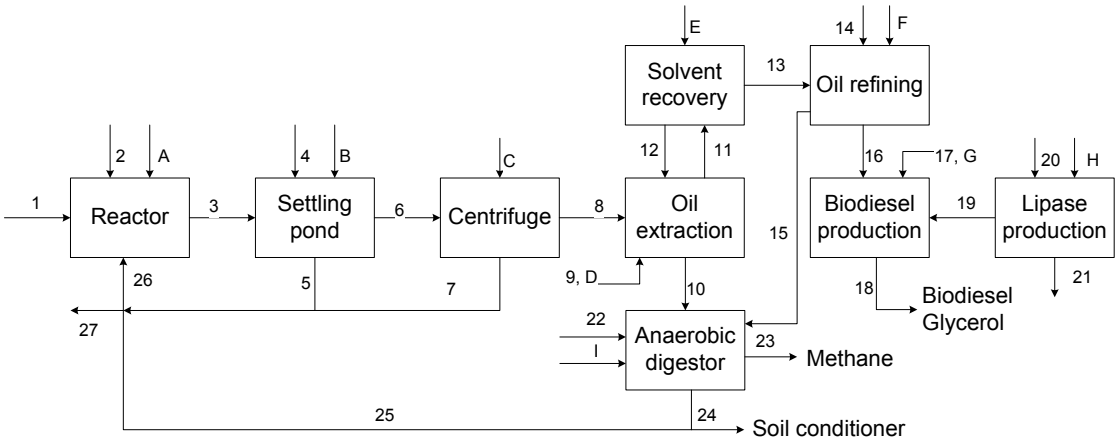

Figure D.1 Process flow-sheet for the production of biodiesel from algae with co-production of methane from anaerobic digestion of algal residue (Richardson, 2011).

Table D.1 Flows (kg day^{-1}) of each component in each of the streams numbered in the process flow-sheet for the simulated algal biodiesel production process inFigure D.1. The flows below represent the quantities when an airlift photobioreactor at a gas flowrate of 2 L min^{-1} was used for algal cultivation.

Flows (kg)	**1**	**2 / 25**	**26**	**3**	**5**	**6**	**7**	**8**	**9**	**10**	**11**
Water	409866	0	1531512	1941378	1903542	37836	10848	26988	0	26988	0
Cells	0	0	499	4304	430	3874	194	3680	0	2664	0
Sodium nitrate	771	0	0	0	0	0	0	0	0	0	0
KH_2PO_4	124	0	0	0	0	0	0	0	0	0	0
Hexane	0	0	0	0	0	0	0	0	42	0	8421
Phosphoric acid	0	0	0	0	0	0	0	0	0	0	0
NaOH	0	0	0	0	0	0	0	0	0	0	0
Methanol	0	0	0	0	0	0	0	0	0	0	0
Biodiesel	0	0	0	0	0	0	0	0	0	0	0
Glycerol	0	0	0	0	0	0	0	0	0	0	0
Cooling water	0	0	0	0	0	0	0	0	0	0	0
Steam	0	0	0	0	0	0	0	0	0	0	0
Glucose	0	0	0	0	0	0	0	0	0	0	0
Yeast	0	0	0	0	0	0	0	0	0	0	0
Precipitating chemical	0	0	0	0	0	0	0	0	0	0	0
CO_2	0	7627	0	0	0	0	0	0	0	0	0
Phosphates	0	0	0	0	0	0	0	0	0	0	0
Urea	0	0	0	0	0	0	0	0	0	0	0
Methane (STP)	0	0	0	0	0	0	0	0	0	0	0
Soil conditioner	0	0	0	0	0	0	0	0	0	0	0
TAG	0	0	0	0	0	0	0	0	0	0	1001
Chlorophyll	0	0	0	0	0	0	0	0	0	0	15
Lipase	0	0	0	0	0	0	0	0	0	0	0
TOTAL	410761	7627	1532012	1945683	1903973	41710	11042	30668	42	29652	9437

Flows (kg)	12	13	14	15	16	17	18	19	20	21	22	23 / 24	27
Water	0	0	115	0	0	56	51	0	32	36	0	26988	382878
Cells	0	0	0	0	0	0	0	0	0	0	0	1833	125
Sodium nitrate	0	0	0	0	0	0	0	0	0	0	0	0	0
KH_2PO_4	0	0	0	0	0	0	0	0	0	0	0	0	0
Hexane	8379	42	0	21	21	0	0	0	0	0	0	0	0
Phosphoric acid	0	0	1	0	0	0	0	0	0	0	8	0	0
NaOH	0	0	3	0	0	0	0	0	0	0	56	0	0
Methanol	0	0	0	0	0	111	2	0	0	0	0	0	0
Biodiesel	0	0	0	0	0	0	1000	0	0	0	0	0	0
Glycerol	0	0	0	0	0	0	106	0	0	0	0	0	0
Cooling water	0	0	0	0	0	97	97	0	22	22	0	0	0
Steam	0	0	0	0	0	1540	0	0	0	0	0	0	0
Glucose	0	0	0	0	0	0	0	0	6	0	0	0	0
Yeast	0	0	0	0	0	0	0	0	4	0	0	0	0
Precipitating chemical	0	0	0	0	0	0	0	0	2	2	0	0	0
CO_2	0	0	0	0	0	0	0	0	0	8	0	413	0
Phosphates	0	0	0	0	0	0	0	0	0	1	0	0	0
Urea	0	0	0	0	0	0	0	0	0	0	3	0	0
Methane (STP)	0	0	0	0	0	0	0	0	0	0	0	126	0
Soil conditioner	0	0	0	0	0	0	0	0	0	0	0	0	0
TAG	0	1001	0	10	991	0	0	0	0	0	0	0	0
Chlorophyll	0	15	0	14	0	0	0	0	0	0	0	0	0
Lipase	0	0	0	0	0	0	0	2	0	0	0	0	0
TOTAL	8379	1058	120	45	1012	1805	1257	2	67	71	66	29359	383003

Table D.2 Flows (kg day^{-1}) of each component in each of the streams numbered in the process flow-sheet for the simulated algal biodiesel production process in Figure D.1. The flows below represent the quantities when an airlift photobioreactor at a gas flowrate of 0.5 L min^{-1} was used for algal cultivation.

Flows (kg)	**1**	**2 / 25**	**26**	**3**	**5**	**6**	**7**	**8**	**9**	**10**	**11**
Water	437867	0	1643515	2081382	2043546	37836	10848	26988	0	26988	0
Cells	0	0	499	4304	430	3874	194	3680	0	2664	0
Sodium nitrate	771	0	0	0	0	0	0	0	0	0	0
KH_2PO_4	124	0	0	0	0	0	0	0	0	0	0
Hexane	0	0	0	0	0	0	0	0	42	0	8421
Phosphoric acid	0	0	0	0	0	0	0	0	0	0	0
NaOH	0	0	0	0	0	0	0	0	0	0	0
Methanol	0	0	0	0	0	0	0	0	0	0	0
Biodiesel	0	0	0	0	0	0	0	0	0	0	0
Glycerol	0	0	0	0	0	0	0	0	0	0	0
Cooling water	0	0	0	0	0	0	0	0	0	0	0
Steam	0	0	0	0	0	0	0	0	0	0	0
Glucose	0	0	0	0	0	0	0	0	0	0	0
Yeast	0	0	0	0	0	0	0	0	0	0	0
Precipitating chemical	0	0	0	0	0	0	0	0	0	0	0
CO_2	0	7627	0	0	0	0	0	0	0	0	0
Phosphates	0	0	0	0	0	0	0	0	0	0	0
Urea	0	0	0	0	0	0	0	0	0	0	0
Methane (STP)	0	0	0	0	0	0	0	0	0	0	0
Soil conditioner	0	0	0	0	0	0	0	0	0	0	0
TAG	0	0	0	0	0	0	0	0	0	0	1001
Chlorophyll	0	0	0	0	0	0	0	0	0	0	15
Lipase	0	0	0	0	0	0	0	0	0	0	0
TOTAL	438762	7627	1644014	2085686	2043976	41710	11042	30668	42	29652	9437

Flows (kg)	**13**	**14**	**15**	**16**	**17**	**18**	**19**	**20**	**21**	**22**	**23 / 24**	**27**
Water	0	0	115	0	0	56	51	0	32	36	0	26988
Cells	0	0	0	0	0	0	0	0	0	0	0	1833
Sodium nitrate	0	0	0	0	0	0	0	0	0	0	0	0
KH_2PO_4	0	0	0	0	0	0	0	0	0	0	0	0
Hexane	0	0	0	0	0	0	0	0	0	0	0	0
Phosphoric acid	8379	42	0	21	21	0	0	0	0	0	0	0
NaOH	0	0	1	0	0	0	0	0	0	0	8	0
Methanol	0	0	3	0	0	0	0	0	0	0	56	0
Biodiesel	0	0	0	0	0	111	2	0	0	0	0	0
Glycerol	0	0	0	0	0	0	1000	0	0	0	0	0
Cooling water	0	0	0	0	0	0	106	0	0	0	0	0
Steam	0	0	0	0	0	97	97	0	22	22	0	0
Glucose	0	0	0	0	0	1540	0	0	0	0	0	0
Yeast	0	0	0	0	0	0	0	0	6	0	0	0
Precipitating chemical	0	0	0	0	0	0	0	0	4	0	0	0
CO_2	0	0	0	0	0	0	0	0	2	2	0	0
Phosphates	0	0	0	0	0	0	0	0	0	8	0	413
Urea	0	0	0	0	0	0	0	0	0	1	0	0
Methane (STP)	0	0	0	0	0	0	0	0	0	0	3	0
Soil conditioner	0	0	0	0	0	0	0	0	0	0	0	126
TAG	0	0	0	0	0	0	0	0	0	0	0	0
Chlorophyll	0	1001	0	10	991	0	0	0	0	0	0	0
Lipase	0	15	0	14	0	0	0	0	0	0	0	0
TOTAL	8379	1058	120	45	1012	1805	1257	2	67	71	66	29359

Table D.3 Flows (kg day^{-1}) of each component in each of the streams numbered in the process flow-sheet for the simulated algal biodiesel production process in Figure D.1. The flows below represent the quantities when a wave photobioreactor at 15 rpm, 4° was used for algal cultivation.

Flows (kg)	**1**	**2 / 25**	**26**	**3**	**5**	**6**	**7**	**8**	**9**	**10**	**11**
Water	406415	0	1517707	1924122	1886286	37836	10848	26988	0	26988	0
Cells	0	0	499	4304	430	3874	194	3680	0	2664	0
Sodium nitrate	771	0	0	0	0	0	0	0	0	0	0
KH_2PO_4	124	0	0	0	0	0	0	0	0	0	0
Hexane	0	0	0	0	0	0	0	0	42	0	8421
Phosphoric acid	0	0	0	0	0	0	0	0	0	0	0
NaOH	0	0	0	0	0	0	0	0	0	0	0
Methanol	0	0	0	0	0	0	0	0	0	0	0
Biodiesel	0	0	0	0	0	0	0	0	0	0	0
Glycerol	0	0	0	0	0	0	0	0	0	0	0
Cooling water	0	0	0	0	0	0	0	0	0	0	0
Steam	0	0	0	0	0	0	0	0	0	0	0
Glucose	0	0	0	0	0	0	0	0	0	0	0
Yeast	0	0	0	0	0	0	0	0	0	0	0
Precipitating chemical	0	0	0	0	0	0	0	0	0	0	0
CO_2	0	7640	0	0	0	0	0	0	0	0	0
Phosphates	0	0	0	0	0	0	0	0	0	0	0
Urea	0	0	0	0	0	0	0	0	0	0	0
Methane (STP)	0	0	0	0	0	0	0	0	0	0	0
Soil conditioner	0	0	0	0	0	0	0	0	0	0	0
TAG	0	0	0	0	0	0	0	0	0	0	1001
Chlorophyll	0	0	0	0	0	0	0	0	0	0	15
Lipase	0	0	0	0	0	0	0	0	0	0	0
TOTAL	407310	7640	1518206	1928426	1886716	41710	11042	30668	42	29652	9437

Flows (kg)	12	13	14	15	16	17	18	19	20	21	22	23 / 24	27
Water	0	0	115	0	0	56	51	0	32	36	0	26988	379427
Cells	0	0	0	0	0	0	0	0	0	0	0	1833	125
Sodium nitrate	0	0	0	0	0	0	0	0	0	0	0	0	0
KH_2PO_4	0	0	0	0	0	0	0	0	0	0	0	0	0
Hexane	8379	42	0	21	21	0	0	0	0	0	0	0	0
Phosphoric acid	0	0	1	0	0	0	0	0	0	0	8	0	0
NaOH	0	0	3	0	0	0	0	0	0	0	56	0	0
Methanol	0	0	0	0	0	111	2	0	0	0	0	0	0
Biodiesel	0	0	0	0	0	0	1000	0	0	0	0	0	0
Glycerol	0	0	0	0	0	0	106	0	0	0	0	0	0
Cooling water	0	0	0	0	0	97	97	0	22	22	0	0	0
Steam	0	0	0	0	0	1540	0	0	0	0	0	0	0
Glucose	0	0	0	0	0	0	0	0	6	0	0	0	0
Yeast	0	0	0	0	0	0	0	0	4	0	0	0	0
Precipitating chemical	0	0	0	0	0	0	0	0	2	2	0	0	0
CO_2	0	0	0	0	0	0	0	0	0	8	0	416	0
Phosphates	0	0	0	0	0	0	0	0	0	1	0	0	0
Urea	0	0	0	0	0	0	0	0	0	0	3	0	0
Methane (STP)	0	0	0	0	0	0	0	0	0	0	0	127	0
Soil conditioner	0	0	0	0	0	0	0	0	0	0	0	0	0
TAG	0	1001	0	10	991	0	0	0	0	0	0	0	0
Chlorophyll	0	15	0	14	0	0	0	0	0	0	0	0	0
Lipase	0	0	0	0	0	0	0	2	0	0	0	0	0
TOTAL	8379	1058	120	45	1012	1805	1257	2	67	71	67	29364	379552